IWANAMI SERIES IN MODERN MATHEMATICS

Translations of
MATHEMATICAL
MONOGRAPHS

Volume 209

# Far-from-Equilibrium Dynamics

Yasumasa Nishiura

American Mathematical Society

# Selected Titles in This Series

209 **Yasumasa Nishiura,** Far-from-equilibrium dynamics, 2002

208 **Yukio Matsumoto,** An introduction to Morse theory, 2002

207 **Ken'ichi Ohshika,** Discrete groups, 2002

206 **Yuji Shimizu and Kenji Ueno,** Advances in moduli theory, 2002

205 **Seiki Nishikawa,** Variational problems in geometry, 2001

204 **A. M. Vinogradov,** Cohomological analysis of partial differential equations and Secondary Calculus, 2001

203 **Te Sun Han and Kingo Kobayashi,** Mathematics of information and coding, 2002

202 **V. P. Maslov and G. A. Omel'yanov,** Geometric asymptotics for nonlinear PDE. I, 2001

201 **Shigeyuki Morita,** Geometry of differential forms, 2001

200 **V. V. Prasolov and V. M. Tikhomirov,** Geometry, 2001

199 **Shigeyuki Morita,** Geometry of characteristic classes, 2001

198 **V. A. Smirnov,** Simplicial and operad methods in algebraic topology, 2001

197 **Kenji Ueno,** Algebraic geometry 2: Sheaves and cohomology, 2001

196 **Yu. N. Lin'kov,** Asymptotic statistical methods for stochastic processes, 2001

195 **Minoru Wakimoto,** Infinite-dimensional Lie algebras, 2001

194 **Valery B. Nevzorov,** Records: Mathematical theory, 2001

193 **Toshio Nishino,** Function theory in several complex variables, 2001

192 **Yu. P. Sol**
operators in

191 **Shun-ichi**
geometry, 2

190 **Alexander N. Starkov,** Dynamical systems on homogeneous spaces, 2000

189 **Mitsuru Ikawa,** Hyperbolic partial differential equations and wave phenomena, 2000

188 **V. V. Buldygin and Yu. V. Kozachenko,** Metric characterization of random variables and random processes, 2000

187 **A. V. Fursikov,** Optimal control of distributed systems. Theory and applications, 2000

186 **Kazuya Kato, Nobushige Kurokawa, and Takeshi Saito,** Number theory 1: Fermat's dream, 2000

185 **Kenji Ueno,** Algebraic Geometry 1: From algebraic varieties to schemes, 1999

184 **A. V. Mel'nikov,** Financial markets, 1999

183 **Hajime Sato,** Algebraic topology: an intuitive approach, 1999

182 **I. S. Krasil'shchik and A. M. Vinogradov, Editors,** Symmetries and conservation laws for differential equations of mathematical physics, 1999

(*Continued in the back of this publication*)

# Far-from-Equilibrium Dynamics

IWANAMI SERIES IN MODERN MATHEMATICS

Translations of
# MATHEMATICAL MONOGRAPHS

Volume 209

# Far-from-Equilibrium Dynamics

Yasumasa Nishiura

Translated by
Kunimochi Sakamoto

**American Mathematical Society**
Providence, Rhode Island

# 非線形問題 1

## パターン形成の数理

HISENKEI MONDAI. 1, PATAN KEISEI NO SURI
(FAR-FROM-EQUILIBRIUM DYNAMICS)

by Yasumasa Nishiura



Originally published in Japanese
by Iwanami Shoten, Publishers, Tokyo, 1999

Translated from the Japanese by Kunimochi Sakamoto

2000 *Mathematics Subject Classification.* Primary 34D15, 35B25, 35B32, 35B40, 35K57, 37D10, 37L10, 74N20.

**Library of Congress Cataloging-in-Publication Data**

Nishiura, Yasumasa, 1950-
[Hisenkei mondai. 1, Patan keisei no suri. English]
Far-from-equilibrium dynamics / Yasumasa Nishiura ; translated by Kunimochi Sakamoto.
p. cm. — (Translations of mathematical monographs, ISSN 0065-9282 ; v. 209)
(Iwanami series in modern mathematics)
Includes bibliographical references and index.
ISBN 0-8218-2625-5 (softcover : alk. paper)
1. Dynamics. 2. Interfaces (Physical sciences) 3. Scaling laws (Statistical physics) 4. Phase transformations (Statistical physics) 5. Pattern formation (Physical sciences) I. Title. II. Series. III. Series: Iwanami series in modern mathematics.

QA852.N5713 2002
510 s—dc21
[531′.11] 2002018242



10 9 8 7 6 5 4 3 2 1 07 06 05 04 03 02

# Contents

# Preface

A pattern is a state in which different scales coexist in space-time. What is a scale? It is a gauge to measure the speed with which things change in space-time. When different scales coexist in the spatial direction, it produces non-uniformity. If the degree of the non-uniformity is not so great, one sees vague inhomogeneity. On the other hand, if the non-uniformity is sharply contrasted, one clearly sees well-discernible perimeters.

The invasion of solid phase into liquid phase in crystal growth processes and the transition from oxidized states to reduced states in chemically reacting systems always accompany changes in states (phases), and often the transition is very rapid. When the direction of alignment changes along an interface, one can also observe a pattern. It could be said that patterns are created wherever states of different natures reside side by side. In other words, it is such a rapid transition between states that enables us to recognize patterns.

An easily understandable example of coexisting scales in the temporal direction is a beat. What we hear is not caused by rapid oscillations of the air but by the gradually changing large amplitudes. Moiré patterns are considered as a spatial version of beats.

The main objective of this book is to investigate the dynamics of spatio-temporal patterns created by the coexistence of different scales.

However, the coexistence of different scales poses, mathematically speaking, a difficult problem, namely, the loss of uniformity. The problem of how to deal with classical secular terms is a typical example of this loss of uniformity. To keep the uniformity, a particular scale has to be fixed through which observations are made. But then the global picture of the system is lost. It may well be said that singular perturbation theories have been developed as an effort to alleviate the dilemma.

Another objective, as may be realized by browsing through the book, is to introduce the reader to the dynamics of dissipative systems. A *dissipative system* is any system which creates structures or orders within itself, supplied with energy or matter from outside, and discards wastes at the same time. The earth and ourselves, as well as the examples described above, are all examples of dissipative systems. To present a bird's-eye view of dissipative systems, which is a rich source of nonlinear dynamical systems, is not so easy a task, even if the scope is restricted to their mathematical aspects. For this reason, I have tried to give a coherent view of several topics from the standpoint of separation and unification of scales, rather than to give a list of various methodologies. Therefore the emphasis is placed more on the overall flow of theories than on fine details of proof.

The boundary of two different phases caused by the difference of spatial scales is usually called an *interface*. Our interest is to study how the interface is created, how it evolves, and what types of configurations it eventually takes. The interface dynamics is taken up as the main theme of the second half of this book, and it is one of the most actively studied areas in dissipative dynamical systems. Water-oil interfaces on one end and nano-structures on the other—interface dynamics reveals itself within various hierarchies from macroscopic to microscopic with the advancement of measurement technologies. The main issue here is to find a mathematical framework with which we can understand the dynamics. Although we study models which come from real phenomena, what we gain at the end will be independent of the particular phenomena.

Many important topics and methodologies are left out of this book, partly due to the limitation of pages. For example, it is regrettable that the geometric theory of singular perturbation and bifurcation theory are not included. Nevertheless, I humbly hope that the book conveys to many readers the excitement of exploring pattern dynamics.

I am indebted to many people for the completion of this book. From my respected friend Hiroshi Matano, who encouraged me to write this book, I received much important advice. My colleague Ryo Kobayashi helped not only through discussion of the contents of the book, but also in drawing many of the figures. Shin-Ichiro Ei of Yokohama City University and Masataka Kuwamura of Wakayama University gave me many pieces of important information to write

Chapter 1. Tatsunari Sakurai of Meme Media Lab of Hokkaido University carried out experiments on the BZ reaction for the book, and Toshiko Ogiwara carefully read the entire manuscript. At the last stage of writing the manuscript, the editorial staff of Iwanami Book Company was of great assistance. Throughout this enterprise many graduate students have been very helpful, especially Daishin Ueyama (presently at Hiroshima University) in producing figures and pictures, and Kei-ichi Ueda in collating the first draft and polishing the final manuscript. I deeply thank them all.

Towards the end of the year, December 24, 1998, my beloved teacher Masaya Yamaguti passed away. I dedicate this book to his gracious and free spirit.

December 1998, Sapporo
Yasumasa Nishiura

# Preface to the English Edition

The English edition of this book has provided the opportunity for correcting many typographial errors and mistakes. The last chapter, "Transient Dynamics", has been almost completely rewritten. I have added considerable new material, including the bifurcational characterization for the onset of self-replication, which, combined with weak interaction of localized pulses, clarifies the interrelation between strong and weak interactions. This plays an important role in undesrstanding the manner of splitting. Also added is a geometrical interpretation of spatio-temporal chaos. The Gray-Scott model is adopted as a representative model in this chapter; however, the methods and the results have a great potential to be applied to many other similar problems.

I would like to thank Nick Alikakos, Shin-ichiro Ei, Paul Fife, Jim Keener, Björn Sandstedt, Gieri Simonett, Peter Sternberg, and Wim van Saarloos for many useful comments to improve the English edition, as well as for updating references and catching typographical errors.

Finally, but not the least, special thanks go to the translator, Kuni Sakamoto. This book would have had no chance to be read outside of Japan without his efforts.

October 2001, Sapporo
Yasumasa Nishiura

# Overview

A dynamic cycle in which a uniform state is disturbed by fluctuations, a particular size of the fluctuations is therein selectively picked up, and a structure emerges, keeps its shape, disintegrates, and returns to the original uniform state, literally resembles the state of being alive. What kind of mathematical mechanism is it that produces such a dynamics? Alan Turing's idea of diffusion-induced instability gives the simplest and most direct explanation of instability, in the sense that random fluctuations may possibly grow into a structure. This idea was received with great surprise because it means that diffusion effects, believed to be a uniformization force, could sometimes function as a driving force of destabilization.

Although the content of Turing's idea was a forerunner of what is nowadays called symmetry-breaking bifurcation, it remained a mere theoretical possibility because its experimental realization proved extremely difficult. However, once its experimental realization became possible in chemically reacting systems in the early 1990's, an explosion of discoveries have followed that exhibited a wide range of dynamic behaviors originating from the Turing instability. At the present time, experimental discoveries are advancing ahead of theory. The self-replicating pattern to be discussed in Chapter 6 is one of the phenomena in this trend of events.

A well known chemical reaction in which the shape and rhythm of patterns are maintained is the BZ reaction, which will be discussed in Chapter 4. This is a sort of oxidation-reduction process in which a chemical marker makes the two states visible. Typically observed in this system are spiral patterns. The mathematical mechanism which drives the motion of the spiral is the same as those for nerve impulses, liquid crystals, and the movement of amoebae, and could be common to other similar phenomena.

When we discern such shapes, we are actually observing their boundary or perimeter. The boundary is exactly the place where

the state (phase) of the matter changes abruptly, or, in other words, observing the boundary enables us to grasp the shape as a whole. Information is, so to speak, concentrated on the perimeter. This line of reasoning naturally leads to the interface dynamics approach. By focusing attention on how the bounding interfaces move and on what kind of configuration they form, one can qualitatively understand the mathematical structures of pattern formation by neglecting fine details in the bulk and considering a substantially reduced system (which describes the movement of hypersurfaces in the simplest case).

Notice here that the viewpoint of separation and unification of various scales is lurking behind the scene. Namely, since the speed of the change near the interface differs substantially from that in the bulk, it is possible to reduce the evolution of the full system to the motion of the interface. The basic idea here is to understand the dynamics of shapes by taking advantage of the difference in the scales and lowering the dimension of the system in geometrically sensible ways. Although some portion of quantitative information may be lost in such a process, a rather universal understanding of qualitative aspects is accomplished. Such a point of view is the keynote of this book.

In the above reductions, the reduced interface dynamics may not be uniquely determined, even if the equations governing the original system are the same. Depending on what aspect of the original phenomenon is of interest, one has to decide what kind of limit procedure to take. It is here that the difficulty appears in dealing with infinite dimensional systems, and this is also where the excitement lies.

Notice also that the separation of scales is intimately related to singularities. It is well known that at a bifurcation point some mode of evolution may be very slow relative to the others, and hence the slow mode asymptotically dictates the evolution of the entire system. Therefore it is possible to separate out particular modes of evolution at bifurcation (or unstable) points, by utilizing the discrepancy in scales. The construction of center manifolds, as well as other types of invariant manifolds, is based upon such a viewpoint.

There are cases, on the other hand, where interest lies in how the system behaves in a certain intermediate time scale, rather than how it ultimately behaves. In other words, it can be said that whether a dynamic structure is viewed as stationary or transient depends on whether it lasts long enough relative to the observer's time scale.

Therefore whether a phenomenon is stationary or transient is a relative concept, and is determined by the relationship between the observer and the observed.

Of particular interest in this context is impermanent dynamics. For a period of time the system keeps its shape. In a longer period of time it loses the shape, and after a while it rebuilds itself into a different shape and then collapses. Sometimes this cyclic process may continue indefinitely. Sometimes it may settle down to a final destination. The shape we refer to here is not necessarily a rigid one which literally survives an erosion of time, but could be a chaos, or any dynamics which has a certain supporting structure in the background. There are cases in which the mechanism of how transient dynamics is produced is clarified by extensive use of computers, not as a naive simulation machine, but to detect the global solution structure. In these cases, computer simulations bridge the gap between the phenomenon and its rigorous theoretical explanation. The reader will encounter one such example toward the end of this book.

Let me now describe the content of each chapter.

Chapter 1 recapitulates the classical secular term problem and the transition layer problem. The former is nothing but the problem of how to deal with an effect of, so to speak, dust piling up to create a mountain. Minute perturbations can result in a huge change over a long period of time. The task here is how to take care of the effects of such a slowly evolving change. A boundary layer in fluid motions is a typical example where two spatially different scales coexist. When fluid passes by a stationary object, the velocity of the fluid rapidly decreases from a finite value to zero in the vicinity of the boundary (the object). The task in this case is to take into account the viscosity, which acts effectively only near the boundary. In pattern formation problems, internal transition layers play important roles. What is it that is responsible for determining the position and shape of internal layers? To provide an approach to such a question is one of the aims of Chapter 1. The approach is related to how to extract the slow mode of freedom in the system. Renormalization group methods can also be treated from the same approach.

In Chapter 2, it is shown that the amplitude equation is nothing but the normal form of dynamics near an unstable point in infinitely extended systems. When the spatial domain is bounded, the distribution of discrete (point) spectra is responsible for the destabilization

of the system, and therefore a great amount of information can be obtained by analyzing the flows on various invariant manifolds, such as center manifolds. In infinitely extended systems, continuous spectra prevail, and it is not an easy task to construct such invariant manifolds as above. However, it is sometimes possible to detect the long-time dynamics of infinitely extended systems near an unstable point. This is done by taking the dominant modes (the modes which correspond to the most unstable eigenfunctions) of the system as the basis of coordinates, and by examining how the amplitude of the dominant modes depends on the slow spatio-temporal scales. Also included in this chapter is a rigorous characterization of asymptotic behavior in terms of renormalization group methods.

Pattern selection problems are taken up in Chapter 3. Nature exhibits diverse varieties of patterns. These patterns, under certain conditions, reproduce themselves. In a crystal growth process, for example, the growth speed and shape of the crystal is uniquely determined by the degree of undercooling in the far-field. What kind of mechanism is it that makes this decision? In this chapter, after a short historical description of dendritic crystal growth, an argument is given for the velocity selection mechanism of travelling waves which invade unstable regions. The argument is not so easy as it may look at first glance, since the problem turns out to be a global one, in the sense that one has to describe the entire process, including the initial perturbations and the final shape of the travelling waves. In fact, the detailed mechanism remains unknown, except for scalar equations to which comparison principles are applicable. A useful viewpoint is provided by a so-called *marginal stability criterion.* This criterion, first proposed as a selection principle of solutions for crystal growth processes, asserts that, among a family of solutions, the one at which the stability property changes is selected. The advantage of the criterion is its potential applicability to a wide class of problems. From a dynamical system point of view, however, the question of why such a solution is selected has not been completely answered.

In Chapter 4, pattern dynamics problems for reaction-diffusion systems are treated. Classes of equations, which are generally called reaction-diffusion systems, contain wide varieties, and the phenomena described by them are diverse. Choosing at first a particular class of system, we discuss the dynamics of the system with specific nonlinearities which are believed to be fundamental. Gradient systems are the most basic of all, and they have played important roles in the

development of infinite dimensional dynamical system theories. The ultimate state of a solution in gradient systems usually converges to an equilibrium state, along with the decrease of the value of the energy functional. It will be shown, however, that when nonlocal terms are involved in the energy functional, the final destination could be quite complicated, and it is sometimes described by a *rugged landscape.*

The second half of the chapter presents the Turing instability, a pioneering work in pattern formation theory, and spiral waves in excitable media. Turing's simple yet brilliant idea, that diffusion effects could give rise to instability, has recently been tested and confirmed to be valid by many experiments, and moreover, has become the rich source of many new dynamical behaviors. A spiral wave observed in the BZ reaction is a representative of spatio-temporal patterns in dissipative systems, and is a typical example to which the method of interface dynamics applies effectively. The evolution law of the spiral wave, in terms of differential equations, is at least formally obtained by the method of matched asymptotic expansions. The pattern selection problem, discussed in Chapter 3, i.e., the problem of what shape and angular velocity of the spiral are selected, appears here again. It is necessary to derive a model which is as simple as possible and yet retains a sufficient amount of information to resolve the issues. In deriving such a model, what is called a *singular limit balanced scaling*, treated in Chapter 5, will play an important role.

In Chapter 5, an overview is given to the theory of *singular limit analysis*, which recently has developed substantially. The method of interface dynamics and the method of matched asymptotic expansions mentioned above are part of this theory. The effectiveness of the singular limit analysis seems to stem from the fact that the method is geometric in nature, and from the fact that it is closely related to the basic premise that when we perceive the motion of patterns we are actually looking at the perimeter or the boundaries. The motion of a hypersurface driven by its mean curvature is mathematically shown to exist globally in time beyond singularities in terms of viscosity solutions. It is also possible to rigorously show that the motion is actually the singular limit of a scalar bistable reaction-diffusion equation. By passing to singular limits of the equations in Chapter 4, one can derive various types of interface equations and can elucidate, with the help of the interface equations, what it is that essentially drives the interfaces. Also treated in this chapter is the *SLEP*-method, which

is instrumental in characterizing spectral properties in the singular limit of reaction-diffusion systems of activator-inhibitor type.

Chapter 6 has a flavour different from other chapters. In this chapter the spotlight is on aspects that have escaped the methods presented in the preceding chapters. Namely, we take a fresh, close look at transient or impermanent dynamics. As discussed earlier, what is transient and what is permanent are relative concepts which depend on the scale through which observations are made. The *self-replicating patterns* treated in this chapter are just a typical example of such a phenomenon. On bounded domains, these are patterns that appear along the way, before the system settles down to the final destination, and, before and after the self-replication, they behave as if they were either genuine equilibrium solutions or spatially periodic solutions (aftereffect of limiting points and unstable manifolds). What drives this process is not seen just by looking at the phase space at a fixed parameter. The driving mechanism becomes uncovered only when we look at the extended phase space in which a global bifurcation diagram is drawn with variable parameter values (hierarchical structures of limiting points). This mechanism also gives us a criterion for the onset and termination of the replicating dynamics. When the system size becomes large or infinite, the interaction among well-separated localized pulses or spots can be reduced to an ODE dynamics. The system of ODE's allows us to understand not only a weak interaction among them, but also more subtle dynamics like oscillatory splitting near singularities.

Generally speaking, transient structures necessarily emerge wherever several different scales coexist and one scale transfers to another. In this sense, transient processes create quite vivid and interesting dynamical behaviors. In fact, when the solutions to which the system eventually settles down either disappear or become unstable, a dynamic behavior appears in which self-replications and self-destructions alternatively occur perpetually. Such a phenomenon is also expected to be understood by the help of the global bifurcation structure of the system. In fact, at the end of this chapter, we demonstrate that a particular type of *spatio-temporal chaos* can be characterized as an aftereffect of heteroclinic cycles in infinite dimensional space.

CHAPTER 1

# Separation and Unification of Scales

The secular term problem in celestial mechanics is a typical example in which naive perturbation expansions in the temporal direction break down. As remedies, the strained coordinate method, the method of multiple time scales, and various other techniques have been developed. These methods, however, cannot escape the criticism that they are the artwork of a craftsman and often require problem-dependent specifics. On the other hand, in the theory of fluid dynamics, L. Prandtl discovered and started the analysis of boundary layer phenomena in 1905, and his analysis quickly produced the first cornerstone example of the coexistence of different scales in the spatial direction. In this chapter, it will be shown that these problems (the secular term problem and the boundary layer problem) are caused by non-uniformity of convergence due to the coexistence of different spatio-temporal scales. We will aslo show that long-term behaviors of such problems can be lucidly described by introducing a coordinate system which suits the so-called *slow* degrees of freedom.

## 1.1. Problem of Cumulative Term Type

**1.1.1. Method of Multiple Scales.** Let us consider the *Duffing equation*, which describes the motion of a nonlinear spring:

$$\frac{d^2x}{dt^2} + x + \epsilon x^3 = 0, \qquad t > 0, \tag{1.1}$$

$$x(0) = \alpha, \qquad \frac{dx}{dt}(0) = 0. \tag{1.2}$$

Here $x$ stands for the deviation from a reference point, and the parameter $\epsilon$ is a small positive number. When $\epsilon = 0$, it reduces to the well known equation for a harmonic oscillator. Since the nonlinear term $\epsilon x^3$ is of lower order, the solution $x(t)$ may be obtained as an

$\epsilon$-power series, as is the case in **regular perturbation** problems:

$$x(t) \sim x_0(t) + \epsilon x_1(t) + \ldots + \epsilon^n x_n(t) + \ldots . \tag{1.3}$$

Substituting (1.3) into (1.1) and rearranging the resulting equation in terms of powers in $\epsilon$, one obtains the first two terms of the solution as follows:

$$x(t) = \alpha \cos t + \epsilon \left\{ -\frac{3}{8}\alpha^3 t \sin t + \frac{\alpha^3}{32}(\cos 3t - \cos t) \right\} + O(\epsilon^2). \tag{1.4}$$

For each finite $T > 0$, the expansion (1.4) is valid uniformly on $[0, T]$. However, it cannot be an approximation on the entire half-axis $[0, \infty)$, because the quantity $-\frac{3}{8}\alpha^3 t \sin t$ in the second term diverges oscillatorily to infinity as $t \to \infty$ (the solutions of (1.1) remain bounded, as can easily be verified by multiplying it by $\frac{dx}{dt}$). For $t = O(1/\epsilon)$, the second term in (1.4) is no longer of the order $O(\epsilon)$. Such a term as $-\frac{3}{8}\alpha^3 t \sin t$, which forces the regular perturbative expansion to break down, is called a **secular term**. For this reason, a problem of the type (1.1) is called a **cumulative type problem**. The equation (1.1) does not have a form in which the highest order derivative term is added as a perturbation. However, it should be treated as a **singular perturbation problem**, since its solutions do not have any regular perturbative expansion which is valid on $[0, \infty)$.

In order to overcome this difficulty, various techniques have been devised. One such technique is the *method of strained coordinate*. In this method the independent variable $t$ is transformed to $\tau$ via

$$t = (1 + \epsilon\omega_1 + \epsilon^2\omega_2 + \ldots)\tau, \tag{1.5}$$

in which the constants $\omega_i$ $(i = 1, 2, 3, \ldots)$ are to be determined to eliminate secular terms. For the moment, the expression

$$1 + \epsilon\omega_1 + \epsilon^2\omega_2 + \ldots \tag{1.6}$$

is assumed to be convergent. In terms of $\tau$ the problem (1.1)-(1.2) is recast as

$$\frac{d^2x}{d\tau^2} + (1 + \epsilon\omega_1 + \epsilon^2\omega_2 + \ldots)^2(x + \epsilon x^3) = 0, \qquad \tau > 0, \tag{1.7}$$

$$x(0) = \alpha, \qquad \frac{dx}{d\tau}(0) = 0. \tag{1.8}$$

Expand $x(\tau)$ as in

$$x(\tau) = x_0(\tau) + \epsilon x_1(\tau) + \epsilon^2 x_2(\tau) + \ldots . \tag{1.9}$$

Substituting it into (1.7), and equating to 0 the coefficients of each power of $\epsilon$, one obtains a series of linear initial value problems. The first two in the series read

(1.10)

$$O(1): \quad \frac{d^2x_0}{d\tau^2} + x_0 = 0, \qquad x_0(0) = \alpha, \quad \frac{dx_0}{d\tau}(0) = 0,$$

(1.11)

$$O(\epsilon): \quad \frac{d^2x_1}{d\tau^2} + x_1 = -(x_0^3 + 2\omega_1 x_0), \quad x_1(0) = 0, \quad \frac{dx_1}{d\tau}(0) = 0.$$

Solving (1.10), one obtains

$$x_0(\tau) = \alpha \cos\tau, \tag{1.12}$$

which upon substitution into (1.11) gives rise to

$$\frac{d^2x_1}{d\tau^2} + x_1 = -\alpha^3(\cos\tau)^3 - 2\alpha\omega_1 \cos\tau \tag{1.13}$$

$$= -\alpha\left(\frac{3}{4}\alpha^2 + 2\omega_1\right)\cos\tau - \frac{\alpha^3}{4}\cos 3\tau.$$

The first term on the right is a solution of the harmonic-oscillator equation and is the source of the secular term. This term is eliminated by choosing

$$\omega_1 = -\frac{3}{8}\alpha^2. \tag{1.14}$$

With this choice, the solution $x_1$ of (1.13) satisfying the initial conditions in (1.11) is given by

$$x_1(\tau) = \frac{\alpha^3}{32}(\cos 3\tau - \cos\tau). \tag{1.15}$$

The expansion (1.9) up to an $O(\epsilon)$-term is therefore given by

$$x(\tau) = \alpha\cos\tau + \epsilon\frac{\alpha^3}{32}(\cos 3\tau - \cos\tau) + O(\epsilon^2). \tag{1.16}$$

Since $\tau = (1 - \frac{3}{8}\alpha^2\epsilon + \dots)^{-1}t$, rewriting the first term on the right hand side of (1.16) in terms of $t$, it is expressed as

$$x(t) = \alpha\cos\left\{\left(1 + \frac{3}{8}\alpha^2\epsilon\right)t\right\} + O(\epsilon). \tag{1.17}$$

Note here that two time scales $t$ and $\epsilon t$ appear on the right hand side. The scale $t$ is called the *fast time*, and $\epsilon t$ the *slow time*. A perturbation method in which the existence of several different time scales is advantageously utilized, such as the method of constrained coordinate, is usually called a **method of multiple time scales**. It can be verified that (1.17) gives an approximation uniformly valid on $0 \leq t \leq T/\epsilon$ with the error estimate inclusive, where $T$ is a constant independent of $\epsilon$. The method above, however, is not satisfactory in the following points.

(i) The method is ad hoc in nature:
It is not clear directly from (1.1) why the transformation (1.5) is effective.

(ii) Convergence:
Whether (1.6) converges is not known in advance.

(iii) The method is not geometric:
The geometric meaning of the transformation (1.5) is not clear.

In the next subsection, in order to remedy these points, at least partially, the problem is re-examined from the standpoint of explicitly utilizing the slow mode of freedom in the system.

**1.1.2. Averaging.** What is the slow mode of freedom in (1.1)? It is the eigenspace corresponding to the **0-eigenvalue** of the linear operator obtained by setting $\epsilon = 0$ in (1.1). Denoting by $L$ the linear operator $L = \frac{d^2}{dx^2} + 1$, the equation (1.1) with $\epsilon = 0$ reduces to

$$Lx_0 = 0. \tag{1.18}$$

The 0-eigenspace of (1.18) is spanned by

$$x_0 = re^{i(t+\theta)}, \tag{1.19}$$

in terms of two parameters $r$ and $\theta$. The reason why $(r, \theta)$ is called the slow mode of freedom is as follows. When $\epsilon = 0$ the pair $(r, \theta)$ is determined by the initial conditions and remains constant in time. Hence it is expected to change slowly in accordance with the magnitude of $\epsilon$ for $\epsilon \neq 0$ $(0 < \epsilon \ll 1)$. In fact, in terms of the polar coordinates $(r, \theta)$ compatible with the space of the slow mode, (1.1) is recast as

$$\begin{cases} \dfrac{dr}{dt} &= \epsilon(r\ \cos(t+\theta))^3 \sin(t+\theta), \\ \dfrac{d\theta}{dt} &= \dfrac{\epsilon}{r}(r\ \cos(t+\theta))^3 \cos(t+\theta). \end{cases} \tag{1.20}$$

This system of equations shows that $r$ and $\theta$ change slowly with the speed of $O(\epsilon)$, if $r$ is bounded away from both 0 and infinity. However the system (1.20), which is obtained by the *phase-amplitude transformation*, looks more complicated than the original (1.1). Since the right hand sides in (1.20) are, on the other hand, a $2\pi$-periodic function of $t$ and $(r, \theta)$ changes slowly, the vector field obtained by averaging (1.20) over one period is expected to be a good approximation. Indeed, the right hand sides in (1.20), after the averaging, have a very simple form which is independent of $t$:

$$\begin{pmatrix} \epsilon \dfrac{1}{2\pi} \displaystyle\int_0^{2\pi} (r\ \cos(t+\theta))^3 \sin(t+\theta) dt \\ \\ \dfrac{\epsilon}{r} \dfrac{1}{2\pi} \displaystyle\int_0^{2\pi} (r\ \cos(t+\theta))^3 \cos(t+\theta) dt \end{pmatrix} = \begin{pmatrix} 0 \\ \\ \dfrac{3}{8}\epsilon r^2 \end{pmatrix}. \tag{1.21}$$

The right hand side of (1.21) defines an autonomous system of equations

$$\begin{cases} \dfrac{d\bar{r}}{dt} &= 0, \\ \\ \dfrac{d\bar{\theta}}{dt} &= \frac{3}{8}\epsilon r^2, \end{cases} \tag{1.22}$$

which is called the **averaged equation** of (1.20). The solutions of (1.22) are expected to give a good approximation valid for a long period of time. In fact, (1.22) gives rise to

$$x_0(t) = \alpha \cos\left\{\left(1 + \frac{3}{8}\epsilon\alpha^2\right)t\right\},$$

which agrees with (1.17). In general, the following theorem is available.

THEOREM 1.1 (Averaging Method [**231**]). *Let $x(t)$, $y(t) \in \mathbb{R}^n$ be the solutions of the following initial value problems:*

$$\frac{dx}{dt} = \epsilon f(t, x), \qquad x(0) = x_0, \tag{1.23}$$

$$\frac{dy}{dt} = \epsilon f_0(y), \qquad y(0) = x_0, \tag{1.24}$$

*where $f$ is sufficiently smooth on $G := [0, \infty) \times D$ (with $D$ being a simply connected domain) and $T$-periodic in $t$. The initial value $x_0$ is*

*an interior point of $D$. The vector field $f_0$ is the average of $f$ given by*

$$f_0(y) = \frac{1}{T}\int_0^T f(t,y)dt, \tag{1.25}$$

*in which the integration is carried out with $y$ being considered as a parameter independent of $t$.*

*Then there exists a subdomain $\tilde{D} \subset D$, independent of $\epsilon$, such that, as long as $x(t), y(t) \in \tilde{D}$, the estimate*

$$|x(t) - y(t)| \leq C\epsilon \tag{1.26}$$

*is valid on $0 \leq t \leq C/\epsilon$, where $C$ is a constant independent of $\epsilon$. In other words, the solution of the averaged equation gives an $O(\epsilon)$-uniform approximation valid on a time interval of length $O(1/\epsilon)$.*

PROOF. Once we switch the time scale from $t$ to $\tau$ via $\tau = \epsilon t$ and set $M = \max_G |f(t,x)|$, the fundamental theory of initial value problems for ordinary differential equations guarantees the existence and uniqueness of the solution $x(t)$ on the time interval $0 \leq t \leq \frac{C}{M\epsilon}$. Since $\max_G |f_0(y)| \leq M$ from the definition of $f_0$, the same assertion holds for $y(t)$ as well. By replacing the constant $C$ by another one if necessary, one may assume that the solution $y(t)$ remains in a subdomain $\tilde{D} \subset D$ which is independent of $\epsilon$. In the sequel, instead of estimating the error of $|x(t) - y(t)|$ directly, the error estimate is given in terms of an approximation with an improved accuracy. By rewriting the right hand side of (1.23) as the sum of the average over one period of length $T$ and the deviation from the average, it is recast as

$$\begin{aligned} \frac{dx}{dt} &= \epsilon\left\{\frac{1}{T}\int_0^T f(t,x)dt + \left(f(t,x) - \frac{1}{T}\int_0^T f(t,x)dt\right)\right\} \\ &= \epsilon f_0(x) + \epsilon\Big(f(t,x) - f_0(x)\Big). \end{aligned} \tag{1.27}$$

Although the averaged part is considered as being well approximated by $y(t)$, the deviation part in the second term is not related to $y(t)$. Therefore in the integrated form of (1.27)

$$x(t) - x_0 = \epsilon\int_0^t f_0(x)d\tau + \epsilon\int_0^t \Big\{f(\tau,x) - f_0(\tau,x)\Big\}d\tau \tag{1.28}$$

we consider an approximate solution $w$ which is the sum of $y(t)$ and the second term on the right hand side of (1.28) with $x$ being replaced

by $y(t)$. Namely,

$$w(t) = y(t) + \epsilon u(t, y), \tag{1.29}$$

$$u(t, y) = \int_0^t \Big\{ f(\tau, y) - f_0(\tau, y) \Big\} d\tau. \tag{1.30}$$

Note that $u$ is $T$-periodic in $t$ and satisfies $|u(t, y)| \leq 2MT$. In order to estimate the difference between $x(t)$ and $w(t)$, rewrite the difference as

$$x(t) - w(t) = \int_0^t \left( \frac{dx}{dt} - \frac{dw}{dt} \right) d\tau, \tag{1.31}$$

in which the integrand is rearranged as follows:

$$\begin{aligned} \frac{dx}{dt} - \frac{dw}{dt} &= \epsilon f(t, x) - \epsilon f_0(x) - \epsilon \nabla u \cdot \frac{dy}{dt} - \epsilon \frac{\partial u}{\partial t} \\ &= \epsilon \Big\{ f(t, x) - f(t, y) \Big\} - \epsilon^2 \nabla u \cdot f_0(y) \\ &= \epsilon \Big\{ f(t, x) - f(t, w) \Big\} + \epsilon \Big\{ f(t, w) - f(t, y) \Big\} \\ &\quad - \epsilon^2 \nabla u \cdot f_0(y). \end{aligned} \tag{1.32}$$

By using (1.30), the smoothness of $f$ and the boundedness of $u$ and $\nabla u$, the integrand is estimated as

$$\left| \frac{dx}{dt} - \frac{dw}{dt} \right| \leq \epsilon L |x - w| + C\epsilon^2. \tag{1.33}$$

Here, $L$ is the Lipschitz constant of $f$. Therefore (1.31) gives rise to

$$|x(t) - w(t)| \leq \epsilon L \int_0^t |x(\tau) - w(\tau)| d\tau + C\epsilon^2 t. \tag{1.34}$$

This is rewritten as

$$|x(t) - w(t)| + \frac{C\epsilon}{L} \leq \epsilon L \int_0^t \left\{ |x(\tau) - w(\tau)| + \frac{C\epsilon}{L} \right\} d\tau + \frac{C\epsilon}{L}, \tag{1.35}$$

to which the Gronwall inequality is applicable. Hence one concludes that

$$|x(t) - w(t)| + \frac{C\epsilon}{L} \leq \frac{C\epsilon}{L} \exp(\epsilon L t). \tag{1.36}$$

From (1.29) and (1.36), the conclusion of the theorem immediately follows. □

Thanks to this theorem, one can guarantee that the solution

$$\alpha \cos\left\{\left(1+\frac{3}{8}\epsilon\alpha^2\right)t\right\}$$

to the averaged equation (1.22) of the Duffing equation (1.1) gives a uniform $O(\epsilon)$-approximation on a time interval of length $O(1/\epsilon)$. The slow mode of freedom in (1.1) is two-dimensional and reveals itself as the slow variation of the phase $\theta$ as in (1.22).

Another example in which the slow variation of the amplitude $r$ appears is the **van der Pol equation**:

$$\frac{d^2x}{dt^2}+x=\epsilon(1-x^2)\frac{dx}{dt}. \tag{1.37}$$

When $\epsilon = 0$ this equation is of the same form as the unperturbed Duffing equation, and hence, applying the phase-amplitude transformation, the solutions $x(t)$ of (1.37) are expected to be uniformly approximated by

$$x(t)=\overline{a}\cos(t+\overline{\theta}(t))+O(\epsilon)$$

on $0 \le t \le t_1/\epsilon$. The pair $(\overline{a}, \overline{\theta})$ is the solution of the averaged equations:

$$\begin{cases} \dfrac{d\overline{a}}{dt}=\dfrac{\epsilon\overline{a}}{2\pi}\displaystyle\int_0^{2\pi}(1-\overline{a}^2\cos^2\varphi)\sin^2\varphi d\varphi=\dfrac{\epsilon\overline{a}}{2}\left(1-\dfrac{\overline{a}^2}{4}\right), \\ \dfrac{d\overline{\theta}}{dt}=\dfrac{\epsilon}{2\pi}\displaystyle\int_0^{2\pi}(1-\overline{a}^2\cos^2\varphi)\sin\varphi\cos\varphi d\varphi=0. \end{cases} \tag{1.38}$$

Integrating this system of equations, one obtains the solution:

$$\overline{a}^2=\frac{4}{1-Ae^{-\epsilon t}}, \qquad \overline{\theta}=\theta_0,$$

where the constants $A$ and $\theta_0$ are uniquely determined by the initial conditions. THEOREM 1.1 guarantees that

$$x(t)=\frac{2}{\sqrt{1-Ae^{-\epsilon t}}}\cos(t+\theta_0)+O(\epsilon) \tag{1.39}$$

uniformly on $0 \le t \le t_1/\epsilon$. When the initial conditions are specified as $x(0)=\alpha>0$, $dx(0)/dt=0$, the constants $A, \theta_0$ are given by

$$A=1-\frac{4}{\alpha^2}, \qquad \theta_0=0. \tag{1.40}$$

Thus it is seen that the amplitude $\overline{a}$ varies slowly in the time scale $\epsilon t$. It is easily understandable that this slow variation is caused by the nonlinear friction term on the right hand side of (1.37).

## 1.2. Problem of Transition Layer Type

**1.2.1. What is a Transition Layer?** In the previous section, it was necessary to introduce a slow time scale $\epsilon t$, in accordance with the perturbation parameter $\epsilon$, in order to obtain an approximation uniformly valid on a sufficiently long $(O(1/\epsilon))$ period of time. The natural system of coordinates in that case was the two-dimensional polar coordinates on the 0-eigenspace of the harmonic-oscillator operator.

Another classical example of singular perturbation, in which several scales are indispensable, is the **layer type problem**. The **boundary layer problem** raised in fluid dynamics by Prandtl is particularly well known. **Internal transition layers**, which recently have attracted a great amount of attention in pattern formation theory and free boundary problems, are an example in which certain quantities change very rapidly in a spatially narrow region. In the latter examples, as a particular parameter tends to zero, two spatial scales, fast-changing and slow-changing, coexist, and the solutions have singularities (discontinuities) in the limit where the thickness of the internal layer is squeezed to zero. When we study the existence and stability of transition layer solutions, the space of slow modes corresponding to (1.18) naturally appears. The slow modes almost identically correspond to the translational freedom of the internal layers. One can observe in the following simple function the separation and unification of scales appearing in a problem of transition layer type:

$$u(x,\epsilon) = e^{-x/\epsilon} + x + \epsilon, \qquad 0 \le x \le 1. \tag{1.41}$$

For each fixed $x$ $(x \neq 0)$, passing to the limit as $\epsilon \to 0$ (outer limit), one obtains

$$\lim_{\epsilon \to 0} u(x,\epsilon) = f(x) = x. \tag{1.42}$$

The function $f(x)$ is an $O(\epsilon)$-approximation of $u(x,\epsilon)$ on $x_0 \le x \le 1$, where $x_0 > 0$ is an arbitrarily fixed constant. This approximation, however, is not uniform in a neighborhood of 0, because $u(x,\epsilon)$ has a boundary layer, as is easily seen from the graph (see FIGURE. 1.1).

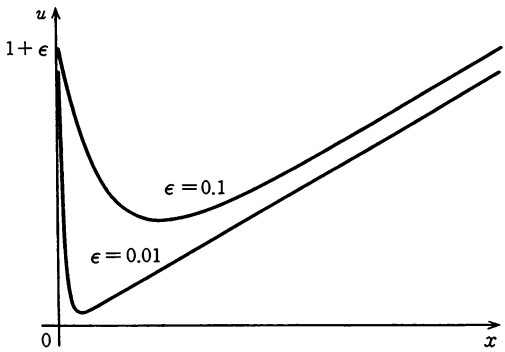


FIGURE 1.1. The coexistence of two spatial scales in a transition layer

Let us rewrite (1.41) in terms of a stretched scale $\tilde{x} = x/\epsilon$:

$$\tilde{u}(\tilde{x}, \epsilon) = e^{-\tilde{x}} + \epsilon\tilde{x} + \epsilon, \qquad 0 \le \tilde{x} \le \frac{1}{\epsilon}. \tag{1.43}$$

For each fixed $\tilde{x}$, passing to the limit as $\epsilon \to 0$ (inner limit), one obtains

$$\tilde{g}(\tilde{x}) = e^{-\tilde{x}}. \tag{1.44}$$

This function $\tilde{g}$ is a uniform approximation of $\tilde{u}$ on the interval $0 \le \tilde{x} \le \tilde{x}_0$ for an arbitrarily fixed constant $\tilde{x}_0 > 0$. It is not, however, a uniform approximation on the entire stretched region $0 \le \tilde{x} \le 1/\epsilon$. In fact, when $\tilde{x}$ is $O(1/\epsilon)$, the term $\epsilon\tilde{x}$ becomes $O(1)$, and hence cannot be neglected. Both the outer limit and the inner limit, by themselves, do not give an approximation uniformly valid on the entire region of relevance, but the sum of the two, $f(x)+\tilde{g}(x/\epsilon) = x+e^{-x/\epsilon}$, is an approximation uniformly valid on the entire region. When several scales coexist, the procedure in which the scales are first separated (outer limit and inner limit) and then unified to construct an approximation uniformly valid on the entire region, such as the method of matched asymptotic expansions, prevails in singular perturbation theories.

**1.2.2. Internal Layer in a Bistable System.** Let us examine how transition layers appear in a concrete system of differential equations. We consider the following parabolic equation:

$$u_t = \epsilon^2 u_{xx} + f(u, x) \qquad -1 < x < 1, \quad t > 0, \tag{1.45}$$

where $\epsilon$ is a sufficiently small positive number. As boundary conditions, the Neumann boundary conditions

$$u_x(-1,t) = 0 = u_x(1,t) \tag{1.46}$$

are imposed. The nonlinearity $f$ is of the form

$$f(u,x) = u(1-u)(u-a(x)), \tag{1.47}$$

in which $a(x)$ is a smooth function satisfying the conditions

$$a(0) = \frac{1}{2}, \quad a_x(0) \neq 0, \qquad 0 < a(x) < 1, \quad x \in [-1,1]. \tag{1.48}$$

As a typical example of $a(x)$, one may think of a strictly monotone function which assumes the value $1/2$ at $x = 0$. The system (1.45) with the nonlinearity defined by (1.47) is said to be of **bistable type**, because for each fixed $x$ the ordinary differential equation obtained by setting $\epsilon = 0$ has two stable equilibria, $u = 0$ and $u = 1$, and solutions tend either to 1 or to 0 according as the initial value is greater than or less than $a(x)$. The value $a(x)$ here plays the role of a separatrix.

REMARK 1.2. If $J(x)$ is defined by $J(x) \equiv \int_0^1 f(u,x)du$, then thanks to (1.48) it satisfies

$$J(0) = 0, \qquad \frac{d}{dx}J(x)\Big|_{x=0} \neq 0. \tag{1.49}$$

In the following we consider only the case where a single transition layer appears. There are several methods to show the existence and the stability of transition layer solutions for (1.45), such as the comparison methods and the method of matched asymptotic expansions. We follow here the Hale-Sakamoto method [**170**], which utilizes a sort of Lyapunov-Schmidt reduction and hence explicitly brings out the slow degree of freedom in the problem.

THEOREM 1.3. *There exist an $\epsilon_0 > 0$ and two families of single layer solutions $u_j(x,\epsilon)$ of (1.45), $j = 0,1$, $0 < \epsilon \leq \epsilon_0$, enjoying the following properties.*

(i) *For an arbitrarily fixed $\delta > 0$,*

$$\lim_{\epsilon \to 0} u_j(x,\epsilon) = j \qquad \textit{uniformly on } [-1,-\delta], \tag{1.50}$$

$$\lim_{\epsilon \to 0} u_j(x,\epsilon) = 1-j \qquad \textit{uniformly on } [\delta,1]. \tag{1.51}$$

(ii) *Moreover, the solution $u_j(x,\epsilon)$ is asymptotically stable (resp. unstable) if*

$$(-1)^j \frac{d}{dx} u_j(0,\epsilon) \cdot \frac{d}{dx} J(0) > \ (resp. <)\ 0. \tag{1.52}$$

*When the solution is unstable, the dimension of the unstable manifold is one.*

### (I) Construction of Approximate Solutions

There are two issues to be dealt with in constructing internal layer solutions:

(i) Where does the transition layer appear?
(ii) How does the thickness of the transition layer depend on $\epsilon$ ?

Issue (i), in general, has to do with the geometry of a global free boundary problem, and issue (ii) is related to the balance among the different terms contained in the equation. Since transition layers, by definition, connect two different states to each other, it is first of all necessary to identify what these two states are. This is called the **outer problem**, which is obtained from the original system by setting the singular perturbation parameter $\epsilon = 0$. In the stationary problem for (1.45), it is given by the algebraic equation

$$f(u,x) = 0. \tag{1.53}$$

The problem (1.53) has three kinds of solutions $u = 0, 1, a(x)$, and hence there is a freedom of choice as to which two of them have to be selected. Hereafter, we choose 0 and 1, which are locally stable with respect to the ordinary differential equation (in fact, they are locally stable with respect to the partial differential equation (1.45), too), and try to construct transition layers which connect these two states.

In general, the solutions of the outer problem (1.53) do not satisfy the boundary conditions. It is known that boundary layers in fluid dynamics appear so as to bridge the gap between the boundary values of the outer solutions and the imposed boundary conditions. In the above example, since we have chosen the constant functions as the outer solutions, the Neumann boundary conditions happen to be satisfied.

Let us return to the two issues raised at the beginning. We first deal with issue (ii), in which the determination of an appropriate scale is demanded. Let the transition layer be located at $x = x_0$ and have thickness $O(\epsilon^\alpha)$, where $\alpha > 0$ is an unknown exponent. In order to

study the asymptotic form of the transition layer, let us introduce a *stretched coordinate* $y$ by

$$y = \frac{x - x_0}{\epsilon^\alpha}. \tag{1.54}$$

In terms of the new function $z(y, \epsilon) = u(x_0 + \epsilon^\alpha y, \epsilon)$, the stationary problem is given by

$$\epsilon^{2(1-\alpha)} \ddot{z} + f(z, x_0 + \epsilon^\alpha y) = 0, \tag{1.55}$$

$$\dot{z}\left(\frac{\pm 1 - x_0}{\epsilon^\alpha}, \epsilon\right) = 0, \tag{1.56}$$

where $\dot{} = d/dy$.

Since the transition layer is expected to connect 0 to 1, the exponent $\alpha$ and the location $x_0$ have to be determined so that the equation (1.55) has a bounded solution connecting 0 to 1 in the limit as $\epsilon \to 0$. If $\alpha \neq 1$, only one of the two terms on the left hand side of (1.55) survives in the limit as $\epsilon \to 0$. Regardless of the choice of $x_0$, neither term meets our requirement. Therefore, $\alpha = 1$ should be the only candidate. In this way, the term which survives in the limit as $\epsilon \to 0$ is closely related to the exponent $\alpha$. Since (1.55) has only two terms, the exponent is determined uniquely. In general, however, the exponent could take various values, depending on which terms out of several choices one wants to retain. According to the different values for the exponent, the limit as $\epsilon \to 0$ in the equation has different **distinguished limits**. We will again encounter such examples in CHAPTER 5.

We next determine the location of the transition layer. The following result is the key for this purpose, and is obtained from a two-dimensional phase plane analysis.

PROPOSITION 1.4. *For each fixed constant $a \in (0, 1)$, consider the equation*

$$\ddot{z} + f(z, a) = 0.$$

*The following statements hold (see* FIGURE 1.2*).*

(i) **Heteroclinic Orbit**

*The necessary and sufficient condition for the existence of a solution satisfying $z(-\infty) = 0$, $z(+\infty) = 1$ (resp. $z(-\infty) = 1$, $z(+\infty) = 0$) is $a = 1/2$. The solution is monotone increasing (resp. decreasing) in $y$, and its orbit is unique and is called a heteroclinic orbit connecting 0 and 1.*

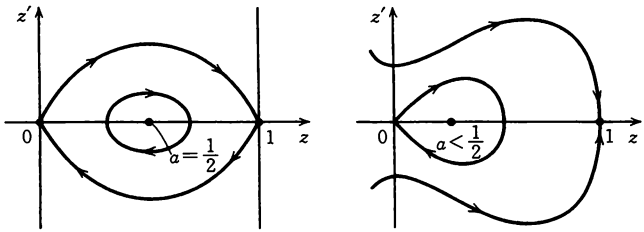


Heteroclinic orbit (a) Homoclinic orbit (b)

FIGURE 1.2. Heteroclinic and homoclinic orbits in a bistable system.

(ii) **Homoclinic Orbit**

*The necessary and sufficient condition for the existence of a solution satisfying* $z(\pm\infty) = 0$ *(resp.* $z(\pm\infty) = 1$*) is* $0 < a < 1/2$ *(resp.* $1/2 < a < 1$*). The orbit of the solution exists uniquely for each fixed* $a$*, and is called an orbit homoclinic to* 0 *(resp.* 1*).*

REMARK 1.5. The condition for the existence of the heteroclinic orbit is expressed as

$$J(a) = 0$$

in terms of $J$ defined in REMARK 1.2. In fact, this equation holds only when $a = 1/2$.

For the limit problem $\ddot{z} + f(z, x_0) = 0$ of (1.55) with $\alpha = 1$, the solutions which satisfy the boundary conditions

$$z(\mp\infty) = 0, \qquad z(\pm\infty) = 1 \tag{1.57}$$

exist only when $x_0 = 0$, because of the conditions in (1.48). This gives an answer to issue (i) raised at the beginning. Namely, the location where the limit problem, defined on $\mathbb{R}$ by introducing the stretched coordinate, has heteroclinic orbits connecting two outer solutions becomes a candidate where a transition layer may appear. This statement is universal, and in fact, heteroclinic orbits are a fundamental ingredient in various interfacial patterns in which transition layers are involved (compare CHAPTER 4).

When $\alpha = 1$ and $x_0 = 0$, the stationary problem is given by

$$\ddot{z} + f(z, \epsilon y) = 0, \tag{1.58}$$

$$\dot{z}\left(\pm\frac{1}{\epsilon}, \epsilon\right) = 0. \tag{1.59}$$

We look for the **inner solution**, which determines the shape of the transition layer, in the following form:

$$z(y, \epsilon) = z_0(y) + \epsilon z_1(y) + O(\epsilon^2). \tag{1.60}$$

Substituting this into (1.58), and equating to zero the coefficient of each power of $\epsilon$, one obtains a series of differential equations. The first two of the series are

$$\ddot{z}_0 + f(z_0, 0) = 0, \tag{1.61}$$

$$\ddot{z}_1 + f_u(z_0(y), 0)z_1 + f_x(z_0(y), 0)y = 0. \tag{1.62}$$

In the sequel, we confine ourselves to the boundary conditions

$$z_0(-\infty) = 0, \quad z_0(+\infty) = 1, \tag{1.63}$$

$$z_1(\pm\infty) = 0, \tag{1.64}$$

which correspond to the transition layer connecting 0 and 1.

As we mentioned, the heteroclinic solution satisfying (1.61) and (1.63) exists uniquely up to phase shifts. We denote by $z_0(y; \gamma)$ the solution satisfying $z_0(0; \gamma) = \gamma$. The constant $\gamma$, unknown at this stage, is uniquely determined later by the solvability condition for $z_1$. The equation (1.62) is a linear inhomogeneous equation. The associated homogeneous equation

$$\ddot{z}_1 + f_u(z_0(y; \gamma), 0)z_1 = 0$$

has a solution $\dot{z}_0(y; \gamma)$ bounded on $\mathbb{R}$, as is easily seen by differentiating (1.61) with respect to $y$. It can in fact be verified that, except for constant multiples of $\dot{z}_0(y; \gamma)$, such a solution does not exist. In this situation, the equation (1.62) has solutions which are bounded on $\mathbb{R}$ if and only if

$$\int_{-\infty}^{+\infty} \dot{z}_0(y; \gamma) f_x(z_0(y; \gamma), 0) y dy = 0. \tag{1.65}$$

(For details, see [**74**], Chapter 11.) This is an example of the **Fredholm Alternative Theorem**. The condition (1.65) uniquely determines $\gamma$. In fact, since

$$C_0(\gamma) := \int_{-\infty}^{+\infty} \dot{z}_0(y;\gamma) f_x(z_0(y;\gamma),0) y dy$$
$$= \int_0^1 f_x(u,0)\left(\int_\gamma^u \left[-2F(v)\right]^{-1/2} dv\right) du,$$

where $F(u) = \int_0^u f(s,0)ds$, (1.49) implies

$$\frac{d}{d\gamma} C_0(\gamma) = -\left[-2F(\gamma)\right]^{-1/2} J'(0) \neq 0,$$

showing the monotonicity of $C_0(\gamma)$. Moreover, since $|C_0(\gamma)| \to \infty$ as $\gamma \to 0, 1$, one can conclude that there exists a unique $\gamma \in (0,1)$ for which (1.65) is satisfied. With such a choice of $\gamma$, $z_0(y;\gamma)$ is simply denoted by $z_0(y)$. Since $z_0(y)$ decays exponentially to 0 and 1, respectively, as $y \to -\infty, +\infty$ and $\dot{z}_0(y)$ also decays exponentially to 0 as $y \to \pm\infty$, the solutions of (1.62), together with their derivatives, converge to 0 at an exponential rate.

In terms of $z_0$ and $z_1$ obtained above, we define the inner solution by

$$Z(y,\epsilon) = z_0(y) + \epsilon z_1(y). \tag{1.66}$$

Combining the outer and the inner solutions, we now construct an approximation which is valid on the entire interval $[-1,1]$. Since the effective regions of the outer and inner solutions are different, we introduce $C^\infty$-functions $\zeta_0$ and $\zeta_+$ satisfying

$$\zeta_0(x) = \begin{cases} 1, & |x| \leq 1/4, \\ 0, & |x| \geq 1/2, \end{cases} \qquad 0 \leq \zeta_0(x) \leq 1, \tag{1.67}$$

$$\zeta_+(x) = \begin{cases} 0, & x \in [-1,0], \\ 1 - \zeta_0(x), & x \in [0,1]. \end{cases} \tag{1.68}$$

The approximate solution is now defined as

$$U(x,\epsilon) = 0 + \zeta_0(x) Z(\frac{x}{\epsilon}, \epsilon) + 1 \cdot \zeta_+(x). \tag{1.69}$$

### (II) The Lyapunov-Schmidt Method and Stability

Based upon the approximate solution, we now outline how to construct the transition layer solution and how to determine its stability. Replacing the equilibrium solution $u$ of the original equation (1.45) by $U(y,\epsilon)+u$, the new variable $u$ is subject to the stationary problem

$$L^\epsilon u + G(\epsilon) + F(u,\epsilon) = 0, \tag{1.70}$$

where

$$L^\epsilon u \equiv \epsilon^2 \frac{d^2}{dx^2} u + f_u(U(x,\epsilon),x)u, \tag{1.71}$$

$$G(\epsilon)(x) \equiv \epsilon^2 \frac{d^2}{dx^2} U(x,\epsilon) + f(U(x,\epsilon),x), \tag{1.72}$$

$$F(u,\epsilon) \equiv f(U(x,\epsilon)+u,x) - f(U(x,\epsilon),x) - f_u(U(x,\epsilon),x)u. \tag{1.73}$$

The operator $L^\epsilon$ is obtained by linearizing the equation (1.45) around the approximate solution $U$, while $F$ is the nonlinear term containing quadratic and higher order terms. The quantity $G(\epsilon)$ measures how well $U$ approximates the transition layer solution, and tends to zero as $\epsilon \to 0$. If $L^\epsilon$ has an inverse which is bounded independently of small $\epsilon$, then, applying $(L^\epsilon)^{-1}$ on both side of (1.70), and solving the resulting equation by the method of successive approximation, one can find the solution $u$. However, since the linear operator $L^\epsilon$ has an (exactly one) eigenvalue $\lambda_1(\epsilon) = O(\epsilon)$ which tends to zero as $\epsilon \to 0$ (this will be described below), one cannot apply the above procedure for all small $\epsilon$. If we denote by $\varphi_1(x,\epsilon)$ the eigenfunction of $L^\epsilon$ corresponding to $\lambda_1(\epsilon)$, then it turns out that the one-dimensional space spanned by $\varphi_1$ is the space of the slow degree of freedom. If transition layers appear at $n$ locations in the solution, this space has dimension $n$ (see §5.4).

The essence of the Lyapunov-Schmidt method is to *reduce the original problem to a problem on the space of slow freedom.* This is done by decomposing the entire phase space into a space of slow freedom and its complementary space, solving the equation on the complementary space by the method of successive approximation. The resulting solution is then substituted into the equation on the space of slow freedom. Let us decompose the unknown as $u = \alpha\varphi_1 + v$, where $\alpha$ is a scalar and $v$ is orthogonal to $\varphi$, $\int_{-1}^{1} \varphi_1(x,\epsilon)v(x)dx = 0$. Substituting this expression into (1.70) and projecting the resulting equation

onto the two subspaces associated with the decomposition, one obtains the equation for $v$ and the equation on the span of $\varphi_1$. Since on the subspace for $v$ the linear operator $L^\epsilon$ is uniformly bounded, the equation for $v$ is solved for small $\alpha$, $\epsilon$ as $v = v^*(\alpha, \epsilon)$ with $v^*(0,0) = 0$. Substituting this solution into the equation on the span of $\varphi_1$, one obtains a reduced equation called a **bifurcation equation** for $(\alpha, \epsilon)$:

$$
\begin{aligned}
(1.74) \qquad B(\alpha,\epsilon) &= \lambda_1(\epsilon)\alpha \\
&+ \frac{1}{\|\varphi_1\|_{L^2}^2} \int_{-1}^{1} \varphi_1(x,\epsilon) \Big[ G(\epsilon)(x) \\
&\qquad + F\Big(\alpha\varphi_1(x,\epsilon) + v^*(\alpha,\epsilon)(x)\Big)\Big] dx \\
&= 0.
\end{aligned}
$$

In order for $U(x,\epsilon)$ to legitimately be called an approximation, its deviation $u$ from a genuine solution has to vanish as $\epsilon \to 0$. Namely, one needs to find the zero of (1.74) satisfying

$$
(1.75) \qquad \alpha = \alpha^*(\epsilon), \qquad \alpha^*(0) = 0.
$$

It is here that the degree of approximation $G(\epsilon)$ of the approximate solution $U(x,\epsilon)$ becomes important. If $G(\epsilon)$ is $O(\epsilon)$, then $v^* = O(\alpha^2 + \epsilon)$. Since $\lambda_1(\epsilon) = O(\epsilon)$, it is not straightforward to find a solution $\alpha^*(\epsilon)$ of (1.74) satisfying $\alpha^*(0) = 0$. This shows that the approximation $U(x,\epsilon)$ has to be accurate enough so that $G(\epsilon) = O(\epsilon^2)$ at least. For such $U$, it is possible to find a zero $\alpha^*(\epsilon)$ of (1.74) that satisfies (1.75). This is the reason why we constructed the approximate solution up to the $O(\epsilon)$-order including the $z_1$-term in the inner solution in the above.

The stability of the solution can be determined by studying the spectral distribution of the linearization around the solution. For now we only give an intuitive meaning of (1.52). For the sake of simplicity, let us assume that $a(x)$ is monotone increasing: $\dfrac{d}{dx} J(0) < 0$. Under this situation, for the ordinary differential equation $u_t = f(u,x)$ with $x$ being a parameter, the basin of attraction in the interval $(0,1)$ of 1 is larger than that of 0 for $x < 0$, and the other way around for $x > 0$. Therefore, it is expected that the solution $u_1(x,\epsilon)$ which assumes values close to 1 for $x < 0$ and close to 0 for $x > 0$ will be stable, while the solution $u_0(x,\epsilon)$ which has the opposite behavior will be unstable. In fact, examination of the sign in (1.52) supports this expectation.

The approximate solution defined in (1.69) solves the stationary problem with an error of $O(\epsilon^2)$ in the following sense.

LEMMA 1.6.

$$\sup_{x\in[-1,1]} |G(\epsilon)(x)| = O(\epsilon^2), \qquad \epsilon \to 0. \tag{1.76}$$

PROOF. The functions $z_0$ and $z_1$, in terms of the stretched variable $y$, together with their derivatives up to the second order decay at an exponential rate for large $|y|$. By using this, the estimate in the lemma is readily verified. □

Decomposing the phase space into regular and singular parts according to the behavior of eigenvalues of $L^\epsilon$, and substituting the regular part into the singular part, the method of Lyapunov-Schmidt is to convert the original problem to an equation (corresponding to the slow degree of freedom) on the space of the singular part which has a substantially reduced degree of freedom. The eigenvalue corresponding to the singular part is the one that tends to zero (or to the imaginary axis, in general) as $\epsilon \to 0$, and it is characterized in the proposition below. Here we consider $L^\epsilon$ as $L^\epsilon : X \longmapsto Y$, where

$$X = \left\{ u \in C^2[-1,1] \;\middle|\; \frac{du}{dx}(\pm 1) = 0 \right\},$$
$$Y = C^0[-1,1],$$

and $X$ is equipped with the norm

$$|u|_{2,\epsilon} = |u|_0 + \epsilon \left|\frac{du}{dx}\right| + \epsilon^2 \left|\frac{d^2u}{dx^2}\right|.$$

The approximate solution $U(x,\epsilon)$ defined in (1.69) clearly belongs to the space $X$.

PROPOSITION 1.7. *There exists an $\epsilon_0 > 0$ such that the following statements hold.*

(i) *The principal eigenvalue $\lambda_1(\epsilon)$ of $L^\epsilon$ is real and simple, and it tends to zero as $\epsilon \to 0$ in the following manner:*

$$\lambda_1(\epsilon) = K_1\epsilon + o(\epsilon), \quad 0 < \epsilon \le \epsilon_0,$$
$$\text{with } K_1 = -J'(0) \Big/ \int_{-\infty}^{\infty} \dot{z}_0(t)^2 dt.$$

(ii) *The principal eigenfunction* $\phi_1(x,\epsilon)$ $(0 < \epsilon \le \epsilon_0)$ *corresponding to* $\lambda_1(\epsilon)$ *decays at an exponential rate. Namely, there exist positive constants* $C_1, C_2$ *such that*

$$|\phi_1(x,\epsilon)| \le C_1|\phi_1(0,\epsilon)|\exp\Big(-\frac{C_2}{\epsilon}|x|\Big), \quad |x| \le 1.$$

(iii) *Eigenvalues other than* $\lambda_1(\epsilon)$ *are all negative and bounded away from zero uniformly in* $\epsilon \in (0,\epsilon_0]$.

PROOF. We refer for the details of the proof to [**170**], and instead explain here why such an eigenvalue appears. The principal part $z_0(y)$ of the internal transition layer tells the source of the small eigenvalue which approaches zero together with $\epsilon$ (cf. (1.61)). In fact, rewriting $L^\epsilon$ in terms of the stretched coordinate $y$ and passing formally to the limit as $\epsilon \to 0$, one obtains

$$\tilde{L}^0\tilde{z} \equiv \ddot{\tilde{z}} + f_u(z_0(y),0)\tilde{z}. \tag{1.77}$$

By differentiating the equation (1.61) with respect to $y$, one finds that $\dot{z}_0$ satisfies the equation

$$\ddot{\tilde{z}} + f_u(z_0(y),0)\tilde{z} = 0. \tag{1.78}$$

This means that $\dot{z}_0$ is an eigenfunction of $\tilde{L}^0$ corresponding to the 0-eigenvalue. Since $\dot{z}_0$ is positive everywhere, 0 is a simple, principal eigenvalue of $\tilde{L}^0$. For sufficiently small $\epsilon > 0$, this eigenvalue is continued to an eigenvalue of $L^\epsilon$, that is precisely $\lambda_1(\epsilon)$. The exponential decay estimate in (ii) and the statement (iii) that the other eigenvalues are all bounded uniformly away from $\lambda_1(\epsilon)$ also follow from the fact that the 0-eigenvalue is simple and principal. The translations of $z_0(y)$ are also a solution of (1.69), and this fact in turn forced its linearization to have 0-eigenvalue. Therefore adding the 0-eigenfunction $\dot{z}_0$ to the transition layer solution is nearly equivalent to the translation of the transition layer solution. In this sense, it might be said that the fact that $L^\epsilon$ has an eigenvalue in an $O(\epsilon)$ neighborhood of the origin stems from the fact that the formal limit problem of the inner problem has a translational invariance. To show that $\lambda_1$ behaves like $K_1\epsilon$ as $\epsilon \to 0$, note first of all that $U_x$ satisfies the following:

$$\epsilon^2\frac{d^2}{dx^2}U_x + f_u(U,x)U_x + f_x(U,x) = O(\epsilon^2). \tag{1.79}$$

On the other hand, the pair $(\lambda_1,\phi_1)$, by definition, satisfies

$$\epsilon^2(\phi_1)_{xx} + f_u(U,x)\phi_1 = \lambda_1\phi_1. \tag{1.80}$$

Taking the $L^2$ inner product between $U_x$ and both sides of the last equation and integrating by parts, one obtains, with the help of (1.79), the following identity:

$$O(\epsilon^2) - \langle f_x(U,x), \phi_1 \rangle = \lambda_1 \langle \phi_1, U_x \rangle. \tag{1.81}$$

Because of the normalization $\|\phi_1\|_{L^2(-1,1)} = 1$, the following relations hold on arbitrary finite $y$-intervals:

$$\sqrt{\epsilon}\phi_1(\epsilon y) \sim \dot{z}_0(y), \tag{1.82}$$

$$\epsilon U_x(\epsilon y, \epsilon) \sim \dot{z}_0(y). \tag{1.83}$$

Thanks to these relations and REMARK1.2, (1.81) leads to the principal part $K_1\epsilon$ of $\lambda_1(\epsilon)$. □

With these preparations at our disposal, we apply the Lyapunov-Schmidt method to (1.70) to prove the existence and stability of the solution stated in THEOREM 1.3.

Based upon the characterization in LEMMA 1.7 of the eigenvalues of $L^\epsilon$, we first decompose the equation (1.70) into the direction of the principal eigenfunction $\phi_1$ and its orthogonal complement (the Lyapunov-Schmidt decomposition). Let $\phi_1$ be normalized so that $\phi_1(0,\epsilon) = \dot{z}_0(0)$, and define the orthogonal projection $E$ onto the span of $\phi_1$ by

$$Eu = \Big\langle u, \phi_1(\cdot,\epsilon) \Big\rangle \frac{\phi_1(\cdot,\epsilon)}{\|\phi_1(\cdot,\epsilon)\|^2_{L^2(-1,1)}}, \tag{1.84}$$

where $\langle \cdot, \cdot \rangle$ is the $L^2(-1,1)$ inner product. According to this projection, the spaces $X$ and $Y$ are decomposed as

$$X = \mathrm{span}\{\phi_1\} \oplus X_1, \qquad Y = \mathrm{span}\{\phi_1\} \oplus Y_1, \tag{1.85}$$

where $X_1$ and $Y_1$ are respectively the kernel of $E$ in $X$ and $Y$. They also satisfy $Y_1 = \mathcal{R}(L^\epsilon) = L^\epsilon X_1$, and $L^\epsilon : X_1 \to Y_1$ is an isomorphism. By decomposing $u$ as $u = \alpha\phi_1(x,\epsilon) + v$ ($\alpha \in \mathbb{R}$, $v \in X_1$), one finds that (1.70) is equivalent to

$$\begin{cases} L^\epsilon v + (I-E)\{G(\epsilon) + F(\alpha\phi_1(\epsilon) + v, \epsilon)\} = 0, \\ \\ \alpha\lambda_1(\epsilon)\phi_1(\epsilon) + E\{G(\epsilon) + F(\alpha\phi_1(\epsilon) + v, \epsilon)\} = 0. \end{cases} \tag{1.86}$$

Since $L^\epsilon : X_1 \to Y_1$ is an isomorphism, the equation $L^\epsilon v = p$ for $p \in Y_1$ is uniquely solvable, and its solution $v(p)$ satisfies

$$|v(p)|_{2,\epsilon} \le C|p|_0, \tag{1.87}$$

where $C > 0$ is a constant independent of $\epsilon \in (0, \epsilon_0]$. Applying this to the first equation of (1.86), we obtain the following lemma.

LEMMA 1.8. *The first equation in* (1.86) *is uniquely solvable in* $v$ *as* $v = v^*(\alpha, \epsilon)$ *in a neighborhood of* $(\alpha, \epsilon) = (0, 0)$. *The solution depends smoothly on* $\alpha$ *and satisfies* $|v^*(\alpha, \epsilon)| = O(\alpha^2 + \epsilon^2)$ *as* $\epsilon + |\alpha| \to 0$.

By using this result in the second equation of (1.86), it becomes

$$\alpha\lambda_1(\epsilon)\phi_1(\epsilon) + E\{G(\epsilon) + F(\alpha\phi_1(\epsilon) + v^*(\alpha, \epsilon), \epsilon)\} = 0, \tag{1.88}$$

which, upon taking the $L^2$ inner product with $\phi_1(\epsilon)$ and using LEMMAS 1.6 and 1.8, is equivalent to finding a zero of the function

$$B(\alpha, \epsilon) = K_1\epsilon\alpha + \tau_0\alpha^2 + \text{h.o.t.} \tag{1.89}$$

The constant $\tau_0$ is determined by the nonlinearity. Note that the contribution from $EG(\epsilon)$ is of order $O(\epsilon^{5/2})$, owing to LEMMA 1.6 and the normalization $\|\phi_1\|_{L^2(-1,1)} = 1$. By using the implicit function theorem, the unique solution $\alpha = \alpha^*(\epsilon)$ of $B(\alpha, \epsilon) = 0$ in $|\alpha| < c_0$, $\epsilon \in (0, \epsilon_0]$ is given by

$$\alpha^*(\epsilon) = -\frac{\tau_0}{K_1}\epsilon + o(\epsilon), \qquad \epsilon \to 0. \tag{1.90}$$

Therefore the family of equilibrium solutions $u_0$ in THEOREM 1.3 is give by

$$u_0(x, \epsilon) = \alpha^*(\epsilon)\phi_1(x, \epsilon) + v^*(\alpha^*(\epsilon), \epsilon)(x) + U(x, \epsilon).$$

Recalling the definition of $U$, $|\alpha^*(\epsilon)| = O(\epsilon)$, and $|v^*(\alpha^*(\epsilon), \epsilon)|_{2,\epsilon} = O(\epsilon^2)$, one can readily show that

$$|u_0(\cdot, \epsilon) - U(\cdot, \epsilon)|_{2,\epsilon} = O(\epsilon), \qquad \epsilon \to 0. \tag{1.91}$$

Property (i) of THEOREM 1.3 follows immediately from the construction of $U$. It is also verified, by the same method as we used for PROPOSITION 1.7, that the following result holds.

PROPOSITION 1.9. *The principal eigenvalue* $\lambda_1^*(\epsilon)$ *of the operator*

$$\mathcal{L}^\epsilon \equiv \epsilon^2 \frac{d^2}{dx^2} + f_u(u_0(x, \epsilon), x) : X \to Y,$$

*which is obtained by linearizing* (1.45) *around the solution* $u_0(x, \epsilon)$, *satisfies*

$$\lambda_1^*(\epsilon) = K_1\epsilon + o(\epsilon), \qquad \epsilon \to 0, \tag{1.92}$$

*where the constant* $K_1$ *is the same as in* PROPOSITION 1.7.

The stability of $u_0$ is determined by the sign of $\lambda_1^*$, and hence by the sign of $K_1$. The sign of $K_1$, on the other hand, is determined by the sign of $J'(0)$. Property (ii) of THEOREM 1.3 for the stability of $u_0$ follows.

REMARK 1.10. The solution $u_0$ has a transition layer which connects 0 to 1. One can also construct a solution, say $u_1(x,\epsilon)$, which has a transition layer connecting 1 to 0. The stability of $u_1$ is judged by the sign of $J'(0)$: it is asymptotically stable (resp. unstable) if $J'(0) >$ (resp. $<$) 0.

REMARK 1.11. When $J(x)$ has several simple zeros, one can prove the existence and the stability of solutions with multiple transition layers (cf. [**170**]). In such a situation, $n$ internal transition layers in a solution give rise to an $n$-dimensional space of slow degree of freedom. This topic will be treated again in CHAPTER 5.

## 1.3. Very Slow Motion Manifolds and Hyperbolicity

**1.3.1. Very Slow Motion.** The following is well known as the simplest non-conservative equation describing phase separation phenomena:

$$u_t = \epsilon^2 u_{xx} + f(u). \tag{1.93}$$

The nonlinearity $f$ is of bistable type, the same as that treated in §1.2:

$$f(u) = \frac{1}{2}u(1-u^2), \tag{1.94}$$

with the difference that the zeros of $f$ do not depend on $x$. The equation (1.93) is called a **scalar bistable reaction-diffusion equation** (or the Allen-Cahn equation). Let us introduce the functional

$$F(u) = \int_{\mathbb{R}} \left\{ \frac{\epsilon^2}{2}|u_x|^2 + W(u) \right\} dx \tag{1.95}$$

$$\text{with} \quad -W(u) \equiv \int_0^u f(s)ds.$$

The function $W$ is called a **double well potential** with two wells of equal depth at $u = \pm 1$. In terms of the functional, (1.93) is formally written as

$$u_t = -\frac{\delta F}{\delta u}.$$

When several interfaces (transition layers) are placed on $\mathbb{R}$, how do they move? Restricting ourselves to the case where there are two interfaces, let us derive heuristically the equation of motion for them. The nonlinearity (1.94) implies that the equation $\epsilon^2 U_{xx} + f(U) = 0$ has the solution with a single transition layer, given by

$$u(x,t) = \pm U(x) = \pm \tanh \frac{x}{2\epsilon}. \tag{1.96}$$

In (1.96), $U(x-\theta)$ is also a solution for each $\theta \in \mathbb{R}$. If the transition layers are located at $x = x_1, x_2$ $(> x_1)$, then the solution will be approximated by

$$\tilde{U}(x) = U(x-x_1) - U(x-x_2) - 1. \tag{1.97}$$

In fact, if $x_2 - x_1 \gg \epsilon$, then (1.97) satisfies the equation (1.93) within an error of the exponentially small order

$$O\left\{\exp\left(-\frac{x_2-x_1}{2\epsilon}\right)\right\}.$$

This remains true as long as $x_1$ and $x_2$ vary within the range where $x_2 - x_1 \gg \epsilon$. Namely, the set

$$\mathcal{W} = \{\tilde{U}(x) \mid x_2 - x_1 \gg \epsilon\} \tag{1.98}$$

is not an invariant manifold for (1.93) because of the exponentially small error, but it is extremely close to being invariant. It is here that a substantial amount of reduction in dynamical degrees of freedom is anticipated. In other words, it is expected that the solution of (1.93) with an initial value of the form (1.97) will move along (1.98) keeping its shape almost unchanged. And hence it will suffice to keep track of the motion of the points $x_1$ and $x_2$ (two-dimensional!), in order to describe the evolution of the solution. It may be said, therefore, that almost all of the dynamical information is concentrated on the transition layers. This is one of the most important points that result from the singular perturbation point of view.

Considering that $x_1, x_2$ depend on the time $t$, let us set

$$u(x,t) = \tilde{U}(x) + b(x,t) \tag{1.99}$$

with $b(x,t)$ being a sufficiently small correction term. Note here that $\tilde{U}(x)$ depends on $t$ through $x_1(t), x_2(t)$. Our goal, then, is to derive the principal part of the equations of motion for $x_1, x_2$ in a closed form. It must be derived from the requirement that (1.99) be a solution of (1.93), and in fact, it is determined by the solvability condition

for the following linearized equation:

$$-\dot{x}_1 U_1' + \dot{x}_2 U_2' + b_t = L^\epsilon b + f(\tilde{U}) - f(U_1) + f(U_2), \tag{1.100}$$

which is obtained by neglecting the quadratic and higher order terms in $b$. In (1.100), "$\dot{}$" $= \frac{d}{dt}$ and $'$ stands for differentiation with respect to the argument, $U_i = U(x - x_i)$, and $L^\epsilon$ is defined by

$$L^\epsilon \equiv \epsilon^2 \frac{d^2}{dx^2} + f'(\tilde{U}). \tag{1.101}$$

The equation of motion for $x_1$ is derived as follows. Since $1 + U_2$ is exponentially small near $x = x_1$, an approximation is possible in the form

$$f(\tilde{U}) - f(U_1) + f(U_2) \cong -3\epsilon(1 + U_2)U_1', \tag{1.102}$$

where $1 - U_1^2 = 2\epsilon U_1'$ is used. The operator $L^\epsilon$ is approximated by

$$L' = \epsilon^2 \frac{d^2}{dx^2} + f'(U_1), \tag{1.103}$$

which, when expressed in terms of $y = x/\epsilon$, agrees with the operator (1.77) in §1.2. The operator $L'$ has the 0-eigenvalue and the associated eigenfunction $\Phi = U_1'$, which originate from the translation invariance. It is known that $L'$ is a self-adjoint operator on $L^2(\mathbb{R})$ and that its 0-eigenvalue is simple. Therefore, the Fredholm alternative applies to (1.100) for solvability in $b$, and hence the inhomogeneous term in (1.100) has to be orthogonal to $U_1'$ in $L^2(\mathbb{R})$. Since $U_2'$ is exponentially small near $x = x_1$, the principal part of the orthogonality condition is given by

$$\dot{x}_1 \langle U_1', U_1' \rangle = -\langle U_1', f(\tilde{U}) - f(U_1) + f(U_2) \rangle, \tag{1.104}$$

where $\langle \cdot, \cdot \rangle$ is the $L^2(\mathbb{R})$ inner product. By using (1.96) and (1.102), both sides of (1.104) can be explicitly computed, giving rise to

$$\dot{x}_1 = 12\epsilon \exp\left[-\frac{x_2 - x_1}{\epsilon}\right].$$

Delegating the explicit computation to [**113**], for example, we now present an intuitive derivation of the result. By the definition of $U_1$, the value of $U_1'$ in an $\epsilon$-neighborhood of $x_1$ is $O(1/\epsilon)$, and it decays as fast as $\exp\left(-\frac{|x - x_1|}{2\epsilon}\right)$ outside of the neighborhood. By using only the first term in the expansion

$$1 + \tanh z = 2 \sum_{n=1}^{\infty} (-1)^{n+1} \exp(2nz),$$

the value of $1+U_2$ near $x_1$ is estimated to be $O\Big[\exp\Big(-\frac{|x_2-x_1|}{\epsilon}\Big)\Big]$. Therefore one obtains

$$\langle U_1', (1+U_2)U_1'\rangle \cong O\Big[\frac{1}{\epsilon}\exp\Big(-\frac{|x_2-x_1|}{\epsilon}\Big)\Big].$$

By using (1.102) and $\langle U_1', U_1'\rangle = O(1/\epsilon)$, one arrives at the desired order of estimate for $\dot{x}_1$. One can also apply the same method to compute $\dot{x}_2$, and one obtains $\dot{x}_2 = -\dot{x}_1$.

Summarizing, the dynamics of $(x_1, x_2)$ are governed by

$$\dot{x}_1 = 12\epsilon\exp\Big[-\frac{x_2-x_1}{\epsilon}\Big], \quad \dot{x}_2 = -12\epsilon\exp\Big[-\frac{x_2-x_1}{\epsilon}\Big]. \tag{1.105}$$

It is clearly read off from this that the motion of the transition layers is very slow and almost stationary. This is why such a motion is called a **very slow motion**. The force acting between $x_1$ and $x_2$ is **attractive**. The attractivity of the force suggests that two internal layers coalesce, leaving behind a nearly constant state 1 or $-1$. This is in accord with the fact that stable equilibrium solutions of (1.93) on a sufficiently large finite interval are identically equal to homogeneous states (cf. §4.2). In general, a process in which larger domains are created by the coalescence of several transition layers is called **coarsening**.

The very slow motion was first treated by the Japanese physicists Kawasaki and Ohta [**205**]. Its rigorous treatment on finite intervals with the Neumann boundary conditions was later carried out in [**58**], [**148**]. See also [**39**] and [**4**] for another treatment in terms of the energy estimates. These rigorous methods also apply to the Cahn-Hilliard equation (which is a conservative system), proving the existence of very slow motions for the one-dimensional case (cf. [**3**], for example). Moreover, the very slow motion of a single bubble and the dynamics of many bubbles were discussed in [**5**]; they yield a higher dimensional version of the transition layers. A similar result, but formal, was obtained in [**351**] for the Allen-Cahn equation with mass conservation.

The method, described above, in which the motion of interfaces is extracted by utilizing the difference of scales, applies not only to dissipative systems, but also to pulse interactions in equations of dispersive type, such as the KdV equation and the Benney equation. For the latter class of equations many interesting results have been obtained by using this approach. For example, the force acting between pulses is **repulsive** (cf. [**113**], [**84**]), contrary to the case above. The

mathematical proof of these results for the original equations, however, is a task yet to be done.

**1.3.2. Invariant Manifold and Normal Hyperbolicity.** The reason why we could derive the interface dynamics as above comes from the fact that the set $\mathcal{W}$ defined in (1.98), consisting of translations of internal layers, very well approximates solutions of (1.93). In fact, it is possible to construct, based on (1.93) as the 0-th approximation, an invariant manifold of (1.93) considered on the finite interval $[0,1]$. The invariant manifold is characterized by being **normally hyperbolic** for all sufficiently small $\epsilon$ including the limit as $\epsilon \to 0$, and we will show in the sequel, following [**147**], that such a characterization naturally enables us to construct the invariant manifold. In other words, such a viewpoint makes it possible to treat the construction of the manifold as a regular perturbation problem.

The normal hyperbolicity of an invariant manifold means that the dynamics in the tangential direction is dominant over that in the normal direction. That is to say, the dynamics in the tangential direction is much slower than that in the normal direction. As we will explain shortly, this property is realized when the spectrum associated with the normal component of the linearized operator around the invariant manifold is separated by a distance from the imaginary axis. Therefore, the notion is a natural extention of hyperbolicity for equilibrium points and periodic orbits of ordinary differential equations. From now on, (1.93) is considered on $[0,1]$ with the Neumann boundary conditions

$$u_x(0,t) = u_x(1,t) = 0.$$

In order to treat the case where there are $N$ transition layers, we introduce some terminology. For sufficiently small $\rho > 0$, let the set $\Gamma_\rho \subset \mathbb{R}$ be defined as the collection of vectors $\xi = (\xi_1, \dots, \xi_N)$ with

$$\Gamma_\rho = \{\xi \in \mathbb{R}^N \mid 0 < \xi_1 < \dots < \xi_N < 1, \quad \xi_{i+1} - \xi_i > 2\rho, \ \ i = 0, \dots, N\}, \tag{1.106}$$

where $\xi_0 = -\xi_1$, $\xi_{N+1} = 2 - \xi_N$. This set is introduced in order to study the motion of interfaces in which the positions of the transition layers and boundary points are all separated by a fixed distance. Denoting $\eta_i = (\xi_{i+1} + \xi_i)/2$ $(i = 0, \dots, N)$, we define a function $u^\xi : [0,1] \to \mathbb{R}$ for each $\xi \in \Gamma_\rho$ by

$$u^\xi(x) = (-1)^{i+1} U(x - \xi_i), \quad x \in [\eta_{i-1}, \eta_i], \quad i = 1, \dots, N, \tag{1.107}$$

where $U$ is the function defined in (1.96). $u^\xi$ is a piecewise $C^1$ function which is obtained by gluing the function $U$ at each $\eta_i$. The collection of $u^\xi$ is an embedded submanifold of class $C^{1,1}$ in $L^2 = L^2(0,1)$. Let us define $\gamma = (\gamma_1, \dots, \gamma_N) : \Gamma_\rho \to \mathbb{R}^N$ by

(1.108)
$$\gamma_i(\xi) = 12\epsilon\left[\exp\left(-\frac{\xi_{i+1}-\xi_i}{\epsilon}\right) - \left(-\frac{\xi_i - \xi_{i-1}}{\epsilon}\right)\right], \quad i = 1, \dots, N.$$

Then we have

THEOREM 1.12 ([**147**]). *Fix a sufficiently small $\rho > 0$ and $N \geq 1$. For each $\epsilon > 0$ sufficiently small, there exist $\hat{u}^\xi \in W^{1,2}$ and $\hat{\gamma}(\xi) \in \mathbb{R}^N$ $(\xi \in \Gamma_\rho)$ such that the following statements hold.*

(i) *The mappings $\xi \to \hat{u}^\xi$ and $\xi \to \hat{\gamma}(\xi)$ are Lipschitz continuous.*

(ii) *The set $\hat{\mathcal{W}} = \{u \mid u = \hat{u}^\xi,\ \xi \in \Gamma_\rho\}$ is an invariant manifold* (**very slow motion manifold**) *of* (1.93) *in $W^{1,2}$.*

(iii) *The flow on $\hat{\mathcal{W}}$ is described by the system of ordinary differential equations $\dot{\xi} = \hat{\gamma}(\xi)$.*

(iv) *We have*

(1.109)
$$\|\hat{u}^\xi - u^\xi\|_{W^{1,2}} = O\left(\exp\left(-\frac{\delta^\xi}{\epsilon}\right)\right),$$

(1.110)
$$|\hat{\gamma}(\xi) - \gamma(\xi)| = O\left(\exp\left(-\frac{3\delta^\xi}{\epsilon}\right)\right),$$

*where $\delta^\xi$ is an arbitrary constant less than $\frac{1}{2}\min\{\xi_i - \xi_{i-1}\}$.*

COROLLARY 1.13. *The very slow motion manifold $\hat{\mathcal{W}}$ contains the unique equilibrium solution $u^{\overline{\xi}}$ of* (1.93). *The equilibrium $u^{\overline{\xi}}$ is hyperbolic (the spectrum of the linearization around it does not have points on the imaginary axis), and $\hat{\mathcal{W}}$ is an open set of the unstable manifold $W^u(u^{\overline{\xi}})$ of the equilibrium.*

The corollary is an immediate consequence of THEOREM 1.12. Although the content of THEOREM 1.12 explains the dynamics in the final stage of the phase separation process, it does not describe the process of **fast dynamics**, where the number of the transition layers changes through coalescence or collision against the boundary. It is, in general, very difficult to construct the invariant manifold which covers the overlapping regions of different scales, because it is not

clear what to take as the 0-th order approximation, and because the normal hyperbolicity breaks down.

**Proof of Theorem 1.12.** In order to avoid technical complications, let us consider only the case where $N = 1$. Our overall strategy is to derive the existence of $\hat{\mathcal{W}}$ from the **normal hyperbolicity** of an invariant manifold $\overline{\mathcal{W}}$ for a reference problem. We now explain what normal hyperbolicity means and give an idea of how to introduce a suitable coordinate system to construct $\hat{\mathcal{W}}$. The reference problem is the following:

$$\begin{cases} u_t = \epsilon^2 u_{xx} + f(u), \quad x \in (0,1), \\ u_x(0) = \phi_0(u), \quad u_x(1) = \phi_1(u), \end{cases} \tag{1.111}$$

where $\phi_i : W^{2,2} \to \mathbb{R}$ $(i = 0, 1)$ are smooth functionals satisfying

$$\phi_0(u^\xi) = u_x^\xi(0), \quad \phi_1(u^\xi) = u_x^\xi(1). \tag{1.112}$$

From the definition of $u^\xi$, we find that both $u_x^\xi(0)$ and $u_x^\xi(1)$ are of order $O(\exp(-\rho/\epsilon))$, and hence $\phi_0, \phi_1$ can be chosen to be globally $O(\exp(-\rho/\epsilon))$-bounded. Therefore, when $\epsilon \ll 1$, the problem (1.111) is considered as a good approximation of (1.93) with the Neumann boundary conditions. Moreover, since $N = 1$, the set $\overline{\mathcal{W}}$ consisting of the functions of the form (1.107) is actually an **invariant manifold** (in fact, a collection of equilibrium points) for (1.111).

It is therefore expected that there exists an invariant manifold $\hat{\mathcal{W}}$ of (1.93) near $\overline{\mathcal{W}}$ if the latter is in some sense nondegenerate up to the limit $\epsilon \to 0$. The normal hyperbolicity is nothing but a condition that assures such a nondegeneracy. In order to be more precise, in a tubular neighborhood $\overline{\mathcal{N}}$ of $\overline{\mathcal{W}}$ let us introduce the following coordinate system:

$$\begin{cases} u = u^\xi + v, \\ \langle v, u_\xi^\xi \rangle = 0, \end{cases} \tag{1.113}$$

where $u_\xi^\xi$ is the derivative of $u^\xi$ with respect to $\xi$. The coordinate system in (1.113) is equivalent to the introduction of the vector bundle $\mathcal{F} = \{\overline{F}^\xi\}$ with the fibre

$$\overline{F}^\xi = \{u \mid u \in L^2(0,1), \quad \langle u, u_\xi^\xi \rangle = 0\} \tag{1.114}$$

at the base point $u^\xi$ for each $\xi$. By the implicit function theorem, (1.113) gives a smooth coordinate transformation from the neighborhood $\overline{\mathcal{N}}$ to an open neighborhood of the 0-section of the vector bundle

$\mathcal{F}$. To express the invariant manifold $\hat{\mathcal{W}}$ as a graph over $\overline{\mathcal{W}}$ is nothing but choosing $\hat{v}^\xi$ and a $C^1$-function $\hat{\gamma}(\xi)$ such that $\hat{u}^\xi = u^\xi + \hat{v}^\xi$ satisfies

$$\text{(1.115)} \qquad \begin{cases} (u^\xi_\xi + \hat{v}^\xi_\xi)\hat{\gamma}(\xi) = \epsilon^2(u^\xi_{xx} + \hat{v}^\xi_{xx}) + f(u^\xi + \hat{v}^\xi), \\ \hat{v}^\xi_x = -u^\xi_x, \quad x = 0, 1, \\ \langle \hat{v}^\xi, u^\xi_\xi \rangle = 0. \end{cases}$$

The first equation represents the invariance condition that the value of the differential operator be parallel to the tangential direction. The quantities $\hat{v}^\xi$, $\hat{v}^\xi_x$, and $\hat{\gamma}(\xi)$ are expected to be sufficiently small for $\epsilon \ll 1$, and hence, as the first approximation of $(\hat{\gamma}(\xi), \hat{v}^\xi)$, the solution $(c(\xi), v^\xi)$ of the following linear approximation of (1.115) will be adequate:

$$\text{(1.116)} \qquad \begin{cases} u^\xi_\xi c(\xi) = \epsilon^2 v^\xi_{xx} + f'(u^\xi)v^\xi, \\ v^\xi_x = -u^\xi_x, \quad x = 0, 1, \\ \langle v^\xi, u^\xi_\xi \rangle = 0. \end{cases}$$

The equation (1.116) can indeed be solved, and its solution $c(\xi)$ gives the principal part of the very slow motion.

PROPOSITION 1.14 ([**148**]). *Assume that $f \in C^3$ and fix a sufficiently small $\rho > 0$. Then, there exists an $\overline{\epsilon} > 0$ independent of $\xi \in \Gamma_\rho$ such that* (1.116) *has a unique solution $(c(\xi), v^\xi)$ for $0 < \epsilon \le \overline{\epsilon}$. The function $c(\xi)$ is of $C^2$-class and $p^\xi = u^\xi + v^\xi$ is of $C^2$-class as a mapping $\Gamma_\rho \to W^{2,2}$. Moreover, $c(\xi)$ satisfies the following estimate:*

$$\text{(1.117)} \qquad c(\xi) = \gamma(\xi)\Big(1 + O\Big(-\frac{\gamma}{\epsilon}\delta^\xi\Big)\Big), \quad \xi \in \Gamma_\rho$$

*(the $\gamma(\xi)$ here is obtained by setting $N = 1$ in* (1.108)*), where $\delta^\xi$ is an arbitrary constant satisfying $\delta^\xi < \min\{\xi, 1 - \xi\}$ (note that $\xi \in (0, 1)$ since $N = 1$).*

In order to construct the restriction of the linear differential operator to the direction normal to $\overline{\mathcal{W}}$, let us define the projections $\overline{P}^\xi$, $\overline{Q}^\xi$ $(\xi \in \Gamma_\rho)$ by

$$\text{(1.118)} \qquad \overline{P}^\xi \phi = \frac{\langle \phi, u^\xi_\xi \rangle}{\langle u^\xi_\xi, u^\xi_\xi \rangle} u^\xi_\xi, \qquad \overline{Q}^\xi = I - \overline{P}^\xi.$$

The following holds (see [3], [282], or [58] for proof).

PROPOSITION 1.15. *Fix a sufficiently small $\rho > 0$. For each $\xi \in \Gamma_\rho$ and $\phi \in C^2[0,1] \cap \overline{F}^\xi$ with $\phi_x = 0$, $x = 0, 1$, define $\overline{A}^\xi$ by*

$$\overline{A}^\xi \phi = \overline{Q}^\xi \left( \epsilon^2 \phi_{xx} + f'(u^\xi)\phi \right). \tag{1.119}$$

*Then $\overline{A}^\xi$ can be extended to a self-adjoint operator on $\overline{F}^\xi = \overline{Q}^\xi L^2(0,1)$, and its spectrum satisfies*

$$\operatorname{spectr} \overline{A}^\xi \leq -c, \tag{1.120}$$

*where the constant $c > 0$ is independent of $\epsilon$ and $\xi$.*

That $\overline{\mathcal{W}}$ is **normally hyperbolic** actually means that the inequality (1.120) holds uniformly in $\epsilon$. As mentioned earlier, $\overline{\mathcal{W}}$ is an invariant manifold for (1.111), and in fact it is a collection of equilibrium points; hence the vector field on it is identically zero. They are considered as the 0-th approximation to the genuine invariant manifold $\hat{\mathcal{W}}$ of (1.93) and the flow on it. If we simply want to show that the flow on the genuine invariant manifold is of order $O(\exp(-c/\epsilon))$, it suffices to compute its deviation from $\overline{\mathcal{W}}$. However, THEOREM 1.12 demands the estimate (1.109) of higher accuracy. In order to achieve the higher accuracy, we use an approximation one degree higher, namely, by using the solution $v^\xi$ in PROPOPSITION 1.14, we construct the manifold

$$\mathcal{W} = \{\, u \mid u = p^\xi = u^\xi + v^\xi, \quad \xi \in \Gamma_\rho \,\}, \tag{1.121}$$

and we search for $\hat{\mathcal{W}}$ as a perturbation from $\mathcal{W}$. Setting

$$\begin{cases} u = p^\xi + w, \\ \langle w, p^\xi_\xi \rangle = 0, \end{cases} \tag{1.122}$$

let us define the tubular neighborhood $\mathcal{N}$ of $\mathcal{W}$ and the vector bundle $\mathcal{F}$ as $\mathcal{F} = \{F^\xi, \xi \in \Gamma_\rho\}$, $F^\xi = \{w | w \in L^2(0,1),\ \langle w, p^\xi_\xi \rangle = 0\}$. We also define the projections $P^\xi, Q^\xi$ in the same way as in (1.118) with $p^\xi_\xi$ replacing $u^\xi_\xi$. Substituting $u = p^\xi + w$ into (1.93), one obtains the following set of equations for $(\xi, w)$:

$$\dot{\xi} = c(\xi)a(\xi, w) + b(\xi, w) \equiv \Theta(\xi, w), \tag{1.123}$$

$$w_t = A^\xi w + \Theta(\xi, w) K^\epsilon w + h(\xi, w), \tag{1.124}$$

where the detailed description of each term is omitted (see [147]). The equation (1.123) represents the principal part of the linear differential

operator along the direction tangential to $\mathcal{W}$, while (1.124) expresses that in the normal direction.

Proving the existence of $\hat{\mathcal{W}}$ by using the normal hyperbolicity of $A^\xi$ is outlined as follows. Let $\Sigma$ be the totality of sections of $\mathcal{F}$. We will show that finding $\hat{\mathcal{W}}$ is equivalent to finding a fixed point of a map $G : \Sigma \to \Sigma$, defined in terms of the equations (1.123) and (1.124). Namely, for each given $\sigma^\xi \in \Sigma$, (1.123) with $w$ replaced by $\sigma^\xi$ is first solved to give a solution $\xi(t)$. Substituting this $\xi(t)$ into (1.124), and solving the resulting equation, a solution $w^{\xi(t)}$ is obtained. The solution $w^{\xi(t)}$ is a section of $\mathcal{F}$, i.e., an element of $\Sigma$. It is the hyperbolicity of $A^\xi$, stated in PROPOSITION 1.15 with $u^\xi$ replaced by $p^\xi$, which guarantees that $w^{\xi(t)}$ is uniquely determined by $\sigma^\xi$ (which defines the map $G$) and that $G$ is a contraction mapping. By performing several estimates on $\hat{\sigma}^\xi \in \Sigma$ which correspond to the fixed point of $G$ and using (1.123), the very slow motion $\hat{\gamma}(\xi)$ of THEOREM 1.12 is obtained. □

## 1.4. Renormalization Group Method

Viewing things from asymptotic perspectives is, in a sense, regarded as a method to extract properties independent of details of the system, such as initial conditions and the specific form of nonlinearities. As we have so far described, good approximations that are valid over a sufficiently long time interval are naturally obtained by separating slow freedoms from fast ones and by taking a good look at the system through the coordinate suited to the separation. Such an approach is effective because the details fade out within the fast time scale and the asymptotically important portion of the dynamics can be well described by the slow scales alone. In other words, the information related to the initial conditions is almost completely forgotten in the long run, and only the universal aspects implicit in the system become manifest. For example, the front of waves on the surface of water in a pond, created by a thrown stone, depends critically on the details at the initial stage, such as the shape of the stone (see FIGURE 1.3). However, after a sufficiently long period of time and seen from a distance, regardless of the initial state, the front approaches a circular shape.

The idea of attentively picking up structures that emerge through coarse-graining of space-time, such as the above, and using those in characterizing the asymptotic behavior of a system, has recently attracted a great amount of attention. One representative of such ideas

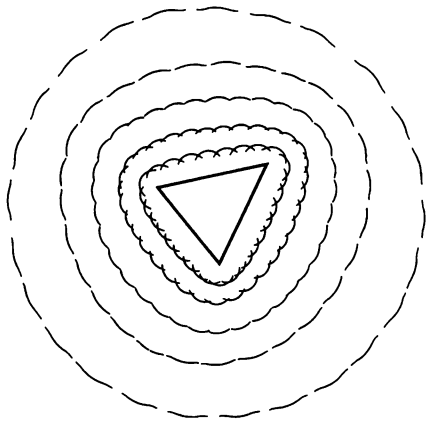

FIGURE 1.3. Waves in a pond. The front of the waves becomes circular after long periods of time.

is called the **renormalization method**. This method, originally developed in field theory and the theory of phase transition to cope with irregularities in critical exponents, has recently proven its effectiveness for various perturbation problems and asymptotic problems in a wide variety of nonlinear non-equilibrium systems, through the works of physicist Y. Oono and his collaborators (cf. [**64**], [**65**], [**299**], and [**157**]), and its further applications are promising.

Of particular interest in this method is the fact that it gives the same result as obtained by traditional methods, by just following a certain set of algorithms which do not require any a priori knowledge of the system to be analyzed. A mathematically rigorous justification of such algorithms remains to be done. Although what will be discussed below has a heuristic flavor, we introduce it as a prelude to the rigorous discussion to be presented later in CHAPTER 2.

Let us return to the secular term problem for the Duffing equation (1.1). Pretending that we do not have any particular knowledge about the system, let us construct local approximate solutions in the form (1.3). We introduce the amplitude $R_0$ and the phase $\Theta_0$ as undetermined constants, in order to accommodate arbitrary initial conditions at an arbitrary initial time $t_0$. Similarly to §1.1, we obtain the following by computing the first few terms in the power series

expansion of the solution:

$$x(t) = R_0 \cos(t + \Theta_0) + \epsilon\left\{ -\frac{3}{8} R_0^3 (t - t_0) \sin(t + \Theta_0) + \frac{1}{32} R_0^3 \Big( \cos 3(t + \Theta_0) - \cos(t + \Theta_0) \Big) \right\} + O(\epsilon^2), \tag{1.125}$$

where $R_0$ and $\Theta_0$ depend on $t_0$. Choosing $R_0$ and $\Theta_0$ adequately, one can make this expansion a good approximation of the solution near $t = t_0$.

However, the expansion breaks down at $t - t_0 = O(1/\epsilon)$. In order to make this expansion meaningful, let us introduce a parameter $\tau$, decompose $t - t_0$ as $(t - \tau) + (\tau - t_0)$, and try to integrate the terms containing $(\tau - t_0)$ into $R_0, \Theta_0$. That is to say, introducing the multiplicative renormalization constant $Z_1 = 1 + \sum_{n=1}^{\infty} a_n \epsilon^n$ and the additive renormalization constant $Z_2 = \sum_{n=1}^{\infty} b_n \epsilon^n$, we set

$$R_0(t_0) = Z_1(t_0, \tau) R(\tau), \tag{1.126}$$

$$\Theta_0(t_0) = \Theta(t_0) + Z_2(t_0, \tau), \tag{1.127}$$

where $a_n, b_n$ are functions of $(t_0, \tau)$, chosen so that the terms involving $(\tau - t_0)$ are eliminated in each power of $\epsilon$. Let us, for example, look at the first order term in $\epsilon$. Since the cosine in the first term on the right hand side of (1.125) is expanded as

$$\cos(t + \Theta_0) = \cos(t + \Theta) - b_1 \epsilon \sin(t + \Theta) + O(\epsilon^2),$$

by choosing $b_1$ as

$$b_1 = -\frac{3}{8} R^2 (\tau - t_0) \tag{1.128}$$

one can eliminate the term involving $(\tau - t_0)$ in the second term which originates from the secular term. If $a_1 = 0$, then $x(t)$ is expressed as

$$x(t) = R \cos(t + \Theta) - \frac{3}{8} \epsilon R^3 (t - \tau) \sin(t + \Theta) + \frac{\epsilon}{32} R^3 \Big( \cos 3(t + \Theta) - \cos(t + \Theta) \Big) + O(\epsilon^2). \tag{1.129}$$

Here $R, \Theta$ are functions of $\tau$. Since the parameter $\tau$ does not appear in the original problem, it should not be involved in the solution $x(t)$ either. Therefore, we must have

$$\frac{\partial x}{\partial \tau} = 0, \tag{1.130}$$

which is called the **renormalization group equation**. Upon differentiation with respect to $\tau$, (1.129) gives rise to

$$\begin{aligned}(1.131)\quad & \frac{dR}{d\tau}\cos(t+\Theta) - R\sin(t+\Theta)\frac{d\Theta}{d\tau} + \frac{8}{3}\epsilon R^3\sin(t+\Theta) \\ & - \frac{9}{8}\epsilon R^2\frac{dR}{d\tau}(t-\tau)\sin(t+\Theta) - \frac{3}{8}\epsilon R^3(t-\tau)\cos(t+\Theta)\frac{d\Theta}{d\tau} \\ & + \ldots + O(\epsilon^2) = 0.\end{aligned}$$

Since the last equation has to hold for each $t$, one obtains

$$(1.132)\qquad \begin{cases} \dfrac{dR}{d\tau} = O(\epsilon^2), \\ \dfrac{d\Theta}{d\tau} = \dfrac{3}{8}\epsilon R^2 + O(\epsilon^2). \end{cases}$$

Solving (1.132), setting $\tau = t$ (this is possible since $\tau$ was an arbitrary time parameter) in the solution, and substituting the resulting solution into (1.129), one obtains

$$(1.133)\qquad x(t) = R\cos\Big(t + \frac{3}{8}\epsilon R^2 t\Big) + O(\epsilon).$$

This is exactly the same as (1.22), which was derived by the averaging method. Although the line of computations described so far is formal in nature, it is amazing that one can arrive at the expression (1.133) only from the local approximation, without any prior knowledge about the solution or a specific scaling.

Since the renormalization group method discussed above seems a little mysterious and god-given, let us interpret it from another viewpoint by using the **envelope method** (which is implicitly contained in the series of papers by Oono and his collaborators cited before, but see [**232**] for the explicit presentation). This method not only gives another perspective to the renormalization group method, but also will be more naturally accepted by the reader who may not be familiar with the renormalization group method. Let the desired orbit be given by the solution $x^*(t)$. By choosing the local solution (1.125) at each $t = t_0$ appropriately, it may be possible to make it tangential to $x^*(t)$ at each $t = t_0$ (see FIGURE 1.4). Note that we regard $R_0, \Theta_0$ as a function of $t_0$, not as a mere parameter. From this viewpoint, as may be clear from FIGURE 1.4, the desired solution $x^*(t)$ is realized as the envelope of the $t_0$-parameter family of curves $x = F(t, t_0)$, where $F(t, t_0)$ stands for the right hand side of (1.125). In order to identify

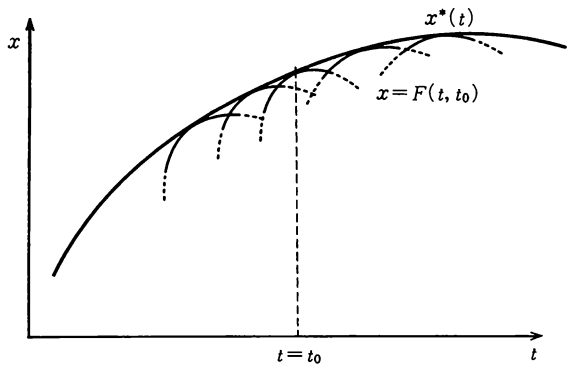


FIGURE 1.4. A global solution is obtained as an envelope of a family of local solutions.

the envelope we first solve

$$\frac{\partial F}{\partial t_0}(t,t_0)=0 \tag{1.134}$$

in $t_0$ as $t_0=t_0(t)$ (elimination of the parameter $t_0$). By using this we obtain the equation for the envelope: $x=F(t,t_0(t))$. However, we already know that the functional form of $t_0$ must be $t_0(t)=t$, because the $t_0$-parameter family of curves had been supposed to be tangential to the desired $x^*(t)$ at $t=t_0$. Thus the desired curve must be described by the equation $x=F(t,t)$.

This observation is very useful when one performs computations on (1.134). Since, as mentioned earlier, $R_0,\Theta_0$ are regarded as a function of $t_0$, the equation (1.134) takes a quite complicated form. If the condition $t=t_0$ is imposed, however, the secular terms disappear all together, giving rise to

$$\begin{cases} \dfrac{dR_0}{dt}=0+O(\epsilon^2), \\ \dfrac{d\Theta_0}{dt}=\dfrac{3}{8}\epsilon R_0^2+O(\epsilon^2). \end{cases} \tag{1.135}$$

This set of equations tells us how to choose the initial values $(R_0,\Theta_0)$ in accordance with the time $t$. Truncating the terms higher than $O(\epsilon)$ in (1.135), and solving it, it will be evident that one obtains the same solution as in (1.17), which is an effective approximation on time intervals of length $O(1/\epsilon)$.

An important point in this method is that only the trivial procedure of solving the equation (1.1) in a short interval around each initial moment $t = t_0$ is required, and that no preparations or techniques, such as rescaling of time or averaging, are necessary. But, this method does not always give an effective way of approximation.

Let us consider the following simple example[1]:

$$\frac{dA}{dt} = \epsilon A^2 - \epsilon^2 A. \tag{1.136}$$

Looking for the solution simply in the form

$$A = A_0 + \epsilon A_1 + \epsilon^2 A_2 + \dots, \tag{1.137}$$

and substituting this into (1.136), one obtains the first few terms:

(1.138)

$$A(t; t_0) = A_0 + \epsilon(t - t_0)A_0^2 + \epsilon^2\Big\{(t - t_0)^2 A_0^3 - (t - t_0)A_0\Big\} + O(\epsilon^3).$$

Secular terms appear on the right hand side. Applying the method above to this situation, we obtain

$$\begin{cases} A(t) = A_0(t) + O(\epsilon^2), \\ \dfrac{dA_0}{dt} = \epsilon A_0^2. \end{cases} \tag{1.139}$$

If this equation is an effective approximation of the original (1.136), then one arrives at the conclusion that the solution $A \equiv 0$ is an unstable equilibrium. But, this conclusion is wrong. What went wrong? Solving the equation (1.136) directly by using the method of separation of variables, one finds that $A(t)$ depends on $t$ only through the term $\epsilon^2(t - t_0)$. The expression (1.137) simply was a bad choice because the $O(\epsilon)$-term approximation was postulated in it. In this particular case, moreover, the existence of the nontrivial equilibrium $A \equiv \epsilon$ and its dependence on $\epsilon$ also make the above formal expansion ineffective.

In fact, it is natural from the form of the equation to set $A = \epsilon\tilde{A}$, and in terms of $\tau = \epsilon^2 t$, the equation (1.136) becomes equivalent to

$$\frac{d\tilde{A}}{d\tau} = -\tilde{A} + \tilde{A}^2. \tag{1.140}$$

The form of the last equation will prevent us from making a mistake like the above. There is another remark to be made. When one

[1]The following discussion is based upon suggestions provided by Shin-Ichiro Ei and Masataka Kuwamura.

intends to find a higher order approximation, for example, an approximation valid on the time scale of $O(\epsilon^{-2})$, by using the renormalization group method, one has to be careful, because the procedure is not simple compared with the case where the approximation valid on $O(\epsilon^{-1})$ time intervals was constructed for the Duffing equation. Indeed, the linear equation

$$\frac{d^2x}{dt^2} + \epsilon\frac{dx}{dt} + x = 0 \tag{1.141}$$

can be explicitly solved by quadrature, with the exact solution being

$$x(t) = Ae^{-\frac{\epsilon}{2}t}\cos\left(\sqrt{1-\frac{\epsilon^2}{2}}t + \theta\right), \tag{1.142}$$

where the constants $A, \theta$ are to be determined by initial conditions. The amplitude of the solution evidently varies with the time scale $O(\epsilon t)$, while the phase varies with the time scale $O(\epsilon^2 t)$. Even if one derives a renormalization group equation similar to (1.130) by formally constructing local approximate solutions of (1.141), it does not necessarily give rise to the desired system

$$\begin{cases} \dfrac{dR}{d\tau} = -\dfrac{\epsilon}{2}R, \\ \dfrac{d\Theta}{d\tau} = -\dfrac{1}{8}\epsilon^2, \end{cases} \tag{1.143}$$

in which $R$ and $\Theta$ stand for, respectively, the amplitude and the phase. Unless one is very careful to select the initial conditions in the construction of each approximate solution, (1.143) cannot be obtained (the reader is encouraged to try this). This example indicates that the nice feature of the renormalization group method (that is, the fact that a good approximation can be constructed without any prior knowledge of the behavior of the solution) seems to be lost.

The last example, although artificial and perhaps evil-minded, warns us that care must be exercised in dealing with more realistic problems (see a discussion in [**299**]). It is a future task to find out under what mathematical framework the formal algorithm automatically determines at least the correct principal part of the solution. At the same time, the development of this method in the future is expected to be fruitful, since the idea and the framework of the renormalization group method and its applicability are potentially much wider than explained here.

## 1.5. Summary

**1.1** The problem related to secular terms for the Duffing equation is solved by using a classical method and an averaging method. The meaning of slow freedom is clarified.

**1.2** The problem of determining the position and width of spatial internal layers is studied through an example of a scalar inhomogeneous second order equation of bistable type.

**1.3** The very slow motion, which evolves with an extremely slow time scale, is characterized as a motion on an invariant manifold by using the concept of normal hyperbolicity.

**1.4** The basic idea of the renormalization group method is explained through an example of nonlinear ordinary differential equations.

CHAPTER 2

# Amplitude Equations

When the system size is quite large compared with the scale of a phenomenon, it is usual, as an approximation, to study the system as defined on the infinite domain. This approximation allows us to be free from considering the effects caused by the presence of the boundary, and to use various tools such as the Fourier transform. For example, in fluid motion between two concentric cylinders, destabilization and pattern formation of various type in the velocity field have been treated mathematically as a problem in the region between two infinite cylinders (Taylor-Couette flow). Although such an approximation gives rise to a neat formulation of the problem, several difficulties arise in dealing with the extended system. Especially, the difficulty caused by the presence of continuous (or essential) spectra has long been a pending problem. In dealing with finite systems, destabilizations are detected by looking at the behavior of discrete spectra, and hence the gaps between eigenvalues allow us to invoke center manifold theory, reducing the problem essentially to a finite dimensional one.

In dealing with infinitely extended systems, such spectral gaps in general cease to exist, and hence a continuum of wave modes destabilize simultaneously, preventing us from using such reduction methods. The problem here is how to control the destabilization of infinitely many degrees of freedom. The physicists Newell, Whitehead, and Segal proposed a partial differential equation, called an **amplitude equation**, which is supposed to describe the original system quite well near the unstable points, and have performed various analyses (cf. [**277**] and references therein).

The best-known example is a nonlinear partial differential equation called the Ginzburg-Landau equation (GLE). This equation may be considered as a **universal equation which is effective near unstable points in extended systems**, because it is derived based solely upon the mechanism of destabilization, independently of the

original phenomenon and its model equation. This situation corresponds to the normal form classification of dynamics on center manifolds near bifurcation points in systems of finite size. The idea was generalized to deal with dynamic behaviors of finite amplitude solutions, and developed into the idea of the phase equation method of Kuramoto and his collaborators (cf. [**270**]).

In this chapter, we survey how the amplitude equation is derived, how well it approximates the original system, and what kind of dynamics it possesses. We also explain how effective the renormalization group method (described at the end of the last chapter) is in studying the properties of the amplitude equation.

## 2.1. Order Parameter

It is not feasible, nor necessarily meaningful, to describe every minute detail of various dynamic behaviors. What is it, then, that dominantly describes an overall picture of a given system? Naturally, one vaguely thinks of the following two things: (1) something that remains after short-lived transient behaviors, and (2) large structures that change slowly and emerge only after coarse-graining. In finite dimensional systems, (1) suggests that we should look at the dynamics on center manifolds, while a good example of (2) is a beat. In the latter, the important part is not the rapidly oscillating waves but the slow variation of the amplitude of their envelope. In both cases (1) and (2), it is easily seen that the difference in spatio-temporal scales is exploited. Generally speaking, an **order parameter** is a variable corresponding to the freedom which is scrutinized by using the difference in scales, and is believed to asymptotically characterize the system. In linear differential equations, it precisely corresponds to the eigenspace associated with the eigenvalues with nonnegative real part. In nonlinear problems, however, more sophisticated tools are necessary to identify an order parameter.

As in TABLE 2.1, order parameters are roughly classified into four categories. In dissipative systems, as long as the domain is finite, the associated spectrum is discrete and contains only a finite number of active eigenvalues with nonnegative real part. Therefore the center manifold theory is applicable to produce ODE (ordinary differential equations) describing the principal part of the dynamics, which is the amplitude equation. In case the system is far from equilibrium, although one cannot treat all the steps of analysis rigorously due to the largeness of the amplitude, it is agreed to some extent that the

TABLE 2.1. Four categories of order parameter.

| Spectrum | Degree of non-equilibrium | |
|---|---|---|
| | Near bifurcation point | Far from equilibrium state |
| Discrete (Finite domain) | Amplitude equation (ODE) Center manifolds | Finite amplitude solution and its stability, Global analysis of multiple bifurcation point |
| Continuous (Infinite domains) | Amplitude equation (PDE) | Phase equation, Envelope equation, Slowly modulated pattern |

situation can in principle be understood by unfolding singularities and clarifying the global behavior of bifurcating branches as well as their connections. However, if the size of the system is large (large aspect ratio) compared with the typical size of the phenomenon (for example, the period of a periodic pattern), the system is often regarded as an infinitely extended system. As such, the destabilization of the system is related in general to a continuum of spectra. Therefore the center manifold theory is not applicable, and one has to come up with a new idea of reduction method to approximate the system.

In order to do so, it is necessary to return to the original phenomenon. In fluid systems, especially in the Bénard convection and the Taylor-Couette flow, periodic structures are often observed and in many situations the variation of the wave numbers evolves slowly. Newell, Whitehead and Segal, assuming that the amplitude part of the fundamental periodic structure depends only on substantially slower spatio-temporal scales, and using it as a necessary condition, derived an equation that the amplitude has to satisfy. This equation for the Bénard convection is called the Newell-Whitehead equation and has the following form (cf. [**270**] for details):

$$\frac{\partial W}{\partial t} = \mu\lambda_1 W + D\left(\frac{\partial}{\partial x} - \frac{i}{2k_c}\frac{\partial^2}{\partial y^2}\right)^2 W - g|W|^2 W.$$

This equation, although a PDE (partial differential equation), is of substantially reduced form compared with the original Bénard system (a coupled system of the Navier-Stokes equation and an equation for temperature field). When the system is in a non-equilibrium state, namely, when it is far away from bifurcation points, it is no

longer possible to describe the dynamics in terms of the amplitude of linear unstable modes. However, even in such a case, the description in terms of phase equations is effective for systems which have certain basic structure and the fluctuation from it varies and propagates slowly. Namely, assuming that the basic structure is almost time-invariant and only the configuration of the structure is gradually changing in space-time, one tries to extract the equation which describes the variation of configuration. A well known equation which is derived by this kind of idea for oscillatory systems is the Kuramoto-Shivashinsky equation, to be treated in §2.4 (cf. [**270**] for details).

In the sequel, the Swift-Hohenberg equation, the simplest model equation describing convection phenomena, is studied. After deriving from it the Ginzburg-Landau equation (GLE) as an amplitude equation, we study the properties of the latter equation. We also give some discussion on how the GLE, as a normal form, approximates the original equation.

## 2.2. Derivation of Amplitude Equations

We will present the following three methods to formally derive amplitude equations:

(1) amplitude expansion method,
(2) spatio-temporal rescaling method,
(3) method exploiting symmetry.

We apply these methods to the Swift-Hohenberg equation (SHE), which describes the convection of fluid, to derive the Ginzburg-Landau equation (GLE).

**Amplitude Expansion Method**

The one-dimensional version of the SHE is the following fourth order one:

$$\frac{\partial u}{\partial t} = -\left(1 + \frac{\partial^2}{\partial x^2}\right)^2 u + \lambda u - u^3, \tag{2.1}$$

where $\lambda$ is a real parameter that stands for the intensity of convective instability. The trivial solution $u \equiv 0$ of (2.1) is unstable for $\lambda > 0$. This is seen from the linearization around $u \equiv 0$:

$$\frac{\partial v}{\partial t} = -\left(1 + \frac{\partial^2}{\partial x^2}\right)^2 v + \lambda v. \tag{2.2}$$

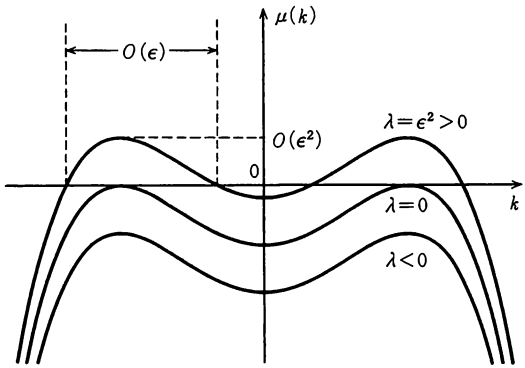


FIGURE 2.1. Destabilization of the trivial solution in the Swift-Hohenberg equation.

Setting $v = e^{\mu t + ikx}$, we find that $\mu(k) = -(1-k^2)^2 + \lambda$, which implies that $u \equiv 0$ is linearly unstable for $\lambda > 0$.

For more detail, we set $\lambda = \epsilon^2$ to find that destabilizations occur near $k_c^{\pm} = \pm 1$ in a band with an $O(\epsilon)$-width and $O(\epsilon^2)$-height (cf. FIGURE 2.1). For $k$ outside these bands, $\mu(k)$ is strictly negative. This means that after a period of time of length $O(1/\epsilon^2)$ the Fourier spectrum of the solution of (2.2) has its peaks only in an $O(\epsilon)$ neighborhood of the wave number $k_c^{\pm}$. Therefore, it is suggested that when $\lambda = \epsilon^2$ new spatio-temporal scales $T = \epsilon^2 t$, $X = \epsilon x$ are appropriate to observe unstable behaviors within an $O(1)$-scale. Speaking in terms of the original physical variables, the rescaling brings out variations over a spatially large region and slow variations in time.

Based on the discussion above, the following formal approximate solution naturally arises:

$$u_A(t,x) = \epsilon\Big\{A(T,X)e^{ix} + \overline{A}(T,X)e^{-ix}\Big\}, \tag{2.3}$$

where $A(T,X)$ is the $(T,X)$-dependent complex amplitude associated with the most unstable Fourier mode $e^{ix}$. Substituting this expression into (2.1) and equating the coefficients of $e^{ix}$ in the resulting equation, one finds that $A$ formally satisfies the GLE

$$\frac{\partial A}{\partial T} = 4\frac{\partial^2 A}{\partial X^2} + A - 3|A|^2 A. \tag{2.4}$$

Note that only slow variables appear as independent variables in this equation. As mentioned earlier, the GLE is a universal equation valid

near unstable points, while the specificity of the original equation is reflected in the coefficients of the GLE. When the instability is of oscillatory nature, the complex amplitude is called for, and different nonlinearities give rise to differences in the coefficients. However, the form of the GLE itself does not change.

**Rescaling Method**

In place of $u$, let us introduce a new dependent variable $v$ which depends on rescaled space-time variables:

$$u(t,x) = 2\epsilon \mathrm{Re}\Big(v(\epsilon^2 t, \epsilon x)e^{ix}\Big). \tag{2.5}$$

One can see in this expression that the independent variables are rescaled in accordance with the dispersion relation of the linearized equation (2.2). The difference from the amplitude expansion method is that the new dependent variable is introduced and the equation itself is rewritten. The transformation (2.5) will turn out to be very useful in dealing with front solutions of SHE by using infinite dimensional versions of center manifold theory, as well as in studying various solutions of other types. The equation for $v = v(T, X)$ is given by

$$\frac{\partial v}{\partial T} = \left(4\frac{\partial^2}{\partial X^2} + 1 - 4i\epsilon\frac{\partial^3}{\partial X^3} - \epsilon^2\frac{\partial^4}{\partial X^4}\right)v - 3v|v|^2 - e^{\frac{2iX}{\epsilon}}v^3. \tag{2.6}$$

When $\epsilon$ is small, $e^{\frac{2iX}{\epsilon}}$ acts as a highly oscillatory coefficient, and hence its contribution is expected to be very small as long as $v$ remains smooth. Therefore, passing formally to the limit as $\epsilon \to 0$ in (2.6), one obtains the GLE as in (2.4).

**Derivation by Using Symmetry**

We will show that the nonlinear term of the amplitude equation is determined by the symmetry of the original equation. We assume that the solution is approximated in the form of (2.3). The linear part of the equation for $A$ is easily shown to be $\frac{\partial A}{\partial T} = 4\frac{\partial^2 A}{\partial X^2} + A$ from the principal part near $k = \pm 1$ of the dispersion relation $\mu(k) = -(1-k^2)^2 + \lambda$ of the linearized problem. In order to determine nonlinearity, we distinguish the following two symmetries which our amplitude equation has to have:

(i) translational symmetry,
(ii) symmetry under conjugation.

The former symmetry is the invariance under $A \mapsto Ae^{i\psi}$ $(\forall \psi \in \mathbb{R})$, while the latter one corresponds to that under $A \mapsto \overline{A}$. Assuming

that the nonlinearity is a polynomial of $(A, \overline{A})$, one finds that all the quadratic nonlinearities $A^2$, $|A|^2$, and $\overline{A}^2$ do not have the translational invariance. Moreover, among the cubic nonlinearities, it is easily seen that only $|A|^2 A$ has the invariance. Therefore one concludes that the equation for $A$ with the lowest order nonlinearity is given by the GLE in (2.4), although the coefficient $-3$ cannot be determined by such a reasoning alone.

## 2.3. Validity of Amplitude Equation

Naturally, the first question to be asked is, when $A$ evolves according to (2.4), how well does the approximate solution $u_A$ in (2.3) approximate the solution $u$ of the original equation (2.1) with the same initial condition? An answer was first given for SHE by Collet and Eckmann ([**75**]), and then by van Harten ([**345**]) for more general scalar equations with quadratic nonlinearities. These results, roughly speaking, say that there exists $T_0 > 0$ such that $u_A$ approximates $u$ uniformly on $(t, x) \in [0, T_0/\epsilon^2] \times \mathbb{R}$ with an error of $O(\epsilon^2)$. The proof of these results is quite complicated. In order to see how the solutions of GLE approximate those of the original equation without touching technical difficulties, we adopt the following assumption:

**Assumption:** The nonlinearity is cubic or higher.

The SHE satisfies this assumption. The following method does not apply directly to equations with quadratic nonlinearity, such as the Kuramoto-Shivashinsky equation. For an extension of the method to such examples, the reader is referred to [**345**] and [**330**].

In order for the two solutions to be compared, they have to live in the same space. Denote by $C_b^m(\mathbb{R})$ the set of functions which are uniformly bounded on $\mathbb{R}$ together with their derivatives up to order $m$ inclusive. It is known for SHE and GLE that the solution with initial value in $C_b^4(\mathbb{R})$ uniquely exists for all $t > 0$ and is bounded in $C_b^4(\mathbb{R})$ (cf. [**76**]). The following theorem holds.

THEOREM 2.1 ([**218**]). *Let $A = A(T, X)$ be a solution of* GLE *and $u_A$ the formal approximate solution given in* (2.3).

*For each $T_0 > 0$ and $d > 0$, there exist constants $\epsilon_0, C > 0$ such that the following statement holds for $\epsilon \in (0, \epsilon_0)$: If $u = u(t, x)$ is the solution of* SHE *with the initial condition satisfying*

$$|u(0, x) - u_A(0, x)| \leq d\epsilon^2,$$

*then*

$$|u(t,x) - u_A(t,x)| < C\epsilon^2 \tag{2.7}$$

*for* $(t,x) \in (0, T_0/\epsilon^2] \times \mathbb{R}$.

PROOF. Our aim is to show that the error $u(t,x) - u_A(t,x)$ remains $O(\epsilon^2)$ for $t \le T_0/\epsilon^2$. However, the $u_A$ in (2.3), as it stands, is not appropriate for this purpose. Actually, the residue upon the substitution of this $u_A$ into SHE is $\epsilon^3 A^3 e^{3ix} + \text{c.c.}$ (where c.c. stands for the complex conjugate), which gives rise only to an error of $O(\epsilon)$ when integrated over $[0, T_0/\epsilon^2]$. Therefore, as an improved approximation, we adopt

$$v_A(t,x) = \epsilon A(T,X)e^{ix} - \epsilon^3 \frac{1}{64} A(T,X)^3 e^{3ix} + \text{c.c.} \tag{2.8}$$

The $O(\epsilon^3)$ terms in (2.8) are chosen so that the $O(\epsilon^3)$ terms in the residue cancel out as in (2.9) below. By using the notation $L_\lambda(\partial_x)u = -(1+\partial_x^2)^2 u + \lambda u$, one has

$$\begin{aligned} &- L_0(\partial_x)(B(\epsilon x)e^{nix}) \\ &= \Big[(1-n^2)^2 B + \epsilon 4in(1-n^2)B' + \epsilon^2(2-6n^2)B'' \\ &\qquad + \epsilon^3 4inB''' + \epsilon^4 B''''\Big] e^{nix}. \end{aligned}$$

Thanks to this, the residue $\rho$, when $v_A$ is substituted into SHE, is given by

$$\begin{aligned} &\rho(\epsilon,t,x) \\ &= \partial_t v_A - L_0 v_A - \epsilon^2 v_A + v_A^3 \\ &= \epsilon^3 \Big[(\partial_T A - 4\partial_X^2 A - A)e^{ix} - (1-3^2)^2 \frac{1}{64} A^3 e^{3ix} + \text{c.c.}\Big] \\ &\quad + \epsilon^3 (Ae^{ix} + \overline{A}e^{-ix})^3 + O(\epsilon^4). \end{aligned} \tag{2.9}$$

Since $A$ satisfies the GLE (2.4), the $O(\epsilon^3)$ terms cancel out, and hence $\rho = O(\epsilon^4)$ is obtained.

In order to estimate $u - v_A$ as $O(\epsilon^2)$, let us set $u(t,x) - v_A(t,x) = \epsilon^2 R(t,x)$ and try to show the uniform boundedness of $R(t,x)$. The equation for $R$ is given by

$$\partial_t R = L_0 R + \epsilon^2 a(\epsilon,t,x)R + \epsilon^3 N(\epsilon,t,x,R) + \epsilon^2 r(\epsilon,t,x), \tag{2.10}$$

$$R(0,x) = \Big(u(0,x) - v_A(0,x)\Big)/\epsilon^2, \tag{2.11}$$

where

$$a(\epsilon,t,x)=1-3(v_A(t,x)/\epsilon)^2,\quad N(\epsilon,t,x,R)=-3(v_A/\epsilon)R^2-\epsilon R^3,$$

and $r=\rho/\epsilon^4$. Thanks to the earlier computation for $\rho$ and the fact that $A$ exists globally in time and is bounded, $r$ remain bounded on $(0,\epsilon_0)\times[0,\infty)\times\mathbb{R}$. By choosing $\epsilon_0$ smaller if necessary, one can assume that $|R(0,x)|\le 2d$.

Transforming the differential equation for $R$ into an integral equation, let us estimate its $C_b(\mathbb{R})$-norm (the usual sup-norm). Let us denote the semigroup associated with $L_0$ by $G(t)=e^{L_0t}$. Taking it for granted that the semigroup is uniformly bounded and strongly continuous on $C_b(\mathbb{R})$ (for a proof, see Lemma 2.3 in [**218**]), the integral equation for $R$ is given by

(2.12)

$$R(t)=G(t)R(0)+\epsilon^2\int_0^t G(t-s)\Big[a(\epsilon,s)R(s)+\epsilon N(\epsilon,s,R(s))+r(s)\Big]ds,$$

where the variable $x$ is omitted, and similarly below. For each $D>0$ there exists $M>0$ such that $\|N(\epsilon,s,R)\|\le M$ for $\|R\|\le D$ and $\epsilon\in(0,\epsilon_0)$. Moreover there exists a $C>0$ such that

$$\|G(s)\|,\ \|r\|,\ \|a(s)\|\le C.$$

Therefore, as long as $R(t)$ stays in a ball of radius $D$, the following is valid:

$$\|R(t)\|\le 2dC+\int_0^t\epsilon^2C^2\|R(s)\|ds+\epsilon^2tC(\epsilon M+C).$$

The Gronwall inequality implies that

$$\|R(t)\|\le\tilde{C}e^{\epsilon^2C^2t},\qquad \tilde{C}=2Cd+T_0C(\epsilon M+C),\tag{2.13}$$

for $t\le T_0/\epsilon^2$. Therefore, choosing $\epsilon_0$ so small that $\epsilon_0M\le C$, and setting

$$\hat{C}:=2Cd+T_0C(C+C),\qquad D:=\hat{C}e^{C^2T_0},$$

one finds by (2.13) that $\|R(t)\|\le D$ for $t\le T_0/\epsilon^2$. Since we have

$$u(t,x)-u_A(t,x)=\epsilon^2R(t,x)-\epsilon^3(A^3e^{3i3x}+\text{c.c.})/64,$$

the proof is complete. □

REMARK 2.2. The above argument does not apply to the case where the nonlinearity contains quadratic terms. The reason is that in this case the second term on the right hand side of (2.10) is $O(\epsilon)$ (in place of $\epsilon^2 aR$), making it impossible to give an error estimate $O(1/\epsilon^2)$ over a long time-period.

REMARK 2.3. There are generalizations of the above method in several directions. By improving the degree of approximation to make $\rho = O(\epsilon^n)$ $(n > 4)$, one can sharpen the error estimate up to $O(\epsilon^{n-2})$ (cf. [**345**] and [**189**]). The method also extends to deal with the case where the nonlinearity $g$ is cubic in $u$ and depends also on the derivatives $\partial_x^k u$ $(k = 1, 2, 3)$ (cf. [**76**] and [**345**]).

REMARK 2.4. Since the magnitude of $u_A$, and hence that of $u$, is $O(\epsilon)$, the $O(\epsilon^2)$ estimate in (2.7) is a meaningful approximation. We note also that the approximation in terms of the amplitude equation is effective within the natural time scale $O(1/\epsilon^2)$ mentioned in §2.1.

### 2.4. Attractivity of the Ginzburg-Landau Equation

The expression (2.3) says the approximation by the Ginzburg-Landau equation (GLE) describes the evolution of functions which have a special Fourier mode distribution with sharp peaks only at the mode numbers $k = \pm 1$. When the original system starts with an initial function of a more general Fourier mode distribution, does the solution tend, as time passes, to have the special Fourier mode distribution? Or, in other words, does the system fall into the GLE-regime? It is indeed numerically confirmed that for SHE and the Kuramoto-Shivashinsky equation (KSE) the solutions with a small initial value tend to have, after a certain period of time, the Fourier mode distribution as depicted in FIGURE 2.2. The distribution in FIGURE 2.2 clearly shows that the strengths of the Fourier modes are selectively high, due to the nonlinear interaction, at the integer multiples of the most unstable wave numbers $|k_c| = 1$. To put it more precisely, the strength of the Fourier mode at $k$ with $|k - nk_c| = O(\epsilon)$ is $\epsilon^{|n-1|}$, and it decays sharply otherwise. This is called the **clustered mode distribution**. It should also be noted that the distribution in FIGURE 2.2 effectively reflects the structure of the higher order approximate solutions for GLE

$$v = \epsilon\{A_1 e^{ix} + \text{c.c.}\} + \epsilon^2\{A_0 + (A_2 e^{2ix} + \text{c.c.})\} + \dots,$$

where the coefficients $A_1, A_0, A_2$ depend only on $T = \epsilon^2 t$, $X = \epsilon x$. It is shown in [**345**] by van Harten that if the initial condition for the

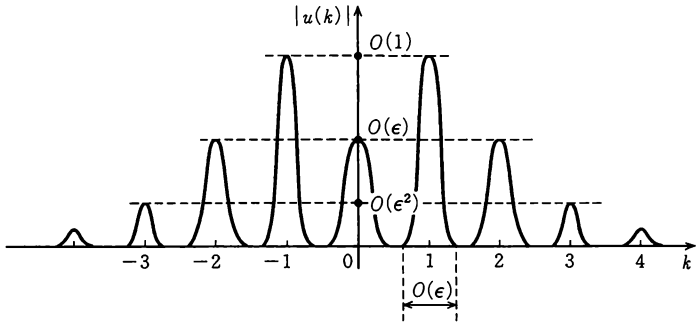


FIGURE 2.2. Clustered mode-distribution of the Fourier spectrum.

original equation has the Fourier mode distribution as in FIGURE 2.2, then the corresponding solution of GLE approximates the solution of the original system in the same sense as in (a slightly weaker version of) THEOREM 2.1.

In this section, we deal with the question raised above for the following equation with quadratic nonlinearity (the quadratic case is the most difficult):

$$\frac{\partial u}{\partial t} = Lu + N(u), \qquad x \in \mathbb{R}. \tag{2.14}$$

Although $u$ here could be vector-valued, we assume for simplicity that it is scalar-valued. $L$ is a real linear differential operator with constant coefficients. We also assume that $L$ depends on a control parameter $R$. $N(u)$ is a nonlinear term which is assumed to be expressed as

$$N(u) = 2\pi\rho(u^2).$$

Here $\rho$ is also a linear differential operator with constant coefficients. The symbols $\mu(k;R)$ and $\rho(k;R)$ of $L$ and $\rho$, respectively, are defined by

$$Le^{-ikx} = e^{-ikx}\mu(k;R),$$
$$\rho\left(e^{-ikx}\right) = e^{-ikx}\rho(k;R).$$

For the sake of simplicity, we assume that $\mu$ and $\rho$ are real-valued, and also that $\mu$ is of higher order than $\rho$ in the sense that

$$\rho(k;R)/\mu(k;R) \to 0 \text{ as } |k| \to \infty.$$

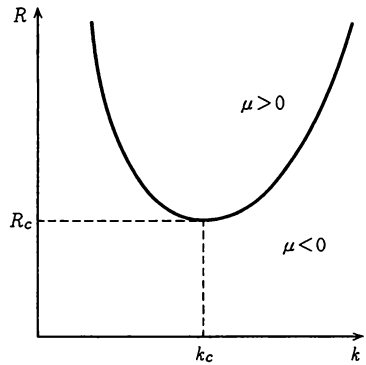


FIGURE 2.3. Parametric destabilization curve for $L$.

As an additional assumption on $L$, we assume that $\mu(k;R)$ behaves as in FIGURE 2.3. More precisely, near the first destabilization point $R = R_c$, namely, for

$$R > R_c, \qquad R - R_c = \epsilon^2,$$

it is assumed that the nullcline of $\mu$ is parabola-like as in FIGURE 2.3. Therefore, the destabilization above the threshold value $R_c$ looks like that in FIGURE 2.1. For later use, let us write down the Fourier transformed version of (2.14). In terms of $\Phi(k,t) = \int_{-\infty}^{\infty} u(x,t)e^{-ikx}dx$, (2.14) is recast as

$$\frac{\partial \Phi}{\partial t} = \mu(k;R)\Phi + \rho(k;R)\Phi * \Phi, \tag{2.15}$$

where $\Phi * \Phi$ stands for the convolution. Denoting by $\Phi^0(k;R)$ the Fourier transform of the initial value $u(x,0)$, one obtains

$$\Phi(k,t) = e^{\mu(k;R)t}\left[\Phi^0(k) + \rho(k;R)\int_0^t e^{-\mu(k;R)t'}\Phi * \Phi dt'\right].$$

A typical example which satisfies all the assumptions listed above is the Kuramoto-Shivashinsky equation (KSE)

$$\frac{\partial u}{\partial t} = -\left(1 + \frac{\partial^2}{\partial x^2}\right)^2 u + \lambda u + u\frac{\partial u}{\partial x},$$

where we set $\lambda = R - R_c$.

Let us first consider the initial conditions whose Fourier transform is of magnitude $O(\epsilon)$ in $L^1 \cap L^\infty$. The totality of such functions does include functions whose Fourier mode distribution is as in FIGURE 2.2,

although the strength of the Fourier modes of its member may not have a sharp peak at integer wave numbers. What has to be proved is that even for functions whose Fourier mode distribution does not have such peaks, after a period of time $T_0/\epsilon^2$ ($T_0 > 0$, $T_0 = O(1)$), the Fourier mode distribution of the solution approaches the clustered mode-distribution. Once this is proven, the dynamics of the solution thereafter is described by GLE due to the result of van Harten. The following result was obtained by Eckhaus [**103**].

THEOREM 2.5. *Let the initial value for the equation* (2.14) *have the Fourier transform* $\Phi^0(k)$ *which satisfies*

$$\Phi^0(k) = \delta_k(\epsilon)\varphi^0(k), \quad \varphi^0 = O(1),$$
$$\delta_k(\epsilon) = \max\{f(k,k_c), \epsilon\},$$
$$f(k,k_c) = \frac{\epsilon^2}{(k-k_c)^2+\epsilon^2}.$$

*Then, for a sufficiently small arbitrary positive number* $\sigma$, *at time*

$$t = \frac{\tilde{T}}{\epsilon^{2-\sigma}}, \qquad \tilde{T} = O(1),$$

*the solution of* (2.15) *satisfies*

$$\Phi(k,t) = \tilde{\delta}_k(\epsilon)\varphi(k,t), \quad \varphi = O(1), \tag{2.16}$$
$$\tilde{\delta}_k(\epsilon) = \max\Big\{\sum_{n=0}^{N} \epsilon^{|1-n|}[f(k,nk_c)]^N, \epsilon^N\Big\},$$

*where* $N$ *is an arbitrarily large integer.*

REMARK 2.6. For $0 < p < 1$, if $|k - nk_c| = O(\epsilon^p)$, then

$$[f(k,nk_c)]^N = O(\epsilon^{2N(1-p)}).$$

Therefore, after a period of time $O(\tilde{T}/\epsilon^{2-\sigma})$, one finds that the strength of the Fourier modes outside the region $|k - nk_c| = O(\epsilon)$ decays very sharply (because of the order of decay, the distribution in (2.16) is called a clustered mode-distribution of polynomial type).

REMARK 2.7. Since $\sigma > 0$, the time needed to settle down to the clustered mode-distribution is much shorter than the duration $O(1/\epsilon^2)$ in which GLE is an effective approximation.

The above result shows that the mode-distribution in FIGURE 2.2 has an attractivity property in the Fourier space, and hence that the

GLE approximation is an attractor. It is a severe restriction that the basin of attraction in Fourier space is characterized only in an $O(\epsilon)$-neighborhood of 0 in $L^1 \cap L^\infty$. Extensions to more realistic cases where bounded functions on $\mathbb{R}$ are included as initial functions have been pursued in recent years. For example, in [**330**] it is shown for KSE that for initial functions $u_0$ with

$$\|u_0\|_{W^{4,\infty}} \le C_0\epsilon, \qquad W^{4,\infty} = \{\partial_x^i u \in L^\infty;\ i = 0, \dots, 4\},$$

the decay rate of the Fourier modes between peaks is $e^{-|k-nk_c|\sqrt{t}}$ for $0 \le t \le O(1/\epsilon^2)$ and $n \in \mathbb{Z}$. The decay rate of the Fourier modes is exponentially fast. It has been also shown that conclusions of the same type as above are valid for more general equations that encompass KSE.

## 2.5. Stability of Stationary Periodic Solutions for the Swift-Hohenberg Equation

The Swift-Hohenberg equation (SHE)

$$\frac{\partial u}{\partial t} = -\Big(1 + \frac{\partial^2}{\partial x^2}\Big)^2 u + \epsilon^2 u - u^3 \qquad (t \ge 0,\ \ x \in \mathbb{R})$$

has a three-parameter family of stationary periodic solutions (roll solutions) for small $\epsilon^2 > 0$:

$$u_0(x;\omega,\varphi,\epsilon) = \epsilon\sqrt{\frac{1-4\omega^2}{3}}\, e^{i(1+\epsilon\omega)x} e^{i\varphi} + O(\epsilon^2). \tag{2.17}$$

In (2.17) $u_0$ is $2\pi/(1+\epsilon\omega)$-periodic in $x$ and is obtained as bifurcated solutions from $u \equiv 0$ if $\epsilon$ is considered as the bifurcation parameter (by fixing the period of the relevant solutions, one can apply the usual bifurcation theory).

It is directly verified that the Ginzburg Landau equation (GLE) (2.4) also has the following three-parameter family of stationary solutions:

$$A_0(X;\omega,\varphi,\epsilon) = \sqrt{\frac{1-4\omega^2}{3}}\, e^{i\omega X} e^{i\varphi}. \tag{2.18}$$

By using (2.3) and $X = \epsilon x$, one can see that the solution (2.18) gives rise to the same principal part as (2.17). It is assumed here that $\omega, \varphi$ vary in the range $|\omega^2| < 1/4, \varphi \in [0, 2\pi)$. In this section, the stability properties of these solutions are discussed. Spectra for GLE will be

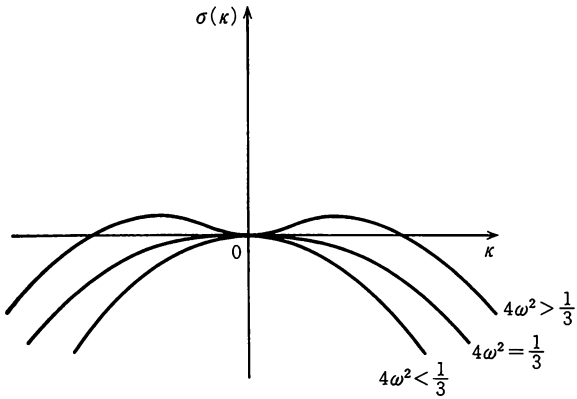


FIGURE 2.4. Spectral distribution for the periodic stationary solutions of GLE (the Eckhaus-instability occurs across the curve $4\omega^2 = 1/3$).

explicitly computed. Let us linearize it around the periodic solution $A_0$, which yields

$$\frac{\partial v}{\partial T} = 4\frac{\partial^2 v}{\partial X^2} + v - 6|A_0|^2 v - 3A_0^2 \overline{v} \equiv Lv.$$

Looking for an eigenfunction in the form

$$v(T, X) = e^{\sigma(\kappa)T}\left(ae^{i(\omega+\kappa)X} + be^{-i(\omega+\kappa)X}\right),$$

one finds that

$$\sigma(\kappa) = -(1 - 4\omega^2) - \kappa^2 + \sqrt{(1 - 4\omega^2)^2 + 16\kappa^2\omega^2}.$$

The behavior of $\sigma(\kappa)$ varies as in FIGURE 2.4, according to different values of $\omega$. One can read off from the graph that the stability property changes at $4\omega^2 = \frac{1}{3}$. Moreover, the following statements hold.

(i) When $4\omega^2 < \frac{1}{3}$, the solution is linearly stable (Eckhaus-stable) in the sense that the spectrum has no intersection with the right half plane, although it touches the origin since the problem is defined on $\mathbb{R}$ and has translational invariance.

(ii) The instability that occurs for $4\omega^2 > \frac{1}{3}$ is called the **Eckhaus instability**, in which destabilization acts to deform the wave length of eigenfunctions rather than to change their shape.

If one selects an Eckhaus-stable periodic stationary solution, does it also have a nonlinear stability property? The fundamental difficulty related to such a question is marginal stability.

**Marginal Stability**

Even for the stationary solution in the Eckhaus-stable region $4\omega^2 < \frac{1}{3}$, the continuous spectrum of the linearization reaches the origin, and hence there is no spectral gap. In such a case, nonlinear stability is not at all trivial.

Even if the issue just mentioned is resolved positively, one has to recall that GLE was introduced as an approximate equation for SHE. Therefore the (nonlinear) stability for GLE does not necessarily imply the same property for SHE. In fact, there is a big obstacle between these two.

**Limitation of the Approximation by GLE**

As mentioned above, even if the nonlinear stability for GLE is established, it does not necessarily mean nonlinear stability for SHE. One reason for this is that approximation by GLE (THEOREM 2.1) is valid only on a finite interval $[0, O(1/\epsilon^2)]$, not on $[0, \infty)$.

The nonlinear stability of the stationary solution for GLE was established in [**38**] by Bricmont and Kupiainen (see also [**81**]). The method employed by them is based upon the idea that renormalization group methods can be utilized to overcome the difficulties originating from the marginal stability. It seems that no attempt has been made to extend the region of validity for GLE approximations to $0 \le t < \infty$ even when the stationary solution is stable. There are, however, some attempts to apply renormalization group methods directly to SHE to establish stability. The following result is due to Schneider [**332**].

THEOREM 2.8. *There exists an $\epsilon_0 > 0$ such that the following statement is valid. For fixed $\omega, \varphi$ and $\epsilon \in (0, \epsilon_0)$, let $u_0 = u_0(\omega, \varphi, \epsilon)$ be an Eckhaus-stable stationary solution of* SHE. *Let $v|_{t=0}$ be a sufficiently small element of an appropriate space $\mathcal{B}$ (for the definition of $\mathcal{B}$, see* [**332**]).

*Let $u_0 + v|_{t=0}$ be an initial data. Then, there exists a positive constant $C_1(\omega, \epsilon)$ such that the solution $v(x,t)$ asymptotically satisfies, in the $L^\infty$-sense,*

$$v(x,t) = \frac{1}{\sqrt{t}} \tilde{A} e^{-\frac{x^2}{4C_1(\omega,\epsilon)t}} \partial_x \tilde{u}_0(\omega, \varphi, \epsilon)[x] + O(t^{p-1}) \qquad (as \ \ t \to \infty)$$

*for each* $p \in (0, 1/2)$, *where* $\epsilon\tilde{u}_0 = u_0$, $\tilde{A}$ *depends only on the initial condition, and* $C_1(\omega, \epsilon)$ *and* $\tilde{A}$ *are both* $O(1)$*-quantities as* $\epsilon \to 0$.

The solution $v$ evidently decays with the same polynomial order as solutions of the heat equation. This phenomenon is a marked difference from exponential decays in problems on bounded domains where spectral gaps are available.

In fact the proof of THEOREM 2.8 consists of the following steps.

First, the spectral properties are studied in detail for the linearization of SHE around the Eckhaus-stable solution. Then one shows that the principal part of the spectrum is the same as that for the heat equation. Finally, to complete the proof, one shows by using renormalization group methods that solutions of SHE behave in the same manner as the solutions of the heat equation in an appropriate function space.

The renormalization group method is one of the most effective techniques to handle the difficulties caused by essential spectra, and it has been used in recent years to study asymptotic behaviors of various types of solutions.

In §2.7, basic ideas of the renormalization group method will be explained by using a simple model equation.

REMARK 2.9 (Pattern Selection Problem). As opposed to problems on a finite interval, infinitely many Fourier modes destabilize all at once in problems on infinite intervals. Therefore, it is not clear which mode ultimately dominates the system immediately after the destabilization sets in. In general, when many patterns coexist in a given system, the problem of determining which one is realized (selected), called a pattern selection problem, depends crucially on how one formulates it. In other words, the most important question is how to set up the framework to capture the essence of the phenomenon. The stability of the stationary solution to SHE has been shown in THEOREM 2.8. This means that each stationary solution can exist stably relative to an appropriate class of perturbations, and hence the pattern is selected according to the initial condition. Therefore, one may not hope that a particular pattern is uniquely selected from a general initial data unless its basin of attraction is completely characterized in an appropriate function space. In reality, of course, it is not satisfactory to restrict the initial conditions to a particular class of small perturbations. More realistic initial conditions are random

fluctuations from a constant state or finite perturbations with support contained in a compact domain. In order to handle such initial conditions, one has to deal with global dynamics of the system, which is at present a very difficult task. We will come back to such pattern selection problems in CHAPTER 3.

REMARK 2.10. Recently, the work in [**108**] made it possible to give a geometric proof of THEOREM 2.8. The result obtained is interesting in the sense that the finite dimensional invariant manifold theory is applicable even though the system is marginally stable.

## 2.6. Front Solutions of the Ginzburg-Landau Equation

In the last section, the problems of existence and nonlinear stability of stationary periodic solutions were discussed for the Swift-Hohenberg equation, which is supposed to describe the periodic roll solutions in the heat convection problem. The same problems were also treated for the Ginzburg-Landau equation, an amplitude equation of SHE. In reality, however, it is rare to have a roll solution with the same period across the entire domain, and it is natural to expect to have a mixture of roll solutions with varying periods. Therefore it becomes important to give an answer to the pattern selection problem as to what period, among many, eventually dominates the system. A complete resolution of this problem is not available yet. As a first approach to such a problem, let us deal with the following problem for the Ginzburg-Landau equation.

**Problem:** When two periodic solutions of different periods are specified at $x = \pm\infty$ as the boundary conditions, how does the system behave in between?

In the sequel, we treat this problem for the normalized Ginzburg-Landau equation

$$\frac{\partial u}{\partial t} = \frac{\partial^2 u}{\partial x^2} + (1 - |u|^2)u, \qquad x \in \mathbb{R}. \tag{2.19}$$

As explained in the last section, this equation has a family of time-independent periodic solutions

$$u_q(x) = \sqrt{1 - q^2}\, e^{i\varphi} e^{iqx}, \qquad q \in [-1, 1], \quad \varphi \in \mathbb{R}, \tag{2.20}$$

where solutions with small amplitude ($q^2 > 1/3$) are unstable and solutions with large amplitude ($q^2 < 1/3$) are marginally stable.

Let the periodic boundary conditions at $\pm\infty$ be give by $u_{q_0}$ (at $x = -\infty$) and $u_{q_1}$ (at $x = \infty$) with $|q_0|,\ |q_1| \leq 1$. One needs to consider first of all the existence and stability of a front solution connecting these periodic solutions. The **front solution** here means a complex-valued function $U(x, \xi)$ such that

$$u(x,t) = U(x, x - ct)$$

is a solution of GLE and $U$ satisfies

$$\lim_{\xi \to -\infty} U(x,\xi) = u_{q_0}(x), \quad \lim_{\xi \to \infty} U(x,\xi) = u_{q_1}(x).$$

The constant $c$ is the speed at which the envelope of the family of solutions $\{U(x,\cdot)\}_{x\in\mathbb{R}}$ propagates. Such a solution is the counterpart of a heteroclinic orbit in finite-dimensional dynamical system theory. When $u_{q_0}$ is a stable roll solution and $u_{q_1}$ is an unstable one, in particular, it is expected that the stable solution $u_{q_0}$ invades the region of $u_{q_1}$ and that the front solution converges to $u_{q_0}$ when observed on arbitrary compact intervals (see FIGURE 2.5).

When $u_{q_1} \equiv 0$ (i.e., $q_1 = \pm 1$), the existence of such a front solution is easily established as follows.

Let us consider a solution in the form $u(x,t) = v(x - ct)e^{iq_0 x}$, where $v$ is a complex-valued function and $q_0 \in (-1,1)$, $c > 0$. Substituting this expression into (2.19), one obtains the ordinary differential equation

$$v''(\xi) + (c + 2iq_0)v'(\xi) + (1 - q_0^2 - |v(\xi)|^2)v(\xi) \tag{2.21}$$

for $v(\xi)$. If the Hamiltonian $H$ is defined by

$$H(v,v') = \frac{1}{2}|v'|^2 + \frac{1}{2}(1 - q_0^2)|v|^2 - \frac{1}{4}|v|^4, \tag{2.22}$$

then (2.21) is considered as a dissipative system with the complex dissipation coefficient $c+2iq_0$. It is easily verified that $\frac{dH}{dt} = -c|v|^2 \leq 0$ along the orbits of (2.21). The boundary condition at $\xi = \infty$ is taken to be $v = 0$, which is a stable equilibrium point of (2.21). On the other hand, the boundary condition at $\xi = -\infty$ is to be on the circle of equilibria: $v = \sqrt{1 - q_0^2}e^{i\varphi}$, which is unstable. Once an orbit enters the region defined by $|v|^2 < 1 - q_0^2$, $H < \frac{1}{4}(1 - q_0^2)^2$, it remains there and converges to the origin $(v, v') = (0, 0)$. The circle of equilibria lies on the boundary of this region, and the unstable manifold of the circle intersects the region. Therefore for any periodic solution $u_{q_0}$ taken as a boundary condition at the left end, (2.19) has a front solution which invades the region $u_{q_1} \equiv 0$.

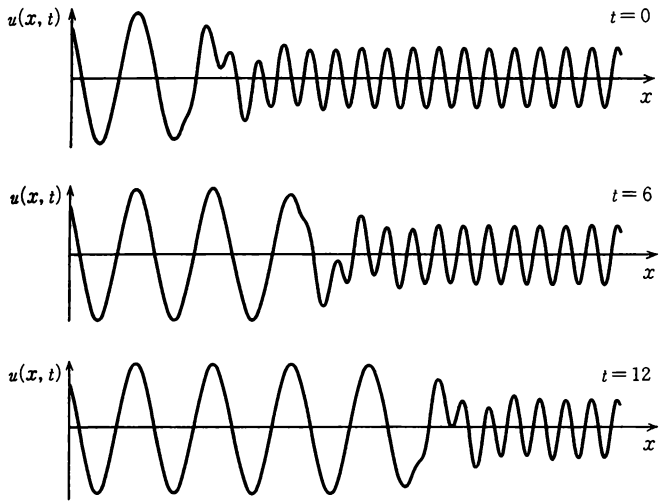


FIGURE 2.5. The front solution connecting a stable roll solution and an unstable one. Two roll solutions corresponding to $q_0 = -0.3$ and $q_1 = 0.9$ for GLE are connected, and the stable roll solution ($u_{q_0}$) is invading the region of the unstable one ($u_{q_1}$) with travelling speed $c = 5$ (transcribed from FIGURE 1 of [**105**]).

If the boundary conditions $u_{q_0}, u_{q_1}$ are both different from 0, the situation is not so simple. In fact, even if one tries the ansatz

$$u(x,t) = v_0(x - ct)e^{iq_0 x} + v_1(x - ct)e^{iq_1 x}$$

for a solution, one immediately finds that the solution has to depend on all wave numbers $q_n = q_0 + n(q_1 - q_0)$ ($n \in \mathbb{Z}$) due to the nonlinear interaction. This means that the solution has to be searched for in the general form

$$u(x,t) = \sum_{n\in\mathbb{Z}} C_n(x - ct)e^{iq_n x}. \tag{2.23}$$

Upon substitution into (2.19), this expression gives rise to a series of ordinary differential equations for $C_n$:

$$C_n' = D_n, \qquad D_n' = -(c + 2iq_n)D_n + C_n(q_n^2 - 1) + F_n(C), \tag{2.24}$$

where $F = (F_n)_{n\in\mathbb{Z}}$, arising from the nonlinear interaction, is given by

$$F_n(C) = \sum_{p+s+r=n} C_p C_s C_{-r}^*. \tag{2.25}$$

In the above, $'$ stands for the differentiation with respect to $\xi = x - ct$. The boundary conditions for the solution $C(\xi) = (C_n(\xi))_{n\in\mathbb{Z}}$ are given by

$$\lim_{\xi\to-\infty} C(\xi) \in C_{-\infty}, \qquad \lim_{\xi\to\infty} C(\xi) \in C_{\infty}, \tag{2.26}$$

where $C_{\pm\infty}$ are defined by

$$C_{-\infty} = \left\{ (C_n)_{n\in\mathbb{Z}} \mid |C_n| = \sqrt{1-q_0^2}\delta_{n,0} \right\}, \tag{2.27}$$

$$C_{\infty} = \left\{ (C_n)_{n\in\mathbb{Z}} \mid |C_n| = \sqrt{1-q_1^2}\delta_{n,1} \right\}, \tag{2.28}$$

with $\delta_{i,j}$ being the Kronecker delta. The sets $C_{\pm\infty}$ represent circles of equilibria for (2.24) which respectively correspond to the equilibrium solutions $u_{q_0}$ and $u_{q_1}$ (note that degeneracy is present because of the freedom in phase shifts). For what values of $q_0, q_1 \in [-1,1]$ does the problem (2.24), (2.26) have a solution? As a partial answer, the following two results have been obtained in [**105**] and [**150**].

THEOREM 2.11 (**Unstable-Unstable Front**). *Let $\alpha$ and $c$ be constants satisfying $0 < \alpha < 1/2$ and $c > 0$. Then there exists a value $\epsilon_1 = \epsilon_1(c) > 0$ such that for $0 < \epsilon \le \epsilon_1$, the problem* (2.24), (2.26) *has a solution with $q_0 = -1+\epsilon$ and $q_1 = 1-\alpha\epsilon$. Moreover, as $c \to \infty$, $\epsilon_1(c)$ converges to a positive constant.*

THEOREM 2.12 (**Stable-Unstable Front**). *Assume that $q_0$ satisfies*

$$-1/\sqrt{3} < q_0 \le 0.$$

*Then there exist constants $\epsilon_1 > 0$ and $c_1 > 0$ such that for all $\epsilon, c$ satisfying $0 < \epsilon \le \epsilon_1$ and $c \ge c_1$, the problem* (2.24), (2.26) *has a solution with $q_1 = \sqrt{1-\epsilon^2}$.*

REMARK 2.13. Corresponding to the invariance of the original GLE (2.29) with respect to rotation and translation, the equations (2.24) also have related invariance. Namely, if one defines $R_\phi$ by $(R_\phi C)_n = e^{i\phi} C_n$ and $T_\delta$ by $(T_\delta C)_n = e^{in\delta} C_n$, then these operators commute with the nonlinearity $F$. This fact implies that if some pair

from $C_{\pm\infty}$ is connected by an orbit of (2.24), then an arbitrary pair from $C_{\pm\infty}$ is also connected by an orbit of the same system.

REMARK 2.14. Front solutions do not necessarily exist for an arbitrary pair $(q_0, q_1)$. For an arbitrary solution $u(x,t)$ of (2.19), the maximum principle for second order parabolic equations implies that the number of zeros of $\mathrm{Re}(u(x,t))$ in any compact interval does not increase in time (this is due to a remark made by S. Angenent). Assuming that $c > 0$, the latter fact tells us that there exists a front solution only when $|q_1| > |q_0|$. Since the equation (2.19) is invariant with respect to the complex conjugation $u \to \overline{u}$, one can rephrase the condition as $q_1 > |q_0|$.

REMARK 2.15. Although the system (2.24) appears to contain infinitely many ordinary differential equations, a substantial amount of reduction is possible. In fact, it can be reduced, by using center manifold theory, to a (complex) two-dimensional problem (see [**105**] for details).

Partial results similar to those cited above have been obtained in [**75**] and [**107**] for the existence of front solutions of the Swift-Hohenberg equation. For this equation, too, center manifold theory applies as in REMARK 2.15, and the reduced problem is defined on real four-dimensional space (cf. [**150**], [**263**], and also [**352**]). The reason why infinite dimensional problems can be essentially reduced to finite dimensional ones is that the solution ansatz (2.23) taken at the beginning has a certain **periodicity condition**.

As for the stability of the front solutions, no discussion is given here, and there are many problems worth investigating in the future. The difficulty of dealing with the stability question is partly due to the fact that one cannot use the maximum principle when one studies complex perturbations of the real front solution connecting 0 and 1 in GLE. Therefore other approaches, such as renormalization group methods, are called for. For partial results in this direction, we refer, for example, to [**38**], [**37**] and [**77**] (cf. [**79**], [**80**], [**106**] too).

## 2.7. Renormalization Group and Its Application

**2.7.1. Idea of the Renormalization Group Method.** We will present the idea of the renormalization group method through an asymptotic characterization of solutions for the following scalar

equation (cf. [**36**]):

$$\dot{u} = u'' + F(u, u', u''), \quad x \in \mathbb{R}. \tag{2.29}$$

The idea remains the same even for the case where $x \in \mathbb{R}^n$. Let us examine whether the solution $u$ can be characterized as

$$u \sim t^{-\frac{\alpha}{2}} f(xt^{-\frac{1}{2}}) \qquad (t \to \infty) \tag{2.30}$$

for some function $f$. This means that the asymptotic form of $u$ is the profile of the function $f$, with the spatial scale being magnified by the time-dependent ratio $t^{1/2}$ and the amplitude being contracted by the ratio $t^{-\alpha/2}$. The exponent $\alpha > 0$ is a number to be determined.

When $F \equiv 0$ in (2.29), the equation is a well known heat equation. Its solutions are expressed and asymptotically characterized in terms of the fundamental solution:

$$u(x,t) = (4\pi t)^{-1/2} e^{-\frac{x^2}{4t}}.$$

In fact, if the initial functions decay appropriately at infinity, one can show that as $t \to \infty$

$$\sup_x \left| u(x,t) - (4\pi t)^{-1/2} U e^{-\frac{x^2}{4t}} \right| \leq O\Big(\frac{1}{t}\Big), \tag{2.31}$$

where $U = \int u|_{t=0} dx$. In this case, $f$ is given by $f(\xi) = (4\pi)^{1/2} e^{-\xi^2/4}$, and hence $\alpha = 1$. A feature of the fundamental solution for the heat equation is that the solution at arbitrary instances $t, t'$ can be transferred to each other by appropriate space-time and amplitude scaling. A solution with such a property is called a **scale-invariant solution**.

We chose the asymptotic form $f(xt^{-\frac{1}{2}})$ in (2.30) with the expectation that the diffusion effect in (2.29) will dominate for sufficiently large $t$. If the solution behaves as in (2.30), then, repeating the space-time and amplitude scaling appropriately, one will be able to extract a scale-invariant part of the solution. The idea of the renormalization group method is to reduce the problem of determining long-term behavior of solutions to the problems of existence and stability of fixed points for an iteration scheme. The iteration scheme here is defined in terms of the solutions of a problem on a fixed finite time interval, together with repeated applications of scaling. Let us roughly describe its framework, neglecting details on nonlinearity and phase space. Let us denote by $\mathcal{S}$ the phase space to which initial functions belong. It is convenient to choose the initial time $t = 1$. For a fixed

constant $L > 1$, let us set

$$u_L(x,t) = L^\alpha u(Lx, L^2 t), \tag{2.32}$$

where $u$ is the solution of (2.29) with initial value $f \in \mathcal{S}$, and $\alpha$ is an unknown exponent to be determined. Notice that the parabolic space-time scaling is adopted on the right hand side of (2.32), which is the one that makes invariant the fundamental solution of the heat equation. The factor $L^\alpha$ is the amplitude scaling.

In terms of $u_L$, the **renormalization group map** $R : \mathcal{S} \to \mathcal{S}$ is defined formally by

$$(Rf)(x) = u_L(x,1). \tag{2.33}$$

That is to say, the operation $R$ consists of solving the equation (2.29) with initial value $f$ up to time $L^2$, reducing the spatial size $L$ to 1, and magnifying the amplitude by the factor $L^\alpha$. The equation for $u_L$ to satisfy is

$$\dot{u}_L = u_L'' + F_L(u_l, u_L', u_L''), \tag{2.34}$$

where $F_L(a,b,c) = L^{\alpha+2}\, F(L^{-\alpha}a, L^{-\alpha-1}b, L^{-\alpha-2}c)$. In particular, if $F$ is a monomial $F(a,b,c) = a^{n_1}b^{n_2}c^{n_3}$ and $\alpha = 1$, then $F_L = L^{-d_F}F$, where

$$d_F = n_1 + 2n_2 + 3n_3 - 3. \tag{2.35}$$

If $d_F > 0$, repeated applications of the renormalization group map lessen the contribution of the nonlinearity. For example, if $F(u) = |u|^p$ with $p > 3$, then $d_F > 0$. In general, the nonlinearity $F$ is called **irrelevant** if $d_F > 0$, **marginal** if $d_F = 0$, and **relevant** if $d_F < 0$.

Since the renormalization group map depends on $L$ and $F$ (as well as on the exponent $\alpha$), we denote it by $R_{L,F}$. A characteristic feature of the map is its **semigroup property** (and hence it should have been called a renormalization semigroup, to be precise):

$$R_{L^n,F} = R_{L,F_{L^{n-1}}} \circ \ldots \circ R_{L,F_L} \circ R_{L,F}. \tag{2.36}$$

Each factor on the right hand side is a map which corresponds to solving the differential equation on a **fixed** time interval, and hence (2.36) means that repeated applications of such maps enable one to compute the long term behavior on the left hand side. Let us now set $t = L^{2n}$; namely, the operator $R$ has operated $n$ times; then the solution at that instant is written as

$$u(x,t) = t^{-\frac{\alpha}{2}}(R_{L^n,F}f)(xt^{-\frac{1}{2}}). \tag{2.37}$$

Assume that there exist $F^*$ and $f^*$ such that

$$F_{L^n} \to F^*, \qquad R_{L^n,F} f \to f^* \tag{2.38}$$

as $n \to \infty$. Note that $f^*$ is a fixed point of $R_{L,F^*}$:

$$R_{L,F^*} f^* = f^*, \tag{2.39}$$

and that it is a scale invariant solution of the equation $\dot{u} = u'' + F^*$. By using such an $f^*$ and (2.37), the asymptotic behavior of $u$ is described as

$$u(xt^{-\frac{1}{2}}, t) \sim t^{-\frac{\alpha}{2}} f^*(x). \tag{2.40}$$

Therefore we have reduced the study of asymptotic behavior of solutions to the study of the existence and stability of fixed points for the renormalization group map $R_{L,F^*}$. The strength of the stability of the fixed point determines the size of the region where one is allowed to take initial functions.

**2.7.2. Application to Nonlinear Parabolic Equations.** Up to this point, we have described from various aspects how effective the renormalization group method is. We now consider a simple nonlinear parabolic equation and show how the method applies. The equation is

$$\frac{\partial u}{\partial t} = \frac{\partial^2 u}{\partial x^2} + u^p \quad (x \in \mathbb{R}), \qquad p > 3. \tag{2.41}$$

We will show the stability of the zero solution $u \equiv 0$. Since $p > 3$ and one can take $\alpha = 1$, the indicator $d_F$ in (2.35) in the present case is positive, and hence the nonlinearity is irrelevant. Let us introduce the function space $H^m(n)$ ($m$ and $n$ are integers) defined in terms of the weight $|x|^n$ at infinity as follows:

$$H^m(n) = \{u \mid u(x)(1 + |x|^2)^{n/2} \in H^m\},$$

where $H^m$ is the usual Sobolev space consisting of functions whose (distributional) derivatives up to order $m$ belong to $L^2(\mathbb{R}, \mathbb{C})$. We have the following result.

THEOREM 2.16. *There exists a constant $\delta > 0$ such that for any initial function $u_0$ satisfying $\|u_0\|_{H^2(2)} < \delta$ the following statement holds.*

*There exists a number $A^* \in \mathbb{R}$, depending on the initial function $u_0$, such that the solution $u$ of (2.41) with $u|_{t=0} = u_0$ behaves*

*asymptotically as follows:*

$$\left\| \sqrt{t}\, u(x\sqrt{t}, t) - \sqrt{\pi} A^* e^{-\frac{x^2}{4}} \right\|_{H^2(2)} = O(t^{-\min\{1,\, p-3\}/2}). \tag{2.42}$$

REMARK 2.17. Since $H^2(2) \subset L^\infty$, the asymptotic characterization (2.42) is also valid in the sense of pointwise convergence.

PROOF. Since it is easily verified that the Fourier transform is an isomorphism from $H^2(2)$ to itself, instead of (2.41) one may consider its Fourier transformed version

$$\frac{\partial \hat{u}}{\partial t} = -k^2 \hat{u} + \hat{u}^{*p}, \tag{2.43}$$

where $*p$ stands for the $p$-fold convolution ($p$-th power of convolution).

Let $L > 1$ and rescale $k, t$ by $k = K/L^n, t = L^{2n}T$. Define a new dependent variable $v_n$ by $v_n(K, T) = \hat{u}(k, t)$. Since the $p$-fold convolution in the second term on the right hand side of (2.23) produces the factor $L^{(1-p)n}$, one obtains

$$\frac{\partial v_n}{\partial t} = -K^2 v_n + L^{n(3-p)} v_n^{*p}. \tag{2.44}$$

Since $T = 1$ means $t = L^{2n}$, the limit as $n \to \infty$ corresponds to $t \to \infty$. One should notice that since $p > 3$ and $L > 1$, the nonlinearity exerts less and less effect as $n \to \infty$. Instead of solving (2.43) on $[1, \infty]$, we solve (2.44) successively as follows.

To begin with, let us define a scaling transformation by

$$\left(\mathcal{L}_{1/L} f\right)(K) = f(K/L).$$

(i) $n = 1$: Solve the equation (2.44) on the interval $[1/L^2, 1]$ and call the solution $v_1$ (in terms of the original time $t$ this corresponds to the interval $[1, L^2]$). Next, solve the equation for $n = 2$ with the initial value $\mathcal{L}_{1/L} v_1(\cdot, 1)$ on the time interval $[1/L^2, 1]$ ($[L^2, L^4]$ in the original time). Namely, $v_2(\cdot, 1/L^2) = \mathcal{L}_{1/L} v_1(\cdot, 1)$.

(ii) $n \to n + 1$: Solving the equation (2.44) on the time interval $[1/L^2, 1]$ and using the solution $v_n$, solve the equation for the next stage $n+1$ taking $\mathcal{L}_{1/L} v_n(\cdot, 1)$ as the initial value, namely, $v_{n+1}(\cdot, 1/L) = \mathcal{L}_{1/L} v_n(\cdot, 1)$.

Repeating this process, one finds that $v_n$ in general satisfies the following integral equation:

$$v_n(K,T) = e^{-K^2(T-1/L^2)} v_{n-1}(K/L,1) + L^{n(3-p)} \int_{1/L^2}^{T} e^{-K^2(T-s)} v_n^{*p}(K,s)ds. \tag{2.45}$$

The following estimate plays an important role in showing the existence of solutions by the contraction mapping principle.

LEMMA 2.18. *For some $\alpha > 5$, let us assume that*

$$\delta < L^{-\alpha} \quad \text{and} \quad \|v_{n-1}|_{T=1}\|_{H^2(2)} < \delta.$$

*Then, there exist $C_1, L_0 > 0$ such that, for any $L > L_0$,*

$$R \equiv \sup_{T\in[1/L^2,1]} \|v_n(T)\|_{H^2(2)} \le C_1 L^{5/2-\alpha}. \tag{2.46}$$

PROOF. From the definition of $H^2(2)$ and of $\mathcal{L}_{1/L}$, one finds that

$$\|\mathcal{L}_{1/L} v\|_{H^2(2)} \le C L^{5/2} \|v\|_{H^2(2)}.$$

The linear part in (2.45) is estimated as

$$\begin{aligned} &\sup_{T\in[1/L^2,1]} \|e^{-K^2(T-1/L^2)} v_{n-1}(K/L,1)\|_{H^2(2)} \\ &\quad \le C \sup_{T\in[1/L^2,1]} \|e^{-K^2(T-1/L^2)}\|_{C_b^2} \|v_{n-1}(K/L,1)\|_{H^2(2)} \\ &\quad \le C L^{5/2} \delta. \end{aligned}$$

On the other hand, the nonlinear term in (2.45) is estimated as

$$\sup_{T\in[1/L^2,1]} \left\| L^{n(3-p)} \int_{1/L^2}^{T} e^{-K^2(T-s)} v_n^{*p}(K,s)ds \right\|_{H^2(2)} \le C L^{n(3-p)} R^p,$$

where the inequality

$$\|u * v\|_{H^2(2)} \le C \|u\|_{H^2(2)} \cdot \|v\|_{H^2(2)}$$

is used. □

After a little more computation, taking $\delta$ as in the last lemma, and choosing $L$ large, one can show that the right hand side in the integral equation (2.45) defines a contraction mapping in the ball of radius $CL^{5/2-\alpha}$ with center at the origin in the space $C([1/L^2,1], H^2(2))$. This establishes the existence and uniqueness of a solution to the integral equation (2.45), as well as the desired estimate in (2.46).

What remains to be proven is that the value $v_n|_{T=1}$ at $T = 1$ of the solution $v_n$ obtained above converges in $H^2(2)$ to $A^* e^{-K^2}$ as $n \to \infty$ for some constant $A^* \in \mathbb{R}$. Referring for details to [**332**], let us explain the main idea. Let $\psi = e^{-K^2}$ and decompose $v_n|_{T=1}$ as

$$v_n|_{T=1} = A_n \psi + \rho_n,$$

where the mean value of $\rho_n$ is 0, namely, $\rho_n(0) = 0$. Next, one estimates $|A_{n+1} - A_n|$, $\|\rho_n\|_{H^2(2)}$, and then shows that $A_n$ converges to $A^*$ at a geometric rate and $\|\rho_n\|_{H^2(2)} \to 0$ as $n \to \infty$. As a byproduct of this process, one can also derive the decay order in time $t$. □

## 2.8. Summary

**2.1** It is shown through examples that an order parameter is nothing but the amplitude in the direction of the slow freedom extracted by using the difference in scales.

**2.2** Three formal ways of deriving amplitude equations are presented.

**2.3** It is shown by the example of the Ginzburg-Landau equation that the amplitude equation approximates the original system on a sufficiently long time interval.

**2.4** The set of orbits which obey the Ginzburg-Landau equation is shown to be attractive in the space of initial functions.

**2.5** It is described how the stability of the periodic stationary solutions for the Swift-Hohenberg equation can be proved by the renormalization group method.

**2.6** We discussed the stability-instability question, related to front solutions, that plays an important role in determining which periodic solution among many is selected.

**2.7** The idea of the renormalization group method is presented, in which a problem on a finite time interval is solved repeatedly, the fixed point is found, and the asymptotic behavior of the original problem is thus determined by the property of the fixed point.

CHAPTER 3

# Marginal Stability Criterion and Pattern Selection

When several stable solutions coexist, why is it that a particular solution is selected? As an example of such a problem, the problem of determining the shape and growth-speed of crystals has long attracted the attention of researchers. We will first take a quick look at what roles singular perturbation effects, such as the surface tension and anisotropy, play in pattern selection. Next, we will study the problem of describing how physically realistic initial values converge, as time progresses, to a particularly selected pattern. This is quite a difficult problem, and there have been almost no results on it. The only exception to this situation is the wave speed selection problem of travelling wave solutions to scalar reaction-diffusion equations. In the latter context, we will introduce a very useful method, called the marginal stability criterion, that does not depend on the comparison principle.

## 3.1. Pattern Selection

It is rather common that there exist many stable solutions of nonlinear systems, and hence the asymptotic destiny of the system may be different, depending on the initial values. On the other hand, it is also a fact that patterns, in many of the phenomena we observe, always reproduce themselves under fairly general conditions. For example, in a crystal growth process in an undercooled medium, the shape and growth speed of the crystal is uniquely determined by the degree of undercooling in the far-field. In this chapter, we will investigate principles that explain why a particular pattern is selected from many possibilities.

To put it very abstractly, the problem raised above asks what attractor has the largest basin of attraction. But this is not so useful a re-phrasing, and moreover, may not be appropriate either. For

example, if the basin is widely spread but very thin in the phase space, perturbation in the thin direction will kick the system out of the basin easily. It is also understandable that the large volume of the basin does not necessarily mean that it contains meaningful initial values. After all, one realizes that neither the problem of pattern selection nor the stability of solutions can be discussed separately from the class of initial values and perturbations that is of concern at the moment. If the class of perturbations is an empty set, then everything is stable, and, on the other hand, if the class is very large, then instability sets in easily. What has just been said is a trivial fact, but it is not trivial at all to appropriately set up the class of meaningful perturbations and its relationship to stability questions for a particular problem.

It often happens that even though the real world system uniquely selects a solution, its model system does not do so. It can possibly happen that degeneracy or multiplicities of solutions are introduced because of our negligence in incorporating various physical effects. As an example of such a situation, in the next section we will review pattern selection in dendritic crystal growth processes. In this example, the effects of surface tension and anisotropy play an essential role. These effects are considered as a singular perturbation effect (we will come back to this topic in CHAPTER 5, considering it as a distinguished limit of the phase-field model). In other words, in this example a structurally unstable system is transformed into a structurally stable one by introducing singular perturbation effects.

The last statement provides a novel viewpoint for pattern selection problems. It indicates that the selected pattern is given as a limit of solutions of structurally stable systems (cf. [**65**]). Here the phrase *structurally stable* is used in the sense that the system does not allow the multiple existence of stable solutions in a reasonable class of function spaces, and that solutions starting with almost all initial values converge to the unique stable state. In §3.3 we investigate a wave speed selection problem for the Fisher-Kolmogorov equation, considering it as a limit of bistable systems (where the wave speed of travelling waves is uniquely determined). In this case, as opposed to the crystal growth process above, structural stability is gained by modifying the nonlinearity of the system.

It is, however, still important to know intrinsic principles that control the selection of patterns, especially because the model equations at hand cannot avoid neglecting some physical effects. Among such principles, we will give a detailed explanation of the **marginal**

**stability criterion** in the context of the Fisher-Kolmogorov equation in §§3.4 and 3.5.

As for the Fisher-Kolmogorov equation (cf. §3.3), the wave speed selection problem was mathematically settled by Aronson and Weinberger [**10**], [**11**]. However, a general selection principle which explains why the minimum speed is selected has not been established. It is therefore necessary to look for a selection rule that is independent of the particular problem at hand. The marginal stability criterion is a candidate for such a selection rule. This criterion is not only useful in practice, but also provides us with some insights into the nature of fundamental instabilities that are encountered in the stability analysis of interfaces, such as in tip-splitting and side-branching. The criterion is also expected to apply effectively to more general equations that do not obey the maximum principle, although its mathematical justification remains open.

## 3.2. A Brief History on Dendrites

According to experiments, for the crystal growth process in an undercooled liquid system, the shape of the crystal (the curvature $1/\rho$ of the tip of the crystal, in particular) and the growth speed of the tip are uniquely determined by the degree $\Delta$ of undercooling given in the far-field. Therefore, it seems that the shape of the interface and its speed of motion are **uniquely selected** by the degree $\Delta$ of undercooling. How to explain such a situation is the content of a **pattern selection problem**. This kind of problem is a universal one in pattern formation, and in fact, the frequency selection problem for spiral waves, to be discussed in CHAPTER 4, is another such problem.

**3.2.1. Stefan Type Model and Geometric Model.** If an interface is smooth in macroscopic scale, then its motion may be described by some system of differential equations (when the interface is a fractal, such as in the diffusion-limited aggregation, the local motion of the interface is not well-defined). There are, roughly speaking, two models to describe the motion of an interface: one in which the interface has no thickness and is considered as a sharp interface where bulk variables may change discontinuously, and the other in which the interface is described as an internal transition layer of a finite (non-zero) thickness. The representative of the former model is the Stefan-type model, and the phase-field model to be discussed

in CHAPTER 5 is well known as an example of the latter. We will hereafter focus our attention on sharp interface models in $\mathbb{R}^2$ or $\mathbb{R}^3$.

In order to describe the growth of a crystal in an undercooled medium, the Stefan-type model utilizes only the temperature $T$ and the location $\Gamma$ of the interface, and is given by

$$\frac{\partial T}{\partial t} = D\Big(\frac{\partial^2}{\partial x^2} + \frac{\partial^2}{\partial y^2} + \frac{\partial^2}{\partial z^2}\Big)T \quad \text{(heat diffusion)} \quad \text{in } \mathbb{R}^3\backslash\Gamma, \tag{3.1}$$

$$Lv_n = C_p D\Big[(n\cdot\nabla)T|_{\text{sol}} - (n\cdot\nabla)T|_{\text{liq}}\Big] \quad \text{on } \Gamma. \tag{3.2}$$

Moreover, $T$ is supposed to satisfy an undercooling condition in the far-field (to be described later). As a boundary condition on the interface $\Gamma$, we adopt one of the following:

$$T|_\Gamma = T_M \quad \text{(locally in thermal equilibrium)}, \tag{3.3}$$

(3.4) Surface tension

$$T|_\Gamma = T_M\Big(1 - \frac{\gamma}{L}\kappa\Big) \quad \text{(curvature effect)},$$

(3.5) Anisotropy (two-dimensional)

$$T|_\Gamma = T_M\left(1 - \frac{\gamma + \frac{d^2\gamma}{d\theta^2}}{L}\kappa\right) \quad \text{(dependency on directions)}.$$

In the above, $T$ stands for the temperature, $D$ the heat diffusion coefficient, $L$ the latent heat, $v_n$ the velocity in the normal direction of the interface $\Gamma$, $C_p$ the specific heat, $T_M$ the melting temperature, $\gamma$ the surface tension, $\kappa$ the mean curvature of $\Gamma$, and $\theta$ the angular variable in $\mathbb{R}^2$. Moreover, $n$ is the unit normal vector on $\Gamma$ pointing to the liquid phase, and the curvature $\kappa$ is taken to be positive when $\Gamma$ is concave seen from the solid phase. The condition (3.3) seems natural in the sense that the temperature is equal to the melting temperature at the interface $\Gamma$; however, this condition is not enough, and it turns out later that (3.4), in which curvature effects are taken into consideration, and (3.5), where anisotropies are included, become more appropriate. The condition (3.4) is often called the Gibbs-Thomson condition. When the interface is flat ($\kappa = 0$), these latter conditions agree with (3.3). Our main concern is, therefore, the case (3.4) or (3,5). Note that when the boundary condition (3.3) is adopted, the

temperature $T$ completely determines the motion of $\Gamma$. The inclusion of surface tension, on the other hand, will no longer allow one to determine the phase merely by the sign of $T$, and moreover one cannot resort to a comparison principle. As a consequence, many of the methods which were successfully applied for the classical Stefan problem are not available for the problem with surface tension. Whether the solidification develops depends crucially on the condition $T_\infty$ at infinity in the liquid phase: $T = T_\infty$, $|x| \to \infty$. The quantity $\Delta = T_M - T_\infty$ is call the **degree of undercooling**.

A naive question is how solidification proceeds according to the above Stefan problem. When a small bulge of crystal is formed, the temperature gradient nearby is increased according to (3.1) (which is similar to the fact that a sharp metal edge is easily struck by lightning). This increase of gradient attracts more molecules, and the crystal grows. The surface tension effect (3.4) has the opposite effect, namely, the heat flux along the interface flows from a convex region to a concave one (seen from the solid); hence small bumps may disappear. The net effect of these two opposite tendencies drives solidification or melting.

> In general, it is very difficult to solve problems of Stefan type!

The reason for this statement is that although the motion of the interface is determined locally as in (3.2), the temperature $T$ on the right hand side is determined **non-locally** in the sense that (3.1) has to be solved in the entire domain under one of the boundary conditions which depend on $\Gamma$ (**non-locality** of the problem). Namely, to follow the motion of the interface in one step, one has to solve the partial differential equation on the whole domain. This is not an easy task, either analytically or numerically (cf. REMARK 3.1). Therefore, in order to pursue the mathematical analysis and to discover the qualitative behavior of the crystal growth, the following **geometric model** ([**41**], [**42**]) has been proposed in $\mathbb{R}^2$, although it may have less degree of connection to the real phenomenon:

$$
\begin{aligned}
&v_n = \kappa + \alpha\kappa^2 - \beta\kappa^3 + \gamma\tfrac{d^2\kappa}{ds^2}, \\
&v_n \ : \text{ the speed of growth in the normal direction,} \\
&s \ : \text{ the arclength along the interface,} \\
&\kappa \ : \text{ the curvature,} \\
&\gamma = \gamma_0(1 - \delta\cos(m\theta)) \ : \text{ the effect of the surface tension} \\
&\qquad (\text{if } \delta = 0, \ \text{isotropic; if } \delta > 0, \ \text{anisotropic}).
\end{aligned}
\tag{3.6}
$$

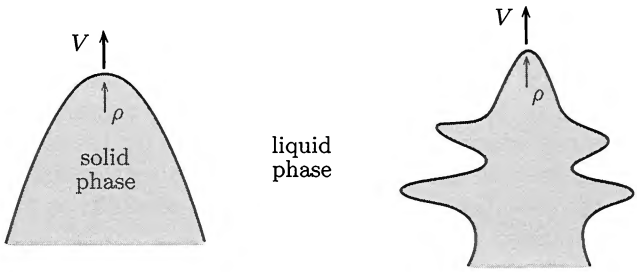


FIGURE 3.1. Needle crystal and dendrite

The sign of $\kappa$ is positive if $\Gamma$ is concave along the normal direction, $\alpha, \beta$ are positive constants, and $m$ is a positive integer.

Moreover, the following kinematic conditions are satisfied (cf. [**85**]):

$$\left.\begin{aligned} \frac{\partial \kappa}{\partial t} &= -\Big(\kappa^2 + \frac{\partial^2}{\partial s^2}\Big) v_n \\ \frac{\partial s}{\partial t} &= \int_0^s \kappa v_n ds \end{aligned}\right\} \text{ kinematic conditions.}$$

There is another type of model, called boundary layer models (cf. [**29**]), derived in the same spirit as geometric ones. We will not deal with them here. These models are supposed to describe the cases where the speed of crystal growth is very large, namely, the case where the **diffusion length** $l = 2D/V$ (the length in which the diffusive medium is affected by the motion of an interface with velocity $V$) is very small compared with the curvature radius $\rho$ of the tip of the crystal. This type of model is useful when one investigates in detail the relationship between the existence of a solution and such effects as surface tension and anisotropy.

Let us here rephrase the problem raised at the beginning of the present section. We consider the following problems for the Stefan-type problem (and for the geometric model later):

**Existence Question**: For a given degree $\Delta$ of undercooling, does there exist a needle crystal whose tip has a constant curvature $1/\rho$ and a constant speed $V$ of growth? Does there also exist a dendrite with side branches? (Cf. FIGURE 3.1.)

**Selection Problem (Stability):** For a fixed degree of undercooling $\Delta$, are the solutions as above determined uniquely? What are the physical factors which play important roles for the solutions to be determined uniquely?

The Stefan problem has been studied for over a century, and here I have only touched the tip of the iceberg. See [**319**], [**261**] and [**350**] (pp.117-120) for a historic account. A more detailed introduction can be found in [**63**] and [**173**]. In [**161**] and [**162**], a theoretical framework is developed starting from general thermodynamical laws. The classical Stefan problem, i.e., with (3.3) as the interfacial condition, is known to admit unique global weak solutions (see, for instance, [**142**], [**143**], [**202**] and [**234**] (pp.496-503)), the proof of which is closely tied up with the maximum principle. For the regularities of weak solutions of the multidimensional one-phase Stefan problem (without surface tension), see for instance, [**45**], [**46**], [**47**], [**144**], [**172**], [**215**], and [**216**]. For more recent progress on the regularity problem, see for instance [**12**], [**13**], [**93**], [**222**], [**260**], [**291**]. Concerning the Stefan problem with surface tension, we have very few analytical results, see [**116**], [**145**], [**248**], and [**260**]; in particular, existence of global weak solutions for the two-phase problem is established in [**248**], using a discretized problem and a capacity-type estimate for approximating solutions. If the heat diffusion equation is replaced by the Laplace equation, then the resulting problem is the quasi-stationary Stefan problem with surface tension, which is also called the Mullins-Sekerka model. Existence, uniqueness, and regularity of solutions for the quasi-stationary approximation have recently been investigated in [**24**], [**66**], [**67**], [**118**], [**119**], [**120**], [**121**]. I owe the reference in this paragraph to [**117**], which proves the existence of a unique smooth solution for the Stefan problem with surface tension.

**3.2.2. Ivantsov's Paradox.** The first partial answer to the above questions was given by Ivantsov [**191**].

PROPOSITION 3.1. *If the effects of surface tension and anisotropy are absent (in this case the interface is in an isothermal state; $T|_\Gamma = T_M$), the Stefan problem* (3.1)–(3.3) *has a one-parameter family of needle solutions for each given degree of undercooling. Therefore, there is no pattern selection mechanism working, and continuum-many solutions coexist.*

To be more precise, the problem has the following type of solutions:

$$z - Vt = \frac{\rho_0}{2} - \frac{1}{2\rho_0}(x^2 + y^2), \tag{3.7}$$

which represent a family of paraboloids in $\mathbb{R}^3$, where the crystal grows in the $z$ direction and the curvature of its tip is $1/\rho_0$. Integrating (3.1) with the help of the parabolic coordinates, we see that the temperature distribution in the liquid phase (in the solid phase the temperature is constant, $T = T_M$) is given as follows:

$$T(x, y, \zeta) = T_\infty + (T_M - T_\infty)\frac{\operatorname{erfc}[(\sqrt{x^2 + y^2 + \zeta^2} + \zeta)/l]}{\operatorname{erfc}(p)}, \tag{3.8}$$

where $\zeta = z - Vt$ is the travelling coordinate in the $z$ direction, and

$$\operatorname{erfc}(x) \equiv \frac{2}{\sqrt{\pi}} \int_x^\infty \frac{e^{-t}}{t} dt \tag{3.9}$$

is the error function. $p$ is a non-dimensional quantity, called the **Peclet number**, defined by

$$p \equiv \frac{\rho_0}{l} = \frac{V\rho_0}{2D}. \tag{3.10}$$

That is to say, $p$ is the ratio of the curvature radius of the tip to the diffusion length $l$ ($\equiv 2D/V$). Moreover, the normalized degree of undercooling $\Delta$,

$$\Delta \equiv C_p(T_M - T_\infty)/L, \tag{3.11}$$

and the Peclet number $p$ have to satisfy the following relation:

$$\Delta = pe^p \operatorname{erfc}(p). \tag{3.12}$$

The relation (3.12) can be obtained by dimension analysis [**305**], too. We have thus obtained the needle crystal solutions. Although the product of the growth speed $V$ and the inverse $\rho_0$ of the curvature of the tip (which is nothing but the Peclet number) is uniquely determined as in (3.12), there are infinitely many combinations of $V$ and $\rho_0$. This indeterminacy is called the Ivantsov paradox.

According to experiments, $V$ and $\rho_0$ are uniquely selected for each given $\Delta$, and therefore, we must admit that there is something missing from our argument. It is not the case that stability analysis offers a selection criterion, either. In fact, all of our solutions are known ([**240**]) to be unstable with respect to the problem (3.1), (3.2), (3.3). Therefore it is necessary to take into account the effects of surface tension and anisotropy, which have so far been neglected.

**3.2.3. Mullins-Sekerka Instability and the Marginal Stability Criterion.** We now present the analysis done by Mullins and Sekerka and its influence on an idea for a selection criterion.

**The surface tension effects and the Mullins-Sekerka Instability.**

Mullins and Sekerka in [**274**] analyzed how the surface tension affects the stability properties of a planar front interface (although the analysis in [**274**] was given to interfaces appearing in a binary alloy, it applies equally to the crystal growth process). The planar interface around which the stability analysis is to be carried out actually exists. In fact, since the interface is planar and hence the curvature $\kappa = 0$, the temperature distribution on the interface is given by $T|_\Gamma = T_M$, regardless of the boundary conditions (3.3), (3.4) or (3.5). A family of solutions of the diffusion equation (3.1) in this case is given by

$$T(z,t) = T_\infty + (T_M - T_\infty)\exp[-2(z - Vt)/l], \tag{3.13}$$

where the crystal is growing in the $z$-direction with velocity $V$ ($T \equiv T_M$ in the solid phase). Here $T_\infty$ is the temperature given at infinity, $V > 0$ is arbitrary, and $l = 2D/V$ is the diffusion length. Applying the condition (3.2) at the interface location $z = Vt$, one obtains the relation

$$\Delta \equiv C_p(T_M - T_\infty)/L = 1 \tag{3.14}$$

to be satisfied. Here, $\Delta$ is the non-dimensionalized degree of undercooling.

What should be noted here is that **the growth speed is indeterminate**. The shape of the interface has been identified as planar, while the indeterminateness is placed on the speed. If sinusoidal perturbations are applied to this planar solution and linear stability analyses are carried out, one finds that perturbations of wave length greater than a certain length destabilize. To be more specific, let $k$ be the wave number of the perturbation; then, under the condition $kl \gg 1$, the **critical wavelength** $\lambda_s$ is given by ([**236**], [**237**])

$$\lambda_s \cong 2\pi\sqrt{ld_0}. \tag{3.15}$$

An amplitude with wave length greater than this critical one grows, while one with shorter wave length diminishes due to the surface tension effect. The constant $d_0$ above is a non-dimensional quantity,

called the **capillary length**, defined by

$$d_0 \equiv \gamma T_M C_p / L^2. \tag{3.16}$$

It is worth noticing that the critical wave length is proportional to the geometric mean of the capillary length $d_0$ and the diffusion length $l$.

### Marginal Stability Criterion

Langer, Müller and Krumbhaar ([**240**]) applied the method in [**274**] to needle crystal growth, and attempted to resolve the issues of the existence of a dendrite and the Ivantsov paradox simultaneously. They first assume that the Stefan problem with the boundary condition (3.4) incorporating the surface tension effect has a needle crystal solution. Then, applying perturbations to it, they analyze the eigenvalues $\Omega(\sigma)$ ($\sigma \equiv (\lambda_s/2\pi\rho)^2$) of the associated linearized eigenvalue problem, and after some reasoning based on physics, they proposed the following criterion (marginal stability criterion):

> The dendrite appears at the value $\sigma = \sigma^*$ where the eigenvalue $\Omega(\sigma)$ associated to the needle crystal is marginally stable, i.e., $\mathrm{Re}\,\Omega(\sigma^*) = 0$.

In other words, the condition $\sigma^* = 2Dd_0/V\rho^2$ has to be realized for a dendrite to grow. This criterion appears to be in reasonable agreement with experimental facts. In particular, the criterion seems to well predict the order of magnitude of the dendrite tip. However, it was later found that the assumption of this criterion was wrong. Namely,

> The Stefan problem (3.1), (3.2), (3.4) incorporating only the isotropic surface tension effect (probably) does not allow needle crystal solutions.

The reason why we used the word "probably" is that the rigorous proof of the non-existence of needle solutions for the Stefan problem has not been established, to the best of the author's knowledge. There are many convincing semi-rigorous analyses and carefully performed numerical experiments that all indicate the non-existence ([**26**], [**259**], [**211**], for example).

The theory developed in the above-mentioned papers is called the **solvability theory.** The reason for such an appellation will become clear in the subsequent sections. For the moment we depart from the Stefan problem, and deal in a mathematically rigorous manner

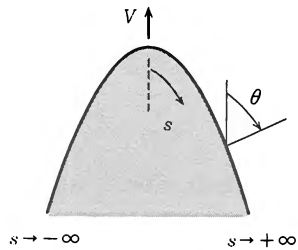


FIGURE 3.2. Geometric model for a needle crystal

with such problems raised above for the simplified geometric model mentioned earlier.

**3.2.4. Surface Tension and Anisotropy.** Denote the position of the interface by $x(t, s)$ in $\mathbb{R}^2$, where $s$ stands for the arclength measured from a reference point. The geometric model attempts to describe the motion of the interface in terms of an equation of the following type:

$$\mathbf{n} \cdot \frac{\partial x}{\partial t} = U\Big(\kappa, \frac{\partial^2 \kappa}{\partial s^2}, \dots\Big), \tag{3.17}$$

where the left hand side represents the outward normal velocity and the right hand side is a nonlinear velocity function depending on even order derivatives (due to the rotational symmetry of $U$) of the curvature $\kappa$. When a needle crystal of parabolic shape is growing with a constant speed $V$ as in FIGURE 3.2, the equation (3.17) takes the form

$$V \cos\theta = U\Big(\kappa, \frac{\partial^2 \kappa}{\partial s^2}, \dots\Big). \tag{3.18}$$

Here $\theta$ is the angle between the direction of growth and the normal vector. As the velocity function $U$, let us adopt the one in (3.6) with $\alpha = \beta = 0$. By using the relation $\kappa = d\theta/ds$, one can reduce (3.18) to

$$V \cos\theta = \theta' + \gamma\theta''', \qquad ' = \frac{\partial}{\partial s}, \tag{3.19}$$

where $\gamma$ corresponds to the surface tension. Using $Vs$ as a new arclength parameter (and denoting it by $s$ again), the last equation becomes

$$\epsilon^2\theta''' + \theta' = \cos\theta, \quad -\infty < s < \infty, \tag{3.20}$$

where we have set $\epsilon \equiv \sqrt{\gamma}V$. By a **needle crystal** for (3.20), we mean a monotonic function $\theta$ of $s$ satisfying the following boundary conditions:

$$\theta(s;\epsilon) \to \pm\frac{\pi}{2}, \quad s \to \pm\infty. \tag{3.21}$$

In case the surface tension effect is absent, namely, when $\epsilon = 0$, (3.20) has the following needle crystal solution:

$$\theta(s;0) = -\frac{\pi}{2} + 2\tan^{-1} e^{s}. \tag{3.22}$$

This corresponds to the Ivantsov solution described in Subsection 3.2.2 (here, indeteminateness of $V$ is not apparent due to the change of variable $s \to Vs$). In (3.20), the surface tension effect appears as the coefficient of the highest order derivative, and hence it serves as a **singular perturbation** effect. When $\epsilon$ is a positive constant and $\delta = 0$ (isotropic case) in (3.6), the following result is obtained by [**230**], [**6**], and [**171**].

THEOREM 3.2 (Non-Existence Theorem). *For any positive constant* $\epsilon$, (3.20) *does not have any needle crystal solution in the isotropic case.*

This theorem says that it is in vain to look for a family of solutions of (3.20) that are continuously connected to (3.22).

Why does (3.20) have no needle crystal?

An intuitive explanation suggests itself, when one views (3.20) from the standpoint of dynamical system theory. Let us consider $(\theta, \theta', \theta'')$ as new unknowns, rewrite (3.20) as a system of first order differential equations, and linearize it around the equilibria $(\pm\pi/2, 0, 0)$. The associated eigenvalues at $(-\pi/2, 0, 0)$ are

$$m_1(\epsilon) = 1 - \epsilon^2 + O(\epsilon^4), \qquad m_{2,3}(\epsilon) = \pm\frac{i}{\epsilon} - \frac{1}{2} + O(\epsilon), \tag{3.23}$$

from which one can show the existence of a one-dimensional unstable manifold corresponding to $m_1$. Similarly, one can show the existence of a one-dimensional stable manifold of $(\pi/2, 0, 0)$. The search for a needle crystal solution for (3.20) is nothing but showing the existence of a heteroclinic orbit connecting the two equilibria. As one can see from FIGURE 3.3, it is almost impossible to make two one-dimensional orbits coincide in a three-dimensional space.

However, it is not so easy as it may look to give a rigorous proof to this theorem, because the problem is more degenerate than the

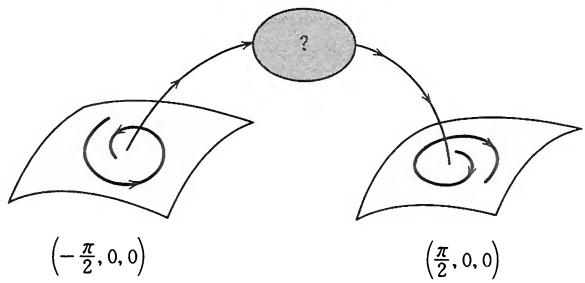


FIGURE 3.3. Heteroclinic orbit for a needle crystal

situation in FIGURE 3.3 due to symmetries inherent in the system. Let us first state the following lemma.

LEMMA 3.3. *For given $C > 0$ and $0 < \epsilon \ll 1$, there exists a solution $\theta(s; \epsilon, C)$ of (3.20), which corresponds to the positive eigenvalue $m_1(\epsilon)$ in (3.23), such that*

$$\theta \to -\frac{\pi}{2} \qquad (as \ \ s \to -\infty), \tag{3.24}$$

$$(\theta + \pi/2)\exp(-m_1(\epsilon)s) \to C \qquad (as \ \ s \to -\infty). \tag{3.25}$$

*Moreover, the constant $C$ is uniquely determined as a function of $\epsilon$, $C = C(\epsilon)$, by demanding that*

$$\theta(0; \epsilon, C) = 0. \tag{3.26}$$

In the sequel, we always understand that $C$ is chosen so that (3.26) is satisfied. The corresponding solution is denoted by $\theta(s; \epsilon)$. The following lemma identifies the condition that makes $\theta(s; \epsilon)$ a needle crystal solution.

LEMMA 3.4. *The necessary and sufficient condition for $\theta(s; \epsilon)$ to be a needle crystal solution (namely, a solution of (3.20) that is monotone increasing and satisfies the boundary conditions (3.21) and $\theta(0) = 0$) is*

$$\theta''(0; \epsilon) = 0. \tag{3.27}$$

In geometric terms, the condition (3.27) is saying that the solution $\theta(s; \epsilon)$ is anti-symmetric around the origin: $\theta(s; \epsilon) = -\theta(-s; \epsilon)$.

Thanks to LEMMA 3.3, the solution $\theta(s; \epsilon)$ of (3.20), (3.24), (3.26) is uniquely determined. If, in addition, this solution satisfies (3.27),

then it is a needle crystal. In fact, one can extend $\theta(s;\epsilon)$ defined on $(-\infty,0]$ to $(-\infty,\infty)$ by reflecting it around $s=0$ as an odd function. The extended function satisfies the differential equation and the boundary conditions. In this sense, the condition (3.27) is called a **solvability condition.**

Unfortunately, the condition (3.27) is never satisfied, as the following result tells us.

THEOREM 3.5. *For each $\epsilon>0$, the solution $\theta(s;\epsilon)$ always satisfies $\theta''(s;\epsilon)>0$ for $s\in(-\infty,0]$. In particular, one has*

$$\theta''(0;\epsilon)\neq 0. \tag{3.28}$$

*Moreover, as $\epsilon\to 0$ the following estimate holds:*

$$\theta''(0;\epsilon)\sim 2k\epsilon^{-5/2}\exp(-\pi/2\epsilon), \tag{3.29}$$

*where $k$ is a nonzero constant.*

One can see from (3.29) that a transcendental part converging to zero faster than any power of $\epsilon$ remains. This means that no conclusion is obtained from merely approximating $\theta(s;\epsilon)$ in ordinary $\epsilon$-power series to test the condition (3.27). In fact, if such an analysis is carried out, then the resulting approximation always satisfies the condition (3.27), and hence an analysis beyond all orders (of $\epsilon$) must be employed. How do we then verify (3.28)? An idea is to extend the variable $s$ to the complex plane as in [**230**], extracting the detailed asymptotic behavior as $\epsilon\to 0$. In this manner, one concludes that (3.20) does not have any needle crystal solution for positive $\epsilon$. Therefore, **the isotropic surface tension effect is not responsible for the pattern selection.**

How about the case where the crystal has anisotropies? It is widely accepted (cf. [**305**], for example) that anisotropy is one of the important factors that determine the magnitude of the tip curvature of growing crystals. Here we take up a geometric model which is slightly different from (3.6), taking an anisotropy into account:

$$\epsilon^2\theta'''+\theta'=g(\theta),\qquad -\infty<s<\infty, \tag{3.30}$$

where

$$g(\theta)=\frac{\cos\theta}{1+\alpha\cos 4\theta},\quad 0<\alpha<1. \tag{3.31}$$

The constant $\alpha$ indicates the intensity of anisotropy, and $\cos 4\theta$ represents the symmetry of the anisotropy. The definition of a needle crystal solution for (3.30) is the same as that for (3.20).

**Question**: For sufficiently small $\epsilon > 0$, can we find values of $\alpha$ $(0 < \alpha < 1)$ for which (3.30) has a needle crystal?

The next result, obtained in [**230**], answers the question.

THEOREM 3.6. *There exist several values of* $\alpha$ *in* (3.31) *for which the anisotropic model* (3.30) *has a needle crystal. The number of such values behaves as* $O(1/\epsilon)$ *when* $\epsilon$ *tends to zero. Therefore there exist infinitely many needle crystal solutions in the limit as* $\epsilon \to 0$.

Roughly speaking, the reason why the new model admits needle crystals is that the anisotropy effect, measured by $\alpha$, introduces oscillatory factors into the right hand side in the asymptotic expansion performed on (3.30) in the same manner as applied to (3.20). A natural question is, of course, among those needle crystal solutions, which will be a physically realizable (stable) one? This is an essential question in pattern selection, to which no decisive answer has yet been given. In terms of the linear stability criterion, it is known ([**41**], [**42**], [**211**]) that the one with largest growth speed is stable.

For the anisotropic Stefan problem (3.1)-(3.2)-(3.5), an integro-differential equation of the interface has been derived by using Green's theorem, and by formally solving its linear eigenvalue problem it has been shown ([**27**], [**17**], for example) that only the solution corresponding to the largest value $\sigma$, which is the parameter in Subsection 3.2.3, is stable in the linearized sense. However, there are several controversies (cf. [**349**]) about these results, and no final conclusion has been reached.

We end this subsection with the following two remarks.

It is in general difficult to experimentally verify the dependency of $\sigma^*$ on the strength $\alpha$ of anisotropy in surface tension. However, for two-dimensional dendrites, there is an interesting prediction made in [**355**].

In the three-dimensional case, a needle crystal solution is *not* close to the Ivantsov paraboloid. This requires us to make some nontrivial corrections and to go through matching arguments with regard to the tail part. A convincing formal analysis was done in [**35**] and [**25**].

**3.2.5. What Causes Side Branches to Grow?** At the end of the last subsection, we mentioned the linear stability of needle crystals. This, however, does not exclude the possibility of growing side branches. In terms of the co-moving coordinate frame that travels with the same speed as the needle crystal, a perturbation given in a

neighborhood of the tip of the crystal grows and at the same time runs away from the tip along the outskirts of the needle crystal. The latter behavior is a propagation type of instability caused by the presence of continuous spectra. Therefore, so long as one observes the tip of the needle crystal from the travelling coordinate system, it keeps its parabolic shape locally (cf. §§3.4 and 3.5).

However, a mathematically rigorous justification (in what kind of function space and for what sort of perturbation class it is stable) of this behavior is yet to be done. If the behavior described in the last paragraph is true, then the **principle of selective noise-amplification** (cf. [**239**] and [**309**]) becomes more convincing; this principle asserts that while a small fluctuation near the tip flows towards the outskirts along the interface, a particular wave length is amplified to produce side branching and gives rise to a dendrite.

Recently, on the other hand, detailed numerical experiments have been performed on the phase-field model (cf. CHAPTER 5) in place of Stefan-type models. For example, according to the work of Kobayashi ([**220**] and [**221**]), it has been discovered that

> the speed of the tip of dendrites is not constant and may become oscillatory depending on the parameters

when the intensity of anisotropy is taken appropriately (cf. §5.4). Such a phenomenon is considered to be caused by Hopf bifurcation, and never occurred in the discussion of Stefan-type models. If this speculation is true, then the emergence of side branches must be related directly to unstable oscillatory modes intrinsic to the system, and hence the principle of selective noise-amplification may be dismissed.

In any case, at present there is no complete explanation of why side branching occurs and what determines the wave length of the side branches. Development of more accurate methods of numerical computation for the phase-field model together with the advancement of theoretical analysis may hopefully bring a breakthrough in the near future.

## 3.3. Wave Speed Selection in the Fisher-Kolmogorov Equation

The fundamental question in the propagation of fronts is to determine in what shape and at what speed local disturbances given in unstable regions spread into the surrounding area. It is, however, very difficult in general to clarify the entire process, starting from the

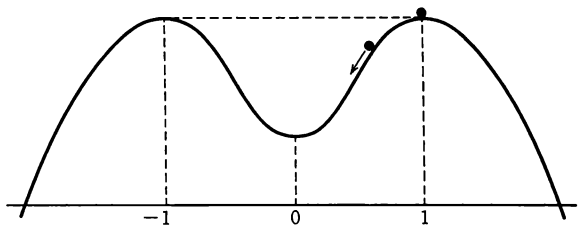


FIGURE 3.4. A particle moving in the quartic potential field with the resistance of friction

initial disturbances, going through the nonlinear dynamic interactions and finally settling down to the most stable propagation mode. In this section, as a prototypical example of propagation waves invading unstable regions, we study the following Fisher-Kolmogorov equation (FKE), with special attention given to how the wave speed is selected:

$$u_t = u_{xx} + u - u^3. \tag{3.32}$$

This equation has the form of GLE, treated in CHAPTER 2, restricted to the one-dimensional real space. Clearly, $u = 0$ is unstable, while $u = \pm 1$ are stable. Let us consider the situation in which the state $u = 1$ is invading the unstable state $u = 0$. What is the speed of this propagation? This is not a trivial question, because if we search for the front solution in the form of a travelling wave $u(x - ct)$ (with $c$ being the speed), then the possible speed is not uniquely determined but exists as a one-parameter family. The latter situation can be intuitively understood by arguing as follows. The front solution $u(\xi)$, together with the unknown speed $c$, has to satisfy the following set of equations:

$$u_{\xi\xi} = -cu_\xi - \frac{d}{du}\Big(\frac{1}{2}u^2 - \frac{1}{4}u^4\Big), \tag{3.33}$$

$$u(+\infty) = 0, \tag{3.34}$$

$$u(-\infty) = 1, \tag{3.35}$$

where $\xi = x - ct$ is the travelling coordinate with speed $c$. The equation (3.33) is thought of as describing the motion of a particle moving in the potential field $V = u^2/2 - u^4/4$ with the resistance $c$ of friction (cf. FIGURE 3.4).

For an arbitrary positive friction coefficient $c$, the orbit emanating from $u = 1$ at time $\xi = -\infty$ (with $u_\xi = 0$) always converges to $u = 0$

at time $\xi = \infty$. If $c$ is not too large, the orbit decays in an oscillatory manner around $u = 0$.

Even if solutions are restricted to nonnegative ones, the indeterminateness of the speed $c$ remains. Namely, if the friction $c$ is larger than a certain critical value, the particle keeps its position at positive $u > 0$ and converges monotonically to $u = 0$. Note that this behavior of the particle is the same for any friction coefficient $c$ greater than or equal to the critical value $c^*$ (which in fact equals 2). Therefore, a wave speed cannot be selected by considering the existence of travelling waves alone.

With regard to the last question, a result was first given by Kolmogorov et al. [**228**], in which it was shown that the solutions with initial conditions of Heaviside function type converge with asymptotic phase to the travelling wave of minimal speed $c^*$. Later, Aronson and Weinberger [**10**] showed that, starting from initial conditions of more general and physically natural type, and including functions with compact support, the wave speed of the corresponding front solutions asymptotically approaches the minimal speed $c^*$ ($c^* = 2$ for (3.32)). The method of proof is an elegant one based upon the comparison principle, and their result was the first, ground-breaking one in this direction of research.

What we want to do in this chapter is to single out the more fundamental framework, if exists, through which the selection mechanism of the wave speed $c^* = 2$ becomes apparent. Such a consideration will give rise to a useful viewpoint in application to a wider class of equations for which the comparison principle does not work, as well as in considering pattern selection problems in general.

Let us first recall the result of [**10**] in terms of the following equation:

$$u_t = u_{xx} + f(u), \tag{3.36}$$

where

$$\begin{aligned} &f \in C^1[0,1], \quad f(0) = f(1) = 0, \\ &f'(0) > 0, \quad f'(1) < 0, \\ &f(u) > 0, \quad 0 < u < 1. \end{aligned} \tag{3.37}$$

We are interested in the solutions $u(x - ct)$, which depend only on $\xi = x - ct$ and satisfy the conditions

$$u(-\infty) = 1, \quad u(+\infty) = 0, \quad 0 \le u \le 1. \tag{3.38}$$

Such functions are called front solutions of (3.36) and satisfy the following ordinary differential equation:

$$w'' + cw' + f(w) = 0, \tag{3.39}$$
$$w(-\infty) = 1, \quad w(+\infty) = 0, \quad 0 \le w \le 1.$$

Let us define the function space

$$X = \{u \mid u \in C^0(\mathbb{R}), \ 0 \le u \le 1\}.$$

Let $c^* > 0$ be the **minimal wave speed** for which (3.39) has a solution. The next result is known ([**10**], [**11**]) for the asymptotic travelling wave speed of front solutions.

THEOREM 3.7. (1) *Let $u(x,t)$ be a solution of* (3.36) *with initial condition $u(x,0) \in X$. If $u(x,0) \equiv 0$ for $x \in [x_0, +\infty)$ for some $x_0$, then, for each $\xi$ and $c > c^*$,*

$$\lim_{t\to\infty} u(\xi + ct, t) = 0.$$

(2) *If, moreover, $u(x,0) \not\equiv 0$, then, for each $\xi$ and $|c| < c^*$,*

$$\lim_{t\to\infty} u(\xi + ct, t) = 1.$$

REMARK 3.8. For the characterization of the critical value $c^*$ in terms of $f$ and the fact that it is uniquely determined, we refer, for example, to Chapter 4 of [**94**]. It is known that for $f(u) = u(1-u)$, the minimum speed is $c^* = 2$, and for $f(u) = u(1-u)(1+\nu u)$ (with $\nu > -1$), it is given by $c^* = 2$ (if $-1 < \nu \le 2$) and $c^* = (\nu+2)/\sqrt{2\nu}$ (if $\nu \ge 2$).

REMARK 3.9. For $0 < c < c' := 2\sqrt{f'(0)}$, there exists no non-negative front solution. The reason is simply that for such a $c$ the point $(0,0)$ is a stable spiral point and hence any orbit approaching $(0,0)$ inevitably goes into the negative side. This implies that $c^* \ge 2\sqrt{f'(0)}$.

REMARK 3.10. Since the equation (3.36) is invariant with respect to the change of variable $x \to -x$, if $u(x,0)$ is of compact support, then for each $\xi$ and $|c| > c^*$ we have that $\lim_{t\to\infty} u(\xi + ct, t) = 0$.

### Wave Speed Selection via the Limit of Structurally Stable Systems

In THEOREM 3.7, it was shown that the asymptotic travelling speed of front waves is $c^*$. What is it that selects the minimal speed?

One way of viewing this is that the existence of a continuum of front solutions is a degeneracy caused by an inadequate setting of the problem, and hence, by looking at the problem as a limit of structurally stable systems, the selection of the wave speed may be naturally understandable (cf. [**65**]). To be more specific, let us consider (3.36) with the following nonlinearity:

$$f(u) = \begin{cases} u(1-u) & (u \geq 0), \\ \\ \frac{u}{b}(u+b) & (u < 0), \end{cases} \qquad (b > 0). \tag{3.40}$$

In the region $u \geq 0$, THEOREM 3.7 is applicable, giving the asymptotic wave speed $c^* = 2$ (cf. REMARK 3.8). In the extended region $u \geq -b$, $f$ is of bistable type and $u = -b, u = 1$ are the stable equilibria. In the two-dimensional first order system associated with (3.39),

$$\begin{cases} w' = z, \\ z' = -cz - f(w), \end{cases} \tag{3.41}$$

the equilibria $(-b, 0)$ and $(1, 0)$ are saddle points; the stable manifold of $(-b, 0)$ and the unstable manifold of $(1, 0)$ are both one-dimensional. Therefore, in this case, by choosing the value $c$ appropriately one expects to find a unique front solution connecting these points. In fact, the following is available ([**139**], [**94**]).

PROPOSITION 3.11. *For the nonlinearity $f$ in* (3.40), *there exists a unique front solution $u^1_{-b}$ connecting $u = -b$ and $u = 1$ with wave speed $c_b$. This solution is exponentially asymptotically stable in the topology of uniform convergence, up to asymptotic phase shifts.*

Bistable systems are structurally stable in the sense of the last proposition. Our aim here is to characterize the wave speed selection of the front solution connecting 1 and 0 as the limit of the front solutions of the bistable system connecting $-b$ and 1 as $b \to 0$. We have

THEOREM 3.12. $\lim_{b \to 0} c_b = 2$.

The proof, to be omitted here, is achieved by a phase plane analysis. Intuitively one can understand it from the profile of the potential in FIGURE 3.5 as follows. In order to go from the higher summit at $u = 1$ through $u = 0$ and reach and stop at the lower summit at $u = -b$, the friction coefficient $c_b$ is uniquely determined, and hence $\lim_{b \to 0} c_b$ has to be the minimal friction coefficient $c^* = 2$.

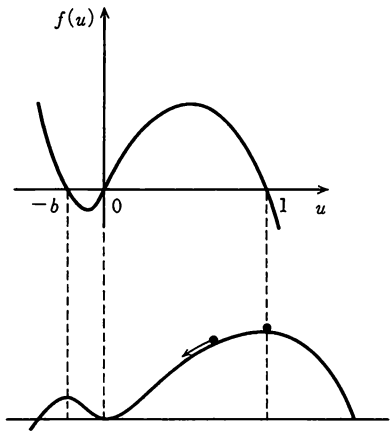


FIGURE 3.5. Wave speed selection via the limit of structurally stable systems

In the above, we described how to treat a degenerate problem as a limit of structurally stable systems only in the wave speed selection of front solutions. Such an idea, hopefully, will prove to be useful in other pattern selection problems.

In the next section, we return to the original Fisher-Kolmogorov equation, and discuss, from the dynamical system point of view, the reason why solutions approach the front solution of minimal speed.

## 3.4. Marginal Stability Criterion and Its Applications

The marginal stability criterion is useful in the pattern selection problem for frontal waves invading an unstable region, especially for the selection of the wave speed, as well as the wave length created behind it. This criterion is believed to be applicable to various equations, ranging from scalar equations to reaction-diffusion systems for which the comparison principle is not available. In particular, the **linear marginal stability criterion** (LMS) is highly valuable in practice, since it requires us to examine only the dispersion relation of the linearized equation in unstable regions.

However, when the effect of nonlinearity becomes substantial, the contribution from the linear part naturally is not sufficient and LMS loses its power. Even in the latter regime, the idea of a marginal stability criterion itself is still effective, and the system in that regime

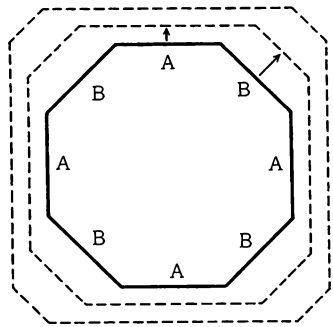


FIGURE 3.6. Slowly growing facets dominate the system.

then enters the territory of **nonlinear marginal stability criteria** (NMS), although the computation of the selected wave speed is not so easy as in LMS. In order to judge the limitation of LMS, it is important to clarify the mechanism of transition from LMS-regime to NMS-regime.

In the next subsection 3.4.1, we will present a physical intuition into pattern selection mechanisms, especially into the reason why the minimal wave speed is selected. In subsection 3.4.2, we will explain the relationship between LMS and NMS by way of the example of a scalar reaction-diffusion equation. In particular, we will discuss a geometric characterization of the transition from LMS to NMS. The content of this subsection was strongly motivated and inspired by an excellent series of works by van Saarloos and his coworkers [**346, 347, 348**].

**3.4.1. Physical Background of Speed Selection.** It seems, at first glance, to go against our intuition that the slowest propagation speed is selected. When waves with faster and slower propagation speed coexist, the faster ones can never be caught by the slower ones and the faster ones catch up with the slower ones ahead, and in any case, one can imagine that the waves as a whole finally propagate with the faster speed. However, this is not the case if we start with natural initial conditions.

Let us consider the situation of crystal growth depicted in FIGURE 3.6. The initial facets are drawn in solid lines, and let us suppose that facets $A$ grow slowly compared with facets $B$. As time passes, the faster growing facets $B$ disappear and the slowly growing facets

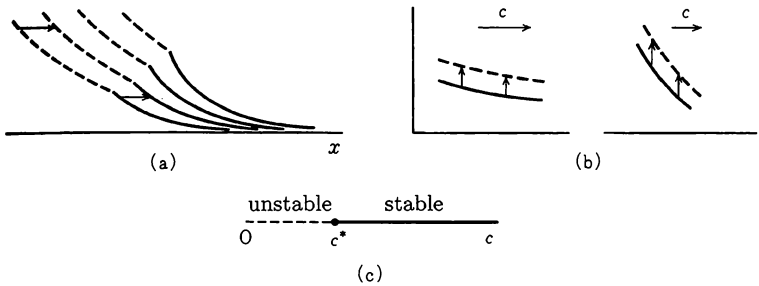


FIGURE 3.7. (a) The migration of intersection points between fast fronts and slow fronts. (b) Propagation speeds of envelopes. (c) Wave speeds and stability. (Transcribed from FIGURE 3 of the reference [**346**])

dominate the entire configuration. Here the rule for determining the position of new facets after a period $\Delta t$ of time is as follows. Each facet grows with its own speed of growth, and the intersecting points among the extensions of translated facets determine the new set of facets.

The same behavior occurs in propagation fronts invading unstable regions. Let us assume that in a neighborhood of an unstable region the rate of growth is constant. As in FIGURE 3.7 (b), let us first note that the smaller the slope of profiles, the faster is the propagation speed of the envelope of the profiles. We take initial functions of compact support and assume that the growth speed is constant near the tip of fronts. Adopting the same rule for the determination of the new profile as for the facets in FIGURE 3.6, it is expected that the intersection of the fast moving envelope and the slowly moving one migrates as in FIGURE 3.7 (a). This means that the slowly moving region expands more and more.

If there exists a family of wave fronts parametrized by the propagation speed $c$, then the waves with extremely slow speed are expected to be unstable because waves invading unstable regions with slow speed are immediately accelerated by the force of diffusion. On the other hand, waves with speed greater than a certain value are considered to be locally stable, and their speed of propagation will decrease as discussed above.

As a result, the minimal speed $c^*$ in the stable region as in FIGURE 3.7 (c) is selected. In other words, the slowest wave speed is selected.

Since the value $c^*$ is a **marginal stability point** where the stability property of the system changes, this selection rule is called the **marginal stability criterion**. In the above, it was said that the waves with speed greater than a certain value are stable. This statement appears contradictory to the slowing down of wave propagation. However, the meaning of stability here is relative to a special class of perturbations that are extremely close to the frontal waves. Moreover, the situation we are concerned with for the moment is outside of this class; hence no contradiction arises (cf. §3.5 for more detail).

**3.4.2. Linear and Nonlinear Marginal Stability Criteria.** The reason why the marginal stability criterion has attracted a great amount of attention is not only that it gives an important guideline to ideas in dealing with pattern selection problems, but also that it serves as a practical criterion. Especially, the linear marginal stability criterion (LMS), despite its limited applicability, is a simple and very useful criterion for a certain range of problems. When waves migrate towards unstable regions, their amplitude at the tip of fronts is not so large. Therefore, LMS may be effective under the premise that the selection criterion obtained from the linearized equation near the tip of fronts (the unstable region) determines the pattern selection of the entire system.

Why is it that LMS applies so effectively to solutions with finite amplitude, despite its foreseen limitation? What we have been considering so far is a wave motion in which a stable constant state invades the region of an unstable state, such as in the FK-equation. Consequently, the existence of a one-parameter family of travelling waves followed. Looking into the dynamics in a neighborhood of the front of the wave to be selected, one will find an eigenmode associated with its center-unstable direction. Since it is also expected that the principal part of the eigenmode is concentrated near the tip of the front, instead of being located in the stable region, the dynamics of the entire system will resemble that of the tip. The situation is completely different in bistable systems. Since in bistable systems there exists only one candidate for the wave speed, the selection mechanism relies genuinely on the nonlinearity and hence cannot be clarified by just looking at a subportion of the system.

The evolution of a small perturbation around an unstable constant state (0, for simplicity) is expected to be determined by a dispersion relation. Namely, substituting a perturbation $\psi$ of the form

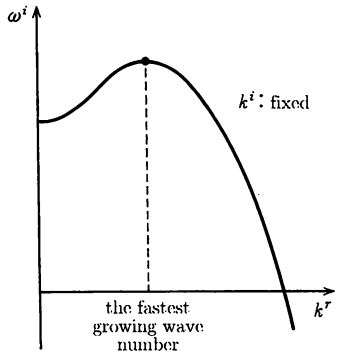


FIGURE 3.8. Wave number vs. growth rate relation.

$\psi \sim e^{-i\omega t+ikx}$ into the linearized equation around 0

$$\psi_t = L\psi, \tag{3.42}$$

one obtains the dispersion relation, expressing $\omega$ as a function of $k$,

$$\omega = \omega(k), \tag{3.43}$$

that determines the dynamics of (3.42). Here and below, $k$ and $\omega$ are allowed to be complex numbers, and the existence of a relation such as (3.43) is taken for granted.

What are the shape and speed of the perturbation that dominates the dynamics? The quantity $k^i := \text{Im } k$ determines the order of spatial decay at infinity and the shape of the envelope, while $k^r := \text{Re } k$ dictates the wave number within the envelope. On the other hand, $\omega^i := \text{Im } \omega$ determines whether the perturbation decays or grows, and $\omega^r := \text{Re } \omega$ describes whether the temporal behavior is oscillatory or monotone. Keeping $k^i$ fixed, assume that the temporal growth rate $\omega^i$, as a function of the wave number $k^r$, has the functional form as in FIGURE 3.8.

The character of the dynamics comes from the wave number $k^r$ at which

$$\frac{\partial \omega^i}{\partial k^r} = 0 \quad \text{and} \quad \frac{\partial^2 \omega^i}{\partial (k^r)^2} < 0. \tag{3.44}$$

If such a value of $k^r$ is unique, then the value $k^r$ is considered as a function of $k^i$. So in the sequel, we treat $k^i$ as being the only

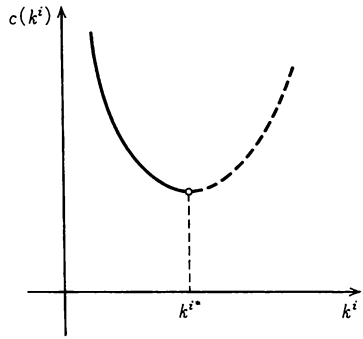


FIGURE 3.9. Decay rate vs. phase velocity relation.

independent variable. The **phase velocity**

$$c = \frac{\omega^i}{k^i} \tag{3.45}$$

of the wave with the largest growth rate is also a function of $k^i$, $c = c(k^i)$.

Let us also assume that the functional form of $c$ is as depicted in FIGURE 3.9. The behavior $c \to \infty$ as $k^i \to \infty$ comes from our hypothesis, namely, that the stationary state 0 is unstable ($\omega^i > 0$) relative to Fourier modes with wave length $k_c$ (corresponding to no decay, and hence $k^i = 0$). If waves with slower speed tend to be dominant, then the wave length with minimum speed, $\frac{\partial c}{\partial k^i} = 0$ ($k^{i*}$ in FIGURE 3.9), will be selected. Since

$$\frac{\partial c}{\partial k^i} = \frac{1}{(k^i)^2}\left(\frac{\partial \omega^i}{\partial k^i}k^i - \omega^i\right), \tag{3.46}$$

the minimum is attained at $\frac{\partial \omega^i}{\partial k^i} = \frac{\omega^i}{k^i}$. Therefore, recalling (3.44), the wave speed to be selected is determined by

$$c^* = \frac{\omega^i}{k^i} = \frac{\partial \omega^i}{\partial k^i}, \qquad \frac{\partial \omega^i}{\partial k^r} = 0. \tag{3.47}$$

The last conditions, obtained by the **linear marginal stability criterion**, give the selected wave speed $c^*$ and the corresponding wave number $k^*$. The significance of the criterion is that it is very simple and practical.

What is an intuitive meaning of the conditions in (3.47) obtained by LMS? What is their relation to marginal stability? It turns out

that the two conditions in (3.47) are closely related to the following two fundamental instabilities pertinent to the propagation of interfaces including frontal waves:

(i) **Growth Instability**;

(ii) **Propagation Instability**;

Growth (resp. propagation) instability is sometimes called *absolute* (resp. *convective*) instability. When a particular wave number $k_0$ is perturbed to $k = k_0 + \Delta k$ ($\Delta k \in \mathbb{R}$), the major variation of amplitude in the $e^{-i\omega t}$-part is given by

$$e^{\frac{\partial \omega^i}{\partial k^r} \Delta k t},$$

and hence if $\partial \omega^i / \partial k^r \neq 0$, then by choosing $\Delta k$ in such a way that $\frac{\partial \omega^i}{\partial k^r} \Delta k > 0$, the amplitude can be made exponentially growing (growth instability). Therefore, the relation

$$\frac{\partial \omega^i}{\partial k^r} = 0$$

is the marginal stability condition.

On the other hand, propagation instability is the instability of a small localized perturbation of the fronts. The instability of this type propagates with the **group velocity** $c_g = \partial \omega^i / \partial k^i$. Recall that the **phase velocity** was defined by $c_{ph} = \omega^i / k^i$. If $c_{ph} < c_g$, the localized perturbation reaches the unstable region prior to the front, giving rise to instability. If $c_{ph} > c_g$, then the front goes ahead of the perturbation and is expected to be stable (in a space with an appropriate weight) in reference to the co-moving coordinate frame with speed $c_{ph}$. Therefore the condition $c_{ph} = c_g$ is the marginal stability condition for this class of perturbations.

Let us apply LMS to the Fisher-Kolmogorov equation (3.32) treated in §3.3. The linearized equation around $u = 0$ is given by

$$\psi_t = \psi_{xx} + \psi, \tag{3.48}$$

which gives rise to the dispersion relation

$$\omega = i - ik^2. \tag{3.49}$$

The condition $\partial \omega^i / \partial k^r = 0$ implies $k^r = 0$. Also, the relation $\omega^i / k^i = \partial \omega^i / \partial k^i$ ($= c^*$) naturally gives $c^* = 2$, which agrees with the rigorous result stated in §3.3 (cf. THEOREM 3.7, REMARK 3.8). It is somewhat surprising that conditions in LMS alone determine the wave speed to be selected, despite the facts that the FK equation is not a small

perturbation of the linear equation (3.48) and that the front solution is a finite amplitude solution connecting the states $u = 0$ and $u = 1$.

This phenomenon may be explained as follows. Due to the concentration of the principal part of the dominant eigenmode near the tip of the wave front, the dynamics of the entire system is essentially reduced to the dispersion relation for the linearized equation around the unstable state; that is to say, there exists a reduction mechanism. However, there is no mathematically rigorous proof of the validity of the criterion based on this reduction mechanism.

LMS naturally has its limitations. When the effect of nonlinearity becomes strong enough, the **nonlinear marginal stability criterion** has to be employed. In order to explain the criterion in concrete terms, let us deal with the following equation, proposed by Ben-Jacob et. al. [**28**]:

$$u_t = u_{xx} + f_b(u), \tag{3.50}$$

$$f_b(u) := \frac{u}{b}(1-u)(b+u) \quad (b > 0). \tag{3.51}$$

Although the equation is qualitatively the same as (3.32), the effect of nonlinearity becomes strong as $b \to 0$. The linearized equation around $u = 0$, however, does not depend on $b$. Therefore, the wave speed of the front connecting $u = 0$ and $u = 1$ that is to be selected according to LMS is $c^* = 2$, independent of $b$.

Is it true that the selected speed $c^* = 2$ is independent of $b$? According to the characterization of $c^*$ due to [**10**], [**11**], $c^* = 2$ is uniquely determined for the case $b \geq 1$, where the nonlinearity $f_b$ is concave on $(0, 1)$, which coincides with the wave speed selected by LMS. However, when $0 < b < 1$, the nonlinear effect is so strong that the validity region of LMS starts to shrink, and one needs a more careful analysis.

To carry out the detailed analysis, let us first note that (3.50) has the following family of special solutions, which is confirmed by direct computations:

$$c = c_b := (2b)^{\frac{1}{2}} + (2b)^{-\frac{1}{2}}, \tag{3.52}$$

$$u_c(x) = \frac{1}{2}\Big(1 - \tanh\frac{q(x-ct)}{2}\Big), \tag{3.53}$$

$$q = \begin{cases} q_1, & b \geq 1/2 \\ q_2, & 0 < b < 1/2, \end{cases} \tag{3.54}$$

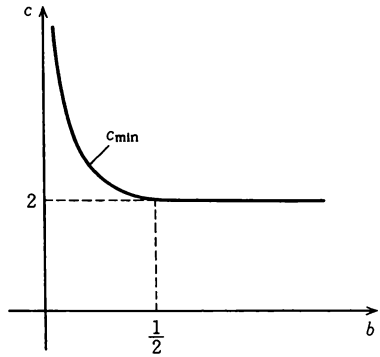


FIGURE 3.10. The selected wave speed varies with the strength of nonlinearity.

where

$$q_1 = \frac{c}{2} - \left[\frac{c^2}{4} - 1\right]^{\frac{1}{2}}, \tag{3.55}$$

$$q_2 = \frac{c}{2} + \left[\frac{c^2}{4} - 1\right]^{\frac{1}{2}}. \tag{3.56}$$

THEOREM 3.7 predicts that the frontal wave that has the minimum speed among positive solutions is to be selected. For the solutions of (3.50) with range $0 \leq u \leq 1$, what is the functional form of the minimum speed as a function of $b$?

PROPOSITION 3.13. *The minimum wave speed of positive solutions of* (3.50) *is given by*

$$c_{\min} = \begin{cases} 2, & b \geq 1/2, \\ c_b = (2b)^{1/2} + (2b)^{-1/2}, & 0 < b < 1/2, \end{cases}$$

*which is at the same time the speed to be selected* (*cf.* FIGURE 3.10).

The special solutions given above actually correspond to those that have the minimum speed. As PROPOSITION 3.13 says, for $0 < b < 1/2$ the wave speed to be selected is not the $c^* = 2$ predicted by LMS, but is larger than that. Moreover, $\lim_{b \to 0} c_b = \infty$, showing that LMS breaks down when the nonlinearity has strong effects. However, as we will see in the next section, the property of **marginal stability** is maintained even in the case where $0 < b < 1/2$; that is to say, solutions with speed larger than $c_b$ are stable while those

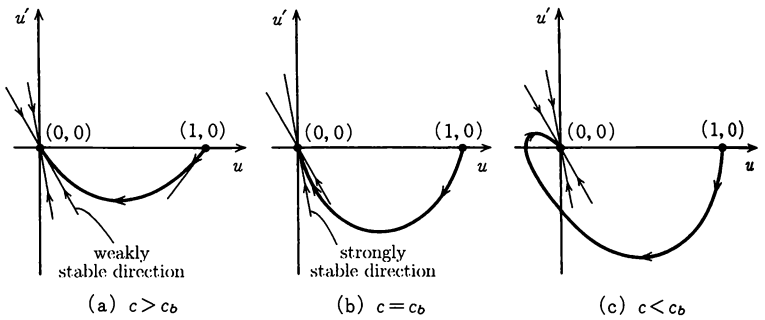


FIGURE 3.11. Varieties of behavior of a nonlinear marginally stable orbit ($0 < b < 1/2$). Only when $c = c_b$ does the unstable manifold of $(1, 0)$ enter into $(0, 0)$ from the strongly stable direction.

with speed slower than $c_b$ are unstable. Again, the selected wave speed $c_b$ is the minimum among the wave speeds of stable solutions. In this sense, one can adequately say that the **nonlinear marginal stability criterion** is valid even in the region $0 < b < 1/2$.

The proof of PROPOSITION 3.13 becomes apparent from the following geometric characterization of the marginally stable wave speed $c_b$. The same geometric information will play an essential role in the next section, when one tries to verify the validity of the stability criterion.

THEOREM 3.14. *In the phase plane, the orbit of the front solution* (3.53) *of* (3.50) *approaches the stable node* $(0, 0)$ *along the* **strongly stable direction** *if and only if its wave speed is the critical one* $c = c_b$ $(0 < b < 1/2)$. *The solution is monotone for* $c \geq c_b$, *while it becomes non-monotone for* $c < c_b$ *and is not always positive any more. The profile of the orbit varies with* $c$ *as in* FIGURE 3.11.

PROOF. We will present only an outline. Rewriting (3.50) as in (3.41), the front solution corresponds to the heteroclinic orbit that joins $(1, 0)$ to $(0, 0)$. The eigenvalues of linearization around the equilibrium $(0, 0)$ are $-q_1$ and $-q_2$ in (3.55) and (3.56), respectively, and hence the equilibrium is a stable node for $c \geq 2$ and a stable spiral for $c < 2$. The latter statement is true independently of $b$. However, the one-dimensional unstable manifold of the saddle point $(1, 0)$ varies as $b$ changes.

Roughly speaking, when the nonlinear effect becomes strong as $b$ gets small, the lower branch of the unstable manifold is pushed downward, and therefore in order to make it converge to $(0,0)$ with its positivity being kept, one needs to employ a large friction rate $c$. Since $(0,0)$ is a stable spiral for $c < 2$, as long as positive front solutions are concerned, one needs to consider the case in which $c \geq 2$. For $c > 2$, there is only one orbit that approaches $(0,0)$ along the strongly stable direction (the eigendirection corresponding to the eigenvalue with largest absolute value) (cf. FIGURE 3.11 (b)).

There are two ways in which the solution on the unstable manifold of $(1,0)$ loses its positivity. One way is, as already mentioned, the case where $(0,0)$ is a stable spiral for $c < 2$. The other is the case in which $(0,0)$ remains as a stable node and the unstable manifold of $(1,0)$ goes around the strongly stable direction and approaches $(0,0)$ along the weakly stable direction on the opposite (negative) side (cf. FIGURE 3.11 (c)).

Depending upon the value of $(b,c)$, one or the other of the two cases is primarily realized, distinguishing whether LMS or NMS is operative. In fact, when $b > 1/2$, the nonlinear effect is not strong enough that the former case is primarily realized as $c$ is decreased. On the other hand, when $0 < b < 1/2$, the unstable manifold of $(1,0)$ converges to $(0,0)$ along the strongly stable direction, as in FIGURE 3.11 (b), at $c = c_b > 2$. As $c$ decreases below this value $c_b$, the unstable manifold overshoots and converges to $(0,0)$ along the weakly stable direction on the opposite side as in FIGURE 3.11 (c), losing positivity and monotonicity. □

REMARK 3.15. We note that the solution selected by NMS is geometrically characterized as an orbit that approaches an equilibrium along a strongly stable direction. This remark is important, because such a geometric characterization of NMS may serve as a guiding principle for more general systems of differential equations (cf. [**310**]).

REMARK 3.16. The effective applicability of LMS and NMS for many types of equations, such as the complex Ginzburg-Landau equation and the Swift-Hohenberg equation treated in CHAPTER 2, is at least numerically well tested (cf. [**91**], [**89**], [**90**], [**346**], [**347**] and [**28**]). A mathematically rigorous theory for these equations with a clear geometric characterization seems to still be missing, and awaits further developments.

## 3.5. Credibility of Marginal Stability Criterion

We will show that the marginal stability criterion actually holds in the wave speed selection problem for front solutions of (3.50) treated in the previous section.

As we have seen in §3.3, among the positive (or monotone) solutions the one with minimum wave speed is selected. The proof of this fact, however, depended on the comparison principle, and hence it is desirable to have a different selection principle applicable to more general cases. We here deal with all the travelling wave solutions, dropping the condition that they be positive (or monotone). We will show in this setting that among the travelling waves in the family, the one at which the stability property changes (the marginally stable one) is selected. This criterion, which already appeared in §3.2 for crystal growth processes, will be rigorously treated for (3.50). As mentioned at the beginning of the present chapter, in order to talk sensibly about stability, a class of relevant perturbations and a gauge to measure the perturbations have to be defined. For example, front solutions are always unstable relative to a class of seemingly natural perturbations, as demonstrated in the following theorem.

THEOREM 3.17. *The front solutions of* (3.50) *that connect* 0 *to* 1 *are unstable relative to perturbations that belong to* $L^p(\mathbb{R})$, $C_{\mathrm{unif}}(\mathbb{R})$ *or* $C_0(\mathbb{R})$.

PROOF. This theorem is established by showing that the essential spectra of the linearization around the front solutions always have positive real part. For this, the following lemma plays a key role (we refer to [**176**] for its proof).

LEMMA 3.18. *Let* $L$ *be a linear operator defined by*

$$Lu = u_{xx} + a(x)u_x + b(x)u, \tag{3.57}$$

$$\lim_{x\to\pm\infty} a(x) = a_\pm, \qquad \lim_{x\to\pm\infty} b(x) = b_\pm, \tag{3.58}$$

*on* $\mathbb{R}$. *On any one of the spaces above, the essential spectrum of* $L$ *is contained in the following parabolic region:*

$$\sigma_e(L) \subset \left\{ \lambda \in \mathbb{C} \;\middle|\; \mathrm{Re}\lambda \le -\frac{(\mathrm{Im})^2}{a_\pm^2} + b_\pm \right\}, \tag{3.59}$$

*in which the right hand side is replaced by the half interval* $(-\infty, b_\pm]$ *when* $a_\pm = 0$. *In particular,*

$$\max \operatorname{Re} \sigma_e(L) = \max(b_+, b_-). \tag{3.60}$$

PROOF OF THEOREM 3.17. Since $f_b'(0) = 1$ (independent of $b$), the last lemma implies that in any one of the spaces above, we have

$$\max \operatorname{Re} \sigma_e(L) = 1, \tag{3.61}$$

where $L$ is the linearization of (3.50) around the front solutions in terms of the co-moving coordinate system. Therefore, applying Corollary 5.1.6 of [**176**], the front solution is unstable. □

One can intuitively understand the reason why the front solutions are all unstable as follows.

Pick a front solution $u_c(x,t) = v_c(x - ct)$ ($v_c(\infty) = 0$, $v_c(-\infty) = 1$) with speed $c$. Since the front solutions exist in the one-parameter family, one can choose $c'$ near $c$ ($c' > c$) and take

$$u_{c'}(x,t) - u_c(x,t) \tag{3.62}$$

as a perturbation. Since all front solutions decay exponentially to both 0 and 1 at $\pm\infty$, by choosing $c'$ sufficiently close to $c$, the perturbation in (3.62) can be made arbitrarily small at $t = 0$ in all of the function spaces in THEOREM 3.17. However, the perturbation, observed from the travelling coordinate system with speed $c$, grows in terms of any one of the norms, since $c' > c$ causes the perturbation to spread forward, resulting in a large deviation of phase. This phenomenon is precisely the propagation instability discussed in §3.4.2. In other words, *propagation instability is caused by essential spectra.*

The situation above differs substantially from the bistable case (compare with PROPOSITION 3.11). The reason is that the travelling waves considered above are those invading the unstable region $u \equiv 0$, and therefore perturbations in this region, unless restricted by strong conditions, will grow immediately. This means that to obtain stability we have to restrict perturbations to a smaller class.

Such a restriction may seem stringent at first glance, but it is not so if one recalls the origin of the problem. In fact, one natural way of setting up the problem is to ask how a small fluctuation evolves when the system is all at once placed in an unstable state, caused by a sudden change of temperature or concentration. In such a situation, naturally, perturbations are localized and of compact support. Also,

in a dendritic crystal growth process, natural perturbations in reference to the travelling coordinate system are those localized at the tip of the crystal. If one uses a norm that uniformly takes account of perturbations far from the tip, then the dendrite is unstable.

Let us introduce the following weighted space in order to eliminate the propagation instability caused by essential spectra:

$$L^p_w(\mathbb{R}) = \left\{ v \;\middle|\; \left( \int_{-\infty}^{\infty} \left| \frac{v(x)}{w(x)} \right|^p dx \right)^{1/p} < \infty \right\}, \quad 1 \le p \le \infty, \tag{3.63}$$

$$w(x) > 0, \quad \frac{w'(x)}{w(x)} \to -\mu, \quad \frac{w''(x)}{w(x)} \to \mu^2, \quad x \to \infty, \tag{3.64}$$

where $\mu$ is any real number that satisfies $\mu^2 + c\mu + 1 < 0$ and $w(x)$ is a smooth function that is uniformly bounded at $x = -\infty$. Note that the weight is chosen so that it has an effect only at $x = \infty$ to eliminate the propagation instability spreading into the unstable region. With the weighted space at our disposal, we have the following.

THEOREM 3.19. *Let* $c_{\min}$ *be as given in* PROPOSITION 3.13. *For* $c > c_{\min}$ (*resp.* $c < c_{\min}$), *the front solution is asymptotically stable* (*resp. unstable*) *in the weighted space* $L^p_w(\mathbb{R})$.

REMARK 3.20. The stability in the last theorem is actually exponential and asymptotic, up to phase shifts. Such a stabilization method with the help of weighted spaces is due to [**327**], [**328**].

PROOF. We first show that for any $c > 2$, independent of $b$, the instability caused by the essential spectrum can be eliminated by choosing the weight appropriately. On the other hand, such a trick is not possible for $c < 2$, and propagation instability occurs there. The instability for $0 < b < 1/2$ where $c_{\min} > 2$ is caused by the discrete spectrum, which will be discussed later. Examining the essential spectrum as in LEMMA 3.18, one finds for $c^2 > 4$ that

$$\max \operatorname{Re} \sigma_e(L_w) = \mu^2 + c\mu + 1 \tag{3.65}$$

(see Chapter 5 of [**176**] for details). Note that the inequality $c^2 > 4$ follows for any $b$ from PROPOSITION 3.13. The operator $L_w$ here is defined by $L_w v \equiv \frac{1}{w} L(wv)$. By choosing $\mu$ so that $\mu^2 + c\mu + 1 < 0$, which is possible because $c^2 > 4$, one can push the essential spectrum to the left half plane.

Note that the two real eigenvalues associated with the stable node $(0, 0)$ are the two roots of the equation $\mu^2 + c\mu + 1 = 0$. This implies

that the decay exponent of the weight function $w$ at $x = \infty$ falls into the interval between these two eigenvalues. Therefore, regardless of the choice of $\mu$, the right end point of the essential spectrum approaches the origin as $c \to 2$. When $c < 2$, the essential spectrum sticks out into the right half plane, and hence the front solution is unstable no matter what type of weight is employed. This indicates that one cannot stabilize the essential spectrum unless the wave speed is rather large. But, why does instability set in when the wave speed is small?

An intuitive answer to this question is as follows. Assume that a perturbation is growing in the form

$$e^{\Omega t - \gamma x} \qquad (\Omega > 0, \ \ \gamma > 0). \tag{3.66}$$

When observed relative to the travelling coordinate $\xi = x - ct$, the perturbation exhibits itself as

$$e^{\Omega t - \gamma(\xi + ct)}. \tag{3.67}$$

The perturbation growing exponentially with respect to the fixed coordinate $x$ now decays exponentially with respect to the travelling coordinate $\xi$ if the condition

$$c > \frac{\Omega}{\gamma} \tag{3.68}$$

is satisfied. This argument is of course not valid for small $c$. The same thing happens even if our attention is restricted to compact intervals. Therefore, even when a front is subjected to a perturbation, the front can keep its shape if it travels faster than the perturbation does. Although the perturbation is growing in the regions far away from the front, it can be regarded as small by adding an appropriate weight. This is an intuitive explanation of why waves travelling fast enough can be made stable with respect to a corresponding travelling coordinate. □

Let us next examine the behavior of the discrete spectrum. We first show the following.

PROPOSITION 3.21. *For a front solution with speed $c > c_{\min}$, discrete eigenvalues of the linearization have negative real part, except for the simple eigenvalue* 0 *which corresponds to translational freedom.*

PROOF. With $w(\xi) = e^{-c\xi/2}$ as the weight function, the eigenvalue problem $L_w v = \lambda v$ takes the following form:

$$L_w v = v'' + \left(-\frac{c^2}{4} + f'(\phi(\xi))\right)v = \lambda v, \tag{3.69}$$

where $\phi(\xi)$ represents the front solution. This problem can be considered as a self-adjoint one on $L^2(\mathbb{R})$, independently of the original weighted function space. The discrete spectra of (3.69), therefore, are all reals. The maximum eigenvalue has the following variational characterization:

(3.70)

$$\lambda = \max_{v \in H^1(\mathbb{R}),\ \|v\|_{L^2(\mathbb{R})}=1} \left\{ \int_{-\infty}^{\infty} -(v')^2 + \left(-\frac{c^2}{4} + f'(\phi(\xi))\right)v^2 d\xi \right\}.$$

If $v$ is a function that realizes the maximum, so is $|v|$, and hence one can assume that $v$ is nonnegative. If $v = 0$ and $v' = 0$ at some point, then $v$ has to be identically zero. Therefore, $v$ is strictly positive. Let us note that the function $\psi(\xi) := \phi'(\xi)e^{-c\xi/2}$ $(\psi > 0)$ obtained from the derivative of the front solution satisfies

$$\psi'' + (-c^2/4 + f'(\phi))\psi = 0;$$

namely, it is an eigenfunction associated with the 0-eigenvalue.

Denoting by $p$ a normalized eigenfunction associated with the maximum eigenvalue $\lambda$, one can express the latter as

$$\lambda = -\int_{-\infty}^{\infty} \psi^2 \left(\frac{d}{d\xi}\left(\frac{p}{\psi}\right)\right)^2 d\xi \tag{3.71}$$

in terms of $\psi$. The last expression immediately implies $\lambda \leq 0$. If $\lambda = 0$, then $p/\psi =$ constant, and hence $p$ essentially coincides with $\psi$, which was obtained from the derivative of the front solution. Therefore, discrete eigenvalues other than 0, if they exist, have to satisfy $\lambda < 0$. Combining this with the previous results, we have the stability of the front solution for $c > c_{\min}$ in a weighted space. □

We next prove the instability of the front solution for $0 < c < c_{\min}$. When $b \geq 1/2$, PROPOSITION 3.13 says $c_{\min} = 2$, and hence the essential spectrum, as established in the previous discussion, intersects the right half plane, proving the instability. On the other hand, since $c_{\min} = c_b > 2$ for $0 < b < 1/2$, the essential spectrum stays in the left half plane even for $c$ smaller than the selected speed $c = c_b$. To show that the state where $c = c_b$ is marginally stable, we will show the existence of positive eigenvalues for $c < c_b$.

Arguing as before, one can obtain the self-adjoint problem (3.69), and hence the maximum eigenvalue is characterized as in (3.70). The function $\psi(\xi) = \phi'(\xi)e^{-c\xi/2}$, obtained from the derivative of the front solution $\phi$, is an eigenfunction associated with the 0-eigenvalue. The front solution $\phi(\xi)$, however, is not monotone in the present situation due to THEOREM 3.14, and hence $\phi'$, and consequently $\psi$, has at least one simple zero, proving that 0 is not the maximum eigenvalue and that $\lambda_{\max} > 0$. We have thus proven that the eigenvalue crosses the origin at $c = c_b$, and the proof of THEOREM 3.19 is complete.

### Stability of the Front with Critical Wave Speed

We have so far shown that there are two selection criteria for asymptotic travelling speed in (3.50): the minimum speed selection criterion and the marginal stability criterion, and that they both give the same result. The former asserts that among positive and monotone front solutions the one with minimum speed is selected, while the latter says that among all possible front solutions the one at which the stability property changes is selected. We have already seen in THEOREM 3.7 that the asymptotic travelling speed of a front solution agrees with the critical speed predicted by these criteria. The basin of attraction of such a behavior is quite large and contains, for example, initial values $u_0(x) \in [0, 1]$ that satisfy $\liminf_{x\to-\infty} u_0(x) > 0$ and $u_0(x) \equiv 0$ for $x \geq 0$ (cf. [**34**]). However, the last result relies on the maximum principle, which means that the method does not apply to cases where the unknown is complex-valued or vector-valued. It is therefore desirable to have a method which does not use the maximum principle. In relation to such a method, we shall now briefly describe what has been known about the local stability of the marginally stable front solution, setting aside the issue of global attractivity for the moment.

When the wave speed was larger than the critical one ($c > c_{\min}$), we obtained exponential stability by introducing the weighted spaces, which enabled us to separate and shift the essential spectrum. However, it is not possible to separate the essential spectrum for the front solutions with the critical speed, and as we will see below, the rate of decay is of polynomial order. In [**217**], Kirchgässner showed that the decay rate to the critical front solution is of order $O(t^{-1/4})$ in an appropriate weighted space, by reducing the linearized operator around the front to a normal form of Floquet type with the help of a

novel change of variables, and by examining the semigroup generated by the normal form operator.

On the other hand, Bricmont and Kupiainen ([**38**], [**37**]) established the stability of front solutions to complex-valued Ginzburg-Landau equations by means of a renormalization group method. And then, Gallay in [**151**], combining the ideas in these two methods, established a polynomial order decay to critical front solutions for the following class of scalar equations:

$$\frac{\partial u}{\partial t} = \frac{\partial^2 u}{\partial x^2} + F(u), \qquad x \in \mathbb{R}, \tag{3.72}$$

where $F$ is either a polynomial or an analytic function satisfying the conditions

$$F(0) = F(1) = 0, \qquad F'(0) > 0, \quad F'(1) < 0, \tag{3.73}$$
$$F''(u) < 0 \quad \text{for all} \quad u \in (0,1).$$

This class contains $u - u^3$ (Ginzburg-Landau type) and $u - u^2$ (Fisher type). Renormalization group methods like those described in CHAPTER 2 are expected to be applicable to determine the stability of critical front solutions for more general equations, and further investigation in this direction seems promising.

## 3.6. Modern Developments[1]

In the marginal stability approach, we have paid much attention to the existence of nonlinear front solutions and the selection mechanism of these nonlinear fronts, as well as the relation between front stability and front selection. It has recently become clear that approaching the front dynamics from a slightly different angle not only clarifies several conceptual issues, but also yields a starting point for systematically calculating the rate of convergence of the speed and shape of fronts to their asymptotic behavior ([**101**]).

A key point in this approach is as follows: The value $c^*$, which is identified as the minimal wave speed among nonnegative front solutions and *is the wave speed selected* via the linear marginal stability criterion (3.47), actually arises more generally as the *asymptotic spreading speed* of a localized initial perturbation. The behavior of this local perturbation is governed by a dynamical equation, which is obtained by linearizing the nonlinear equation around the unstable state. In essence, the equations (3.47) arise as saddle-point

[1]This section is based on communication with Wim van Saarloos.

equations in the complex $k$-plane, when the long-time asymptotics of the Green's function of the linearized equation is extracted from its Fourier representation by deforming the $k$-contour so as to go through this saddle point ([**235, 31, 101**]). The importance of this result is its independence of the precise nonlinearities. Namely, the evolution dynamics, obtained by linearizing the dynamical equation about the unstable state, leads by itself to ever-growing perturbations whose level-lines spread asymptotically with the speed $c^*$ given by (3.47).

From this perspective, it becomes clear that in the presence of the nonlinearities in the dynamical equations, there can be, in practice, only two possibilities for nonlinear front propagation: Either the asymptotic front speed $c_{\rm as}$ of a nonlinear front is equal to $c^*$, $c_{\rm as} = c^*$, or it is larger than $c^*$, $c_{\rm as} > c^*$. Although there is no rigorous proof, the third possibility that $c_{\rm as}$ would be less than $c^*$ is practically considered to be dynamically impossible. This is because for the nonlinearities to have any effect at all on a nonlinear front, the front must propagate at least as fast as the small perturbations grow out and spread with velocity $c^*$.

The first case, in which $c_{\rm as} = c^*$, corresponds to the linear marginal stability regime. In the recent literature, however, fronts of this type are often called *"pulled" fronts*, as the linear spreading of small perturbations about the unstable state almost literally "pulls" the nonlinear front back [**338, 101**]. The second case, where fronts propagate asymptotically faster than $c^*$, corresponds to the nonlinear marginal stability regime. Fronts of this type are referred to as *"pushed" fronts*, to contrast them with the pulled fronts.

A remarkable and general result which has recently been derived starting from the above perspective is the following. If one measures an instantaneous speed $c(t)$ by following a level line $u(x,t) = const.$ of a pulled front as it approaches its asymptotic velocity $c^*$, one finds the exact result ([**101**]) for the convergence of wave speeds:

$$c(t) = c^* - \frac{3}{2k^{i*}t} + \frac{3\sqrt{\pi}}{2(k^{i*})^2\sqrt{D}\,t^{3/2}} + \mathcal{O}\left(\frac{1}{t^2}\right), \tag{3.74}$$

while the shape of the profile is given by

$$u(x,t) = U_{c(t)}(\xi_X) + \mathcal{O}\left(\frac{1}{t^2}\right), \quad \xi_X \ll \sqrt{t}. \tag{3.75}$$

In the above, $U_c(\xi)$ is the solution for the front profile moving with uniform speed $c$, $\xi_X$ the non-uniformly moving coordinate

$$\xi_X = x - \int^t c(t')dt',$$

and $k^{i*}$ the solution of (3.47) with $D$ given by

$$D = \frac{i}{2}\frac{d^2\omega}{dk^2}\bigg|_{k^*}$$

playing a role of a diffusion coefficient.

The interesting feature of these results is their universality.

For the Fisher-Kolmogorov equation the first term of order $1/t$ in $c(t)$ was derived rigorously almost twenty years ago by Bramson in [**34**], but the $t^{-3/2}$ term was not known before. Moreover, it turns out that the equations (3.74) and (3.75) are valid for all pulled fronts in the much more general situation where the asymptotic profile of the front is uniformly translating, except for the bifurcation point from the pulled to the pushed regimes. Thus, they even apply to coupled reaction-diffusion equations and to difference equations ([**101, 102**]). Quite surprisingly, all the terms in (3.74) are independent of the nonlinear terms in the dynamical equation under study. An interesting aspect of (3.74) is that the velocity always approaches $c^*$ asymptotically *from below*, and hence the front shape, according to (3.75), is for long times close to a uniformly translating front solution with instantaneous speed below $c^*$!

A related recent finding concerns the sensitivity of "pulled" fronts to changes in the dynamics near the unstable state: For nonlinearities $f(u)$ in (3.36) of the form

$$f(u) = \begin{cases} u - u^3 & \text{for } u > \epsilon, \\ 0 & \text{for } u < \epsilon, \end{cases}$$

the asymptotic speed converges only logarithmically slowly in $\epsilon$ to $c^*$ as $\epsilon \to 0$ ([**43**]). This behavior seems to be relevant to the propagation of fronts in stochastic lattice models, where a natural cutoff is set by the discrete particles.

An important experimental realization of front propagation into unstable states is found in the pearling instability of tubular membranes [**22**]. The propagating fronts are of the pulled type [**311**], in spite of the strong nonlinearities behind the front that eventually lead to the pinching of droplets.

## 3.7. Summary

**3.1** The meaning of the pattern selection problem is explained.

**3.2** By using the simplest geometric model describing a dendritic crystal growth process, it is explained how pattern selection is related to surface tension effects and anisotropies.

**3.3** The minimum speed criterion for front solutions in the Fisher-Kolmogorov equation is elucidated by regarding the equation as a limit of structurally stable systems.

**3.4** An intuitive account is given for the minimum speed criterion. By using a scalar equation, the limitation of a linear marginal stability criterion is pointed out, and a geometric characterization of a nonlinear marginal stability criterion is given.

**3.5** The validity of the marginal stability criterion is established for scalar equations.

**3.6** Recent developments oconcerning marginal stability criteria are discussed. The notions of pulled and pushed fronts are introduced.

CHAPTER 4

# Pattern Formation

Pattern, interpreted in the broadest sense of the word, means an order formed at the expense of consuming some kind of energy and materials. Mathematical theories for pattern formation that encompass such a wide interpretation of the terminology, however, have not been established. The situation at the present moment is rather that new types of dynamic behaviors are being discovered one after another, enlarging the horizon of varieties, so to speak, while the discovery of universal mathematical structures that pierce through the varieties of pattern formation phenomena remains as a future task. It is also true, on the other hand, that many pattern formation phenomena have given an impetus to develop fruitful methodologies. For example, bifurcation theory and singular perturbation theory are very effective tools for finding solutions in a constructive manner. Also, asymptotic analysis and ideas from infinite dimensional dynamical systems have been very helpful in uncovering the ultimate behavior of a system. We will introduce the reader to some of these theories in this and the next chapter. We will also discuss, in these chapters, what one can say about higher dimensional pattern formation from the viewpoint of scaling.

## 4.1. What is Pattern Formation?

Among many distinguished works done by Alan Turing, who is famous for his *Universal Turing Machine*, there is a paper predicting that a simple combination of reaction and diffusion can cause a spontaneous formation of inhomogeneous structures, called Turing patterns. This remarkable result revealed that diffusion effects, considered as a driving force of uniformization, had a counterintuitive aspect: they could function cooperatively with reaction to create spatially inhomogeneous ordered structures. At first the Turing

mechanism was considered as having little to do with real phenomena. However, recent experiments have clarified that Turing's idea gets at the essence of dynamics in chemical reactions and morphogenesis. Moreover, the universality of the mechanism, which does not depend so much on particular real phenomena, has been recognized as a very important principle for understanding varieties of hierarchical structures in nonlinear phenomena.

A well known example of a model equation for the Turing mechanism is a system of semilinear parabolic partial differential equations, called a reaction-diffusion system.

A characteristic feature of nonlinear reaction kinetics in such a system is a balanced interaction between a self-catalytic growth and an inhibition effect that tends to suppress the growth. The population of a metropolis or an outbreak of a virus increases or spreads rapidly once an impetus is given. Eventually, the population either settles down to an appropriate size or declines, and sometimes exhibits an oscillatory behavior. Such behaviors are caused by inhibitory effects due to a limited source of food, or by the response of immune systems.

Another aspect of reaction-diffusion systems is spatial dispersion due to diffusion effects. To understand such effects, imagine the spread of flu or a combustion process (such as wildfire). There are three different states, namely, the population susceptible to the disease (combustible state), the infected (burning state) and the immunized (burned state). In order to describe the spatial dispersion of the disease or flame, it is not necessary to know all of these three states. It is enough to only know the infected population or the flame fronts. This type of argument naturally leads to the idea of interface dynamics. Namely, it is sufficient to describe only the motion of internal layers (interfaces) where the state changes abruptly. By employing such a procedure, one is able not only to substantially reduce the degree of freedom in the original model, but also to explicitly characterize the essence of intrinsic dynamics.

Such an idea has a wide range of applicability. It is not too much to say that the idea is effective in describing some sort of transition from one state to another in any situation where two or more different states coexist, such as in crystal growth, combustion processes, morphogenesis, and population biology. When one deals with distinguished limits, in which one tries to reduce the motion of a system to that of an interface, it is necessary to rescale space and time. In order to obtain meaningful limits, one needs to pay attention to the balance

between several forces which are related to the motion of the interface. Depending upon the adopted forces which interact and compete with each other, there are many different distinguished limits and scaling laws.

The aim of this chapter is to clarify the existence and dynamics of typical patterns in reaction-diffusion systems by using mainly asymptotic methods as described above.

## 4.2. Gradient System and Its Dynamics

It is an old and natural idea that the dynamics of a state evolves in such a way that the value (energy) of a functional (free energy) decreases in the most efficient way. In such a situation, the ultimate destiny of the state will be the one of the points where the energy assumes a minimal value. This is an inherent reason why it is often so effective to investigate stability properties by using Lyapunov functions in the theory of ordinary differential equations.

In spatially extended systems, interactions between neighboring positions are usually expressed in terms of spatial derivatives (for example, material or heat flows with a speed in proportion to its spatial gradient). As a typical example of energy functional, the following simple but basic one, called the van der Waals type,

$$F_\epsilon(u) = \int_\Omega \frac{\epsilon^2}{2}|\nabla u|^2 + W(u)dx, \tag{4.1}$$

is often employed, where $\Omega$ is a smooth bounded domain in $\mathbb{R}^N$. As is mentioned in §4.1, at least two different states are observable in phase transition, like solid and liquid or unburnt and burned. Therefore, for the density function $W(u)$, we employ what is called a double-well potential, which typically is expressed by the quartic polynomial $W(u) = (u^2 - 1)^2/4$ as in FIGURE 4.1.

Taking $L^2(\Omega)$ as the basic function space, we choose $H^1(\Omega)$ as the admissible class of functions for the functional. In order to minimize the value of the functional, it is preferable to assign either $+1$ or $-1$ to $u$ pointwise, and at the same time, to reduce the spatial gradient of $u$ as much as possible. Therefore, if there is no constraint imposed on $u$, then one of the two homogeneous states $u \equiv \pm 1$ gives rise to the minimum value of the functional. The description of the dynamics leading to these states will be discussed in §4.2.2. On the other hand, in the case where there is a mass conservation condition imposed on $u$, such as in the phase separation of a binary alloy, the Cahn-Hilliard

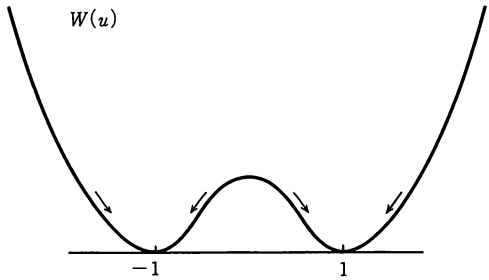


FIGURE 4.1. A double-well potential.

equation will be suitable (to be treated in §4.2.3). In the latter situation, the **minimizer** of the functional is a non-constant function, giving rise to the interesting problem of geometrically characterizing the shape of its interface.

Moreover, a good deal of attention has been directed in recent years to variational problems associated with a functional of the form of (4.1) with non-local terms added, and to the gradient dynamics generated by such a functional. In such a system, interesting types of solutions appear, produced by the interplay of local and global effects, such as a minimizer with a fine structure. Since all of these examples are considered as a gradient system in an infinite dimensional space, we will briefly review the framework of such systems in the next subsection.

**4.2.1. Global Attractor of Gradient System.** The theory of dynamical systems, initiated as qualitative theories for ordinary differential equations, has developed in many directions. In particular, during the last couple of decades notable advances have been achieved in infinite dimensional spaces. Studies of functional differential equations with delays and model equations in dissipative systems have been a strong driving force in such advances. Systems which evolve while dissipating energies and information provide us with an ideal material by which to understand what is the essential degree of freedom that controls dynamical behaviors.

One of the most important notions in this context is that of **global attractor**. A global attractor is such that it is often finite dimensional, and once its structure is known the asymptotic behavior of the system is well-understood, substantially reducing the degree of

freedom in the dynamic behaviors of the original systems. The idea of reducing the entire dynamics to the flow on global attractors is a typical example of qualitative approaches in nonlinear problems. The presentation in this section mainly follows that of [**166**].

DEFINITION 4.1 (**Global Attractor**). Let $T(t)$ be a $C^r$-semigroup on a Banach space $X$ ($r \geq 0$). An invariant set $A$ of the semigroup is called a **global attractor** if it satisfies the following conditions:

(i) $A$ is a maximal, compact invariant set.

(ii) $A$ attracts each bounded set $B \subset X$, i.e.,

$$\lim_{t\to\infty} \operatorname{dist}(T(t)B, A) = 0.$$

REMARK 4.2. From the definition, it follows immediately that the $\omega$-limit set $\omega(B)$ of $B$ is compact and contained in $A$.

For the rest of this section, $X$ is always a Banach space and the semigroup is always a strongly continuous $C^r$-semigroup. It is convenient to introduce the following two notions before we state the conditions that guarantee the existence of a global attractor.

The semigroup $T(t)$ is called **asymptotically smooth**, if for each non-empty bounded closed set $B$ satisfying $T(t)B \subset B$ ($t \geq 0$), there exists a compact set $J \subset B$ that attracts $B$. $T(t)$ is called **point dissipative**, if there exists a bounded set $B \subset X$ that attracts each point of $X$.

A positive orbit $\gamma^+(x)$ through $x \in X$ is defined by $\gamma^+(x) = \{T(t)x \mid t \geq 0\}$. Since $T(t)$ is, in general, neither surjective nor injective, a negative orbit $\gamma^-(x)$ is defined as follows:

$$\gamma^-(x) = \bigcup_{t\geq 0} H(t, x), \tag{4.2}$$

$$H(t,x) := \{y \in X \mid \text{there exists an orbit } \phi : (-\infty, 0] \to X \text{ such that } \phi(0) = x \text{ and } \phi(-t) = y\},$$

where $\phi(s)$ is an orbit (of $T(t)$) if it satisfies

$$T(t)\phi(s) = \phi(s+t) \qquad (s \in (-\infty, -t],\ t \geq 0).$$

THEOREM 4.3. *Let $T(t) : X \to X$ be asymptotically smooth and point dissipative. If positive orbits of bounded sets remain bounded, then there exists a connected global attractor $A$ for $T(t)$.*

THEOREM 4.4. *If $T(t) : X \to X$ is completely continuous and point dissipative, then there exists a connected global attractor $A$. Moreover, in this case, there exists an equilibrium in $A$.*

These theorems may look very abstract. However, if they are applied to a restricted class of dynamical systems, called gradient systems, then the global attractor $A$ can be expressed in fairly concrete terms. Since the notion of **hyperbolicity** of equilibria plays a key role later on, we define this terminology. An equilibrium $x$, namely $T(t)x = x$ for each $t \geq 0$, is hyperbolic if the spectrum $\sigma(DT(t)(x))$ does not intersect the unit circle in the complex plane for $t > 0$.

DEFINITION 4.5 (**Gradient System**). A $C^r$-semigroup

$$T(t) : X \to X$$

is called a **gradient system** if the following conditions hold:

(i) Bounded positive orbits are precompact.
(ii) There exists a continuous Lyapunov function $V : X \to \mathbb{R}$ that satisfies the following conditions:
  (a) $V(x)$ is bounded below;
  (b) $\lim_{|x|\to+\infty} V(x) = +\infty$;
  (c) for each $x \in X$, $V(T(t)x)$ is non-increasing in $t$;
  (d) if $T(t)x$ is defined for all $t \in \mathbb{R}$ and $V(T(t)x) = V(x)$ for all $t \in \mathbb{R}$, then $x$ is an equilibrium.

Let $E$ denote the totality of equilibria of $T(t)$. The following is known.

LEMMA 4.6. *When $T(t)$ is a gradient system, for each $x \in X$ its $\omega$-limit set $\omega(x)$ belongs to $E$. If the negative orbit $\gamma^-(x)$ through $x$ is precompact, then the $\alpha$-limit set $\alpha(x)$ of $x$ also belongs to $E$.*

For gradient systems, the existence of a global attractor is guaranteed by the next theorem.

THEOREM 4.7. *If a gradient system $T(t)$ $(t \geq 0)$ is asymptotically smooth and the set $E$ of equilibria is bounded, then there exists a connected global attractor $A$. In this case, the attractor $A$ is represented as follows:*

$$A = W^u(E) := \{y \in X \mid T(-t)y \text{ is defined for } t \geq 0, \quad T(-t)y \to E \text{ as } t \to +\infty\}. \tag{4.3}$$

*Moreover, if each element of $E$ is hyperbolic, then $E$ is a finite set and $A$ has a simpler expression:*

$$A = \bigcup_{x \in E} W^u(x). \tag{4.4}$$

PROOF. Because of the boundedness of $E$, LEMMA 4.6 implies that the semigroup is point dissipative. Thanks to the properties of the functional $V$, orbits of bounded sets are bounded. Therefore, THEOREM 4.3 implies the existence of the connected attractor $A$. In order to show that $A = W^u(E)$, note that the orbit of each point $x \in A$ is defined for all $t \in \mathbb{R}$, and in particular, that the negative orbit $\gamma^-(x)$ is precompact. Therefore, it follows from LEMMA 4.6 that its $\alpha$-limit set $\alpha(x)$ belongs to $E$. This means $A \subset W^u(E)$. The inclusion $A \supset W^u(E)$ obviously holds. If, moreover, each element of $E$ is hyperbolic, then elements of $E$ are isolated. Therefore, from the compactness of $A$ it follows that $E \subset A$ is a finite set, showing that $A = \bigcup_{x \in E} W^u(x)$. □

If $T(t)$ is completely continuous, then it is asymptotically smooth. Hence we have the following result.

THEOREM 4.8. *Let $T(t)$ $(t \geq 0)$ be a gradient system. If $T(t)$ is completely continuous and $E$ is bounded, then the conclusions of* THEOREM 4.7 *hold true.*

When semiflows (semigroups) are defined by partial differential equations, their domain of definition usually cannot be the entire function space $X$. To apply the results above to such problems, one needs to set up appropriate function spaces on which the solution operator $T(t)$ defines a $C^r$-semigroup. Fortunately, for systems of differential equations that appear in dissipative systems, their linear part is usually a **sectorial operator** which generates an analytic semigroup. By using the analytic semigroup, one can show that the solution operator generates $C^r$-semigroups on various function spaces (cf. [**176**] for the details). We will deal with the simplest and most typical example of such a system in the next subsection.

**4.2.2. Non-Conservative Gradient System.** As typical examples of gradient dynamical systems, we will first deal with two types of non-conservative systems to which the general theory presented above applies nicely. They are governed, respectively, by scalar bistable reaction-diffusion equations and compex-valued Ginzburg-Landau equations.

### Scalar Bistable Reaction-Diffusion Equation

If one thinks of the states $u = \pm 1$ related to the functional in (4.1) as describing directions of spin, up or down, liquid or solid state, or oxidized or reduced state, then the minimum value of the functional is attained at the states $u = \pm 1$. Therefore, in such a system one is mainly interested in how orbits settle down to the states $u = \pm 1$. The $L^2(\Omega)$-gradient system associated with the functional in (4.1) is the following Euler-Lagrange equation:

$$\begin{aligned} u_t &= \epsilon^2 \Delta u + f(u) \quad (\text{in } \Omega), \qquad f(u) = -W'(u), \\ \frac{\partial u}{\partial n} &= 0 \quad (\text{on } \partial\Omega). \end{aligned} \tag{4.5}$$

If the second order derivative term is missing in (4.5), the system converges to either $+1$ or $-1$ (except for the case where 0 is taken as the initial value), exhibiting bistability. For this reason, (4.5) is called a **scalar bistable reaction-diffusion equation** of non-conservative type (or the Allen-Cahn equation). This is one of the fundamental equations in the theory of pattern formation.

Let us apply the dynamical system theory prepared in the previous subsection to the one-dimensional version of (4.5) with the boundary conditions replaced by Dirichlet ones:

$$\begin{cases} u_t = u_{xx} + f(u), & 0 < x < 1, \\ u = 0, & x = 0, 1, \end{cases} \tag{4.6}$$

where we set $\epsilon = 1$ for simplicity and the nonlinearity is given by $f(u) = u - u^3$.

REMARK 4.9. Although we deal with a special case where the boundary conditions are Dirichlet ones and the nonlinearity is the cubic $f(u) = u - u^3$, the methods used below are equally applicable to more general nonlinearities and boundary conditions, including Neumann ones (cf. [**166**]).

Considering (4.6) as an evolution equation in an infinite dimensional space, let us apply the results of the previous subsection. In order to define a time-global $C^1$-semigroup $T(t)$, we choose to take $X = L^2(0,1)$ as our basic space. If the domain of definition of $L \equiv -\frac{d^2}{dx^2}$ is defined by $D(L) = H_0^1(0,1) \cap H^2(0,1)$, then $L$ is a positive definite self-adjoint operator. Moreover, it is a sectorial operator with compact resolvent. If we define $X^{1/2} \equiv D(L^{1/2}) = H_0^1(0,1)$,

then the nonlinear map $f : X^{1/2} \to X$ is of $C^1$-class. Therefore, applying the variation of constants formula, one can easily verify that (4.6) generates a time-local $C^1$-semigroup $T(t)$ on $X^{1/2}$.

The existence of the following energy functional $V$ and the dissipativity of $f$ (meaning $\overline{\lim}_{|u|\to\infty} f(u)/u \leq 0$) imply that the $C^1$-semigroup $T(t)$ is defined globally in time. In fact, let $V$ be defined by

$$V(\phi) = \int_0^1 \left\{ \frac{1}{2}\phi_x^2(x) + W(\phi(x)) \right\} dx, \quad W(u) = -\int^u f(s)ds. \tag{4.7}$$

Then it follows that

$$\frac{d}{dt} V(u(t,\cdot)) = -\int_0^1 u_t^2 dx \leq 0,$$

and hence the $C^1$-semigroup $T(t)$ generated by (4.6) is a gradient system on $X^{1/2}$. Since $T(t)$ is completely continuous for $t > 0$, one can express its global attractor $A$ as $A = \bigcup_{\phi\in E} W^u(\phi)$, thanks to THEOREM 4.7, if each element of $E$ is hyperbolic. In the present situation, furthermore, the structure of $A$ is understood in detail, due to the following result.

PROPOSITION 4.10 (**Transversality** (cf. [**177**], [**7**])). *Let $\phi$ and $\psi$ be hyperbolic equilibria of* (4.6). *Then the unstable manifold of $\phi$ and the stable manifold of $\psi$ intersect transversely:*

$$W^u(\phi) \pitchfork W^s(\psi).$$

One of the most important consequences of the last propostion is that, as $f$ varies, **the global attractor $A$ changes its qualitative structure only through the loss of hyperbolicity of equilibria**, or in other words, **only through local bifurcations of equilibria**. This, in particular, means that as long as the equilibria remain hyperbolic, there are no qualitative changes in the dynamics on the attractor $A$, which in turn enables us to understand $A$ in constructive terms from bifurcation theories. Let us, indeed, embed (4.6) in the following one-parameter ($\lambda > 0$) family of problems:

$$\begin{cases} u_t = u_{xx} + \lambda^2 f(u), & 0 < x < 1, \\ u = 0, & x = 0, 1. \end{cases} \tag{4.8}$$

When $\lambda$ is small, (4.8) has only one equilibrium solution $u \equiv 0$. As $\lambda$ increases, successive bifurcations take place at $u \equiv 0$ (cf. FIGURE 4.2), and their unstable manifolds constitute the attractor $A$.

To be precise, the next theorem holds true.

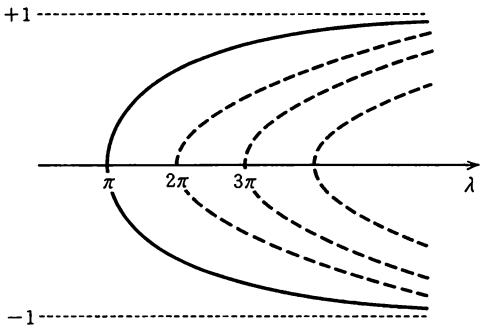


FIGURE 4.2. A bifurcation diagram in the scalar bistable reaction-diffusion equation. Under the Dirichlet boundary conditions, only the branch bifurcating from $\lambda = \pi$ is stable.

THEOREM 4.11 ([**62**], [**176**]). *In* (4.8), *if* $\lambda \in (n\pi, (n+1)\pi)$ *for a positive integer* $n$, *then there exist* $(2n+1)$ *equilibria* $\phi_0 \equiv 0$, $\phi_j^+$, $\phi_j^-$ $(j = 1, 2, \dots, n)$. *All of these equilibria are hyperbolic for* $\lambda \in (n\pi, (n+1)\pi)$ *with* $\dim W^u(\phi_0) = n$ *and* $\dim W^u(\phi_j^\pm) = j - 1$ $(j = 1, 2, \dots, n)$. *The global attractor* $A_\lambda$ *is given as*

$$A_\lambda = W^u(\phi_0) \cup \Big( \bigcup_{j=1}^{n} W^u(\phi_j^\pm) \Big).$$

REMARK 4.12. When $\lambda \in (n\pi, (n+1)\pi)$, the semigroup $T(t)$ generated by (4.8) is a Morse-Smale system (see [**166**] for details).

REMARK 4.13. **Spatially inhomogeneous stable** equilibria are only those on the branch that bifurcates from $\lambda = \pi$.

Although the manner of connections between solutions on the global attractor $A_\lambda$ increases the degree of complexity as $\lambda$ varies (cf. FIGURE 4.3), we only need to look at local bifurcations from $u \equiv 0$ to detect its structural changes.

REMARK 4.14 ([**252**], [**360**], [**167**]). For an arbitrary orbit $\phi$, it is known that $\omega(\phi)$ consists of a single point.

In the example above with Dirichlet boundary conditions, the only stable inhomogeneous equilibria are those on the branch bifurcating at $\lambda = \pi$, as already mentioned in REMARK 4.13. On the other

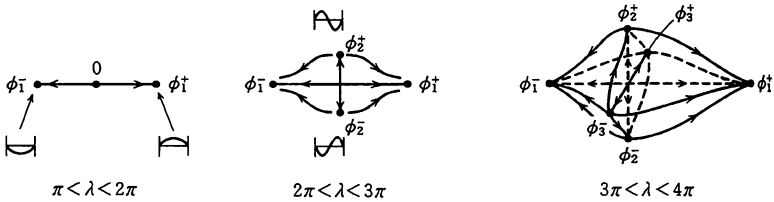


FIGURE 4.3. The dimension of the global attractor increases as $\lambda$ increases. Compare with the bifurcation diagram in FIGURE 4.2.

hand, under the Neumann boundary conditions, the inhomogeneous equilibria are all unstable ([**61**], [**253**], [**358**]).

The latter result remains true in higher dimensional spaces.

THEOREM 4.15 ([**59**], [**253**]). *For the higher dimensional version of* (4.6),

$$\begin{cases} u_t = \Delta u + f(u), & x \in \Omega, \\ \dfrac{\partial u}{\partial n} = 0, & x \in \partial\Omega, \end{cases} \tag{4.9}$$

*the nonconstant equilibria of* (4.9) *are all unstable, provided that the domain* $\Omega$ *is convex.*

REMARK 4.16 ([**253**]). The last theorem is not true in general if $\Omega$ is **non-convex**. Namely, for appropriate non-convex dumbbell shape domains and a nonlinearity $f$, one can construct a non-constant stable equilibrium for (4.9).

When the domain $\Omega$ is convex, the ultimate destiny of the system governed by (4.9) is a constant state. Our interest naturally lies in the process by which it reaches the final state. This means that one has to describe dynamic behaviors on the global attractor. Such a description is in general a very hard problem. For one-dimensional singularly perturbed systems in which the diffusion rate is very small, the dynamics on the global attractor is characterized as that on a **very slow motion manifold** ([**58**], [**148**]), as explained in §1.3. A similar characterization applies to the Cahn-Hilliard equation (to be discussed later; cf. [**3**] and [**5**]).

The key to success in singularly perturbed systems is the fact that the motion along unstable manifolds is very well approximated

by translational motions of *quasi-equilibrium solutions*. The speed of such a motion is exponentially small, and hence it is called a very slow motion. It is, however, very difficult in this approach to rigorously describe the coalescence-disappearance of transition layers and the behavior of layers near the domain boundary, since in such situations faster time scales come into the problem. Despite this difficulty, it is expected that the motion tends to decrease the number of transition layers, following along the unstable manifolds as in FIGURE 4.3.

In higher space dimensional cases, the detail of the dynamics on the attractor is not well understood, because it is quite hard to find all of the equilibrium solutions. Moreover, the structure of heteroclinic connections between them is far more complicated than in the one-dimensional case. Therefore, it seems practical to consider the motion of solutions of special type, such as bubble solutions in the Cahn-Hilliard equation ([**5**]), or to use the method of singular limit analysis (to be discussed in CHAPTER 5) which helps us reduce the problem to interfacial dynamics. In fact, the singular limit of (4.9) is described by the mean curvature flow, which allows us to understand how the domains where $u$ takes values $\pm 1$ evolve.

### Complex-valued Ginzburg-Ladau Equation

As the second example of gradient dynamical systems, we now deal with a case in which the functional is defined on the space of complex-valued order parameters. Namely, it is given by

$$E(\Phi) = \int_\Omega \Big( |\nabla \Phi|^2 + \frac{\lambda}{2}(1 - |\Phi|^2)^2 \Big) dx, \tag{4.10}$$

and the associated Euler-Lagrange equation reads as follows:

$$\Phi_t = \Delta \Phi + \lambda(1 - |\Phi|^2)\Phi, \qquad \frac{\partial \Phi}{\partial n} = 0. \tag{4.11}$$

The equation in (4.11) is called the **time-dependent complex Ginzburg-Landau equation** (without magnetic effects). This equation is well known as a model describing superconducting states.

The equation generates a smooth semiflow on $C(\overline{\Omega}; \mathbb{C})$. Purely superconducting states are represented by $|\Phi| = 1$, while $\Phi = 0$ corresponds to the normal state. The functional is minimized at $\Phi = e^{ic}$ (with $c$ being any real), called a minimizer, corresponding to purely superconducting states. Therefore, from a variational point of view, nonconstant **local minimizers** are of interest.

In this direction, recent papers by Jimbo and Morita ([**193**], [**194**], [**195**]) have contributed to clarifying the solution structure. From the standpoint of physics, the following types of solutions are important:

(i) Nonconstant solutions $\Phi$ such that $|\Phi(x)| > 0$ everywhere on $\Omega$ (corresponding to local minimizers).

(ii) Nonconstant solutions that have zeros in $\Omega$ (corresponding to vortex lines).

The following result, however, shows that one needs to take $\Omega$ carefully to realize such solutions.

THEOREM 4.17. *If the domain $\Omega$ is convex, then nonconstant equilibrium solutions are all unstable, regardless of the value $\lambda > 0$.*

Stable equilibria are only those that take values of modulus 1. Here, an equilibrium is stable if it gives a local minimum value to the functional (4.10) on $H^1(\Omega, \mathbb{C})$, and it is unstable otherwise. It is known ([**334**]) that stability in this sense coincides with Lyapunov stability for the evolution equation. THEOREM 4.17 is also a natural generalization of THEOREM 4.15, which deals with real valued situations. If the initial function has several zeros, then these zeros (vortices) evolve so that they either hit the boundary, or collide with each other and disappear. There have been a lot of investigations of the motion of vortices on the entire space $\mathbb{R}^2$ and the stability of vortex lines ([**276**], [**354**]).

The last theorem suggests that in order to realize local minimizers or vortex lines, the topology of the domain has to be nontrivial. Indeed, the following result is known for domains with nontrivial homotopy ([**196**]).

THEOREM 4.18. *If the domain has nontrivial homotopy (such as annuli), then stable local minimizers (corresponding to solutions with no zero) are realized provided that the parameter $\lambda$ is suitably large.*

On the other hand, if the domain has trivial homotopy (such as simply connected domains), nonconstant solutions always have zeros. Although we know that to stabilize these solutions the domain has to be nonconvex, we still do not have a complete characterization of such domains. As another approach, by considering the equation with variable diffusion coefficient, it is possible to stabilize a solution with zeros at specified points for an arbitrary domain ([**71**]). Although it may be rather artificial in view of the original problem, another

situation is the case of the Dirichlet boundary conditions, in which minimizers have zeros. In the latter case, it is known ([**32**]) that the behaviors of the vortex lines for large values of $\lambda$ are very informative to clarify the singularity structure of harmonic maps from $\Omega$ to $S^1$.

**4.2.3. Conservative Gradient System.** We now deal with conservative systems.

**Cahn-Hilliard Equation**

So far, we have not put any restriction on the function for which energy functionals of the Ginzburg-Landau type are defined. It is natural, and often the case, that the functionals have to be considered under certain constraints. Among such situations, one of the most important examples is the class of conservative systems.

For example, if the states $\pm 1$ in the double-well potential represent different materials in an alloy, then the following quantity determined by the initial condition $u_0(x)$ has to be conserved:

$$\overline{u(t,\cdot)} \equiv \frac{1}{|\Omega|}\int_\Omega u(t,x)dx = \frac{1}{|\Omega|}\int_\Omega u_0(x)dx, \qquad -1 < \overline{u}_0 < 1.$$

The Euler-Lagrange equation for (4.1) under the last constraint in $L^2(\Omega)$ is given by

$$\begin{aligned} u_t &= \epsilon^2 \Delta u + f(u) - \overline{f(u)} \quad (\text{in } \Omega), \\ \frac{\partial u}{\partial n} &= 0 \quad (\text{on } \partial\Omega), \end{aligned}$$

which is an example of an equation with a non-local term (integral term). This equation, however, is not a satisfactory model of the original phenomenon, because it is not realistic to imagine that the alloy instantaneously detects the state of the entire system and responds to it in a non-local manner. Therefore, it is necessary to find a model equation which depends only on local interactions and, at the same time, conserves the mass constraint. Fife in [**135**] pointed out that if one considers (4.1) as defined on $H_0^{-1}(\Omega)$ (the subspace of $H^{-1}$ consisting of functions with null average) and gradient operation is taken with respect to the $H^{-1}$ inner product, then the resulting equation naturally becomes conservative. The Euler-Lagrange equation in this case is given by

$$\begin{aligned} u_t &= -\Delta(\epsilon^2 \Delta u + f(u)), \qquad x \in \Omega, \\ n \cdot \nabla u &= n \cdot \nabla \Delta u = 0, \qquad x \in \partial\Omega, \end{aligned} \tag{4.12}$$

which is a fourth order equation. This is called the **Cahn-Hilliard equation** and is one of the basic equations in conservative reaction-diffusion equations ([**54**]). Since in (4.12) $-\Delta$ operates on the linear term $u$ coming from the nonlinearity $f(u)$, it has a backward diffusion effect. However, because of the fourth order term $-\epsilon^2\Delta^2 u$, the existence and smoothness of its solutions are saved ([**176**], [**292**], [**114**]). In fact, let $H^2_E(\Omega)$ be defined by

$$H^2_E(\Omega) = \{u \in H^2(\Omega) \mid n \cdot \nabla u = 0, \ \ \overline{u} = 0\}$$

(for simplicity we set $\overline{u} = 0$). Then the linear operator $L = \epsilon^2\Delta^2$ with domain

$$D(L) = \{u \in H^2_E(\Omega) \mid \Delta u \in H^2_E(\Omega)\}$$

is a sectorial operator on $X = L^2(\Omega)$ with $X^{1/2} = D(L^{1/2}) = H^2_E(\Omega)$. Moreover, the functional in (4.1) is a Lyapunov function for (4.12), and hence the next result follows from the discussions in §4.2.1.

THEOREM 4.19. *Let $u_0 \in H^2_E(\Omega)$. Then the solution $u(t,x)$ of (4.12) exists globally in time and its $\omega$-limit set is a compact connected invariant set in $H^2_E(\Omega)$. If, moreover,the equilibrium solutions are all isolated, then $u(t,x)$ converges to one of them as $t \to \infty$.*

The Cahn-Hilliard equation is one of the basic model systems that describes the dynamics of spinodal decomposition, nucleation, and phase separation. See [**136**] for an elementary introduction.

### Characterization in Terms of Γ-Convergence

To which equilibrium does the solution $u(t,x)$ converge? It is reasonable to expect that it will eventually settle down to the **minimizer** of the energy functional, since the system is gradient. While the minimizers in the non-conservative case are the trivial ones $u = \pm 1$, they necessarily have to be non-constant in our conservative case because of the constraint. In the sequel, we will deal with the case where the parameter $\epsilon$ is small, since in this case it is possible to geometrically characterize the minimizers.

Thus our concern is the following singularly perturbed variational problem for a nonconvex potential:

$$\begin{cases} \inf\left\{ \hat{F}_\epsilon(u) \;\middle|\; u \in H^1(\Omega), \displaystyle\int_\Omega u dx = c \right\}, \\ \hat{F}_\epsilon(u) = \displaystyle\int_\Omega W(u) + \epsilon^2 |\nabla u|^2 dx, \end{cases} \tag{4.13}$$

where $W(u) = (u^2 - 1)^2/4$ is a double-well potential and $\Omega$ is a bounded domain with Lipschitz continuous boundary in $\mathbb{R}^n$. The constant $c$ in the constraint is assumed to satisfy $-|\Omega| < c < |\Omega|$.

The existence of a minimizer is guaranteed by the direct method in the calculus of variations ([**164**]). Let us denote it by $u_\epsilon$. Now our problem is how to identify $u_\epsilon$. Because of the constraint, $u_\epsilon$ has to take values close to $\pm 1$, and hence, one needs to take into account the contribution from the spatial gradient term $|\nabla u|$. In order to minimize the contribution as much as possible, how should the solution arrange the boundary (called an interface) between the two regions where it takes values $+1$ or $-1$? Our aim here is to characterize the interface in geometric terms.

In the formal limit as $\epsilon \to 0$, the singularly perturbed term $\epsilon^2 |\nabla u|^2$ drops out from the functional, and one is left with

$$\inf \int_\Omega W(u) dx.$$

In the latter situation, to minimize the functional, one is allowed to distribute the values $\pm 1$ arbitrarily, with the only constraint $\int_\Omega u = 1$, giving rise to a continuum of minimizers. Therefore, it is not clear which one can be the limit of $u_\epsilon$.

Are there any distinguished limits that retain some sort of information on the shape and location of the interface as $\epsilon \to 0$? An answer to this question is provided by the concept of **$\Gamma$-convergence** due to De Georgi ([**86**]). A key point of the idea is to characterize the principal part of the variational problem itself, instead of expanding the minimizer $u_\epsilon$ in $\epsilon$-power series. Namely, in the asymptotic expansion of the functional

$$\inf \hat{F}_\epsilon = \epsilon(\inf F_0) + o(\epsilon),$$

one attempts to characterize the problem associated with $F_0$.

This viewpoint is very fruitful. First of all, the problem associated with $F_0$ is simpler than the one associated with $\hat{F}_\epsilon$ in many

cases. More importantly, the reduced problem has a clear geometric meaning. Before we describe $F_0$ in precise terms, let us introduce some terminology. The variational problem for $F_0$ is posed on a basic space $BV(\Omega)$ consisting of functions of bounded variation. The space is defined, together with its norm, by

$$BV(\Omega) = \{u \in L^1(\Omega) \mid \|u\|_{BV(\Omega)} < \infty\}$$
$$\text{with } \|u\|_{BV(\Omega)} := \int_\Omega |u| dx + \int_\Omega |\nabla u|,$$

where the *gradient* of $u \in L^1(\Omega)$ is defined by

$$\int_\Omega |\nabla u| := \sup_{g \in C_0^1(\Omega, \mathbb{R}^n), |g| \le 1} \left\{ \int_\Omega u(x)(\mathrm{div} g(x)) dx \right\}.$$

Clearly, the inclusion $W^{1,1}(\Omega) \subset BV(\Omega)$ holds, while the reverse inclusion is not true. An example of the latter is a characteristic function of a set $A$. In fact, for $u = \chi_A \notin W^{1,1}$ it follows from the definition that

$$\int_\Omega |\nabla u| := \sup \left\{ \int_A \mathrm{div} g(x) dx \;\middle|\; g \in C_0^1(\Omega, \mathbb{R}^n) \quad |g| \le 1 \right\},$$

while for $A$ with smooth boundary the divergence theorem implies

$$\int_\Omega |\nabla u| = H^{n-1}(\partial A \cap \Omega) < \infty,$$

and hence $u \in BV(\Omega)$. The symbol $H^{n-1}$ on the right hand side stands for the $(n-1)$-dimensional Hausdorff measure. This observation makes it natural to define the perimeter of an arbitrary subset $A$ of $\Omega$ by the following formula:

$$\mathrm{Per}_\Omega A = (\text{perimeter of } A \text{ in } \Omega) = \int_\Omega |\nabla \chi_A|. \tag{4.14}$$

If the boundary of $A$ is smooth, $\mathrm{Per}_\Omega A$ is the area of the part of the boundary $\partial A$ contained in $\Omega$. The next two propositions are direct consequences of the definition above (see [**156**] for proof).

PROPOSITION 4.20 (**Lower Semicontinuity**). *If* $\lim_{\epsilon \to 0} u_\epsilon = u$ *in* $L^1(\Omega)$, *then*

$$\liminf_{\epsilon \to 0} \int_\Omega |\nabla u_\epsilon| \ge \int_\Omega |\nabla u|.$$

PROPOSITION 4.21 (**Compactness of** $BV$ **in** $L^1(\Omega)$). *Bounded sets of* $BV$ *are compact in* $L^1(\Omega)$.

Now we are ready to state a main result for (4.13).

THEOREM 4.22 ([**268**], [**337**]). *Let $u_\epsilon$ be the solution of* (4.13). *Assume that, for some subsequence $\epsilon_j$ with $\epsilon_j \to 0$ as $j \to \infty$,*

$$u_{\epsilon_j} \to u_0 \qquad \text{in } L^1(\Omega).$$

*Then $u_0$ is a solution of the following variational problem:*

(4.15)

$$\inf\Big\{\mathrm{Per}_\Omega\{u=-1\} \;\Big|\; u \in BV, W(u(x))=0 \text{ a.e.}, \int_\Omega u dx = c\Big\}.$$

REMARK 4.23. The problem (4.15) is a geometric problem in the sense that it asks how one should minimize, under the integral constraint, the area of the boundary of the region where $u = -1$.

PROOF. It is easy to construct an $H^1(\Omega)$-function that gives a value of $O(\epsilon)$ to the functional in (4.13). In fact, we first construct a step function $u = \pm 1$ and modify it by transition layers in an $O(\epsilon)$ neighborhood of the surface of discontinuity. From this observation, we expect that the original functional divided by $\epsilon$ will give rise to a meaningful limit. Therefore let us define a rescaled functional $F_\epsilon$ by

$$F_\epsilon(u) = \begin{cases} \displaystyle\int_\Omega \frac{1}{\epsilon} W(u) + \epsilon |\nabla u|^2 dx, & u \in H^1(\Omega), \quad \displaystyle\int_\Omega u dx = c, \\ +\infty, & \text{otherwise,} \end{cases}$$

and its associated candidate in the limit $F_0 : L^1(\Omega) \to \mathbb{R}$ by

$$F_0(u) = \begin{cases} \Big(2\displaystyle\int_{-1}^{1} \sqrt{W(s)}\, ds\Big)\mathrm{Per}_\Omega\{u=-1\}, & u \in BV, \\ \qquad W(u(x)) = 0 \text{ a.e.}, \ \displaystyle\int_\Omega u dx = c, \\ +\infty, \qquad \text{otherwise.} \end{cases} \tag{4.16}$$

Thanks to the penalty $+\infty$, the two functionals above are both defined on the same space $L^1(\Omega)$, which in turn enables us to introduce the following notion of **$\Gamma$-convergence**.

DEFINITION 4.24 (**$\Gamma$-Convergence**). The functional $F_\epsilon$ is said to $\Gamma$-converge to the limit functional $F_0$ in the $L^1(\Omega)$-topology if the following two conditions are satisfied:

(i) $v_\epsilon \to v$ in $L^1(\Omega)$ implies $\liminf_{\epsilon \to 0} F_\epsilon(v_\epsilon) \geq F_0(v)$.

(ii) For each $v \in L^1(\Omega)$, there exists a subsequence $\{v_{\epsilon_j}\}$ in $L^1(\Omega)$ such that

$$v_{\epsilon_j} \to v \text{ in } L^1(\Omega) \qquad \text{and} \qquad \lim_{j \to +\infty} F_{\epsilon_j}(v_{\epsilon_j}) = F_0(v).$$

Once the last two conditions are established, THEOREM 4.22 follows immediately. In fact, if $u_{\epsilon_j} \to u_0$ in $L^1(\Omega)$, then the condition (i) implies

$$\liminf_{j \to \infty} F_{\epsilon_j}(u_{\epsilon_j}) \geq F_0(u_0).$$

On the other hand, let us choose an arbitrary $w_0 \in L^1(\Omega)$ and a sequence $\{w_{\epsilon_j}\}$ which converges to $w_0$ in $L^1(\Omega)$. Since $u_{\epsilon_j}$ minimizes $F_{\epsilon_j}$, we have

$$F_{\epsilon_j}(u_{\epsilon_j}) \leq F_{\epsilon_j}(w_{\epsilon_j}).$$

Applying the condition (ii), one obtains

$$F_0(u_0) \leq \liminf_{\epsilon} F_{\epsilon_j}(u_{\epsilon_j}) \leq \lim_{j \to \infty} F_{\epsilon_j}(w_{\epsilon_j}) = F_0(w_0),$$

showing that $u_0$ is a solution of (4.15).

We now have to verify the two conditions in $\Gamma$-convergence. First of all, notice that we need to consider functions that satisfy the condition

$$W(v(x)) = 0, \text{ a.e.}, \qquad \int_\Omega v dx = c,$$

since, otherwise, the two conditions hold trivially because of the penalty in the functionals. It also suffices to consider functions that satisfy $-1 < v_\epsilon < 1$. We henceforth assume that these conditions are fulfilled.

Let us now prove that the condition (i) holds. By applying the Cauchy-Schwarz inequality to $F_\epsilon(v_\epsilon)$, one obtains

$$F_\epsilon(v_\epsilon) \geq 2 \int_\Omega \sqrt{W(v_\epsilon(x))}\, |\nabla v_\epsilon(x)| dx.$$

This is rewritten as

$$F_\epsilon(v_\epsilon) \geq \int_\Omega |\nabla \phi(v_\epsilon(x))| dx,$$

where the function $\phi : \mathbb{R} \to \mathbb{R}$ is defined by

$$\phi(t) = 2 \int_{-1}^{t} \sqrt{W(s)}\, dx.$$

Since $v_\epsilon$ converges to $v$ in $L^1(\Omega)$, we have

$$\phi(v_\epsilon) \to \phi(v) \qquad \text{in } L^1(\Omega).$$

From PROPOSITION 4.20, it follows that

$$\liminf_{\epsilon\to 0} F_\epsilon(v_\epsilon) \geq \liminf_{\epsilon\to 0} \int_\Omega |\nabla\phi(v_\epsilon)|dx \geq \int_\Omega |\nabla\phi(v)|dx.$$

Since we have

$$\phi(v(x)) = \begin{cases} 0, & v = -1, \\ 2\displaystyle\int_{-1}^{1} \sqrt{W(s)}\, ds, & v = 1, \end{cases}$$

the condition $W(v(x)) = 0$ a.e. implies

$$\int_\Omega |\nabla\phi(v)|dx = \Big(2\int_{-1}^{1} \sqrt{W(s)}\, ds\Big)\mathrm{Per}_\Omega\{v = -1\} = F_0(v),$$

establishing the property (i).

Let us now show that the second property (ii) in the definition of $\Gamma$-convergence is satisfied. Namely, we show that there exists an $L^1(\Omega)$-convergent sequence $\rho_{\epsilon_j} \to v$ for each element $v \in L^1(\Omega)$ such that the energy $F_{\epsilon_j}(\rho_{\epsilon_j})$ converges to $F_0(v)$. From the definition of $F_0$ in (4.16), it suffices to deal with only those $v \in L^1(\Omega)$ that satisfy

$$v \in BV(\Omega), \quad W(v(x)) = 0 \ \text{ a.e.}, \quad \int_\Omega v dx = c,$$

since otherwise $F_0(v) = \infty$. Since $v$ takes values $+1$ or $-1$ everywhere, it is represented as

$$v(x) = \begin{cases} -1, & x \in A, \\ 1, & x \in B, \end{cases}$$

where $A$ and $B$ are subsets of $\Omega$ with finite perimeter satisfying

$$-|A| + |B| = c.$$

Let $\Gamma = \partial A \cap \partial B$, and assume that $\Gamma \in C^2$ (from which the validity of the proof in the general case immediately follows).

In the sequel, we will give only an outline of how to construct the approximating sequence, and refer to [**337**] for details. What is crucial in constructing the approximation is how to bridge the gap between $-1$ and $+1$ smoothly. For this purpose let us define an internal transition function $z(s)$ and a signed distance function $d(x)$ to $\Gamma$. We define $z(s)$ as the solution of the following differential equation:

$$\frac{dz}{ds} = \sqrt{W(z)}, \qquad z(0) = 0. \tag{4.17}$$

The solution is defined on all of $\mathbb{R}$ and decays to $\pm 1$ at an exponential rate as $s \to \pm\infty$:

$$\begin{aligned} -1 < z(s) < 1 \qquad & \forall s \in \mathbb{R}, \\ |1 - z(s)| \le C_3 e^{-C_4 s} \qquad & (s \to \infty), \\ |1 + z(s)| \le C_3 e^{C_4 s} \qquad & (s \to -\infty), \end{aligned}$$

where $C_3$ and $C_4$ are positive constants determined by $W$.

The signed distance function $d : \Omega \to \mathbb{R}$ is defined by

$$d(x) = \begin{cases} \operatorname{dist}(x, \Gamma), & x \in B, \\ -\operatorname{dist}(x, \Gamma), & x \in A. \end{cases}$$

The internal transition layer function $g_\epsilon(s)$ that joins $-1$ and $+1$ is defined in terms of $z$ in (4.17) as follows:

$$g_\epsilon(s) = \begin{cases} 1, & s > 2\sqrt{\epsilon}, \\ \left(\dfrac{1 - z(1/\sqrt{\epsilon})}{\sqrt{\epsilon}}\right)\left(s - 2\sqrt{\epsilon}\right) + 1, & \sqrt{\epsilon} \le s \le 2\sqrt{\epsilon}, \\ z(s/\sqrt{\epsilon}), & |s| \le \sqrt{\epsilon}, \\ \left(\dfrac{1 + z(-1/\sqrt{\epsilon})}{\sqrt{\epsilon}}\right)\left(s + 2\sqrt{\epsilon}\right) - 1, & -2\sqrt{\epsilon} \le s \le -\sqrt{\epsilon}, \\ -1, & s < -2\sqrt{\epsilon}. \end{cases}$$

In order to align the profile of this function along $\Gamma$, we replace $s$ by $d(x)$ and define a sequence of functions $\{\tilde{\rho}_\epsilon(x)\}$ by

$$\tilde{\rho}_\epsilon(x) = g_\epsilon(d(x)).$$

For $\epsilon > 0$ sufficiently small, $d(x)$ is Lipschitz continuous in the region $\{x \mid |d(x)| < 2\sqrt{\epsilon}\}$, and hence $\tilde{\rho}_\epsilon \in H^1(\Omega)$. From the definition of $g_\epsilon$, one finds that it becomes sharper as $\epsilon$ gets smaller, and that $\tilde{\rho}_\epsilon$ converges, as $\epsilon \to 0$, to a discontinuous function that joins $-1$ and $+1$ all the way along $\Gamma$.

Therefore, it is now easy to see that $\tilde{\rho}_\epsilon \to v$ in the $L^1(\Omega)$-topology as $\epsilon \to 0$. However, the constraint

$$\int_\Omega \tilde{\rho}_\epsilon(x) dx = c$$

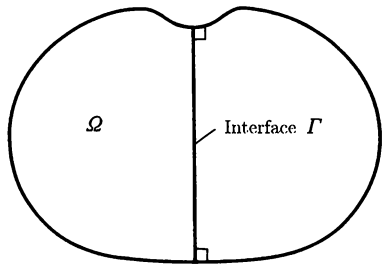


FIGURE 4.4. The location of an interface predicted by Γ-convergence. When the boundary has a dent, an interface passing through it minimizes its length.

may not be satisfied. It is possible to modify the function $\tilde{\rho}_\epsilon$ to $\rho_\epsilon$ by adding a constant of size $O(\epsilon)$ so that the constraint is fulfilled. The sequence of modified functions $\{\rho_\epsilon\}$ is the desired one. □

REMARK 4.25. When the domain $\Omega$ is two-dimensional, having a dent as in FIGURE 4.4, and the average is set equal to zero ($c = 0$), THEOREM 4.22 implies that the position of an interface is placed on one end at the bottom of the dent.

REMARK 4.26. The minimizer of (4.13) in one-dimensional space is a monotone function that converges as $\epsilon \to 0$ to a step function with a unique point of discontinuity ([**57**]).

**4.2.4. Gradient System with Non-local Terms.** We now deal with gradient systems with non-local effects.

**Source of Non-local Effects**

There are cases where the very nature of a problem naturally gives rise to non-local terms in the associated functional. Representative examples are as follows:

(1) the case where physical long-range interactions are present, such as in di-block co-polymers;
(2) the case where extremely different time scales coexist, such as the relaxation time scale due to an elastic response and that due to a reaction-diffusion process.

In case (1), the long-range interaction, caused by chains of polymers which are very long compared with some spatial scale (the thickness of interfaces, for example) in a di-block co-polymer mixture, naturally brings non-local effects into the system. (2) is the case in which a process proceeds at a very rapid rate compared to the time scale with which one is concerned (for example, the time scale of diffusion). For example, it is often the case that elastic effects in a system may relax considerably faster than, say, diffusion. In chemically reacting systems, taking advantage of the difference in time scales of various reacting substances, a so-called **pseudo-steady state approximation** often enables us to substantially reduce the number of unknowns. In fact, almost all of the model equations consisting of few variables to which a rigorous analysis is applicable are obtained by such a procedure.

**Minimizer with Fine Structure**

We consider a mixture of di-block co-polymers. For such a system, the energy functional $\mathcal{F}^{\epsilon,\sigma}$ is given by

$$\mathcal{F}^{\epsilon,\sigma} = \int_\Omega \Big\{ \frac{\epsilon^2}{2}|\nabla u|^2 + W(u) + \frac{\sigma}{2}\big((-\Delta_N)^{-1/2}(u-m)\big)^2 \Big\} dx \tag{4.18}$$

$$\text{with } u \in H^1(\Omega) \quad \text{and} \quad m = \frac{1}{|\Omega|}\int_\Omega u dx,$$

where $W(u)$ is a double-well potential with the two minima attained at $u = \pm 1$, while $m$ $(-1 < m < 1)$ is a parameter that represents the mass ratio of two polymers, and hence is a quantity to be conserved. The third term in the functional accounts for a non-local effect that is expressed as the one-half fractional power of the inverse of the Laplacian $(-\Delta_N)^{-1}$ under homogeneous Neumann boundary conditions. From the last condition in (4.18), the spatial average of $u - m$ is always equal to 0. The parameter $\sigma > 0$ is a constant that has to do with the length-scale of the polymers.

The formulation above is based on [**285**], and its original form is due to [**295, 14**]. In the same way as we did for the Cahn-Hillard equation, computing the gradient of (4.18) in $H^{-1}(\Omega)$, we obtain,

with $f = -W'$, the following system:

$$(4.19)\quad \begin{cases} u_t &= -\Delta\{\epsilon^2\Delta u + f(u) - \sigma(-\Delta_N)^{-1}(u-m)\} \\ &= -\Delta\{\epsilon^2\Delta u + f(u)\} - \sigma(u-m), \\ \dfrac{\partial u}{\partial n} &= \dfrac{\partial(\Delta u)}{\partial n} = 0, \\ u(x,0) &= u_0(x), \qquad \overline{u_0} = m. \end{cases}$$

In (4.19), the over-lined $\overline{u_0}$ stands for the spatial average of $u_0(x)$ on the domain $\Omega$. The difference in (4.19) from the Cahn-Hilliard equation (4.12) is simply that a linear reaction term that stabilizes the state $u = m$ is added to the right hand side. The difference, however, drastically changes the shape and dynamics of patterns. We restrict our attention here to a one-dimensional variational problem:

$$(4.20)\quad \min_{u\in A_m} \mathcal{F}^{\epsilon,\sigma}(u)$$

$$\text{with } A_m := \Big\{ u \;\Big|\; u \in H^1(0,1),\ \int_0^1 u dx = m \Big\}.$$

By applying Müller's method of [**271**], we obtain the following result on the minimizer [**286, 293**].

THEOREM 4.27. *Let us assume that $m = 0$ and $W(z) = W(-z)$. There exists an $\epsilon_0 > 0$ such that for $0 < \epsilon < \epsilon_0$ the problem* (4.20) *admits a minimizer $u^{\epsilon,\sigma}$ with the following properties:*

(i) *The minimizer $u^{\epsilon,\sigma}$, generically speaking, is uniquely determined and has a spatially periodic structure as depicted in* FIGURE 4.5. *The period $P^{\epsilon,\sigma}$ is characterized as follows:*

$$P^{\epsilon,\sigma} = 2\Big(3\sqrt{2}\, A\frac{\epsilon}{\sigma}\Big)^{\frac{1}{3}} + O(\epsilon^{\frac{2}{3}}).$$

(ii) *The value of the functional on the minimizer is characterized as*

$$\mathcal{F}^{\epsilon,\sigma}(u^{\epsilon,\sigma}) = \frac{\sigma}{8}\Big(3\sqrt{2}\, A\frac{\epsilon}{\sigma}\Big)^{\frac{2}{3}} + O(\epsilon^{\frac{4}{3}}).$$

*In the above,*

$$A = 4\int_{-1}^{1} \sqrt{W(s)}\, ds.$$

REMARK 4.28. The period of the minimizer ($= O(\epsilon^{\frac{1}{3}})$) is an intermediate scale (meso-scale) between the width ($= O(\epsilon)$) of transition layers separating the two kinds of polymers and a macro-scale ($= O(1)$). Since the period converges to 0 as $\epsilon \to 0$, the minimizer can be said to have a **fine structure** (FIGURE 4.5).

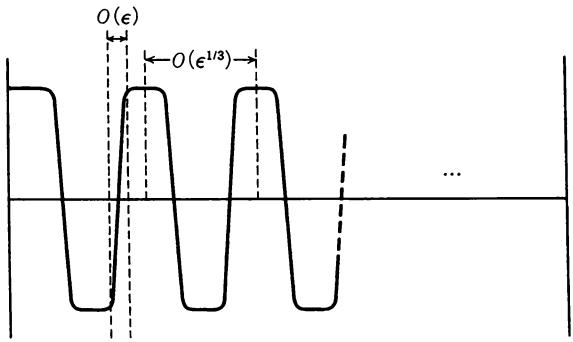


FIGURE 4.5. The period of length $O(\epsilon^{\frac{1}{3}})$ goes to zero together with $\epsilon$. However, it is very long compared with the width $O(\epsilon)$ of the interface.

REMARK 4.29. An extension of THEOREM 4.27 to three-dimensional space was recently obtained by [**73**]. The symmetry condition $W(z) = W(-z)$ is a technical assumption and could be removed. In fact, a recent work of Ren and Wei [**314**] shows that this is the case.

Why is it that the minimizer has a spatially oscillating fine structure? For the Cahn-Hilliard equation without non-local term, the interface (in one-dimensional space) consists of a single point, generating only a macroscopic phase separation. If a solution with such an interface is substituted into $\mathcal{F}^{\epsilon,\sigma}$, then the third term is $O(1)$, and hence it is far from being a minimizer. On the other hand, a function with a profile that oscillates rapidly around $u = m$ tends to minimize the third term. This is because the operator $(-\Delta_N)^{-1/2}$ is a compact operator, and hence the contribution from the third term tends to 0 as $u - m$ converges weakly to 0. However, if the profile oscillates too rapidly, then it makes the first and second terms large. This suggests that there must be an intermediate scale that is equally favorable for all three terms. Such an intermediate scale is nothing but the scale of $O(\epsilon^{1/3})$.

Setting $v(x) = \int_0^x u(x)dx$, choosing $\overline{u} = m = 0$, and noting that

$$\int_0^1 |(-\Delta_N)^{-1/2}u|^2 dx = \int_0^1 \left|\int_0^x u dx\right|^2 dx,$$

we find that (4.20) with $m = 0$ is equivalent to the following variational problem:

$$\min_{v\in H^2(0,1),v(0)=v(1)=0}\left\{\int_0^1 \frac{\epsilon^2}{2}|v_{xx}|^2 + W(v_x)^2 + \frac{\sigma}{2}|v|^2\,dx\right\}. \tag{4.21}$$

The functional in (4.21) appears also as a model functional in the phase transition of a metal crystal ([**271**]). If the first term is missing from the functional, the problem reduces to

$$\min_{v\in H^2(0,1),v(0)=v(1)=0}\left\{\int_0^1 (v_x^2 - 1)^2 + \frac{\sigma}{2}|v|^2\,dx\right\}. \tag{4.22}$$

A minimizing sequence of (4.22) does not necessarily give rise to its minimizer. For example, if we consider a sequence of functions that have gradient equal to either $+1$ or $-1$ (saw-tooth shape functions) with their absolute value decreasing to zero, then it is a minimizing sequence, and the limit of the sequence is $v \equiv 0$, which is not a minimizer of the problem (4.22).

This example shows that the functional in (4.22) is not lower semicontinuous. If the first term involving the second derivative is added as in (4.21), then it acts so as to prohibit the process of creating finer and finer structures. This is why the characteristic spatial scale of $O(\epsilon^{1/3})$ appears. It is also possible to derive the scale of the same order by using only dimensional analysis, as demonstrated in [**14**].

REMARK 4.30. The above scaling suggests that the problem (4.19) has a well-defined singular limit system as $\epsilon$ goes to zero. In fact, a sharp interface model of Mullins-Sekerka type (see CHAPTER 5) was formally obtained by [**285**]. Well-posedness of the resulting singular limit system was obtained by [**115**]. A detailed study was done for a one-dimensional case by Fife and Hilhorst [**138**].

### Rugged Landscape

Non-local terms not only produce a fine structure, but also give rise to a great number of **local minimizers**.

THEOREM 4.31 ([**286**]). *As $\epsilon \to 0$, the number of local minimizers for the functional of di-block co-polymers* (4.18) *goes to infinity.*

This theorem is proved, not by variational methods, but by showing that the number of locally asymptotically stable equilibria for the

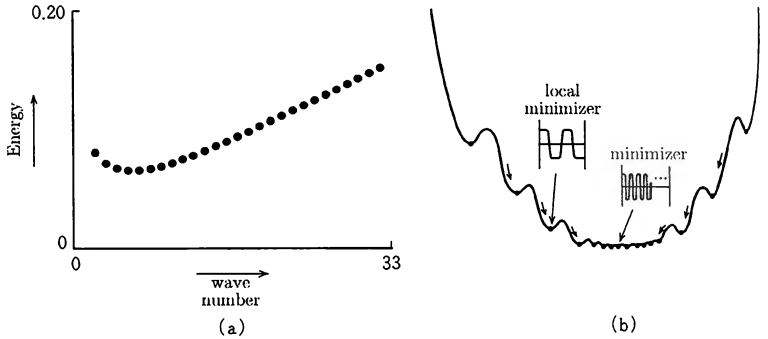


FIGURE 4.6. (a) The distribution of local minimizers for a model equation $u_t = -[\epsilon^2 u_{xx} + u(1-u^2)]_{xx} - \sigma(u-\overline{u})$. Here $\overline{u}$ is the average of $u$ and the boundary conditions are $u_x = u_{xxx} = 0$. In the computation, the parameters are chosen as $\epsilon = 5 \times 10^{-3}$, $\sigma = 50.0$, and the domain size is 1. (b) Other than the minimizer with a fine structure, there exist many local minimizers. The final destiny of the system depends on the initial condition.

gradient system (4.19) goes to infinity as $\epsilon \to 0$. In fact, introducing a new variable $v$ via

$$v = -\epsilon^2 \Delta u - f(u),$$

we can recast (4.19) as

$$\begin{cases} 0 = \epsilon^2 \Delta u + f(u) + v, \\ 0 = \Delta v - \sigma(u-m) - u_t, \end{cases}$$

to which the method to be discussed in CHAPTER 5 applies, giving rise to the existence of normal $n$-layer solutions and their stability. However, these solutions do not possess a fine structure as $\epsilon \to 0$.

By solving (4.19) numerically, one can show as in FIGURE 4.6 (a) that it has a lot of locally asymptotically stable equilibria (solid circles represent local minimizers). Therefore, the profile of the functional is schematically depicted as in FIGURE 4.6 (b), exhibiting a complicated shape with a great number of bumps and dents. In this situation, we say that (4.18) has a **rugged landscape**.

## 4.3. Dynamics of Open Systems

In open systems where mass or energy flows in and out, one cannot in general find functionals which decrease monotonically along the orbits of solutions, and hence such systems cannot be expected to be gradient systems. In such systems, the diversity of dynamics (such as creation of varieties of orders and rhythmical motions) is in sharp contrast to gradient systems, where everything tends to equilibrium states.

The horizon of research in open systems, which originated partly from the study of the diffusion-induced instability considered first by Turing, is still continuously spreading. Naturally it is very difficult to summarize briefly the full range of results for open systems. We therefore introduce here several typical model equations from phenomenological viewpoints, and discuss the basic patterns produced by these equations from the standpoint of scaling. Interfacial dynamics will be treated in CHAPTER 5, by means of the method of singular limit analysis. We recommend the reader to concurrently refer to [**270**], [**275**], [**160**], [**84**] in order to deepen the understanding of the following discussions.

**4.3.1. Basic Models of Reaction-Diffusion System.** A group of equations, called reaction-diffusion equations, appears in many fields of research with various outlooks. Hence for a newcomer to this area of research, it may give the impression that there is no coherence and the state of matter is confusing. Such an impression is probably caused by the following reasons. There are many ways of modelling in different levels, and nonlinearities differ slightly from one problem to another. Therefore it is not clear how and on what base one should understand research in reaction-diffusion systems.

In this subsection, we will take up probably the most prominent and simplest model equations of basic type. Using them as a guiding principle, we will discuss their relations to the properties of other equations of various types. These model equations, though they are derived rather phenomenologically compared with amplitude equations, serve qualitatively as prototypes of many other equations.

The basic model equations have two unknowns $(u, v)$, both of which diffuse in space. As the reaction kinetics of $(u, v)$,

$$u_t = f(u, v), \qquad v_t = g(u, v), \tag{4.23}$$

we require the following.

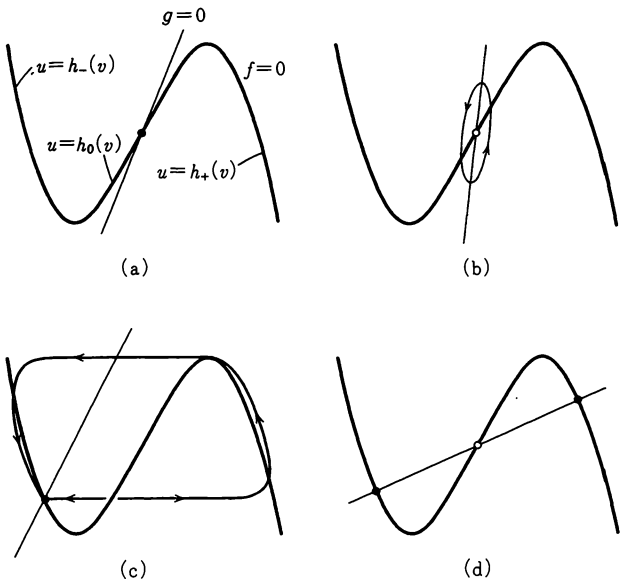


FIGURE 4.7. Dynamics of basic model equations. (a) Turing system, (b) oscillatory system, (c) excitable system, (d) bistable system.

**Hypothesis 1**: When $v$ is fixed, the kinetics is of bistable type with respect to $u$. The other variable $v$ plays the role of controlling the strength of the bistability of two equilibria. We also assume that $\partial f/\partial v < 0$ in an appropriate domain.

The bistable nature often stems from the fact that many systems possess at least two stable states, such as oxidized-reduced states and solid-liquid phases. A typical example of bistability is given by $f_0(u) = u - u^3$, which has already been encountered in §4.2.2. The simplest way to incorporate into this system a variable $v$ that controls the strength of the bistability is to choose $f(u, v) = f_0(u) - v$.

As one can see from FIGURE 4.7, considering the one-dimensional ordinary differential equation $u_t = f(u, v)$ with $v$ being regarded as a parameter, the basins of attraction for the two stable equilibria $u = h_-(v)$ and $u = h_+(v)$ are controlled by the value of $v$. The variable $u$ that exhibits the bistability property is usually called an **activator** or

a **propagator**. The former appellation, as will be clarified in the next subsection, expresses the feedback of its self-enhanced growth effect, while the latter one symbolizes, as we will see in later subsections, that the variable is regarded as a carrier of spatially propagating ordered structures. As for the nonlinearity $g(u,v)$ that controls the dynamics of the variable $v$, we choose those satisfying the following conditions.

> **Hypothesis 2**: The nonlinearity $g(u,v)$ satisfies the conditions $\partial g/\partial u > 0$ and $\partial g/\partial v < 0$.

The simplest example is $g(u,v) = u - \gamma v + k$ with $\gamma$ and $k$ being positive constants. The variable $v$ is often called an **inhibitor** or a **controller**. The variable $v$ is inhibitory because increase in $v$ inhibits the growth of $u$, as one can see from the functional form of $f(u,v)$. The variable $v$ is also called a controller because it controls the speed and direction of travelling wave solutions.

Employing the nonlinearity explained above, we arrive at a model system of reaction-diffusion equations:

$$\begin{cases} u_t = D_u \Delta u + f(u,v), \\ \\ v_t = D_v \Delta v + g(u,v), \end{cases} \qquad x \in \Omega, \tag{4.24}$$

where $\Omega$ is a smooth and bounded domain in $\mathbb{R}^N$. As boundary conditions, we always adopt in the sequel the Neumann conditions, unless otherwise stated:

$$\frac{\partial u}{\partial n} = \frac{\partial v}{\partial n} = 0, \qquad x \in \partial\Omega. \tag{4.25}$$

The system above is called a **reaction-diffusion system of propagator-controller** (or **activator-inhibitor**) **type**. Although there is no necessity to restrict the nonlinearity $(f,g)$ to polynomials as above (see CHAPTER 5 and [**281**] for a more general class of nonlinearities), we use the particular form as a concrete example in the discussions below. It should be also noted that the nonlinearity employed above naturally guarantees the $L^\infty$-boundedness of solutions of the initial value problem associated with (4.24).

Equations of propagator-controller type are classified into four categories according to their kinetics (i.e., the behavior of a two-dimensional dynamical system obtained by ignoring the diffusion effects) as follows:

(1) Turing System,
(2) Oscillatory System,

(3) Excitable System,
(4) Bistable System.

As one can see from FIGURE 4.7, in the first three cases there is only one attractor, while in the fourth case two attractors are present, giving rise to bistability. Bistability here should be understood in terms of a two-dimensional dynamical system, being different from that in a scalar equation $u_t = f(u, v)$ with $v$ fixed as a parameter as in **Hypothesis 1**.

Among the cases in which there is only one attractor, if the attractor is a **limit cycle** then the system is called oscillatory. If the attractor is an equilibrium, the system is called either a Turing system or an excitable system according to whether the equilibrium is located on the middle branch of the nullcline $\{f(u, v) = 0\}$ or on the left branch as in FIGURE 4.7 (c). The appellation "Turing system" is a convention only in this chapter. As we will see later, in Turing systems the equilibrium is destabilized by spatially inhomogeneous perturbations, while in excitable systems it remains locally asymptotically stable against such perturbations. Moreover, excitable systems have a property called excitability that characterizes a specific behavior of orbits. In the sequel, we will focus our discussions on (1) Turing systems and (3) excitable systems.

**4.3.2. Turing System and Standing Wave.** In this section, we describe what Turing instability is, and its connection, via singular perturbation theory, to large-amplitude standing wave solutions.

**Diffusion-Driven Instability**

We have already encountered scalar reaction-diffusion equations in §4.2.2. Since scalar equations are a gradient system, their solutions asymptotically settle down to one of the equilibria. Moreover, it is also shown that the equilibria are (*generically*) a constant state. This means that the system settles down to minima of the energy functional and creates no inhomogeneous structures, confirming our intuition that diffusion effects eliminate inhomogeneity and drive the system to a uniform state.

On the contrary, when **several** diffusive substances interact, this intuition is not necessarily correct, as pointed out first by Rachevsky [**312**] and Turing [**342**]. The idea in these works, which is basically accounted for in terms of linear stability analysis, has tremendously influenced the subsequent research activities in pattern formation,

leading up to the present time. It took, however, a long time for this idea to be realized in real experiments (see, for instance, [**60**] and [**87**]) due to the difficulty of avoiding fluid dynamical effects such as convection and surface tension.

Let us consider two diffusive substances $(U, V)$ and denote their concentrations by $(u, v)$. Assuming that these substances not only diffuse but also undergo a nonlinear interaction described by $(f, g)$, we consider the reaction-diffusion system (4.24). We assume that there exists a spatially homogeneous equilibrium state $X_0 = (u_0, v_0)$, i.e., $f(X_0) = 0$ and $g(X_0) = 0$. To analyze the linear stability of the constant state against spatially inhomogeneous perturbations, it suffices to deal with the following linearized equation:

$$\begin{cases} \dfrac{\partial w}{\partial t} = D_u \Delta w + f_u w + f_v z, \\ \dfrac{\partial z}{\partial t} = D_v \Delta z + g_u w + g_v z. \end{cases} \tag{4.26}$$

In the above, the derivatives of a nonlinearity are evaluated at $X_0$.

Turing imposed the following requirements on $X_0$ in order to guarantee that fluctuations grow and eventually give rise to spatially inhomogeneous ordered states.

> **(T) Diffusion-Driven Instability**
> $X_0$ is a stable equilibrium with respect to the ODE (4.23), while it is susceptible to destabilization with respect to the PDE (4.26). This instability is also called the Turing instability.

This requirement cannot be realized in scalar reaction-diffusion equations, as one can verify easily. It is necessary to consider systems with more than one component in order to realize non-constant ordered states from homogeneous states by adding spatially inhomogeneous fluctuations to it. Here, of course, we assume that our systems depend only on reaction and diffusion mechanisms like (4.24); in fact, if we introduce other effects such as time-delays, nonlocalities or higher order derivatives, then the requirement **(T)** could be satisfied even for scalar equations. This is, however, almost equivalent to introducing another unknown variable.

Let us now analyze (4.26). For simplicity, we first consider the problem on the entire space $\mathbb{R}^N$. It is sufficient to look for solutions

of the following form:

$$\begin{pmatrix} w \\ z \end{pmatrix} = \Phi_k \exp(\omega_k t + i\mathbf{k}\cdot\mathbf{r}).$$

That is to say, we look for solutions that have a temporal growth rate $\exp(\mathrm{Re}(\omega_k)t)$ for perturbations with wave number $\mathbf{k} \in \mathbb{R}^N$. Substituting this into (4.26), we obtain the following characteristic equation for $\omega_k$ and $k = |\mathbf{k}|$:

$$\omega_k^2 - T\omega_k + \delta = 0, \tag{4.27}$$

where

$$T = T(k^2) = f_u + g_v - k^2(D_u + D_v), \tag{4.28}$$

$$\delta = \delta(k^2) = f_u g_v - f_v g_u - (D_v f_u + D_u g_v)k^2 + D_u D_v k^4. \tag{4.29}$$

Since the diffusion and the reaction are isotropic, the equation (4.27) depends only on $h := k^2$. The first requirement in **(T)** that $X_0$ be a stable equilibrium of the ODE is fulfilled by imposing the conditions

$$T(0) = f_u + g_v < 0, \tag{4.30}$$

and

$$\delta(0) = f_u g_v - f_v g_u > 0. \tag{4.31}$$

We therefore assume in the sequel that these conditions are satisfied. The second half of **(T)** demands that (4.27) has a solution with positive $h$ at $\mathrm{Re}(\omega_k) = 0$, where instabilities set in. The first half of **(T)**, the definition of $T(h)$, and the fact $D_u + D_v > 0$ imply that the instability occurs only when a real eigenvalue crosses the origin, i.e., $\delta = 0$. This means that the destabilization is induced not by a Hopf bifurcation but by a static bifurcation. By the requirement (4.31), the condition

$$D_v f_u + D_u g_v > 0 \tag{4.32}$$

is necessary for $\delta$ to be zero ($\delta(h) = 0$) with positive $h$. In order for the destabilization to be the first one, it is also necessary to have the double-root condition:

$$(D_v f_u + D_u g_v)^2 - 4(f_u g_v - f_v g_u)D_u D_v = 0.$$

Under these conditions the unstable wave number $k_c$ (the value of the double root) is given by

$$k_c = \left\{ \frac{f_u g_v - f_v g_u}{D_u D_v} \right\}^{\frac{1}{4}}. \tag{4.33}$$

What is remarkable here is that spatial structure to be produced through such a bifurcation has a **characteristic wave length intrinsic to the system**,

$$L = \frac{2\pi}{k_c}, \tag{4.34}$$

which is proportional to the geometric mean of the diffusion lengths of $U$ and $V$, independent of boundary conditions. This is in sharp contrast to the Rayleigh-Bénard problem, in which the size of a convection cell is determined by external factors such as boundary conditions.

(4.30) and (4.32) imply that $f_u$ and $g_v$ cannot have the same sign. Therefore, from (4.31) we obtain

$$f_u g_v < 0, \qquad f_v g_u < 0. \tag{4.35}$$

Up to this point, we have not made any distinction between $u$ and $v$. Here we need to abandon such a symmetry to identify the signs of the entries in the coefficient matrix. Mathematically speaking, one can arbitrarily choose the sign of $f_u$. Let us choose

$$f_u > 0, \qquad g_v < 0. \tag{4.36}$$

$f_u > 0$ means that the increase of $u$ enhances its growth speed. Namely, we have chosen to regard $u$ as an **activator**. If we adopt the opposite signs, $v$ can be considered as an activator. As for the sign of $f_v$, we only have the constraint in (4.35). If we choose $f_v < 0$, the increase of $v$ inhibits the growth of the activator $u$, giving to $v$ the role of an **inhibitor**. With such choices of signs, the system is called an **activator-inhibitor system**, which already appeared in subsection 4.3.1. From the conditions (4.30) and (4.32), in order for the Turing instability to occur, the condition

$$D_v > D_u \tag{4.37}$$

must be satisfied. Namely, only when the inhibitor diffuses faster than the activator, can the Turing instability occur. The Turing instability could be intuitively explained as follows: For a fixed $v$, $u$ starts to increase thanks to (4.36). If there is no diffusion effect, $v$ also increases and suppresses the growth of $u$, and the orbit returns to the equilibrium (ODE dynamics). On the other hand, if a diffusion effect is added and $v$ diffuses faster than $u$, then $v$ quickly spreads widely and its local concentration is not high enough to prevent the growth of $u$; hence the instability occurs.

On the other hand, when $f_v > 0$ the system is called a **substrate-depleted system**, in which $v$ is considered as a substrate of the reaction. For example, $u$ may represent the temperature and $v$ the fuel, and the presence of $v$ serves to increase the growth rate of $u$ ($f_v > 0$). The Gray-Scott model, to be treated in CHAPTER 6, is another example of such a system.

REMARK 4.32. The classification in the above as an activator-inhibitor or a substrate-depleted system depends only on the linear part of the equations around the constant equilibrium under consideration, and has nothing to do with the global property of nonlinearity. Therefore, the global nonlinear dynamics of a system may be different from the dynamics suggested by the appellation of the system. In fact one can regard a substrate-depleted system as an activator-inhibitor system of indirect type in the following sense: when substrate is consumed, the activator does not have enough resources to be available, which causes the decrease of the activator. We will see in CHAPTER 6 that the Gray-Scott model and the Gierer-Meinhardt model display a similar dynamics, called pulse-splitting in a regime far from equilibrium.

REMARK 4.33. When the system has only a linear part, it may satisfy the condition **(T)**, but this clearly does not guarantee the boundedness of solutions, let alone the bistability.

The Lengyel-Epstein model is a representative example of a Turing system. This model is a realistic one, based on an actual chemical reaction called the CDIMA-reaction ([**244**]), given by

$$\begin{cases} \dfrac{\partial u}{\partial t} = a - u - \dfrac{4uv}{1+u^2} + \Delta u, \\ \dfrac{\partial v}{\partial t} = \delta\left[b\dfrac{u - uv}{1+u^2} + c\Delta v\right], \end{cases}$$

where $u$ stands for the concentration of iodide and $v$ that of chlorine dioxide.

### Bifurcation Theory vs. Singular Perturbation Theory

We have explained how a diffusion-driven instability occurs. In order to describe how such an instability produces spatially ordered structures, several nonlinear analytic methods have been developed.

**Local Bifurcation Theory** (for small amplitude solutions)

When the strength of a nonlinearity or a diffusion changes, it happens that a finite band of wave numbers is destabilized simultaneously. On bounded domains with appropriate boundary conditions (the Neumann conditions, for example), only a finite number of discrete eigenvalues are destabilized, to which one can apply bifurcation theory and center manifold theory directly. General theories have been established for such problems, even for cases of high space dimension. We do not explain the details here, but only recommend the reader to consult [**233**], [**74**] and [**163**].

**Singular Perturbation Theory** (for large amplitude solutions)

In many situations, bifurcation theories can deal only with a small neighborhood of trivial solutions. To describe global behaviors far from bifurcation points, qualitative theories based on topological arguments are available. However, such theories are not satisfactory to examine the detail of solutions and dynamics. One of the powerful theoretical tools for handling large amplitude solutions is the method of singular perturbation. In cases of space dimension one, the methods of matched asymptotic expansion ([**131**], [**134**], [**266**], [**190**]) and geometric singular perturbation theories ([**199**]), which have been rapidly developed in recent years, enable us to obtain large-amplitude solutions and their stability properties. A glimpse of these theories will appear in CHAPTER 5.

In multi-dimensional cases, however, it is very difficult, first of all, to find a solution to the lowest order approximation problem (the so-called reduced problem) which is a seed for singular perturbation procedures to grow from. Rigorous theories for the existence and stability of large-amplitude solutions are still in their infancy (cf. [**137**], [**321**], [**340**]). It is, however, possible to obtain interesting results from scaling viewpoints, which will be treated in CHAPTER 5. On the other hand, computer-assisted investigations of nonlinear dynamics in infinite dimensional phase spaces have been rapidly developing in recent years. Tracing global bifurcation branches by such methods is becoming practical, as we will explain in CHAPTER 6. Developments of new theories based upon such computer-assisted investigations will be indispensable for going beyond perturbational methodologies.

**4.3.3. Excitable Systems and Spiral Waves.** At the beginning of the 1970's, when spiral chemical patterns as in FIGURE 4.8

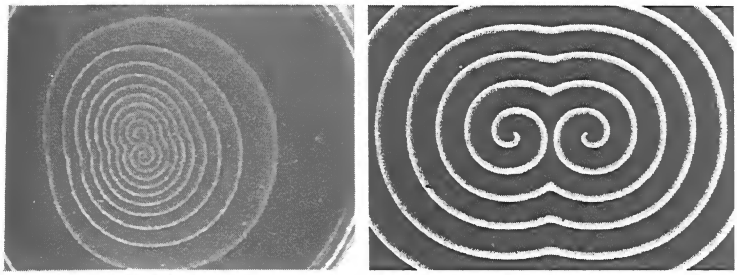


FIGURE 4.8. (a) An experiment of the BZ reaction. (b) A numerical simulation on the model system: $u_t = D\Delta u + u(1-u)(u-a) - v, \quad v_t = \epsilon(u - \gamma v)$ with $D = 2 \times 10^{-6}$, $a = 0.25$, $\gamma = 7.1$ (mono-stable), $\epsilon = 1 \times 10^{-3}$, domain size $= 2.0 \times 1.5$.

were discovered in an actual oxidation-reduction reaction, it was received with great surprise. Such dynamic spiral patterns that spontaneously choose a certain angular velocity and tip form, observed in the **BZ reaction** (Belousov-Zhabotinsky reaction), had never been even imagined to exist in chemical reactions, since chemical reaction had been thought to occur homogeneously and to monotonically reach an equilibrium.

Theoretical issues for such a phenomenon are mainly focused on the shape and the velocity, and especially on how the shape of the core (center of spiral) and its angular velocity are selected. The same type of issues were encountered in crystal growth. To resolve such problems, it is necessary to have a simple model equation that is easily analyzed and has a close relevancy to experiments. Although the details of the BZ reaction are quite complicated, a two-dimensional system of reaction-diffusion equations has been widely used to describe its essential reaction steps. The system of reaction-diffusion equations and its interface dynamics capture very well the macroscopic behaviors of the reaction.

The dynamic mechanism therein extracted has a wide range of applicability in many areas other than the BZ reaction. For example, it can be used to describe spiral patterns that appear in equations modeling nerve-impulse propagation, colonies of bacteria (slime mold), the Rayleigh-Bénard convection, and nematic liquid-crystals. Moreover,

a special case of such dynamics reduces to the mean-curvature flow that will be treated in CHAPTER 5. These examples suggest that the formation of spiral waves is one of the universal types of dynamics which do not depend too much on individual phenomena or on their detailed mechanisms.

### Dynamics of Excitable Systems

A basic kinetics in an excitable system is given by

$$u_t = f(u,v), \qquad v_t = \epsilon g(u,v) \tag{4.38}$$

with $u$ and $v$ respectively being fast and slow variables. The small positive parameter $\epsilon$ here reflects the difference in the time scales of $u$ and $v$. In the BZ reaction, $u$ and $v$ are the concentrations of Ferrien and $HBrO_2$, while in the nerve impulse model they correspond to the action-potential and ionic conductance of the nerve membrane, respectively.

The most notable characteristic feature in excitable kinetics is the existence of a threshold value. As one can see from FIGURE 4.9, all orbits, regardless of initial values, eventually converge to the asymptotically stable equilibrium $U_s = (u_s, v_s)$. However, consider for example the initial values on the line $v = v_s$. The way in which orbits converge to the equilibrium differs sharply across the point $u = a$. If $u < a$, the orbit immediately converges to $U_s$. Since $\epsilon$ is such that $0 < \epsilon \ll 1$, if $u > a$, on the other hand, the orbit takes a large detour, first moves to the right, up, and jumps down to the left, and finally settles down to $U_s$. The value $u = a$ in this sense deserves to be called a *threshold* value, giving a measure for us to judge how sensitively the system reacts to excitation.

When diffusion effects are added to the excitable kinetics, we have the following model equations:

$$\begin{cases} u_t = \Delta u + f(u,v), \\ v_t = \delta \Delta v + \epsilon g(u,v), \end{cases} \tag{4.39}$$

where $\delta = D_v/D_u$ stands for the ratio of the diffusion effects of $u$ and $v$. The diffusion effects induce propagating waves of excitation in spatial directions. Namely, once an excitation is given that lies above the threshold at a spatial point, the diffusion effect forces neighboring points to rise above the threshold, causing $u$ to be excited, and the excitation propagates. The values once excited above the threshold return to the rest state ($U_s$) after an interval of time. Therefore, one

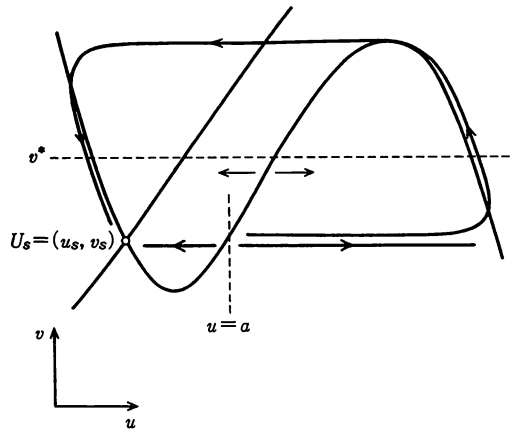


FIGURE 4.9. Dynamics of an excitable system. $v^*$ is a value such that $J(v^*) = 0$, at which the speed of the front solution connecting $h_-(v^*)$ and $h_+(v^*)$ is zero. As $v_s$ gets near $v^*$, the threshold value becomes higher. If the value of $u$ rises above this threshold value, orbits quickly jump to the right branch and follow the branch, jump back to the left branch near the top of the right branch, then gradually approach the equilibrium.

can expect to observe impulsive waves in the case of one space dimension, and a spreading ring of pulses in the case of two space dimensions. If the system is forced periodically, periodic travelling waves in one-dimensional spaces and target patterns in two-dimensional spaces could be produced.

We may not be allowed to take the period of the forcing too short. The reason for this is, if it is too short $u$ may not be excited easily even by somewhat high intensity of forcing, since the value of the controller $v$ (which is a slow variable) is not necessarily low (cf. FIGURE 4.9). On the other hand, if the period of the forcing is very large, the behavior of the orbit becomes closer to that of a single-pulse solution.

The diffusion ratio $\delta$ may not be chosen arbitrarily in order to have such propagating waves. First of all, note that a role of $v$ is to control (inhibitively) the susceptibility of $u$ to excitation. As one

can see from FIGURE 4.9, the larger the $v$-value is, the higher the threshold-value, and hence $u$ is hard to excite (excitation of $u$ is inhibited). Therefore, if $\delta$ is large, $v$ diffuses rapidly and blocks the propagation of excited $u$-states. In fact, for large $\delta$, stationary solutions of Turing type are dominant instead of propagating waves (cf. (4.37)).

Therefore, $\delta$ has to be of order $O(1)$, at most. In the BZ reaction, $\delta \approx 1$, reflecting the fact that most chemical substances diffuse at almost the same rate. In the nerve impulse model, $\delta = 0$. These two cases are compatible with the theoretical prediction.

For later use, let us deal with the existence and wave speed of one-dimensional travelling fronts for the scalar equation obtained from the first of (4.39) by freezing $v$ as a parameter. Introducing the travelling coordinate $\xi = x - ct$, and assuming that $v$ lies in the range where $h_\pm(v)$ are defined, we have the following result.

PROPOSITION 4.34 ([**94**], [**139**], [**140**]). *The problem*

$$\begin{cases} u_{\xi\xi} + cu_\xi + f(u,v) = 0, & \xi \in \mathbb{R}, \\ \lim_{\xi \to \pm\infty} u(\xi) = h_\pm(v) \end{cases}$$

*has a unique solution up to phase shifts, and the wave speed $c$ is uniquely determined as a function $c = c(v)$ of $v$. The sign of $c(v)$ is determined as*

$$c(v) \begin{cases} > 0 \\ = 0 \\ < 0 \end{cases} \iff J(v) \equiv \int_{h_-(v)}^{h_+(v)} f(s,v)ds \begin{cases} < 0, \\ = 0, \\ > 0. \end{cases}$$

*Moreover, there exists a unique $v^*$ such that $J(v^*) = 0$.*

Introducing slow variables $t' = \epsilon t$ and $x' = \epsilon x$ (and rewriting them as $(t,x)$), the model equation (4.39) is recast as

$$\begin{cases} \epsilon u_t = \epsilon^2 \Delta u + f(u,v), \\ v_t = \epsilon\delta \Delta v + g(u,v). \end{cases} \tag{4.40}$$

This system has a convenient form for us to apply singular perturbation methods. The system (4.39) is called the **fast system**, while (4.40) is called the **slow system**.

A concrete example of nonlinearity for the nerve impulse model is given by that of the basic model equation which appeared in §4.3.1:

$$\begin{cases} u_t = \Delta u + u(1-u)(u-a) - v, \\ v_t = \epsilon(u - \gamma v), \end{cases} \tag{4.41}$$

which is called the **FitzHugh-Nagumo equation**. In this model a (one-dimensional) travelling impulse and sequences of impulses propagating along the nerve axon carry the information.

As another example, in the BZ reaction as in FIGURE 4.8, a model called the **Oregonator**, given by

$$\text{(4.42)} \qquad \begin{cases} \epsilon u_t = \epsilon^2 \Delta u + \left[ u(1-u) - \dfrac{\gamma v (u-k)}{u+k} \right], \\ v_t = \epsilon \delta \Delta v + u - v, \end{cases}$$

is a representative among many proposed models. In (4.42), $\gamma, k$ are positive constants (cf. [**356**] and the references therein for details). The nonlinearity of (4.42) satisfies the two hypotheses imposed in §4.3.1, as one can easily verify by examining the nullclines of the nonlinearity.

In an excitable system, in particular in the BZ reaction, the most important two-dimensional pattern may be the spiral pattern. We can simply extend a one-dimensional pulse solution to a two-dimensional planar pulse solution. If we cut across the planar pulse to create an edge, then spiral waves emerge. A characteristic feature of spiral waves is that no external stimulus is necessary to sustain its motion; they are produced spontaneously. Such a feature is a source of the universality of spiral waves. In the sequel, after briefly explaining about properties of one-dimensional pulse solutions, we focus our investigation on spiral waves.

**Travelling Pulse Solution and Dispersion Relation**

**(i) Travelling Pulse Solutions**

The most basic pattern in excitable systems is a travelling pulse solution (also simply called a pulse solution), which is a travelling solitary wave with constant shape and velocity, as depicted in FIGURE 4.10. It essentially depends on one variable $\xi = x - ct$ and is a solution $U(\xi) = U(x-ct) \equiv (u(x-ct), v(x-ct))$ of the following problem:

$$\text{(4.43)} \qquad \begin{cases} 0 = DU_{\xi\xi} + cU_\xi + F(U), \\ \lim_{\xi \to \pm\infty} U(\xi) = U_s, \end{cases}$$

where

$$D = \begin{pmatrix} 1 & 0 \\ 0 & \delta \end{pmatrix}, \qquad F(U) = (f, \epsilon g), \qquad U_s = (u_s, v_s).$$

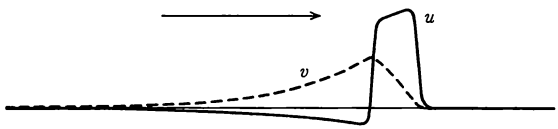


FIGURE 4.10. Travelling pulse wave. This is a single travelling pulse for the model excitable system below. The amplitude of $v$ is magnified six times for visualization. $u_t = D_u \Delta u + u(1-u)(u-a) - v$, $v_t = \epsilon(u - \gamma v)$, $D_u = 2 \times 10^{-4}$, $a = 0.25$, $\epsilon = 1 \times 10^{-3}$, $\gamma = 3.0$, Domain size $= 6.0$.

The point here is only how we choose the value $c$, which corresponds to travelling wave speed, so that the ordinary differential equation (4.43) has an orbit homoclinic to $U = U_s$.

For the FitzHugh-Nagumo equation, the existence of pulse solutions was first established, independently, in [**55**] and [**174**], and later in [**241**] a geometric proof was given. The method in [**200**] made it easy to track orbits in slow-fast systems in terms of a sophisticated tool called an exchange lemma, and gave a simpler proof to the results in [**241**]. The method in [**200**] is a prototype of geometric singular perturbation ([**199**]).

THEOREM 4.35 (Existence of Pulse Solution). *For sufficiently small $\epsilon > 0$, the FitzHugh-Nagumo equation* (4.41) *has a pulse solution $U_p$ with wave speed $c_p(\epsilon)$. As $\epsilon \to 0$ the speed $c_p(\epsilon)$ approaches the speed $c_p^*$ of the singular orbit determined by the nonlinearity* (*cf.* FIGURE 4.11 (a)).

In FIGURE 4.11, the orbits expressed by broken lines represent front solutions for the scalar equation with $v = v_f$ (or $v = v_b$) being fixed. PROPOSITION 4.31 guarantees that such orbits uniquely exist, and that $c(v_b)$ must coincide with $c(v_f)$ in order to make a pulse solution.

As for the stability of the pulse solution, Evans ([**122**] - [**125**]) linked the distribution of eigenvalues of the linearized problem to that of zeros of the so-called Evans function. This idea initiated a trend of using a topological method in stability analysis, which is now called the stability index ([**1**], [**152**], [**199**], [**278**], [**322**]).

The stability of pulses in the FitzHugh-Nagumo equation was rigorously established by [**198**], [**359**]. Stability analyses by analytical methods have been available for propagator-controller systems, which

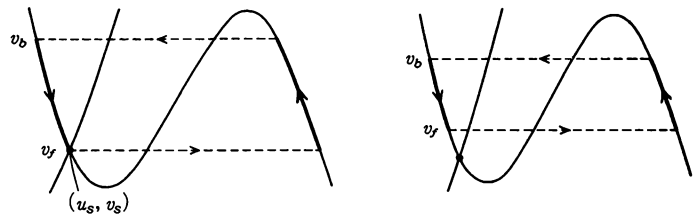


(a) singular orbit of one-pulse solution

(b) singular orbit of periodic travelling wave solution

FIGURE 4.11. (a) Singular orbit of a single pulse solution. The value of $v_b$ is determined so that the speeds of the front and back waves for the scalar bistable equation with fixed $v$ coincide at $v = v_f$ $(= v_s)$ and $v_b$. (b) Singular orbit of a periodic wave train. In the same manner as for pulse solutions, the values $v_f$ and $v_b$ are determined so that the speeds of the front and back waves are equal. Since the orbit does not pass through the equilibrium, it represents a periodic solution.

will be described in §5.4. It is also known ([**187**]) that the topological and analytical methods have a very close connection.

THEOREM 4.36 (Stability of pulse solutions). *For $\gamma > 0$, the pulse solution $U_p$ to (4.41) is asymptotically stable in the $C_b(\mathbb{R})$-sense with asymptotic phase shifts. Here $C_b(\mathbb{R})$ is the set of bounded uniformly continuous functions on $\mathbb{R}$.*

### (ii) Periodic Wave Train and Dispersion Relation

It is known that two-dimensional planar pulse solutions obtained by extending one-dimensional periodic travelling waves give a good approximation to the behavior of spiral and target patterns in the region far away from their cores.

The most important piece of information in characterizing a periodic travelling wave is its dispersion relation. It describes the relation between spatial period and wave speed. When we introduce a new coordinate $z = x - ct$, finding a periodic travelling wave is equivalent to finding a solution which is $T$-periodic in $z$, where $c$ is the speed of

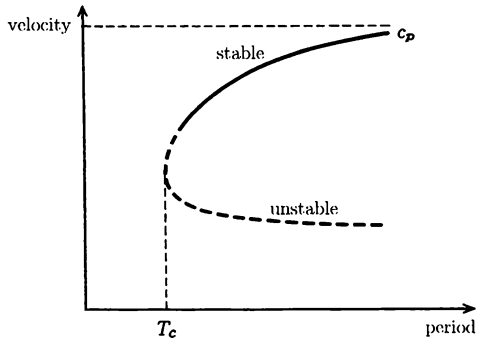


FIGURE 4.12. A typical dispersion relation for a periodic travelling wave. The solid (resp. broken) line stands for the stable (resp. unstable) branch.

the periodic travelling wave. The equation (4.40) is recast as

$$\begin{cases} \epsilon^2 u_{zz} + \epsilon c u_z + f(u,v) = 0, \\ \\ \epsilon\delta v_{zz} + c v_z + g(u,v) = 0, \end{cases} \tag{4.44}$$

in terms of the new variable. In general this system of equations has a $T$-periodic solution only if there is a relation between $c$ and $T$:

$$c = H(T;\epsilon,\delta), \tag{4.45}$$

which is called a **dispersion relation**.

It is in general difficult to rigorously determine such a relation. When $\delta$ is not so large compared with $T$ and $c$, it is known ([**343**], [**95**], [**249**], [**250**]) that the graph of such a relation is as given in FIGURE 4.12. When the period $T$ is sufficiently large, the wave speed must be close to that $c_p$ of the single-pulse solution. When $0 < \epsilon \ll 1$, a singular perturbative construction of periodic travelling waves for (4.44) is possible by using the method of matched asymptotic expansions as in [**185**]. Singular orbits as $\epsilon \to 0$ in such a construction behave as in FIGURE 4.11 (b), in which $v_f$ and $v_b$ are the values at the front and back and satisfy $c(v_f) = -c(v_b)$.

When $\delta = 0$, the lowest order relation between the period $T$ and the speed $c$ is given by

$$T = T_+ + T_- = c\left\{\int_{v_f}^{v_b} \frac{dv}{g(h_+(v),v)} + \int_{v_b}^{v_f} \frac{dv}{g(h_-(v),v)}\right\}. \tag{4.46}$$

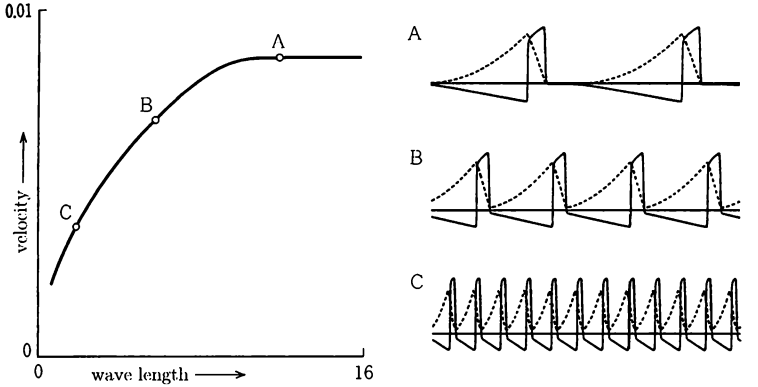


FIGURE 4.13. Dispersion relation and the concentration profile of the inhibitor $v$. The model equation is the same as in FIGURE 4.10 with $\gamma = 0.0$ and domain size $= 24.0$. The concentration of $v$ is magnified six times for ease of visualization. In case A, the concentration of $v$ between two pulses is almost equal to 0, while in B and C, it gets higher as the interval between pulses decreases, and the speed slows down.

This is immediately obtained as follows. In the lowest order of outer expansion for (4.44), we have

$$\begin{cases} f(u,v) = 0, \\ cv_z + g(u,v) = 0. \end{cases}$$

Solving the first equation as $u = h_{\pm}(v)$, then substituting them into the second equation, and integrating the resulting equation, we obtain (4.46). As $v_f$ approaches $v_s$, since $g(h_-(v_f), v_f) \to 0$, $T_-$ diverges, and $c$ converges to the speed $c_p$ of the single pulse solution.

A characteristic feature of FIGURE 4.12 is that as the period becomes short, the speed decreases, and the graph has a folding point at $T = T_c$. The stability property of the periodic travelling wave changes before the folding point is reached, and for $T$ below the value $T_c$ there is no solution. This behavior is natural because, as the period between pulses gets shorter, the inhibitor accumulates in between the pulses, and hence the wave speed decreases (cf. PROPOSITION 4.31).

In fact, if one performs numerical simulations on the FitzHugh-Nagumo equation, one can actually observe, as in FIGURE 4.13, that the inhibitor $v$ accumulates between pulses. The corresponding singular orbit on the phase plane, as in FIGURE 4.11 (b), becomes an elongated cycle with the increase of $v_f$. If the period of external stimuli gets shorter, the threshold value becomes so high (the refractory state) that the system cannot be excited, and hence propagation fails. Note that whether the system can be excited or not is determined not only by $v$, but also by the strength of the external stimulus.

### Matched Asymptotic Expansion and Velocity-Curvature Equation

When we deal with spiral patterns, the most serious difficulty comes from the fact that they are genuinely two-dimensional (dynamic) patterns. A spiral consists, as in FIGURE 4.8, of the core (center part) and arms extending outwards. Near the core, the curvature cannot be ignored. It is not an easy task to find directly a whole spiral as a solution of the reaction-diffusion equations (4.40).

Instead of dealing directly with (4.40), we attempt to characterize the behavior of spirals by solving an approximate problem. The approximation is obtained by expanding (4.40) as an asymptotic series in $\epsilon$ and by truncating it at a finite order. We first describe a general framework for matched asymptotic expansions, and use it to derive a basic equation of interface dynamics, called a velocity-curvature equation, following the presentation by Fife [**134**].

Let us assume that a smooth function $u(x, t; \epsilon)$ is a solution of a differential equation and that the function also depends on a small parameter $\epsilon$ (for simplicity, the space dimension is assume to be two: $x = (x_1, x_2)$). As we have observed so far, instead of directly examining the behavior of $u$ itself, it is more illuminating, and more efficient in bringing out the dynamics of the original system, to investigate the motion of an internal layer $\Gamma(t; \epsilon)$ (often called an *interface*) where $u$ jumps up or down from one branch to another for small $\epsilon$. One of the most effective ways to determine (at least formally) how the interface moves is to use the method of matched asymptotic expansion and associated solvability conditions. Although such an idea is quite old and simple, it has not been widely utilized, probably because procedures to implement it are cumbersome. In one-space-dimensional

cases, the method of geometric singular perturbation ([**199**]) is also successful.

The interface $\Gamma$ as above cannot be determined uniquely, even if the associated solution $u$ (with $\epsilon > 0$) is given. In fact, it usually has a thickness of $O(\epsilon)$, and its exact location has to be artificially specified. Practically it is defined as a level set of some solution of an inner problem. As a preparation, let us explain about inner and outer problems for a given interface $\Gamma$, as well as compatibility (matching) conditions between the two problems.

Let us suppose that the interface $\Gamma(t;\epsilon)$ is given as a curve on the plane. We treat the motion of $\Gamma$ as the evolution of the signed distance function $r(x,t;\epsilon)$ to $\Gamma$:

$$\Gamma(t;\epsilon) = \{\, x \in \mathbb{R}^2 \mid r(x,t;\epsilon) = 0 \,\}. \tag{4.47}$$

Assuming that $\Gamma$ subdivides $\mathbb{R}^2$ into two regions $\mathcal{D}_\pm$, we assign $r$ a positive (resp. negative) sign in $\mathcal{D}_+$ (resp. $\mathcal{D}_-$). Let $\Gamma_\delta(t;\epsilon)$ denote the $\delta$-neighborhood ($|r| \le \delta$) of $\Gamma$, and let $\mathcal{D}_\delta(t;\epsilon) = \mathbb{R}^2 \backslash \Gamma_\delta$. If the function $u$ is smooth in the regions other than $\Gamma$ up to $\epsilon = 0$, then it will be well approximated by the following **outer expansion**:

$$u(x,t;\epsilon) \simeq \sum \epsilon^n u_n(x,t). \tag{4.48}$$

The meaning of this expression is as follows. Let us denote by $u^{(N)}$ the partial sum up to the $N$-th order term. Then we demand the existence of a $\delta(N,\epsilon) > 0$ such that $\delta(N,\epsilon) \to 0$ as $\epsilon \to 0$ and

$$|u - u^{(N)}| = O(\epsilon^{N+1}), \quad \epsilon \to 0,$$

uniformly on $\mathcal{D}_{\delta(N,\epsilon)}$. Each term $u_n$ in the outer expansion is in general discontinuous or non-smooth across the interface $\Gamma$. It is, however, smooth up to $\Gamma$ if restricted to either $\mathcal{D}_-$ or $\mathcal{D}_+$. In order to study the detailed behavior of $u$ near $\Gamma$, it is convenient to introduce a local orthogonal curvilinear coordinate system $(r(x,t;\epsilon), s(x,t;\epsilon))$, in which $s$ stands for the arclength measured along $\Gamma$. We also define a stretched variable $\rho$ in the normal direction by

$$\rho(x,t;\epsilon) \equiv \frac{r(x,t;\epsilon)}{\epsilon}. \tag{4.49}$$

An **inner expansion** of $u$ near $\Gamma$ is the following power series:

$$U(\rho,s,t;\epsilon) \simeq \sum \epsilon^n U_n(\rho,s,t), \tag{4.50}$$

where $U$ is the function $u$ expressed in terms of $(\rho,s,t)$. The precise meaning of the last expression is this. There exists a function $K(\epsilon,N)$

such that $K \to \infty$ as $\epsilon \to 0$ and, for the partial sum $U^{(N)}$,

$$|u - U^{(N)}| = O(\epsilon^{N+1}), \quad \epsilon \to 0,$$

uniformly for $|\rho| \leq K(\epsilon, N)$.

The normal speed $\gamma(s,t;\epsilon)$ of $\Gamma$ in the positive $r$-direction is given by $-r_t$ $(= -\frac{\partial r}{\partial t}(s,t;\epsilon))$. Notice that we need the minus sign. If $\Gamma$ depends smoothly on $(t,\epsilon)$, then so does $(r,s)$, and hence $\gamma$ is a smooth function of $(s,t,\epsilon)$. Note also that once $r$ is determined, so is the arclength $s$ by virtue of the orthogonality condition. The outer expansion $u_n$ and the inner expansion $U_n$ are coefficients in the expansion of the same function, and hence they cannot be independent. In fact, it is natural to require that the following **matching conditions** hold true:

$$U_0(\pm\infty, s, t) = u_0(0\pm, s, t), \tag{4.51}$$

$$U_1(\rho, s, t) = u_1(0\pm, s, t) + \rho\partial_r u_0(0\pm, s, t) + o(1), \tag{4.52}$$

$$U_2(\rho, s, t) = u_2 + \rho\partial_r u_1 + \frac{1}{2}\rho^2\partial_{rr}u_0 + o(1), \tag{4.53}$$

as $\rho \to \pm\infty$. The outer expansion $u_n$ is regarded here as a function of $(\rho, s)$, instead of being one of $x$. The symbols $0\pm$ stand for limits on $\Gamma$ from $\mathcal{D}_\pm$ in the $r$-direction with $s$ being fixed. We do not attempt here to rigorously derive these matching conditions (cf. [**134**]). The condition (4.51), for example, is a natural one for the function $u$ to be smoothly joined from the inner region to the outer region. These conditions will later play important roles as boundary conditions associated with the differential equations for $u_n$ and $U_n$.

It is well-known ([**131**], [**266**], [**185**], [**247**], etc.) that by combining these outer and inner expansions in an appropriate manner one can construct a genuine solution in one-space-dimensional settings. Such a method is called the method of **matched asymptotic expansion**.

For high space-dimensional cases, rigorous constructions based on inner-outer expansions are very difficult, and hence the analysis of approximate equations is more realistic. Such approximate equations should indeed be considered as a new model of original phenomena, and the analysis of these equations often gives us deep insights into the problems.

For later conveniences, let us here describe some properties of the coordinate system $(r,s)$ and an expression of the Laplacian. First of

all, we have

$$|\nabla r| = 1, \qquad \Delta r = \kappa \tag{4.54}$$

on $\Gamma$. Here, both $\nabla$ and $\Delta$ act on functions of the space variable $x$, and $\kappa$ stands for the curvature of $\Gamma$. The sign of $\kappa$ is taken positive when $\Gamma$ is concave from $\mathcal{D}_-$. The identity $|\nabla r| = 1$ holds not only on $\Gamma$ but also in its neighborhood where $r$ is well-defined.

When $u$ is regarded as a function of $(r, s, t)$, both $r$ and $s$ are considered as functions of $(x, t)$. The Laplacian and time derivative are, respectively, rewritten as

$$\Delta u = \partial_{rr} u + \Delta r \partial_r u + \partial_s u \Delta s + \partial_{ss} u |\nabla s|^2, \tag{4.55}$$

$$\partial_t u = \partial_t u + r_t \partial_r u + s_t \partial_s u, \tag{4.56}$$

where, of course, $u$ on the left is regarded as $u(x, t)$.

Let us now apply the method of matched asymptotic expansion to the reaction-diffusion system (4.40).

In the sequel, we consider the case where $\delta = 0$ for simplicity. We also drop references to $\epsilon$ from notation so long as no confusion arises. The lowest order outer expansion is given by

$$f(u_0, v_0) = 0, \tag{4.57}$$

$$\partial_t v_0 = g(u_0, v_0). \tag{4.58}$$

Since $f$ is of bistable type, we adopt the following two stable branches as solutions of (4.57). That is to say,

$$u_0 = \begin{cases} h_-(v_0), & x \in \mathcal{D}_-, \\ h_+(v_0), & x \in \mathcal{D}_+. \end{cases} \tag{4.59}$$

If $G_\pm$ are defined by

$$G_\pm(v) = g(h_\pm(v), v), \tag{4.60}$$

then (4.58) gives

$$\partial_t v_0 = G_\pm(v_0), \qquad x \in \mathcal{D}_\pm. \tag{4.61}$$

Namely, $v_0$ is governed by an ordinary differential equation in the outer region, and $u_0$ is dictated by $v_0$ through the relations in (4.59). Before we go into detailed computations of the inner expansion, let us recall that the interface $\Gamma$ agrees with the zero-level set of $U$, the inner variable of $u$. In other words,

$$U(0, s, t) \equiv 0. \tag{4.62}$$

Although computations are done at this stage regarding $\Gamma$ as given, in actual applications the location of the interface is determined by

(4.62). Since points on the interface $\Gamma(t)$ are uniquely described by $(s,t)$, we express them as $X(s,t)$. Points near $\Gamma$ then are represented as $X(s,t)+re_r$, where $e_r$ is the unit normal vector on $\Gamma$ at $X(s,t)$, pointing to the direction in which $r$ increases. By using (4.55) and (4.56), we find that the differential equations for the inner variables $U(\rho,s,t)$, $V(\rho,s,t)$ are given by

$$r_t\partial_\rho U+\epsilon\partial_t U+\epsilon s_t\partial_s U=\partial_{\rho\rho}U+f(U,V)+\epsilon\Delta r\partial_\rho U+\epsilon^2\Big(\partial_{ss}U|\nabla s|^2+\partial_s U\Delta s\Big), \tag{4.63}$$

$$\epsilon^{-1}r_t\partial_\rho V+\partial_t V+s_t\partial_s V=g(U,V). \tag{4.64}$$

Since the normal speed $\gamma$ of $\Gamma$ is given by $-r_t$ and $\Gamma$ is assumed to depend smoothly on $(t,\epsilon)$, we have that $(s,r)$ and $\gamma$ are also expanded in an $\epsilon$-power series. The lowest order terms in the expansion are the following:

$$\partial_{\rho\rho}U_0+\gamma_0\partial U_0+f(U_0,V_0)=0, \tag{4.65}$$

$$\gamma_0\partial_\rho V_0=0. \tag{4.66}$$

The latter equation evidently implies that $V_0=V_0(s,t)$ does not depend on $\rho$ if $\gamma_0\neq 0$.

On the other hand, the matching condition (4.51) applied to $V_0$ forces $V_0$ to be equal to the limits of $v_0$ on $\Gamma$ from both sides, and hence $v_0$ should be continuous across $\Gamma$ (one needs a more careful argument when $\gamma_0=0$, cf. [**134**]). We can therefore write $V_0(s,t)=v_0(X(s,t),t)$. The equation (4.65) is of the same form as the scalar equation of bistable type which we encountered in PROPOSITION 4.31. Under the matching condition (4.51) for $U_0$, the solution of (4.65) is uniquely determined, and hence the lowest order approximation $\gamma_0$ of the normal speed has to agree with the wave speed $c$ of the travelling front in the proposition. That is to say, we have

$$\gamma_0=c(v_0(X(s,t),t)) \tag{4.67}$$

and

$$U_0(\rho,s,t)=\psi(\rho,v_0(X(s,t),t)), \tag{4.68}$$

where $\psi(\rho,v_0)$ is the travelling front solution that is uniquely determined by the value $v_0$.

The second lowest order approximations for the inner problem are given as follows. In the sequel, we sometimes use the shorthand

symbol $v_0(X,t)$ in place of $v_0(X(s,t),t)$:

$$\begin{aligned}(4.69)\quad &\partial_{\rho\rho}U_1+\gamma_0\partial_\rho U_1+f_u(U_0,v_0(X,t))U_1\\ &\quad=(-\gamma_1-\kappa(s,t))\partial_\rho\psi(\rho,v_0(X,t))-f_v(U_0,v_0(X,t))V_1\\ &\qquad+(\partial_t+(\partial_t s)\partial_s)\psi(\rho,v_0(X,t)),\\ (4.70)\quad &-\gamma_0\partial_\rho V_1=-(\partial_t+(\partial_t s)\partial_s)v_0(X,t)+g(U_0,v_0(X,t)).\end{aligned}$$

Let us rewrite the operator $(\partial_t+(\partial_t s)\partial_s)$ that appears in the third and first term on the right hand side of (4.69) and (4.70), respectively. Our purpose here is to express $(\partial_t s)\partial_s$ explicitly in terms of the normal speed and the normal derivative of $v_0$. Although the function $v_0(x,t)$ is smooth along the interface (hence the subscript $\pm$ is dropped), its normal derivative in general is discontinuous. Therefore, denoting by $v_0^\pm$ an extension of $v_0$, defined on $\mathcal{D}_\pm$, onto the entire domain, we obtain

$$\begin{aligned}(4.71)\quad &(\partial_t+(\partial_t s)\partial_s)v_0^\pm(X(s,t),t)\\ &=\partial_2 v_0^\pm(X(s,t),t)+\gamma_0\partial_r v_0^\pm(x,t)|_\Gamma\end{aligned}$$

(cf. [**134**] for details). It turns out that either choice of $\pm$ in (4.71) gives the same result. The symbol $\partial_2$ means to differentiate with respect to the second variable, and hence the first term on the left of (4.71) is equal to $G_\pm(v_0(X,t))$ due to (4.61). We can thus reduce (4.69), (4.70) to

$$\begin{aligned}(4.72)\quad &\partial_{\rho\rho}U_1+\gamma_0\partial_\rho U_1+f_u(U_0,v_0(X,t))U_1\\ &\quad=(-\gamma_1-\kappa(s,t))\partial_\rho\psi(\rho,v_0(X,t))-f_v(U_0,v_0(X,t))V_1\\ &\qquad+\psi_v(\rho,v_0(X,t))\Big(G_\pm(v_0(X,t))+\gamma_0\partial_r v_0^\pm(x,t)|_\Gamma\Big),\\ (4.73)\quad &-\gamma_0\partial_\rho V_1\\ &\quad=-\gamma_0\partial_r v_0^\pm(x,t)|_\Gamma-G_\pm(v_0(X,t))+g(U_0,v_0(X,t)).\end{aligned}$$

Let us now employ a solvability theory. Denoting by $\mathcal{L}$ the differential operator on the left side of (4.72), one finds that it acts on $L^2(\mathbb{R})$ and has a simple eigenvalue 0. The latter statement easily follows from the fact that $p=\partial_\rho\psi(\rho,v_0)$ satisfies $\mathcal{L}p=0$. The **solvability condition** says that the necessary and sufficient condition for the equation $\mathcal{L}q=f$ with $f\in L^2(\mathbb{R})$ to have a solution in $L^2(\mathbb{R})$ is $\langle f,p^*\rangle_{L^2(\mathbb{R})}=0$. In the condition, $p^*$ is an eigenfunction of the adjoint operator $\mathcal{L}^*$ associated with the 0-eigenvalue. Applying the

condition to (4.72), one obtains

$$(-\gamma_1 - \kappa)A(s,t) + \hat{B}(s,t) = 0, \tag{4.74}$$

in which

$$A(s,t) = \langle p, p^* \rangle > 0, \tag{4.75}$$

$$\begin{aligned} \hat{B}(s,t) &= \Big\langle p^*, \Big[ -f_v(U_0, v_0(X,t))V_1 \\ &\quad + \psi_v(\rho, v_0(X,t)) \Big( G_{\pm}(v_0(X,t)) + \gamma_0 \partial_r v_0^{\pm}(x,t)|_\Gamma \Big) \Big] \Big\rangle. \end{aligned} \tag{4.76}$$

We have thus obtained from (4.67) and (4.74) the normal velocity of the interface up to an $O(\epsilon)$ as

$$\gamma(X,t) = c(v_0(X,t)) - \epsilon\kappa(X,t) + \epsilon\hat{B}(s,t)/A(s,t). \tag{4.77}$$

There are two contributions to the order $O(\epsilon)$, one from the curvature of the interface and the other from the $v$-dependence of $f$ and $\psi$. The equation (4.77) is called the **velocity-curvature equation** (or, eikonal-curvature equation).

One may notice, however, that in well known forms (cf. [**206**], [**262**]) of interface velocity the third term in (4.77) is missing. Except for trivial cases where $f$ is independent of $v$, it is often the case that the omission of the third term is justified by additional hypotheses. For example, if $v$ is a slow variable, then one often replaces $v$ by a constant, and hence the $v$-dependence of $f$ disappears.

A more significant situation is when the curvature is large and $\epsilon\kappa \gg \epsilon$, in which case the third term becomes a higher order one. The latter situation will be typically encountered when we derive a free boundary problem for spiral waves by rescaling. In such a situation, of course, we need to work out the derivation of the velocity-curvature equation with respect to appropriate powers of $\epsilon$ in accordance with the rescaling (note that (4.77) is derived under the condition that $\kappa = O(1)$). For later convenience, let us exhibit a simpler form of the velocity-curvature equation without the third term:

$$c_n(\mathbf{r}_I) = c(v(\mathbf{r}_I)) - \epsilon\kappa(\mathbf{r}_I), \tag{4.78}$$

where $\mathbf{r}_I$ stands for the position of the interface, and $c_n$ is the speed of the interface in the normal direction. The right hand side of (4.78) consists of the dispersion of the medium and the Gibbs-Thomson effect.

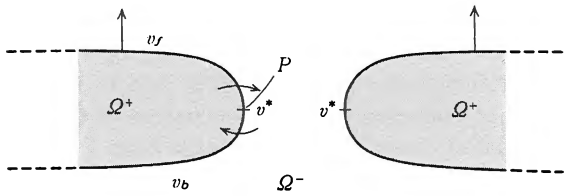


FIGURE 4.14. Defects trigger spiral waves.

As we have seen in the dispersion relation (4.45) for periodic travelling waves, the travelling velocity varies with the value of $v$. Therefore, the first term $c(v(\mathbf{r}_I))$ in (4.78) expresses the dispersion. The curvature-dependent second term adjusts the velocity in accordance with the curvature and thus contributes to smoothing the interface. Such a term appears in many applications, for example, as the Gibbs-Thomson effects in the Stefan-type model of crystal growth (cf. CHAPTER 3 and [**236**], [**237**]). In particular, if $c(v) \equiv 0$ does not depend on $v$, then (4.78) is nothing but the mean curvature flow. It is of interest to note here that the dispersion represents a characteristic of hyperbolic equations, while the Gibbs-Thomson effect represents a characteristic of parabolic equations.

### Emergence of a Spiral Wave and Singularity

Before we analyze the behavior of spiral waves, let us give an intuitive discussion as to why such waves emerge spontaneously. Consider a situation in which a stable two-dimensional pulse solution is given and it is cut half in the middle as in FIGURE 4.14.

If $u$ quickly converges to one of the two stable states $u = h_\pm(v)$ due to the high reactivity, we may assume that according as $u \approx h_\pm(v)$ the domain is divided into two parts $\Omega^\pm$ bounded by a smooth boundary which has finite curvature as in FIGURE 4.14. Assuming that $v$ is continuous, there must be a point $P$ on the interface where $v = v^*$. Here, $v^*$ is a value for which $c(v^*) = 0$; namely, it is a point that does not move (cf. PROPOSITION 4.31).

In the part of the interface below and near the point $P$, we have $v > v^*$, and hence $g > 0$, and consequently $v$ increases with a speed of $O(1)$ if $v$ is diffusion-less ($\delta = 0$). If the curvature is not significantly large, then the part of the interface lower than $P$ moves in the $\Omega^+$-direction, due to the velocity-curvature equation (4.78). On the other

hand, a similar reasoning reveals that the part of the interface above $P$ moves in the $\Omega^-$-direction. As this process progresses, the angular velocity of the interface around $P$ diverges, and hence $v$ tends to be discontinuous. At the same time, the curvature of the interface also becomes unbounded, creating a singularity near $P$. Therefore the velocity-curvature equation (4.78) is not valid any more. In reality, however, the curvature effect cannot be neglected, and if $v$ diffuses ($\delta > 0$) then its gradient is bounded by some constant and singularity formation does not occur. Even in such a case, the stationary behavior around $P$ is equally rotational as above.

Pushing the thought-experiment further, one can imagine that $P$ remains almost stationary and the interface nearby rotates around $P$. On the other hand, in the part far away from $P$ the interface will propagate upward with a constant velocity, keeping the shape of a planar pulse.

Combining such speculations, one can expect that dynamics as in FIGURE 4.15 (a) will spontaneously emerge, in which spiral movement around $P$ and planar travelling pulse are joined together. In fact, such a process is realized in experiments on the BZ reaction as in FIGURE 4.15 (b).

**Kinematic equation**

Before we construct spiral wave solutions by using the velocity-curvature equation and (4.61), let us introduce a simplified version of the geometric model. The basic idea in such a model is to regard a spiral wave as the motion of a one-dimensional curve with an end point. The motion of the curve is determined by its normal velocity, depending on the curvature, and by the tangential velocity of the end point. The time evolution of the spiral arm is described by a partial differential equation related to the curvature. Such a description is expected to be a good approximation when the width of the excited region (the thickness of the arm) is very small, the radius of the core region is large, and the period of rotation is long.

The latter situation is not unrealistic, as exemplified in the following description. Let us first set $\delta = 0$ in the model equation (4.39). The smaller the value of the parameter $\epsilon$ is, the faster the excitation sets in, and as demonstrated in [**85**] and [**264**], there exists some value $\epsilon = \epsilon_{c_2}$ at which the initial state of FIGURE 4.14 keeps its bar-shape. If $\epsilon$ is larger than the critical value, the bar shrinks and quickly disappears. When $\epsilon$ is slightly smaller than $\epsilon_{c_2}$, the radius of the core

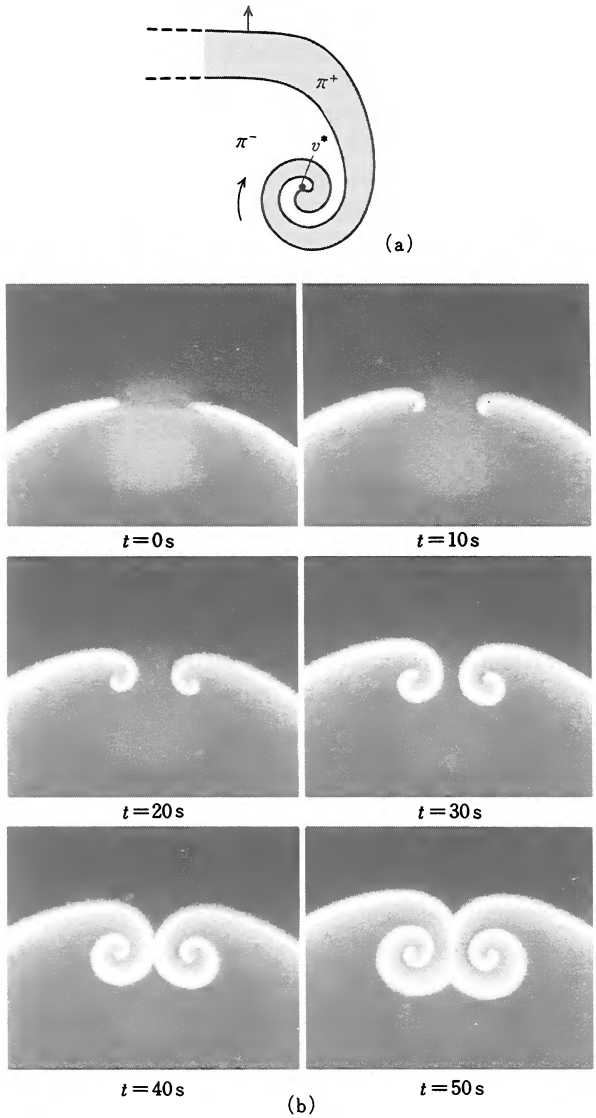


FIGURE 4.15. (a) Spiral wave and planar travelling wave. (b) Emergence of spiral waves in the BZ reaction.

region is sufficiently large, and in comparison, the arm is thin enough, making the above approximation valid.

Another situation is the case of high threshold value. There is a threshold value $H_c$ such that if $H = v - v_s$ is smaller than this value, the arm does not grow. When $H$ is slightly larger than the threshold value, it is expected that the same approximation as above is effective. In this case, however, rigorous relationships to the original reaction-diffusion system (4.39) are not well understood.

If the radius of the core region is large and the arm is thin enough, one may regard the spiral as a string, to the crudest approximation, and hence $v$ is constant on it. Therefore the normal velocity, to the first order approximation, may be treated as depending only on the curvature, thanks to the relation (4.78). Let us thus consider the motion of a half-infinite curve with an end point $P$. It is well known that the motion of a planar curve is completely determined, once the curvature $K$ is given in terms of the arclength $l$ measured from the end point $P$, as $K = K(l,t)$ (natural equation).

The curve evolves according to the following two rules.

(i) The normal velocity $V$ is determined solely by the curvature $K$.

(ii) The tangential velocity $G$ of the end point $P$ is also determined only by the curvature at the point.

The curvature $K_0$ at the end point is defined by

$$K_0 = \lim_{l \to 0} K(l),$$

where $l$ is the arclength measured from the end point, and hence, one can write $G = G(K_0)$.

Once $V$ and $G$ are given, the evolution equation of $K(l,t)$ is given by

$$\frac{\partial K}{\partial t} + \Big( \int_0^l VK dl' + G \Big) \frac{\partial K}{\partial l} = -K^2 V - \frac{\partial^2 V}{\partial l^2}, \tag{4.79}$$

which is call a **kinematic equation**.

The equation is derived by expressing the curvature in terms of polar coordinates and by observing that variation in arclength is caused by the combined effects of variation in curvature and motion of the end point:

$$dl = \Big( \int_0^l VK dl' \Big) dt + G dt$$

(consult [**85**] for details).

A frequently employed choice for $(V, G)$ is

$$V = V_0 - DK, \tag{4.80}$$

$$G = \gamma(K_{c_2} - K_0), \tag{4.81}$$

where $D, \gamma$ are positive constants. The critical curvature $K_{c_2}$ is related to the curvature at which the normal velocity becomes zero in the velocity-curvature equation (cf. [**264**]).

We will describe below how the angular velocity of stationary spiral waves is determined, following the presentation in [**264**]. Let us first determine a stationary spiral wave for (4.79). We assume that the end point does not move in a tangential direction, namely, we impose the boundary condition

$$K_0 = K_{c_2}, \tag{4.82}$$

and hence $G \equiv 0$. Assuming also that the spiral is approximated by a planar wave in the region far away from the core, we also impose

$$\lim_{l \to \infty} K(l, t) = 0. \tag{4.83}$$

Then stationary solutions satisfy

$$\Big(\int_0^l VK dl'\Big)\frac{\partial K}{\partial l} = -K^2 V - \frac{\partial^2 V}{\partial l^2}, \tag{4.84}$$

which upon integration gives rise to

$$\frac{dV}{dl} + K\int_0^l VK dl' = \omega. \tag{4.85}$$

The integration constant $\omega$ gives the angular velocity of the desired spiral solution, as we can in fact see from (4.85): $\omega = (dV/dl)_{l=0}$. The boundary conditions (4.82), (4.83) together with the equation (4.85) constitute a **nonlinear eigenvalue problem** that determines the angular velocity $\omega$. Introducing non-dimensional variables $\kappa = K/K_{c_2}$ and $y = K_{c_2} l$, and using (4.80), one can rewrite (4.85) as

$$\kappa \int_0^y \kappa(1 - \beta\kappa) dy' = \Omega + \beta \frac{d\kappa}{dy},$$

where $\Omega = \omega/V_0 K_{c_2}$, $\beta = DK_{c_2}/V_0$, and the boundary conditions become

$$\kappa(0) = 1, \qquad \lim_{y \to \infty} \kappa(y) = 0.$$

Let us first consider the case where $D = 0$ in (4.80) (i.e. $\beta = 0$), which corresponds to the situation in which one of the boundary conditions

is neglected, the core radius is sufficiently large, and the curvature effect is absent. Since in this case $\kappa \int_0^y \kappa dy = \Omega$, we obtain

$$\kappa(y) = \left(\frac{\Omega}{2y}\right)^{\frac{1}{2}}.$$

This solution satisfies the boundary condition at infinity, although $\kappa(0) = 1$ is not satisfied, indicating that the curvature effect should not be neglected in the core region. The solution represents an involute of a circle, which at far distance approaches the Archimedean spiral with pitch $2\pi/\Omega$. It is therefore realized that the normal velocity $V$ has to depend on the curvature ($\beta \neq 0$) for the boundary condition at $l = 0$ to be satisfied. Numerically, $\Omega$ is determined as a function of $\beta$, and for small $\beta$ it is approximated as

$$\Omega \approx 0.685\beta^{\frac{1}{2}} - 0.06\beta - 0.293\beta^2 + \ldots .$$

The period $T_0$ of rotation in this case is given by

$$T_0 = \frac{2\pi D}{V_0^2 \beta \Omega(\beta)}. \tag{4.86}$$

The angular velocity is thus determined from (4.86). It is, however, too much to ask for the result to be compared with actual experiments of the BZ reaction. The reason is that it is difficult to realize the situation under which the kinematic equation is derived, and hence there is no natural way of selecting the parameters on the right hand side of (4.86).

### Scaling and Free Boundary Problem

A spiral wave consists of an excited region which is surrounded by two interfaces, called **front** and **back**, and the rest, called unexcited regions. These two interfaces meet at the tip of the spiral, which moves along a sphere of radius $r^*$ (FIGURE 4.16). Similarly to the case of crystal growth processes in CHAPTER 3, the most fundamental problem in spiral waves is to know how their shape and angular velocity are determined from the governing model equation.

Difficulties encountered in constructing a spiral wave stem from the fact that its behavior near the core region is different from that in the region far away. To be more precise, it is approximated by a one-dimensional periodic travelling wave in the far-away region, where curvature effects are small. On the other hand, in the core region, a spiral is genuinely a two-dimensional pattern, and hence the curvature effect is essential.

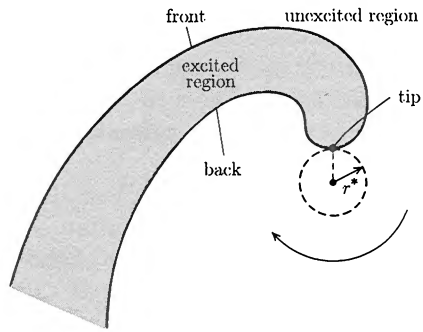


FIGURE 4.16. The tip of a spiral wave.

Historically, investigations of spiral waves were initiated from the standpoint of treating them as perturbations of one-dimensional periodic travelling waves. Attempts to treat them as genuinely two-dimensional patterns began in the mid-1980's. One major point in these attempts was to decide what are the most suitable scales for space-time and unknown variables that bring out all of the spiral solutions.

Our standpoint is to understand the motion of a spiral with the help of an interface that separates sharply excited and unexcited regions in the limit as $\epsilon \to 0$. However, it is not a priori clear that such an interface can be defined at all in the core region. Therefore, it is necessary to start with a careful examination as to whether or not interface-equation methods are valid for spirals. Such an examination has naturally given rise to the so-called **Fife scaling** ([**133**], [**134**]), which will play an important role. We have already utilized the difference in scales to reduce the original system. Namely, taking advantage of the difference in time constants of $u$ and $v$, we derived the velocity-curvature equation (4.77) and the evolution equation (4.61) of $v$ from the original reaction-diffusion system (4.40).

When $v$ does not diffuse, the interface dynamics is described by the ordinary differential equation

$$\frac{dv}{dt} = G_{\pm}(v) \tag{4.87}$$

and the velocity-curvature equation

$$c_n = c(v) - \epsilon\kappa. \tag{4.88}$$

Let us recall that $G_\pm(v) = g(h_\pm(v), v)$ and that $u = h_\pm(v)$ correspond, respectively, to excited and unexcited regions. In the above, we also neglected the term in (4.77) that comes from the $v$-dependency of $f$ (this will be justified later). These two regions are divided by the interface $\Gamma$, and $v$ is supposed to be continuous in the entire domain, including $\Gamma$.

Under what circumstances is the free boundary problem (4.87)-(4.88), and in particular the velocity-curvature equation, effective? We will discuss this question in two cases (cf. [**262**]).

**(i) High-threshold Limit**

One of the conditions for the velocity-curvature equation to be valid is that the radius of curvature be much larger than the width of the interface (compare with the section where the velocity-curvature equation is derived). In particular, this must hold even at the tip of the spiral, where the curvature radius is minimum:

$$R_{\rm tip} \gg O(\epsilon), \qquad R_{\rm tip} = \kappa(r^*)^{-1}. \tag{4.89}$$

How does $R_{\rm tip}$ behave as $\epsilon$ varies, and how small should $\epsilon$ be in order for the last inequality to hold? Note that the normal velocity is zero at the tip. We also assume that $v = v_s$ (equilibrium) holds at the tip. Since the core radius is $r^*$, we have $0 = c(v_s) - \epsilon\kappa(r^*)$, and hence, recalling that $c(v_s) > 0$, we find that (4.89) is equivalent to

$$c(v_s) \ll 1. \tag{4.90}$$

This means that $v_s$ is very close to $v^*$, namely,

$$H = v^* - v_s \ll 1. \tag{4.91}$$

$H$ measures the level of the excitation threshold (note that the smaller $H$ is, the higher the threshold), and therefore the condition (4.91) demands that the threshold be high. Expanding $c(v_s)$ around $v^*$, we have $c(v_s) \sim v^* - v_s$. Now the width $\lambda_+$ of the excited region, measured at a place where the distance from the tip is more than $O(R_{\rm tip})$, is considered as given by

$$\lambda_+ \sim R_{\rm tip}.$$

One the other hand, we also have $\lambda_+ \sim c(v_s)T_+$ and $R_{\rm tip} \sim \epsilon c(v_s)^{-1}$, where $T_+$ is the duration of the excited region, given by

$$T_+ = \int_{v_f}^{v_b} \frac{dv}{G_+(v)} \sim v_b - v_f \sim v^* - v_s.$$

Therefore, we have $c(v_s)^2 T_+ \sim \epsilon$, and hence

$$H \sim \epsilon^{1/3}.$$

At the same time, we also find the following scaling:

$$R_{\text{tip}} \sim \epsilon^{2/3}, \qquad T_+ \sim \epsilon^{1/3}, \qquad c(v_s) \sim \epsilon^{1/3}. \tag{4.92}$$

Therefore, by choosing $\epsilon$ so small that $\epsilon \ll 1$, one can realize the situation in (4.90). Moreover, (4.89) is also valid in the sense that $\epsilon^{2/3} \gg \epsilon$. This suggests that it is appropriate to rescale near the core region $v$ by $\epsilon^{1/3}$ around $v^*$, the space variable by $\epsilon^{2/3}$, and the time by $\epsilon^{1/3}$.

Since the importance of such a scaling was first pointed out by Fife ([**132**]), and later proved to be very useful ([**203**]), it is called the **Fife scaling**. We can now justify neglecting the third term in (4.77), which is one of the $O(\epsilon)$-terms and comes from the dependency of $f$ on $v$. Namely, the curvature term near the core region is of order $O(\epsilon^{1/3})$, instead of $O(\epsilon)$.

The next case to be treated is the low-threshold limit, in which the above scalings are required to be valid on the whole region, not only around the core region.

**(ii) Low-threshold Limit.**

The discussion thus far has been carried out under the condition that $v$ takes the value $v = v_s$ near the core region. Consequently, it was necessary to consider excitable media that have a high threshold value for excitation, so that (4.89) can be satisfied. In general, however, $v$ is not so close to $v_s$. Indeed, for low-threshold (highly excitable) media, it is expected that spiral patterns are maintained even if the inhibitor concentration $v$ is high, which is in fact supported by numerical simulations in [**356**] and agrees with experiments performed to determine the angular velocity.

In the present case, $v^* - v_f(r^*) \ll 1$ is required for (4.90) to hold. Since in low-threshold media, repeated excitation is possible even if $(u, v)$ is not recovered from excitation to a sufficiently close neighborhood of the equilibrium, it is natural to assume that $v^* - v_f \ll 1$ holds on the entirety of spirals. One can in fact find, after a line of arguments similar to the ones above, that scalings

$$v^* - v_f \sim \epsilon^{1/3} \ll 1, \qquad c(v_f) \sim \epsilon^{1/3} \ll 1$$

are adequate for low-threshold media (cf. [**134**]). Since the spatial scale is $O(\epsilon^{2/3})$, the latter scalings imply that the angular velocity $\omega$ has to satisfy $\omega \sim \epsilon^{-1/3}$.

In both cases, the same type of scalings are demanded, except for the difference in the position of the equilibrium point $v_s$.

### Angular Velocity Selection Problem

Let us now deal with the angular velocity selection problem. We will exclusively work with the second case above: (ii) Low-threshold limit. The spatio-temporal scaling and the scaling for the unknown are given by

$$v - v^* = \epsilon^{1/3}\tilde{v}, \qquad x = \epsilon^{2/3}\tilde{x}, \qquad t = \epsilon^{1/3}\tilde{t}. \tag{4.93}$$

These scalings mean that $v$ is almost identical to $v^*$, the space coordinate is stretched by $\epsilon^{-2/3}$, and dynamics is to be observed in the slow time scale of $\epsilon^{1/3}$. Since the thickness $O(\epsilon)$ of transition layers is much finer than the spatial scale in (4.93), we should note that there are limitations to knowing detailed structures of the core of size $O(\epsilon)$ (on the other hand, however, if an $O(\epsilon)$-spatial scaling is employed, then one can discern well the core region, while losing sight of the outer region). Since (4.93) enables us to approximate the wave speed as

$$c(v_I) \approx \epsilon^{1/3} c_v \tilde{v}_I, \qquad c_v = \left.\frac{dc(v)}{dv}\right|_{v=v^*},$$

the principal part of (4.88) is expressed as in

$$c_n(\mathbf{r}_I) = c_v v(\mathbf{r}_I) - \kappa(\mathbf{r}_I). \tag{4.94}$$

In the expression (4.88) before the scaling, the curvature was multiplied by $\epsilon$, while after the Fife scaling the two terms have comparable contributions. The situation shares a common reasoning with §4.2.2, in which polymer patterns and meso-scopic patterns in Turing patterns are discussed (cf. CHAPTER 5).

Since the principal part of $v$ in the scaling (4.93) is $v = v^*$, the nonlinearity for the $v$-equation can be well approximated by $G_\pm(v^*) = g(h_\pm(v^*), v^*)$, which are constants of different signs. Denoting these constants by $g^\pm$, we obtain

$$\frac{\partial v}{\partial t} = g^\pm, \tag{4.95}$$

in which the right hand side is independent of $v$. Therefore, (4.94) and (4.95) give an $\epsilon$-independent rescaled free boundary problem.

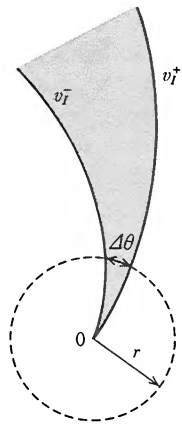


FIGURE 4.17. Spiral wave that has a cusp-like tip.

The equation for the stationary rotating spiral wave is rewritten as

$$\begin{cases} c_n(\mathbf{r}_I) = c_v v(\mathbf{r}_I) - \kappa(\mathbf{r}_I), \\ \omega \dfrac{\partial v}{\partial \theta} + g^{\pm} = 0 \end{cases} \tag{4.96}$$

in terms of the co-rotating coordinate system. In the equation, we have introduced a new angular velocity $\omega \equiv \epsilon^{-1/3}\tilde{\omega}$. Note that $\omega$ is an unknown parameter. Integrating the second equation of (4.96), one obtains

$$v^{\pm}(r,\theta) = -g^{\pm}\frac{\theta}{\omega} + b^{\pm}(r),$$

in which $b^{\pm}(r)$ are integration constants. The excited and rest regions are bounded by the interfaces represented by $\theta = \theta^{\pm}(r)$ (cf. FIGURE 4.17). We assume that $\theta^{\pm}(r) \sim r$ as $r \to \infty$ (Archimedean spirals). Moreover, we also assume that $v$ is continuous across the interface, namely, $v^+(\theta^+(r)) = v^-(\theta^-(r))$ and $v^+(\theta^+(r)) = v^-(2\pi + \theta^-(r))$. Under these conditions, the width $\Delta\theta(r) \equiv \theta^-(r) - \theta^+(r)$ of the excited region is determined as

$$\Delta\theta = \frac{2\pi g^-}{g^- - g^+}, \tag{4.97}$$

which does not depend on $r$. This means that each of the two interfaces is obtained from the other by an appropriate constant rotation. Let us now compute the value $v_I(\theta^{\pm}(r))$ of $v$ on the interface. Since the spiral wave is a stationary pattern, the equality $c_n(\theta^+(r)) = -c_n(\theta^-(r))$ has to be satisfied. Symmetry forces $\kappa(\theta^+) = -\kappa(\theta^-)$, and hence the interface equation implies that the values of $v$ on $\theta^{\pm}(r)$ are of opposite sign. We thus conclude that

$$v_I(\theta^{\pm}(r)) \equiv v_I^{\pm} = \pm \frac{g^+ g^- \pi}{\omega(g^+ - g^-)}, \tag{4.98}$$

which apparently shows that $v$ does not depend on $r$ on the interface.

The spiral wave thus obtained has a cusp singularity at the tip at which $v$ is discontinuous. Although this is a natural consequence of the particular rescaling employed, it does not necessarily mean that our formulation above breaks down in the angular velocity selection problem. In order to eliminate the singularity, it is necessary to introduce another scaling near $r = 0$ and to take into account the diffusion effect of $v$. We do not discuss these points (cf. REMARK 4.34).

In order to determine the shape of the spiral, let us derive an ordinary differential equation for $\theta^+(r)$. The curvature and the normal velocity are computed as

$$\kappa = -\frac{1}{(1+\psi^2)^{3/2}} \frac{d\psi}{dr} - \frac{\psi}{r\sqrt{1+\psi^2}},$$
$$c_n = \frac{\omega r}{\sqrt{1+\psi^2}},$$

respectively, where $\psi(r) = r\frac{d\theta^+}{dr}$. Inserting these expressions into the interface equation (4.96), and using (4.98), one obtains the following equation for $\psi$:

$$\frac{d\psi}{d\rho} = \left(\rho - \frac{\psi}{\rho}\right)(1+\psi^2) - B(1+\psi^2)^{3/2}, \tag{4.99}$$

where $\rho = \sqrt{\omega} r$ and $B = c_v v_I^+ / \sqrt{\omega}$. The equation is supplemented by the following boundary conditions:

$$\psi(\rho) \sim \rho \quad \text{as} \quad \rho \to \infty, \qquad \psi(0) = 0. \tag{4.100}$$

Finally, the angular velocity selection problem is reduced to solving the **nonlinear eigenvalue problem** with respect to $B$ (i.e. with respect to $\omega$), consisting of the equation (4.99) and the boundary conditions (4.100). We do not go into the details, but it is known that the eigenvalue problem has a unique solution, and that a shooting

method gives an approximate value of $B$ as 1.738. Using the value $B$, the angular velocity of the spiral wave is given by

$$\omega^* = \left(\frac{c_v g^+ g^- \pi}{B(g^+ - g^-)}\right)^{2/3}. \tag{4.101}$$

At the same time, the shape of the spiral solution is completely determined except near the tip.

As $r \to 0$, this solution exhibits singularity (i.e. $v$ is discontinuous and the interface has a cusp singularity at the tip). In order to correct the singularity, one needs to solve an inner problem derived by way of scaling

$$x = \epsilon \tilde{x}$$

from the original system of reaction-diffusion equations. No matter what kind of scaling one employs, the width of the excited region and that of the interface near the core region for solutions of the original reaction-diffusion system are comparable. Therefore, one cannot in general capture the entirety of spiral solutions in terms of the solutions of a limit problem obtained by employing one particular scaling.

In other words, in order to characterize a particular quantity of interest, one accordingly needs to find a suitable scaling, and in the chosen scaling some other types of information may necessarily be dropped out.

In this sense, it is accepted that the solution of the outer problem after the Fife scaling gives the correct principal part for the solution of the angular velocity selection problem. Relationships between the solutions of the outer problem and the original system of reaction-diffusion equations, as well as the stability properties of spiral solutions, are currently being intensively investigated (cf. [**213**], [**214**], [**203**], [**30**] and [**306**]), and they will be clarified, hopefully, in the near future.

REMARK 4.37. The solution obtained above by using the Fife scaling has a singularity at the tip. Boundary conditions ensuring that the interface is smoothly joined at the tip $r = r^*$ are given by

$$\Delta(r^*) = 0, \qquad \psi_f(r^*) = +\infty, \qquad \psi_b(r^*) = -\infty, \tag{4.102}$$

where the front $\theta = \psi_f(r)$ and back $\theta = \psi_b(r)$ of the interface are defined as in (4.99) and $\Delta(r) = \psi_f(r) - \psi_b(r)$. Under these conditions, Keener [**207**] rigorously proved that (4.87)-(4.88) have solutions. In the proof, it is essential that $G_\pm$ depends explicitly on $v$ (as opposed to the situation above where $g^\pm$ are constants). The first condition

in (4.102) ensures that the front and back of the interface meet at $r = r^*$, and the other two conditions mean that they meet along the direction orthogonal to the radial direction. In this case, the problem to be solved is a nonlinear eigenvalue problem with respect to the angular velocity $\omega$ and $r^*$, consisting of ordinary differential equations for the two interfaces $\psi_f$ and $\psi_b$. We note that the initial step in the search for $\psi_f$ and $\psi_b$ is the solution $\psi_f \equiv \psi_b \equiv \psi$, that is, the solution of (4.99). Based upon the initial step, the solution is constructed perturbatively by skillfully using shooting methods and comparison theorems so that the boundary conditions (4.102) are satisfied.

REMARK 4.38. As a scaling different from the Fife scaling, there is for example the one by Keener [**208**] (although the system treated is not excitable any more, since the nonlinearity is odd-symmetric). The core region is scaled as $\tilde{x} = x/\epsilon^{1/2}$, and the diffusion effect of $v$ is taken into account ($\delta > 0$). The resulting free boundary problem, however, has a divergent term (as $\epsilon \to 0$) of $O(\epsilon^{-1/2})$, and hence it is expected to become an effective approximation for large $\epsilon$ instead of sufficiently small $\epsilon > 0$.

REMARK 4.39 (**Destabilization of spiral waves: meandering and spiral breakups**). Although we focus on rigidly rotating stable spiral waves, they can also destabilize in many different ways. For instance, they may begin to meander or to drift (see [**335**] and the reference therein). Barkley [**20**] was the first who noticed the relevance of the Euclidean symmetry group to this transition, and it is attributed to a Hopf bifurcation. This idea was made rigorous in [**326**]. Transverse instabilities may occur [**165**] that are characterized by a degenerate dispersion relation between asymptotic wavelength and wave speed. Another common instability is the breakup of spiral waves into a turbulent region. It occurs at either the core [**15**] or the far field [**302**], [**16**]. Quite recently a first rigorous step was made in [**323**], [**324**] based on a linear stability analysis. That approach is also useful to understand the super-spiral structures of meandering and drifting spiral waves [**325**]. Note that the existence of rigidly rotating spiral waves was assumed in the aforementioned works.

REMARK 4.40 (**Destabilization of spiral waves in the singular limit**). Kessler et.al. in [**214**] investigated numerically the stability property of spiral waves with respect to the limit system as

$\epsilon \to 0$, separating the core and outer regions, for both cases, where $v$ diffuses and does not diffuse. According to the results, the core region destabilizes due to a simple real eigenvalue crossing zero. There is a discrepancy between this result and experiments or simulations in which doubly periodic meandering occurs through Hopf bifurcation (see also REMARK 4.39). If the limit system is slightly perturbed to $\epsilon > 0$, then it is conjectured that the simple real eigenvalue coalesces with other eigenvalues and becomes complex, giving rise to possible Hopf bifurcations, although the details are not known. Despite such instability, it is believed that the result discussed above for the angular velocity selection problem remains valid. The rationale for this is that as far as meanderings are concerned, the destabilization is believed to be restricted to the core region and not to influence the outer region ([**214**]). However, a rigorous justification has yet to come.

## 4.4. Summary

**4.1** Pattern formation is explained by using familiar examples.

**4.2** Dynamic properties in gradient systems are briefly described from the standpoint of infinite dimensional dynamical systems. We discuss dynamics of conservative systems and systems with non-local terms.

**4.3** Dynamics of open systems are explained for Turing systems and excitable systems. It is shown that rescaling plays an important role in determining the angular velocity of spiral waves. A concrete method of computation in the matched asymptotic expansion is described.

CHAPTER 5

# Method of Singular Limit Analysis

When we observe patterns, we often understand their behavior by keeping track of the interface where the state of matter abruptly changes (water-ice), or by tracing the movement of the boundary that separates two different materials (water-oil). That is to say, instead of observing the entirety of a system, we (unconsciously) think that the dynamics of patterns is concentrated on the motion of interfaces. The method of singular limit analysis is very instrumental in clarifying how the information on the entire dynamics is condensed into the dynamics of the interface. As already mentioned in CHAPTERS 1 and 4, there are several singular limits (distinguished limits) according to different scales with which things are observed. On one hand, the multiple existence of singular limits in turn enables us to understand the mutual relationships between various model equations we have so far encountered. On the other hand, the method of analysis for interface equations obtained as singular limits has recently made remarkable progress. We will first consider the mean curvature flow as a typical example of such interface equations.

## 5.1. Mean Curvature Flow

It has already been thoroughly explained that tracing the motion of the interface is very important in order to understand the dynamics of pattern formation. We will discuss in this section the simplest yet most fundamental example of mean curvature flow. The level-set method to be described below is effective even after singularities are formed. This method will later play an important role in showing that a singular limit of a scalar bistable reaction-diffusion equation is indeed the mean curvature flow.

**5.1.1. What is Mean Curvature Flow?** Let $\Gamma_0$ be an $(n-1)$-dimensional, closed, smooth hypersurface in $\mathbb{R}^n$. Starting from this surface, each point on the hypersurface moves in the normal direction

with a speed proportional to the mean curvature at the point. Such a motion of the interface, described by a family $\{\Gamma_t\}_{t\geq 0}$, is called the **mean curvature flow** starting at $\Gamma_0$. To be more precise, let $\mathbf{N}$ be the unit normal vector on $\Gamma_t$ pointing into the exterior of $\Gamma_t$. The mean curvature $\kappa$ in the direction of $\mathbf{N}$ is defined by

$$\kappa = \kappa_1 + \ldots + \kappa_{n-1} \tag{5.1}$$

in terms of the principal curvatures $\kappa_i$ $(i = 1, \ldots, n-1)$. The mean curvature flow is a family of moving hypersurfaces in which the normal velocity $V$ of $\Gamma_t$ is given by

$$V = \kappa \mathbf{N}. \tag{5.2}$$

Since the mean curvature is also given by $\kappa = -\mathrm{div}(\mathbf{N})$, (5.2) can be expressed as

$$V = -\mathrm{div}(\mathbf{N})\mathbf{N}. \tag{5.3}$$

Here, divergence is computed with regard to the vector field $\mathbf{N}$ that is smoothly extended to a neighborhood of $\Gamma_t$.

REMARK 5.1 (**Equation of constant growth**). For a constant $c > 0$, let us consider

$$V = c\mathbf{N}. \tag{5.4}$$

This equation describes the motion of surfaces growing in the outward direction with a constant speed. Although such a motion may look simple, it is often the case that singularities are formed in finite time even if the initial surface $\Gamma_0$ is smooth. In CHAPTER 4, velocity-curvature equations were introduced. These equations are a combination of (5.2) and (5.4), with $c$ being allowed to be non-constant and to change its sign.

**5.1.2. Signed Distance Function and Partial Differential Equation.** Let us now assume that the mean curvature flow (5.2) has a smooth solution $\Gamma_t$ on $0 \leq t \leq t_*$ and that there is a bounded open set $U_t$ such that

$$\Gamma_t = \partial U_t, \qquad 0 \leq t \leq t_*. \tag{5.5}$$

We now define:

DEFINITION 5.2. For $t \geq 0$, $d(x,t)$ is defined by

$$d(x,t) = \begin{cases} \mathrm{dist}(x, \Gamma_t), & x \in \mathbb{R}^n \backslash \overline{U}_t, \\ -\mathrm{dist}(x, \Gamma_t), & x \in U_t. \end{cases} \tag{5.6}$$

The function $d$ is called the **signed distance function** for the family $\{\Gamma_t\}_{0\le t\le t_*}$.

Even if the family $\{\Gamma_t\}_{0\le t\le t_*}$ is smooth as above, the map $x \mapsto d(x,t)$ is not necessarily smooth. However, in a sufficiently small neighborhood of $\Gamma_t$, it is smooth. In the sequel, the signed distance function is always considered in such regions.

Since $d$ is determined by $\Gamma_t$, it is expected to carry the geometric information of $\Gamma_t$. We will now bring out such information explicitly in the form of differential equations involving the derivatives of $d$ up to the second order.

Let $x$ be a point near $\Gamma_t$ with $d(x,t) > 0$. There exists a unique $y \in \Gamma_t$ such that $d(x,t) = |x-y|$. The outward normal unit vector of $\Gamma_t$ at $y$ is given by

$$\mathbf{N} = Dd(x,t). \tag{5.7}$$

Information on the curvature of $\Gamma_t$ is contained in the second derivative $D^2d$. Let us denote by $\lambda_1, \dots, \lambda_n$ the eigenvalues of the Hessian matrix $D^2d(x,t)$. The principal curvatures $\kappa_i$ $(i = 1, \dots, n-1)$ of $\Gamma_t$ at $y$ are expressed (cf. [**155**]) as

$$\kappa_i = \frac{\lambda_i}{\lambda_i d - 1} \quad (i = 1, \dots, n-1), \qquad \lambda_n = 0. \tag{5.8}$$

Now, fixing $x$ so that $d(x,t) > 0$, we have

$$d_t = -V \cdot \mathbf{N} = -\kappa := \sum_{i=1}^{n-1} \frac{\lambda_i}{1 - \lambda_i d}. \tag{5.9}$$

The same computation is valid for $d(x,t) \le 0$. Therefore, in a neighborhood of $\Gamma_t$ the mean curvature flow is expressed as

$$d_t = F(d, D^2 d), \tag{5.10}$$

where $F$ is defined by

$$F(p, X) = f(p, \Lambda) := \sum_{i=1}^{n} \frac{\lambda_i}{1 - \lambda_i p}, \tag{5.11}$$

in which $X$ belongs to the set $\mathbf{S}^n$ of real symmetric $n \times n$ matrices and $\Lambda = \Lambda(X)$ stands for the collection of the eigenvalues $(\lambda_1, \dots, \lambda_n)$ of $X$. The equation (5.10) should be always considered in a sufficiently small neighborhood of $\Gamma_t$ so that the denominators $1 - \lambda_i d$ are positive.

Now, in the region $\{d > 0\}$, it is easy to verify that $\lambda_i/(1-\lambda_i d) \geq \lambda_i$, regardless of the sign of $\lambda_i$. Therefore,

$$0 = d_t - \sum_{i=1}^{n} \frac{\lambda_i}{1-\lambda_i d} \leq d_t - \sum_{i=1}^{n} \lambda_i = d_t - \Delta d; \tag{5.12}$$

that is to say,

$$d_t - \Delta d \geq 0 \qquad \text{in the region } \{d \geq 0\}. \tag{5.13}$$

Similarly,

$$d_t - \Delta d \leq 0 \qquad \text{in the region } \{d \leq 0\}. \tag{5.14}$$

In particular, we have

$$d_t = \Delta d \qquad \text{on } \Gamma_t. \tag{5.15}$$

The latter equation, as will be shown later, turns out to be valid on the entire domain $\mathbb{R}^n \times (0, \infty)$ in the sense of viscosity solutions. Due to the form (5.15), the mean curvature flow is also called a *geometric heat equation.*

Let us now examine the nonlinearity in (5.10).

For $A, B \in \mathbf{S}^n$ we define $A \geq B$ if and only if $\lambda_i(A) \geq \lambda_i(B)$ $(i = 1, \ldots, n)$. For fixed $p \in \mathbb{R}$ and $A, B \in \mathbf{S}^n$ with $A \geq B$, we have

$$F(p, A) = f(p, \Lambda(A)) \geq f(p, \Lambda(B)) = F(p, B), \tag{5.16}$$

which follows immediately from the fact that

$$\frac{\partial f(p, \Lambda)}{\partial \lambda_i} = \frac{1}{(1-\lambda_i p)^2} > 0 \qquad (i = 1, \ldots, n).$$

Such a nonlinearity $F$ that satisfies the monotonicity condition (5.16) will be called (degenerate) elliptic (cf. §5.2).

So far, we have assumed that the mean curvature flow $\{\Gamma_t\}$ exists, and based upon this, the equation (5.10) has been derived. On the other hand, starting with a smooth initial hypersurface $\Gamma_0$, one can prove the existence of a classical mean curvature flow $\{\Gamma_t\}_{0 \leq t \leq t_0}$ for sufficiently small $t_0 > 0$. To be more precise, let $g(x)$ be the signed distance function to $\Gamma_0$, $V = \{x \in \mathbb{R}^n \mid -\delta_0 < g(x) < \delta_0\}$, $W = V \times (0, t_0)$, and $\Sigma = \partial V \times [0, t_0]$. Here $\delta_0 > 0$ is so small that $g(x)$ is smooth on $\overline{V}$. With these preparations at our disposal, let us consider the following initial-boundary value problem:

$$\begin{cases} v_t = F(v, D^2 v) & \text{in } W, \\ |Dv|^2 = 1 & \text{on } \Sigma, \\ v = g & \text{on } V \times \{t = 0\}. \end{cases} \tag{5.17}$$

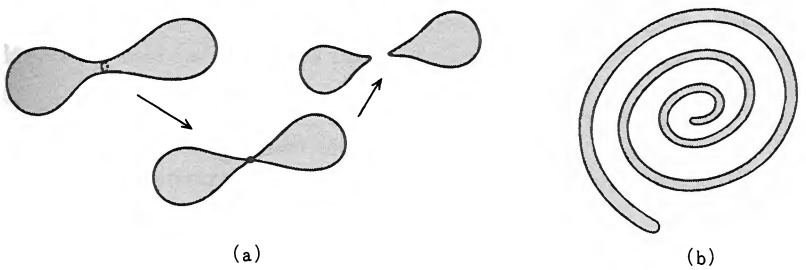


FIGURE 5.1. (a) Formation of singularities by the mean curvature flow in $\mathbb{R}^3$. (b) Singularity is not formed in $\mathbb{R}^2$, and instead the interface shrinks to a point.

If $\{\Gamma_t\}_{0\le t\le t_0}$ is a classical mean curvature flow, then $v = d$ satisfies (5.17). Our assertion here is that if $t_0 > 0$ is sufficiently small, then (5.17) has a classical solution $v \in C^{2+\alpha,\frac{2+\alpha}{2}}(\overline{W}) \cap C^\infty(W)$. If, moreover, we define $\{\Gamma_t\}_{0\le t\le t_0}$ by

$$\Gamma_t = \{x \in V \mid v(x,t) = 0\} \qquad (0 \le t \le t_0), \tag{5.18}$$

then $v(\cdot,t)$ is the signed distance function associated with the $\Gamma_t$ in (5.18) (cf. [**128**]). We have thus reduced the geometric existence problem for the mean curvature flow to the existence of solutions for the partial differential equation (5.17).

## 5.2. Level-set Method and Viscosity Solution

In this section, we will describe the level-set method and an associated notion of viscosity solution.

**5.2.1. Idea of the Level-Set Method.** Even if the initial surface is sufficiently smooth, the mean curvature flow in general develops singularities in finite time. For instance, starting at a sphere, the solution of the mean curvature flow shrinks to a point in finite time. If the initial surface is two-dimensional ($\subset \mathbb{R}^3$), such as in FIGURE 5.1 (a), with a pinched narrow portion in the middle, then it will be torn apart in finite time. Now, a question suggests itself: How can we, in a natural way, define a generalized mean curvature flow beyond such singularities?

REMARK 5.3. In the two-dimensional case, even if the initial closed curve is highly nonconvex, such as in FIGURE 5.1 (b), one

can prove that the curve eventually becomes convex and shrinks to a point in finite time. For details, we refer to [**159**]. See also [**184**] and [**149**].

In §5.1, the mean curvature flow was transformed to the partial differential equation (5.17) with the aid of the signed distance function, enabling us to trace the motion of the hypersurface as the level-set $\{v = 0\}$. This viewpoint is valid, not only for classical solutions, but also for a wide class of solutions which may have singularities. Intuitively speaking, even if a level-set of a function contains singularities, the function itself can still remain smooth.

The idea of using level-sets appeared already in a paper [**294**] by physicists Ohta, Jasnow, and Kawasaki, and later the same idea was introduced by Osher and Sethian [**300**] in order to perform numerical simulations of the mean curvature flow.

The basic idea of the **level-set method** is to first represent the surface $\Gamma_t$ as the 0-level set of a function $u$. Then, the equation of motion for $\Gamma_t$ is rewritten as a partial differential equation for $u$. Then, applying to the partial differential equation the method of viscosity solution, to be discussed later, a unique global-in-time solution will be obtained.

Let us write down the equation for $u$ for which each level-set $\Gamma_t^\gamma = \{x \in \mathbb{R}^n | u(x,t) = \gamma\}$ moves according to the mean curvature flow. We assume that $u$ is smooth and that $|Du| \neq 0$ holds in the region of our concern. Under such conditions, $\Gamma_t^\gamma$ is a smooth hypersurface and its unit normal vector $\mathbf{N}$ and mean curvature $\kappa$ are respectively given by $\mathbf{N} = Du/|Du|$ and

$$\kappa = -\mathrm{div}(\mathbf{N}) = -\mathrm{div}\left(\frac{Du}{|Du|}\right). \tag{5.19}$$

On the other hand, the velocity $V$ of $\Gamma_t^\gamma$ in the direction of $\mathbf{N}$ takes the form

$$V = -\frac{u_t}{|Du|}\mathbf{N}. \tag{5.20}$$

Therefore the equation for the mean curvature flow is expressed as

$$u_t = |Du|\mathrm{div}\left(\frac{Du}{|Du|}\right) \tag{5.21}$$

along $\Gamma_t^\gamma$. Computing the divergence on the right hand side, (5.21) is rewritten as

$$u_t = \sum_{i=1}^{n}\sum_{j=1}^{n}\left(\delta_{ij} - \frac{u_{x_i}u_{x_j}}{|Du|^2}\right), \tag{5.22}$$

where $\delta_{ij}$ is Kronecker's delta and the subscript $x_i$ stands for differentiation with respect to $x_i$.

REMARK 5.4. When the normal speed is a constant (cf. REMARK 5.1), the level-set equation becomes $u_t = c|Du|$.

The right hand side of (5.22) is written in a concise form by using the following function:

$$F(\mathbf{p}, X) = \sum_{i=1}^{n}\sum_{j=1}^{n}\left(\delta_{ij} - \frac{p_i p_j}{|p|^2}\right) X_{ij}, \tag{5.23}$$

where $\mathbf{p}$ is an $n$-vector and $X$ a symmetric $n \times n$ matrix. In terms of this notation, (5.22) is recast as

$$u_t = F(Du, D^2u), \tag{5.24}$$

where $D^2u$ is the Hessian matrix $(u_{x_i x_j})_{1\le i,j\le n}$. The function $F$ can further be written as follows:

$$F(\mathbf{p}, X) = \operatorname{trace}\Big[(I - \overline{\mathbf{p}}\otimes\overline{\mathbf{p}})X\Big], \qquad \overline{\mathbf{p}} = \frac{\mathbf{p}}{|\mathbf{p}|}, \tag{5.25}$$

where $I$ stands for the identity matrix and the tensor product $\mathbf{p}\otimes\mathbf{p}$ is the $n\times n$ matrix whose $ij$-th entry is $p_i p_j$. By direct computations, one can verify that $F$ satisfies the following two properties for $\mathbf{p} \neq \mathbf{0}$:

(i) $F(s\mathbf{p}, sX) = sF(\mathbf{p}, X)$ for $s > 0$.
(ii) $F(\mathbf{p}, X + r\mathbf{p}\otimes\mathbf{p}) = F(\mathbf{p}, X)$ for $r \in \mathbb{R}$.

Functions satisfying these conditions are called **geometric** by Chen, Giga, and Goto [**72**].

Moreover, $F$ enjoys the following **monotonicity** property:

$$F(\mathbf{p}, X) \le F(\mathbf{p}, X + Y) \qquad \text{for } Y \ge 0, \tag{5.26}$$

where $Y \ge 0$ means that $Y$ is a symmetric nonnegative matrix. Note that the latter property has already appeared in (5.16).

When $F$ satisfies the monotonicity (5.26), it is called **(degenerate) elliptic**, and the equation $u_t = F$ is called a **(degenerate) parabolic** equation. For a geometric $F$, strict monotonicity can never be satisfied, since the matrix $\mathbf{p}\otimes\mathbf{p}$, appearing in (ii) in the definition for $F$ to be geometric, is positive definite. On the other hand, for

the heat equation $u_t = \Delta u$ we have $F(\mathbf{p}, X) = \text{trace}X$, and hence strict monotonicity holds. When $F$ is geometric, it is degenerate in the direction of $\mathbf{p} \otimes \mathbf{p}$, and the diffusion effect is not operative in that direction. This is why the geometric $F$ is called *degenerate* elliptic.

REMARK 5.5. In case $F(\mathbf{p}, X)$ does not depend on $X$ (such as in the equation of constant speed), $u_t = F$ is a first order equation, which in our definition above is called degenerate parabolic (degenerate in all directions).

**5.2.2. Viscosity Solutions.** An example in which solutions develop singularities in finite time even if the initial condition is smooth is the shock formation in solutions of the one-dimensional nonlinear hyperbolic equation $u_t + (u^2/2)_x = 0$ (which is a special case of the first order equation in REMARK 5.5). The latter equation is also a special case of nonlinear conservation laws. In fact, it is obtained by differentiating the Hamilton-Jacobi equation

$$v_t + H(v_x) = 0 \tag{5.27}$$

with respect to $x$ and setting $u = v_x$ (with $H(p) = p^2/2$). When $H(p)$ is convex in $p$, generalized weak solutions for such laws are characterized in terms of the Hopf-Lax formula (cf. Chapter 3 of [**126**], for instance).

The weak solutions discussed above are solutions in the sense of distribution. In partial differential equations of divergence form, one can successfully obtain a definition of weak solution, by shifting spatial derivatives from unknown functions to test functions, thanks to integration by parts. However, such a procedure does not fit our present situation, because the degenerate parabolic equation obtained from the mean curvature flow is not of divergence form.

The notion of viscosity solution is proposed to rescue the situation. As the name indicates, the notion is closely linked to the method of vanishing viscosity (see, for instance, [**126**]), in which a weak solution is defined as the limit of solutions of regularized equations obtained by adding a second order *viscosity* term to the Hamilton-Jacobi equation. But it is more than that.

It was first shown in [**72**] and [**127**] that the method of viscosity solutions is very useful in studying interface equations, including the mean curvature flow. In particular, the following results were established in [**72**] for a general geometric nonlinearity $F$; however, we restrict our presentation to the minimum that will be necessary for understanding the subsequent material. For details, consult [**83**],

[**18**], and references therein. Let us now explain the idea in the following setting.

For a given hypersurface $\Gamma_0 \subset \mathbb{R}^n$, we find a bounded continuous function $g$ whose 0-level set is $\Gamma_0$, namely, $\Gamma_0 = \{x | g(x) = 0\}$. We then solve the initial value problem

$$\begin{cases} u_t = \left(\delta_{ij} - \dfrac{u_{x_i} u_{x_j}}{|Du|^2}\right) u_{x_i x_j}, & (x,t) \in \mathbb{R}^n \times (0,\infty), \\ \\ u = g \qquad \text{on } \mathbb{R}^n \times \{t = 0\}, \end{cases} \tag{5.28}$$

by means of viscosity solutions, and define the mean curvature flow starting at $\Gamma_0$ by

$$\Gamma_t = \{x \mid u(x,t) = 0\}. \tag{5.29}$$

In order for $\{\Gamma_t\}_{t \geq 0}$ to be a **generalized mean curvature flow**, it is necessary not only that (5.28) have time-global solutions beyond singularity formation, but also that the solution be unique and coincide with the classical one when the latter exists. Viscosity solutions are weak solutions that meet these requirements.

DEFINITION 5.6 (**Viscosity Solution**). A bounded continuous function $u$ is called a **viscosity sub-solution** (**super-solution**) of (5.28) if $u = g$ on $\mathbb{R}^n \times \{t = 0\}$ and satisfies the following requirements: For each $\phi \in C^\infty(\mathbb{R}^n \times (0,\infty))$ such that $u - \phi$ attains a local maximum (resp. local minimum) at $(x_0, t_0) \in \mathbb{R}^n \times (0,\infty)$, then either

$$\phi_t \leq (\geq) \left(\delta_{ij} - \frac{\phi_{x_i} \phi_{x_j}}{|D\phi|^2}\right) \phi_{x_i x_j} \quad (\text{if } D\phi(x_0,t_0) \neq 0) \tag{5.30}$$

or

$$\phi_t \leq (\geq)\ (\delta_{ij} - \eta_i \eta_j) \phi_{x_i x_j} \quad (\text{if } D\phi(x_0,t_0) = 0) \tag{5.31}$$

for some $|\eta| \leq 1$, holds at $(x_0, t_0)$. When $u$ is both a viscosity sub- and super-solution, it is called a **viscosity solution**.

THEOREM 5.7 (Existence and Uniqueness of Viscosity Solution). *Viscosity solutions of* (5.28) *exist globally in time and are unique.*

PROOF. We refer to [**72**], [**127**]. □

THEOREM 5.7 guarantees the unique existence of solutions of (5.28). However, there are infinitely many ways of choosing $g$ that give rise to the level set $\Gamma_0$. One could choose as the initial function another $\hat{g}$ such $\Gamma_0 = \{x | \hat{g}(x) = 0\}$. It is therefore not clear that the solution $\hat{u}$ of (5.28) with initial condition $\hat{g}$ would give the same mean

curvature flow as the previous one. The following proposition ensures that the choice of initial function does not matter.

PROPOSITION 5.8. *Let $u$ be the unique viscosity solution of* (5.28) *and $\Phi : \mathbb{R} \to \mathbb{R}$ a continuous function. Then*

$$\tilde{u} := \Phi(u) \tag{5.32}$$

*is the viscosity solution of* (5.28) *with the initial condition $\tilde{g} := \Phi(g)$.*

As for the compatibility between viscosity and classical solutions, the following is known.

THEOREM 5.9. *Let $\Gamma_0$ be a smooth hypersurface embedded in $\mathbb{R}^n$. The generalized mean curvature flow $\{\Gamma_t\}_{t\geq 0}$ starting at $\Gamma_0$, constructed by means of viscosity solutions, coincides with the mean curvature flow constructed via classical solutions, as long as the latter exist.*

**5.2.3. Convergence to Mean Curvature Flow.** We examined in CHAPTER 4 the relationship between a reaction-diffusion system and the corresponding velocity-curvature equation, by using the method of formal matched asymptotic expansions. If, in that example, the controller variable $v$ is fixed at the value where the double-well potential has two wells of equal depth, then the corresponding interface dynamics is described by the mean curvature flow.

It is in general important to clarify the relationship between reaction-diffusion systems and the corresponding interface equations. The reason is, not only because two objects (reaction-diffusion systems and interface equations) are linked to each other, but also because it clarifies, for instance, why the phase-field model is effective to describe crystal growth processes (cf. §5.3). In this sense, to understand how these two objects are related is also useful when one tries to construct a mathematical model for some natural phenomenon.

In this subsection, we will rigorously prove the convergence of a scalar bistable reaction-diffusion equation (the Allen-Cahn equation) to its interface equation. This is the most basic result. The equation is

$$u_t = \Delta u - W'(u) \qquad \text{in } \mathbb{R}^n \times (0, \infty), \tag{5.33}$$

where $W(u)$ is a double-well potential. One can show at a formal level that, due to the bistability of $W'(u)$, a front structure emerges in the solution of (5.33) after a long period of time, and that its normal

speed $V$ behaves as

$$V = \alpha + \kappa t^{-1} + O(t^{-2}), \qquad t \gg 1. \tag{5.34}$$

The symbol $\kappa$ stands for the mean curvature of the front, and $\alpha$ is a constant determined by $W(u)$. The constant $\alpha$ in (5.34) is a driving force originating from the potential difference between two local minima of $W$, while the second term is the surface tension generated by the diffusion term (these terms already appeared in velocity-curvature equations treated in CHAPTER 4). In order to characterize these two modes of motion (due to the constant speed $\alpha$ and the curvature effect), it is necessary for us to employ different spatio-temporal scales. Indeed, to characterize the motion due to the constant speed $\alpha$ in the first term of the asymptotic expansion (5.34), a hyperbolic scaling $(x,t) \mapsto (\epsilon^{-1}x, \epsilon^{-1}t)$ is adequate. When we scale $u(x,t)$ as in

$$u^\epsilon(x,t) = u(\epsilon^{-1}x, \epsilon^{-1}t), \tag{5.35}$$

the equation for $u^\epsilon$ becomes

$$u_t^\epsilon = \epsilon \Delta u^\epsilon - \epsilon^{-1} W'(u^\epsilon), \tag{5.36}$$

and we need to consider the singular limit of the latter equation as $\epsilon \to 0$. If $\alpha = 0$ (the potential $W$ assumes the same value at the two local minima), then a parabolic scaling $(x,t) \mapsto (\epsilon^{-1}x, \epsilon^{-2}t)$ is suitable to characterize the motion due to the second term in (5.34). In this case, the function

$$u^\epsilon(x,t) = u(\epsilon^{-1}x, \epsilon^{-2}t) \tag{5.37}$$

satisfies the equation

$$u_t^\epsilon = \Delta u^\epsilon - \epsilon^{-2} W'(u^\epsilon), \tag{5.38}$$

whose singular limit (as $\epsilon \to 0$) has to be considered.

As a preparation for rigorous treatment, let us review some of the properties of the double-well potential $W$ (cf. PROPOSITION 4.31). Let us assume that $W : \mathbb{R} \to \mathbb{R}$ is a double-well potential that has local minima at $u = \pm 1$ and a unique local maximum at $\mu \in (-1,1)$ (and has no other critical points). There exist a unique $c \in \mathbb{R}$ and a function $q : \mathbb{R} \to \mathbb{R}$ that satisfy

$$\begin{cases} c\dot{q} + \ddot{q} = W'(q) & \text{on } \mathbb{R}, \\ q(\pm\infty) = \pm 1, \quad q(\mu) = 0, \quad \dot{q} > 0 & \text{on } \mathbb{R}. \end{cases} \tag{5.39}$$

Moreover, $c$ can be explicitly given by

$$c = \left( \int_{-\infty}^{\infty} \dot{q}(\xi)^2 d\xi \right)^{-1} \Big( W(1) - W(-1) \Big). \tag{5.40}$$

We take the function

$$u_0(x) = q(\epsilon^{-1} d_0(x)) \qquad \text{on } \mathbb{R} \times \{t = 0\} \tag{5.41}$$

as our initial value, where $d_0$ is the signed distance function to the initial interface $\Gamma_0$. Due to the results in [**70**], one can substantially weaken the condition on the initial function. The following theorems hold true.

THEOREM 5.10 (**Hyperbolic Scaling**). *Assume that $W$ satisfies* (5.39) *and* (5.40). *Let $u^\epsilon$ be the solution of* (5.36) *with the initial condition $u_0$ in* (5.41). *We define*

$$\Omega_0 = \{x |\ u_0(x) > 0\}, \qquad \Gamma_0 = \{x |\ u_0(x) = 0\},$$

*and assume that $\Gamma_0 = \partial\Omega_0 = \partial(\mathbb{R}^n \backslash \overline{\Omega}_0)$. Let $(\Gamma_t, \Omega_t^+, \Omega_t^-)$ denote the evolution of level sets according to the constant normal speed with the initial condition $(\Gamma_0, \Omega_0, \mathbb{R}^n \backslash \overline{\Omega}_0)$.*

*Then as $\epsilon \to 0$, $u^\epsilon$ converges to a step function:*

$$u^\epsilon \to \begin{cases} 1 & \text{on } \theta = \bigcup_{t>0} (\Omega_t^+ \times \{t\}), \\ -1 & \text{on } \theta' = \bigcup_{t>0} (\Omega_t^- \times \{t\}), \end{cases} \tag{5.42}$$

*with the convergence being locally uniform.*

THEOREM 5.11 (**Parabolic Scaling**). *Assume that $W$ satisfies $W(-1) = W(1)$, in addition to the conditions in the previous theorem. Let $u^\epsilon$ be the solution of* (5.38) *with the initial condition $u_0$ in* (5.41). *We define $\Omega_0$, $\Gamma_0$ as above, and assume that $\Gamma_0 = \partial\Omega_0 = \partial(\mathbb{R}^n \backslash \overline{\Omega}_0)$.*

*If $(\Gamma_t, \Omega_t^+, \Omega_t^-)$ is the mean curvature flow starting from $(\Gamma_0, \Omega_0, \mathbb{R}^n \backslash \overline{\Omega}_0)$, then as $\epsilon \to 0$, $u^\epsilon$ converges to a step function:*

$$u^\epsilon \to \begin{cases} 1 & \text{on } \theta = \bigcup_{t>0} (\Omega_t^+ \times \{t\}), \\ -1 & \text{on } \theta' = \bigcup_{t>0} (\Omega_t^- \times \{t\}), \end{cases} \tag{5.43}$$

*with the convergence being locally uniform.*

In the sequel, we will outline the proof for THEOREM 5.11. For the proof of THEOREM 5.10, consult [**129**] and [**21**], for example.

PROOF. We consider the modified nonlinearity $W'(u) - \epsilon a$, which is a small perturbation of $W'(u)$, in order to construct super- and sub-solutions that control the behavior of $u^\epsilon$ from above and below, respectively. We assume that $\epsilon$ and $a$ are sufficiently small so that

the equation $W'(u) - \epsilon a = 0$ has exactly three solutions $h_-^{a,\epsilon} < h_0^{a,\epsilon} < h_+^{a,\epsilon}$ which converge to $-1, 0, 1$, respectively, as $\epsilon \to 0$. By the same reasoning as for (5.39) and (5.40), the following problem for one-dimensional travelling waves has a unique solution $(c(a,\epsilon), q^{a,\epsilon})$:

$$\text{(5.44)} \qquad \begin{cases} \ddot{q}^{a,\epsilon} + c(a,\epsilon)\dot{q}^{a,\epsilon} = W'(q^{a,\epsilon}) - \epsilon a & \text{on } \mathbb{R}, \\ \\ q^{a,\epsilon}(\pm\infty) = h_\pm^{a,\epsilon}, \qquad q^{a,\epsilon}(0) = h_0^{a,\epsilon}, \qquad \dot{q}^{a,\epsilon} > 0. \end{cases}$$

Since $W$ has two wells at $u = \pm 1$ with equal depth, the relations

$$\text{(5.45)} \qquad c(a,\epsilon) \to 0, \qquad \epsilon^{-1} c(a,\epsilon) \to c(a) \qquad (\text{as } \epsilon \to 0),$$

$$\text{(5.46)} \qquad c(a) \to 0 \qquad (\text{as } a \to 0)$$

hold true. These relations mean that when the potential $W$ is perturbed by an amount proportional to $\epsilon$, the corresponding wave speed for the perturbed potential also deviates from the original one in the same order of magnitude. We now construct a super-solution of (5.38) to control the behavior of $u^\epsilon$ from above. Let us denote by $u^{\delta,a}$ the solution of the following singular limit equation, corresponding to the perturbed potential:

$$\text{(5.47)} \qquad \begin{cases} u_t^{\delta,a} = \operatorname{trace}\left[\left(I - \dfrac{Du^{\delta,a} \otimes Du^{\delta,a}}{|Du^{\delta,a}|^2}\right) D^2 u^{\delta,a}\right] \\ \qquad\qquad\qquad -c(a)|Du^{\delta,a}| \quad \text{in } \mathbb{R}^n \times (0,\infty), \\ \\ u^{\delta,a} = d_0 + \delta \qquad \text{on } \mathbb{R}^n \times \{0\}, \end{cases}$$

where $\delta$ represents an adjustment in the signed distance function at the initial moment, and $c(a)$ is defined in (5.45). Note that the singular limit does not involve $\epsilon$, simply because the perturbation of the potential was $\epsilon a$ (first order in $\epsilon$). One can see that level sets of the solutions to (5.47) evolve according to

$$\text{(5.48)} \qquad V = \text{mean curvature} - c(a).$$

Moreover, denoting by $d^{\delta,a}$ the signed distance function to the set

$$\{x \mid u^{\delta,a}(x,t) = 0\},$$

one can verify (cf. (5.13)) that

$$\text{(5.49)} \qquad d_t^{\delta,a} \geq \Delta d^{\delta,a} - c(a)|Dd^{\delta,a}|$$
$$\text{and } |Dd^{\delta,a}| = 1 \qquad \text{on } \{d^{\delta,a} > 0\}.$$

We are going to construct a super-solution for $u^\epsilon$ by utilizing the signed distance function $d^{\delta,a}$. For that purpose, it is convenient to introduce the following auxiliary function $w^{\delta,a}$:

$$w^{\delta,a} = \eta_\delta(d^{\delta,a}) \qquad \text{on } \mathbb{R}^n \times (0,\infty), \tag{5.50}$$

where $\eta_\delta : \mathbb{R} \to \mathbb{R}$ is a smooth function with the following properties:

$$\begin{cases} \eta_\delta(z) = -\delta & (z \le \delta/4), \\ \eta_\delta = z - \delta & (z \ge \delta/2), \\ \eta_\delta \le -\delta/2 & (z \le \delta/2), \\ 0 \le \eta_\delta' \le C, \quad |\eta_\delta''| \le C\delta^{-1} & \text{on } \mathbb{R}, \end{cases} \tag{5.51}$$

in which $C$ is a constant independent of $\delta$.

By using $w^{\delta,a}$, let us define $\Phi^\epsilon$ by

$$\Phi^\epsilon = q^{a,\epsilon}(\epsilon^{-1} w^{\delta,a}) \quad \text{on } \mathbb{R}^n \times (0,\infty) \tag{5.52}$$

to obtain

PROPOSITION 5.12. *For each $a > 0$, there exist some $\epsilon_0(\delta, a)$ and $\delta_0(a)$ such that for $(\epsilon, \delta)$ with $\epsilon \le \epsilon_0(\delta, a)$, $\delta \le \delta_0(a)$, the function $\Phi^\epsilon$ is a super-solution of* (5.38).

PROOF. Details of the proof can be found in [**129**] and [**21**]. In the sequel, we only show how the computations go, assuming that $w^{\delta,a}$ is smooth. To be rigorous, we would have to show that these computations are also valid in the sense of a viscosity solution.

Let us now examine the sign of $\Phi_t^\epsilon - \Delta\Phi^\epsilon + (1/\epsilon^2)W'(\Phi^\epsilon)$. By using (5.44) and (5.52), we have

$$\begin{aligned} \Phi_t^\epsilon - \Delta\Phi^\epsilon + \frac{1}{\epsilon^2} W'(\Phi^\epsilon) &= \epsilon^{-1}\dot{q}^{a,\epsilon}\left[w_t^{\delta,a} - \Delta w^{\delta,a} + \epsilon^{-1}c(a,\epsilon)\right] \\ &\quad - \epsilon^{-1}\ddot{q}^{a,\epsilon}\left[|Dw^{\delta,a}|^2 - 1\right] + \epsilon^{-1}a, \end{aligned} \tag{5.53}$$

where $\dot{q}^{a,\epsilon}$ and $\ddot{q}^{a,\epsilon}$ are evaluated at $\epsilon^{-1}w^{\delta,a}$. We now use the following lemma (cf. [**129**] for its proof) to estimate the right hand side of (5.53).

LEMMA 5.13. *There exists a constant $C$, independent of $\delta, a$, such that the following properties hold:*

(i) $w_t^{\delta,a} - \Delta w^{\delta,a} + c(a)|Dw^{\delta,a}| \ge -\delta^{-1}C$ *in* $\mathbb{R}^n \times (0, t^*)$;

(ii) $w_t^{\delta,a} - \Delta w^{\delta,a} + c(a)|Dw^{\delta,a}| \ge 0$ *in* $\{d^{\delta,a} > \delta/2\}$;

(iii) $|Dw^{\delta,a}| = 1$ *in* $\{d^{\delta,a} > \delta/2\}$.

*In* (i) *above,* $t^*$ *is the extinction time at which the set* $\{x|u^{\delta,a}(x,t) = 0\}$ *becomes empty.*

We now deal with two cases according to the value of $d^{\delta,a}$:

(I) When $d^{\delta,a} > \delta/2$.

By applying LEMMA 5.13 to (5.53), we obtain, for small $\epsilon > 0$,

$$\Phi_t^\epsilon - \Delta\Phi^\epsilon + \frac{1}{\epsilon^2}W'(\Phi^\epsilon) \geq \epsilon^{-1}\dot{q}^{a,\epsilon}\left[\epsilon^{-1}c(a,\epsilon) - c(a)\right] + \epsilon^{-1}a \geq 0. \tag{5.54}$$

(II) When $d^{\delta,a} \leq \delta/2$.

According to the definition of $\eta_\delta$, we have

$$w^{\delta,a} \leq -\frac{\delta}{2}. \tag{5.55}$$

Therefore, on account of the exponentially decaying property of the travelling wave solution $q^{a,\epsilon}$ at $\pm\infty$, one can show the existence of a constant $K > 0$ such that

$$\epsilon^{-1}\dot{q}^{a,\epsilon} + \epsilon^{-2}|\ddot{q}^{a,\epsilon}| \leq Ke^{-K\delta/\epsilon}. \tag{5.56}$$

On the other hand, one can prove that $|Dw^{\delta,a}| \leq C$ by using the boundedness of $\eta_\delta'$ in (5.51) and $|Dd^{\delta,a}| \leq 1$. Together with (i) of LEMMA 5.13, we can therefore find a constant $\hat{C} > 0$ such that

$$\begin{aligned}\Phi_t^\epsilon - \Delta\Phi^\epsilon + \frac{1}{\epsilon^2}W'(\Phi^\epsilon) \\ \geq Ke^{-K\delta/\epsilon}\left[-\delta^{-1}C - \hat{C}\right] + \epsilon^{-1}a \geq 0,\end{aligned} \tag{5.57}$$

by choosing $\epsilon > 0$ appropriately small for a given $\delta$. This completes the proof of PROPOSITION 5.12. □

We are now ready to prove THEOREM 5.11.

By using the initial condition (5.41), PROPOSITION 5.13, and the maximum principle, one can show that

$$u^\epsilon \leq \Phi^\epsilon \qquad \text{on } \mathbb{R}^n \times [0, t^*), \tag{5.58}$$

by choosing $\epsilon$ small.

Denoting by $u$ the solution of the mean curvature flow

$$\text{(5.59)}\quad \begin{cases} u_t = \operatorname{trace}\left[\left(I - \dfrac{Du \otimes Du}{|Du|^2}\right) D^2 u\right] & \text{in } \mathbb{R}^n \times (0,\infty), \\ u = d_0 \qquad \text{on } \mathbb{R}^n \times \{0\}, \end{cases}$$

let $(x_0, t_0) \in \mathbb{R}^n \times [0, t^*)$ be a point such that $u(x_0, t_0) = -\beta < 0$. Thanks to the stability of viscosity solutions, we have that $u^{\delta,a} \to u$ as $\delta,\ a \to 0$ uniformly in $(x_0, t_0)$. Therefore by choosing $\delta,\ a$ small, we have

$$\text{(5.60)}\qquad u^{\delta,a}(x_0, t_0) < -\frac{\beta}{2} < 0,$$

which means $d^{\delta,a} < 0$. It therefore follows that

$$\text{(5.61)}\qquad \limsup_{\epsilon \to 0} u^\epsilon(x_0, t_0) \le \limsup_{\epsilon \to 0} \Phi^\epsilon(x_0, t_0) = -1.$$

Since the initial condition (5.41) and the maximum principle imply $u^\epsilon \ge -1$, we finally conclude that

$$\text{(5.62)}\qquad u^\epsilon \to -1 \qquad \text{in} \bigcup_{0<t<t^*} \{x \mid u(x,t) < 0\}.$$

By constructing a sub-solution similarly, one can also prove that

$$u^\epsilon \to 1 \qquad \text{in} \bigcup_{0<t<t^*} \{x \mid u(x,t) > 0\}.$$

This completes the proof of THEOREM 5.11 on $\mathbb{R}^n \times (0, t^*)$. For the extension of the proof to the entire domain $\mathbb{R}^n \times (0,\infty)$, we refer to [**129**] and [**21**]. □

## 5.3. Distinguished Limits of the Phase Field Model

By using the phase-field model (which describes solidification-melting processes)

$$\text{(5.63)}\quad \begin{cases} \partial_t u + \lambda \partial_t \phi = \Delta u, \\ \alpha \epsilon^2 \partial_t \phi = \epsilon^2 \Delta \phi + f(\phi, u; \epsilon) \end{cases}$$

as an example, we will examine in this section various distinguished limits (as $\epsilon \to 0$) and the relationship between them. The meaning of the variables in (5.63) will be explained in §5.3.1. In order to describe the evolution of an interface, there are two approaches: one in which the interface is treated as having thin but finite width, a typical example being the equation (5.63); and the other in which

the interface is treated as a surface of infinitesimal width where the relevant variables exhibit discontinuity and the motion of the surface of discontinuity is scrutinized. An example of the latter is the Stefan type model from CHAPTER 3.

There have been many discussions from physical viewpoints as to what kind of model is adequate in order to describe original phenomena. From the standpoint of singular limits, however, the difference in various models is nothing but the difference of spatio-temporal scales through which the phenomenon is observed, and hence each model can be considered as the most adequate one within the scale employed. Moreover, these different models are interrelated. In fact, one can derive several different interface equations from the phase-field model, according to different ways of passing to the singular limit (cf. [**49**], [**52**]).

There are at least three problems to be examined:

(i) To determine singular limit equations associated with various scales employed.
(ii) Well-posedness of the singular limit equations.
(iii) To investigate various properties of the singular limit equations.

There has been substantial progress in these problems, and research is ongoing. The research activities on the three problems above are considered as an attempt to classify various model equations, with the singular limit procedure being a pivot. We will present some of the results thus obtained in terms of the phase-field model, centering mainly around problem (i).

**5.3.1. Phase-Field Model.** The word *phase* (expressed by the symbol $\phi$) in *phase field* means an order parameter. In case of a crystal growth process, it indicates if a system is either in solid phase or liquid phase. Therefore, it is different from *phase* that appears in periodic solutions. In the example (5.63), $\phi$ signifies that the system is in solid phase when it is near $-1$ and in liquid phase if it is close to 1. To be precise, we impose the following conditions on $f$:

$$\text{(5.64)} \qquad \begin{cases} \text{For each fixed } u,\ f \text{ is of bistable type satisfying} \\ f(\phi,0,\epsilon) = -f(-\phi,0,\epsilon), \qquad f(\pm 1,0,\epsilon) = 0, \\ \displaystyle\int_{h_-(u,\epsilon)}^{h_+(u,\epsilon)} f(\phi,u,\epsilon)d\phi \neq 0 \quad \text{for } u \neq 0. \end{cases}$$

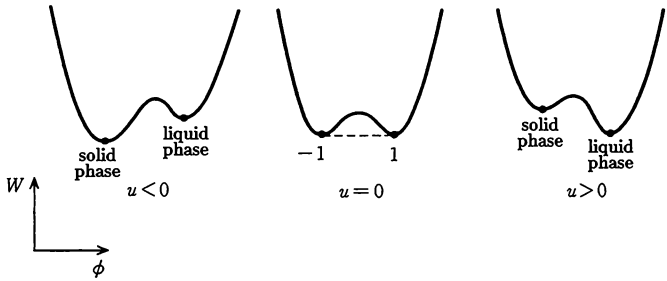


FIGURE 5.2. Temperature dependence of a double-well potential in the phase-field model.

In the above $\phi = h_{\pm}(u, \epsilon)$ are two stable equilibria of the ordinary differential equation for $\phi$ which is obtained by neglecting the diffusion term for each fixed $u$. In the sequel, it will suffice for us to keep in mind a typical example, say, $f(\phi, u) = k(\phi - \phi^3) + u$. The odd symmetry of $f$ in (5.64) is only for the sake of simplicity and is not essential.

The variable $u$ stands for the temperature field. The profile of the potential $W(\phi) = \int^{\phi} f(\phi, u, \epsilon) d\phi$ (cf. FIGURE 5.2) shows that the well corresponding to liquid phase (resp. solid phase) is deeper for $u > 0$ (resp. $u < 0$). The difference in the potential values gives the driving force of phase transition under the variation of temperature.

The parameter $\lambda$ stands for the latent heat, meaning that heat is released at the rate $\lambda\phi_t$ under the temporal variation of phase. The first equation in (5.63) therefore expresses the conservation of heat. For more details, consult [**48**] and [**220**]. In our treatment here, we assume that the latent heat $\lambda$ is constant. It is, however, natural and reasonable from the viewpoint of thermodynamics that it is phase-dependent: $\lambda = \lambda(\phi)$ (cf. [**307**]).

As a classical model for crystal growth, the Stefan model treated in CHAPTER 3 is well known and its physical meaning is easily understood. On the other hand, since the phase-field model was introduced in a more phenomenological manner by employing an order parameter $\phi$, its significance and relevance to actual phenomena were not clear at first. As we will clarify in the next subsection, however, it turns out that the phase-field model gives rise to various models of Stefan type according to different ways of passing to the singular limit.

Therefore, these two models, phase-field and Stefan, are not dealing with different phenomena. In the former one, phase boundaries are considered as layers of finite thickness of order $O(\epsilon)$, while in the latter they are interpreted as sharp interfaces with infinitesimal thickness. Such an observation not only clarifies the mathematical relationships between the model equations, but also gives an important perspective in constructing model equations for new phenomena.

**5.3.2. Distinguished Limits of the Phase-Field Model.** The phase-field model contains many parameters, such as the latent heat parameter $\lambda$, the parameter $\epsilon$ corresponding to the thickness of the interface, and the relaxation parameter $\alpha$ which represents the difference in time constants of $\phi$ and $u$. It is not clear in advance under what kind of combination of these parameters one should pass to the singular limit. In any event, the thickness $O(\epsilon)$ of the interface is required to go to zero. It is therefore convenient to first derive candidates for singular limits by applying the method of matched asymptotic expansion (discussed in §4.3.3) to (5.63), and then to start discussing the issue backward.

The interface $\Gamma$ is the boundary between the liquid phase $\mathcal{D}_+$ ($r > 0$) and the solid phase $\mathcal{D}_-$ ($r < 0$). We use uppercase letters $U, \Phi$ to represent inner variables and lowercase letters $u, \phi$ for outer variables, as in §4.3.3. For simplicity, we consider the case where the space dimension is two and $f$ does not depend on $\epsilon$. Symbols, such as the stretched variable $\rho = r/\epsilon$, are the same as before. The location of the interface $\Gamma$ ($r = 0$) is defined by the level set $\Phi = 0$. The following derivation is due to [**52**].

**Outer Expansion**. We have

$$\text{(5.65)} \qquad \begin{cases} \partial_t u_0 + \lambda \partial_t \phi_0 = \Delta u_0 \quad (r \neq 0), \\ f(\phi_0, u_0) = 0, \end{cases} \qquad O(1),$$

$$\text{(5.66)} \qquad \begin{cases} \partial_t u_1 + \lambda \partial_t \phi_1 = \Delta u_1, \\ f_\phi(\phi_0, u_0)\phi_1 + f_u(\phi_0, u_0)u_1 = 0, \end{cases} \qquad O(\epsilon).$$

We assume that the second equation in (5.65) solves as $\phi_0 = h_+(u_0)$ near $\phi = +1$ and that $f_\phi(\phi_0, u_0) < 0$ is satisfied there (these assumptions are satisfied for the cubic $f$ above and are related to solvability

conditions at the $O(\epsilon)$-level). Substituting this into the first equation, one obtains the following equation that has to be valid in the liquid phase ($r > 0$):

$$\partial_t \left(u_0 + \lambda h_+(u_0)\right) = \Delta u_0, \tag{5.67}$$

which is a nonlinear heat equation for $u_0$. Similar procedures work for the solid phase ($r < 0$), giving rise to $\phi_0 = h_-(u_0)$ and a relevant equation for $u_0$.

One can derive, in the same manner as above, the equations for higher order terms $u_k$ in the expansion. In order to determine these terms, one needs to impose conditions on the interface ($r = 0$), in addition to initial and boundary conditions. Inner expansions bring out these conditions.

**Inner Expansion**. By rewriting (5.63) in terms of the coordinate system $(\rho, s, t)$ near the interface, one obtains the following:

$$\begin{aligned} 0 = {} & \partial_{\rho\rho} U + \epsilon\Big(-r_t \partial_\rho U - \lambda r_t \partial_\rho \Phi + \Delta r \partial_\rho U\Big) \\ & - \epsilon^2 \Big(\partial_t U + \partial_s U s_t + \lambda \partial_t \Phi + \lambda \partial_s \Phi s_t \\ & \qquad - \left(\partial_{ss} U |\nabla s|^2 + \partial_s U \Delta s\right)\Big), \end{aligned} \tag{5.68}$$

$$\begin{aligned} 0 = {} & \partial_{ss}\Phi + f(\Phi, U) + \epsilon\Big(-\alpha r_t \partial_\rho \Phi + \partial_\rho \Phi \Delta r\Big) \\ & + \epsilon^2 \Big(\partial_{ss}\Phi |\nabla s|^2 + \partial_s \Phi \Delta s - \alpha \partial_t \Phi - \alpha \partial_s \Phi s_t\Big). \end{aligned} \tag{5.69}$$

Therefore, the equations for $O(1)$ terms are given by

$$\partial_{\rho\rho} U_0 = 0, \tag{5.70}$$

$$\partial_{\rho\rho}\Phi_0 + f(\Phi_0, U_0) = 0. \tag{5.71}$$

Since we are looking for bounded solutions, (5.70) implies that $U_0$ is a constant. On the other hand, (5.71) demands the existence of a nonzero standing wave solution with wave speed zero. PROPOSITION 4.31 applies to give $U_0 \equiv 0$. By using the matching condition (4.51), we have

$$u_0\Big|_{\Gamma_\pm} (= U_0) = 0, \tag{5.72}$$

and hence $\Phi_0$ is given by

$$\Phi_0 = \Phi_0(\rho) = \psi(\rho) \tag{5.73}$$

thanks to (1.61). Again, applying the matching condition to $\phi_0$, we have

$$\phi_0\Big|_{\Gamma_\pm} = \pm 1. \tag{5.74}$$

Now the $O(\epsilon)$ term in (5.68) is written as

$$\partial_{\rho\rho} U_1 = r_{0t}\partial_{\rho\rho} U_0 + \lambda \partial_t r_0 \partial_\rho \Phi_0 - \Delta r_0 \partial_\rho U_0 = \lambda r_{0t} \psi'(\rho), \tag{5.75}$$

in which the second equality follows from (5.72) and (5.73). When we integrate once with respect to $\rho$, the last equation becomes

$$\partial_\rho U_1 = \lambda r_{0t} \psi(\rho) + c_1(s,t), \tag{5.76}$$

where $c_1(s,t)$ is a constant of integration. The matching condition (4.52) applied to (5.76) (as $\rho \to \infty$) gives rise to

$$\partial_r u_0\Big|_{\Gamma_\pm} = \pm \lambda r_{0t} + c_1(s,t). \tag{5.77}$$

Denoting by $v$ the normal speed of $\Gamma$ (which was denoted by $\gamma$ in CHAPTER 4), we see that the lowest order speed $v_0$ is given by $v_0 = -r_{0t}$. Therefore we obtain from (5.77)

$$\Big[\partial_r u_0\Big]\Big|_\Gamma = -2\lambda v_0, \tag{5.78}$$

where

$$\Big[\partial_r u_0\Big]\Big|_\Gamma := \partial_r u_0\Big|_{\Gamma_+} - \partial_r u_0\Big|_{\Gamma_-}.$$

The latter equation gives the lowest order Stefan condition exactly (the jump in the temperature gradient is proportional to the normal speed of the interface).

Under suitable conditions, the system of equations (5.67), (5.72), (5.78) has a unique solution $u_0(x,t)$, which in turn determines $\phi_0(x,t)$ and $r_0(x,t)$ uniquely. The function $c_1(s,t)$ is determined by using (5.77). Integrating (5.76) once more, we obtain

$$U_1(\rho,s,t) = -\lambda v_0 \Psi(\rho) + c_1(s,t)\rho + c_2(s,t), \tag{5.79}$$

where $\Psi(\rho) = \int_0^\rho \psi(z)dz$ and $c_2(s,t)$ is another constant of integration. Since $\psi(\rho)$ approaches $\pm 1$ exponentially as $\rho \to \pm\infty$, (5.79) is rewritten as

$$\begin{aligned} &U_1(\rho,s,t) \\ &\quad = \lambda v_0 \int_0^\rho \Big(\operatorname{sgn} z - \psi(z)\Big)dz - \lambda v_0|\rho| + c_1(s,t)\rho + c_2(s,t). \end{aligned} \tag{5.80}$$

Note that the second and third terms on the right hand side are linear in $\rho$. Applying the matching condition (4.52) again, we obtain

$$u_1\Big|_{\Gamma_\pm} = c_2(s,t) + \lambda v_0 \int_0^{\pm\infty} \Big(\operatorname{sgn} z - \psi(z)\Big) dz. \tag{5.81}$$

We have thus established that the temperature field $U_1$ behaves as a linear function of $\rho$ for large $|\rho|$. However, in order to determine it completely, we need to know $u_1$ and $c_2$. For the latter, we have to examine $\Phi_1$. The equation coming from the $O(\epsilon)$-term of (5.69) is given by

$$\begin{aligned} &\partial_{\rho\rho}\Phi_1 + f_\phi(\Phi_0, U_0)\Phi_1 + f_u(\Phi_0, U_0)U_1 \\ &= -\alpha v_0 \psi'(\rho) - \kappa_0 \psi'(\rho). \end{aligned} \tag{5.82}$$

Let us define $\mathcal{L} \equiv \partial_{\rho\rho} + f_\phi(\psi(\rho), 0)$ and apply the $L^2(\mathbb{R})$-solvability condition. In the sequel, computations are all carried out for the nonlinearity $f = k(\phi - \phi^3) + u$. Recasting (5.82) as

$$\mathcal{L}\Phi_1 = -U_1 - \Big(\alpha v_0 + \kappa_0\Big)\psi'(\rho), \tag{5.83}$$

and using the fact that $\psi'(\rho)$ is an eigenfunction associated with the simple 0-eigenvalue of $\mathcal{L}$, we see that the solvability condition is given by

$$\int U_1 \psi' d\rho + (\alpha v_0 + \kappa_0) \int (\psi')^2 d\rho = 0. \tag{5.84}$$

Inserting (5.79) into (5.84), we determine $c_2(s,t)$ as follows:

$$c_2 = v_0 \left[\frac{\lambda}{2} \int_{-\infty}^{\infty} \Psi(z)\psi'(z) dz - \frac{1}{2}\alpha A\right] - \frac{1}{2}\kappa_0 A, \tag{5.85}$$

where $A \equiv \int_{-\infty}^{\infty} (\psi')^2 dz$. Therefore $u_1\big|_{\Gamma_\pm}$ is determined from (5.81) and (5.85) as

$$u_1\Big|_{\Gamma_\pm} = v_0 \left[\lambda B - \frac{1}{2}\alpha A\right] - \frac{1}{2} A\kappa_0, \tag{5.86}$$

in which $B \equiv \int_0^{\infty} (1 - \psi(z))^2 dz$.

We have so far determined the lowest and second lowest order terms for the outer expansion $u, \phi$ and the inner expansion $U, \Phi$, and the lowest order term for $r$ (or $v$). One can continue such expansions

to higher order terms. Let us list the equations obtained so far:

$$\left(u+\lambda f^{-1}(u)\right)_t = \Delta u + O(\epsilon^2), \qquad x \notin \Gamma(t), \tag{5.87}$$

$$\left[u_r\right] = -2\lambda v + O(\epsilon^2), \qquad x \in \Gamma(t), \tag{5.88}$$

$$u = \epsilon v\left[\lambda B - \frac{1}{2}\alpha A\right] - \frac{1}{2}\epsilon A\kappa + O(\epsilon^2), \qquad x \in \Gamma(t). \tag{5.89}$$

In (5.87), the outer expansion $h_\pm(u)$ is expressed as $f^{-1}(u)$.

Equation (5.89) gives a dynamic version of the Gibbs-Thomson relation in which the temperature on the interface depends on the curvature and speed of the interface. These quantities in general contribute to the stability of the interface.

Up to this point, we have neglected scalings in time $t$ and in the unknown $u$. Let us introduce new scales $t'$ and $\overline{u}$ for time and the unknown via

$$t' = pt, \qquad \overline{u} = \delta^{-1}u, \tag{5.90}$$

where $p, \delta$ are both positive parameters satisfying $p \leq 1$, $\delta \ll 1$ and $\overline{u} = O(1)$. When the degree of undercooling is small, the temperature field is expected to quickly become almost uniform. In such a situation, the scaling $u = \delta\overline{u}$ is useful. With these scales, the equations (5.87), (5.88), (5.89) are rewritten as

$$p\left(\overline{u}+\lambda\delta^{-1}f^{-1}(\delta\overline{u})\right)_{t'} = \Delta\overline{u} + O\left(\frac{\epsilon^2}{\delta}\right), \tag{5.91}$$

$$\left[\overline{u}_r\right] = -\frac{2\lambda p}{\delta}\overline{v} + O\left(\frac{\epsilon^2}{\delta}\right), \tag{5.92}$$

$$\overline{u} = \frac{\epsilon p}{\delta}\overline{v}\left[\lambda B - \frac{1}{2}\alpha A\right] - \frac{1}{2}\frac{\epsilon}{\delta}A\kappa + O\left(\frac{\epsilon^2}{\delta}\right), \tag{5.93}$$

where $v = p\overline{v}$ is used. When $\delta$ is small, $f^{-1}(\delta\overline{u})$ is approximated as

$$f^{-1}(\delta\overline{u}) = \pm 1 + m\delta\overline{u}, \tag{5.94}$$

where $m = (f'(\pm 1))^{-1}$. Substituting this into (5.91), we obtain (since $\pm 1$ is eliminated upon differentiation)

$$p(1+\lambda m)\overline{u}_{t'} = \Delta\overline{u} + O\left(\frac{\epsilon^2}{\delta}\right). \tag{5.95}$$

In the sequel, we deal with the outer region in terms of (5.95). We will show formally that various free boundary problems arise according to relative orders of magnitude among $\alpha, \lambda, p$, and $\delta$.

**(I) Stefan Type**

(i) When the thermal relaxation is slow ($p = 1$) and the effect of latent heat is small ($\lambda = \epsilon\overline{\lambda}$), and hence the variation of the temperature field is of order $O(\epsilon)$ ($\delta = \epsilon$), and the time constant $\alpha = O(1)$, then one obtains the following limit system:

$$\begin{cases} \overline{u}_t = \Delta\overline{u}, \\ \left[\overline{u}_r\right] = -2\overline{\lambda}v, \\ \overline{u} = -\frac{1}{2}A(\alpha v + \kappa). \end{cases} \tag{5.96}$$

(We have omitted the reference to whether $x$ is *on* or *off* the interface $\Gamma(t)$.)

(ii) The conditions are almost the same as (i), except that $\alpha \to 0$ as $\epsilon \to 0$. In this case we obtain

$$\begin{cases} \overline{u}_t = \Delta\overline{u}, \\ \left[\overline{u}_r\right] = -2\overline{\lambda}v, \\ \overline{u} = -\frac{1}{2}A\kappa. \end{cases} \tag{5.97}$$

(iii) In the two cases above, both $\lambda/\delta$ and $\epsilon/\delta$ are of order $O(1)$, and hence the effects of latent heat $2\overline{\lambda}v$ and surface tension $\frac{1}{2}A\kappa$ both appeared in the limit. We now assume $\lambda = O(\delta)$ and $0 < \epsilon \ll \delta \ll 1$. Since $\epsilon/\delta \to 0$ in this case, setting $\lambda = \delta\overline{\lambda}$, we obtain the following limit system:

$$\begin{cases} \overline{u}_t = \Delta\overline{u}, \\ \left[\overline{u}_r\right] = -2\overline{\lambda}v, \\ \overline{u} = 0, \end{cases} \tag{5.98}$$

when the thermal relaxation is slow ($p = 1, \alpha \to 0$). This is the classical **Stefan problem** in which the curvature effect is missing.

We now deal with cases in which the thermal relaxation is fast:

$$p \to 0, \ \epsilon \to 0.$$

### (II) Mullins-Sekerka Type

(i) When the thermal relaxation is fast ($p \to 0$), we can in particular set $p = \epsilon/\lambda \to 0$ with $\delta = \epsilon$, and assume that $\alpha \ll \lambda/\epsilon$ (and hence $\alpha p \to 0$). We then obtain the following limit system:

$$\begin{cases} \Delta \overline{u} = 0, \\ \left[\overline{u}_r\right] = -2\overline{v}, \\ \overline{u} = -\frac{1}{2}A\kappa. \end{cases} \tag{5.99}$$

(ii) When $p, \delta$, and $\epsilon/\lambda$ satisfy the same conditions as in (i), assuming $\alpha = O(\lambda/\epsilon)$ with $\alpha = (\lambda/\epsilon)\overline{\alpha}$, we obtain another limit system:

$$\begin{cases} \Delta \overline{u} = 0, \\ \left[\overline{u}_r\right] = -2\overline{v}, \\ \overline{u} = -\frac{1}{2}A\Big(\overline{\alpha v} + \kappa\Big). \end{cases} \tag{5.100}$$

It may not be clear why the particular scales above are so chosen. Let us try to clarify the reason for this, taking case (ii) of Mullins-Sekerka type as an example. In this case, since the thermal relaxation is fast, it is natural to expect that (5.91) will reduce to the Laplace equation in the limit. Therefore both $p$ and $p\lambda$ are expected to go to zero. In order to retain the effect of surface tension $\kappa$ in (5.93), we need to take $\delta = \epsilon$. Then the coefficient of $\overline{v}$ in (5.93) becomes $-\frac{1}{2}p\alpha A$, and hence the behavior of $p\alpha$ determines whether or not $\overline{v}$ survives in the limit. Since we already assumed that $p\lambda \to 0$, if it is given as $p\lambda = \epsilon$, then $\alpha p = \alpha(\epsilon/\lambda)$ follows and the latter survives in the case of (ii), giving rise to (5.100). To summarize, we first determine what kind of physical effects we want to include in the final interface equation to be derived from (5.91), (5.92), (5.93); then we choose appropriate scales of parameters and unknowns so that the desired effect remains in the limit. We have thus found that the phase-field model encompasses interface equations of various types as its distinguished limits.

Active mathematical research is ongoing to rigorously justify various aspects of the problems in the list above. We briefly report on part of the progress. Let us classify the results into three groups;

(1) To show the convergence in specific classes of solutions of (5.63), such as equilibrium, travelling wave and radially symmetric solutions, to those of the limit interface equations.

(2) To show the existence of classical or weak solutions of the limit interface equations in general situations.
(3) To show the convergence of solutions of the phase-field equation to those obtained in (2).

It is in general not easy to find solutions (be they classical or weak) of the interface equations above, and it is only recently that some satisfactory results have been obtained. One reason for the difficulty is that the maximum principle is not applicable.

Case (1) is the situation where classical solutions of the limit problem are easily obtained ([**48**], [**53**], [**50**]). As for (2), time-global existence of weak solutions has been established for **(I) Stefan type** problems; we refer to [**336**] for (i) (cf. [**68**] for local solutions) and to [**248**] for (ii). For **(II) Mullins-Sekerka type** problems, time-global existence is not known for weak solutions that allow singularities. On the other hand, on the existence of classical solutions, there has been some progress ([**67**], [**120**], [**121**]). As for (3), although [**336**] proves the convergence of the phase-field model to the problem (i) of **(I) Stefan type**, there are many questions open for further investigations.

**5.3.3. Singular Limit of the Cahn-Hilliard Equation.** As a model equation to describe phase separation in isothermal media, the following Cahn-Hilliard equation was introduced in CHAPTER 4:

$$u_t + \Delta\left\{\epsilon\Delta u - \frac{1}{\epsilon}W'(u)\right\} = 0. \tag{5.101}$$

It turns out that the singular limit of the latter equation as $\epsilon \to 0$ is the free boundary problem (5.99) in (i) of Mullins-Sekerka type described in §5.3.2. According to the volume-preserving property of (5.101), the solution $\Gamma_t$ of (5.99) evolves in such a way that the volume enclosed by it is preserved. This is verified from the following computation:

$$\frac{d}{dt}\mathrm{vol}(t) = \int_{\Gamma_t} \overline{v}\, d\sigma = -\int_{\Omega} \Delta\overline{u}\, dx = 0. \tag{5.102}$$

On the other hand, the surface area of $\Gamma_t$ ($\subset \mathbb{R}^n$) is decreasing in $t$, as the next computation shows:

$$\frac{1}{n-1}\frac{d}{dt}\mathrm{area}(t) = -\int_{\Gamma_t} \kappa\overline{v}\, d\sigma = -\frac{2}{A}\int_{\Omega} |\nabla\overline{u}|^2 dx \le 0. \tag{5.103}$$

Although the convergence of (5.101) to the limit (5.99) was already established formally in [**304**], we now have available the following rigorous result, due to [**2**].

THEOREM 5.14. *Let $\Omega$ be a smooth domain and $\Gamma_{00}$ a smooth hypersurface contained in it. Assume that the Mullins-Sekerka problem* (5.99) *has a smooth solution $(v, \Gamma)$ (note the symbol is switched from $u$ to $v$) on $[0,T]$ starting with the initial interface $\Gamma_{00}$ such that $\overline{\Gamma}_t \subset \Omega$ $(t \in [0,T])$.*

*If there exist functions $u_0^\epsilon(x) \in C^\infty(\Omega)$ and $J^\epsilon \in C^\infty(\overline{\Omega}_T)$ which are uniformly bounded on $(x,t) \in \overline{\Omega}_T$ $(\Omega_T = \Omega \times (0,T))$ for $\epsilon \in (0,1]$, and if $u^\epsilon(x,t)$ is a solution of the Cahn-Hilliard equation:*

$$u_t^\epsilon + \Delta\left\{\epsilon\Delta u^\epsilon - \frac{1}{\epsilon}W'(u^\epsilon)\right\} = 0, \qquad (x,t) \in \Omega_T, \tag{5.104}$$

$$u^\epsilon(x,0) = u_0^\epsilon(x), \qquad x \in \Omega, \tag{5.105}$$

$$\frac{\partial}{\partial n}\left\{\epsilon\Delta u^\epsilon - \frac{1}{\epsilon}W'(u^\epsilon)\right\} = 0, \qquad (x,t) \in \partial\Omega_T, \tag{5.106}$$

$$\frac{\partial}{\partial n}u^\epsilon(x,t) = \epsilon^4 J^\epsilon(x,t), \qquad (x,t) \in \partial\Omega_T, \tag{5.107}$$

*then the following hold true:*

$$\lim_{\epsilon\to 0} u^\epsilon(x,t) = \begin{cases} -1, & (x,t) \in Q_0^-, \\ \\ 1, & (x,t) \in Q_0^+, \end{cases}$$

$$\lim_{\epsilon\to 0}\left(\epsilon\Delta u^\epsilon - \frac{1}{\epsilon}W'(u^\epsilon)\right)(x,t) = v(x,t), \quad (x,t) \in \Omega_T, \tag{5.108}$$

*where $Q_0^+$ and $Q_0^-$ are respectively the interior and exterior of the free boundary $\Gamma$ determined by the solutions of the Mullins-Sekerka problem* (5.99). *Moreover, if $W'(u)$ is linear near $u = \pm 1$, one can choose $J^\epsilon \equiv 0$.*

In the last theorem, the existence of classical solutions of the Mullins-Sekerka problem is postulated. However, as we noted in the previous subsection §5.3.2, this was established in [**67**] and [**120**], so the assumption can be omitted.

The proof of THEOREM 5.14 is accomplished by constructing approximate solutions, based on information about spectra of the linearized operator of the Cahn-Hilliard equation. We do not give the details. Instead, in order that we may intuitively understand that the Mullins-Sekerka problem is the singular limit, let us set $u \equiv -\epsilon\Delta\phi + (1/\epsilon)W'(\phi)$ and rewrite (5.101) as

$$\text{(5.109)} \qquad \begin{cases} \phi_t = \Delta u, \\ 0 = \epsilon\Delta\phi - \frac{1}{\epsilon}W'(\phi) + u. \end{cases}$$

This system is a special case of the phase-field model (5.63) in the sense that $\alpha = 0, \lambda = 1$ and thermal relaxation is fast (and hence the temperature field is of constant value away from the interface). The quantity $u$ defined above is called the *chemical potential*. This terminology is justified, because the jump in the normal derivative of $u$ on the interface is the driving force of motion in the singular limit.

In the singular limit, $\phi$ develops a discontinuity on the interface and otherwise equals either 1 or $-1$. Therefore, interpreting the first equation in (1.109) in the weak sense, one can obtain the first and second equations of (5.99). Arguing in the same manner as in the phase-field model, the third equation (the Gibbs-Thomson relation) of (5.99) can be derived from the second equation of (5.109).

**5.3.4. Dendrites and Anisotropy.** We have emphasized in CHAPTER 3 the importance of the surface tension and anisotropy effects in order to explain growth patterns of crystals. We have also found in §5.3.2 that singular limits of the phase-field model (without anisotropy) are capable of accommodating various important physical effects, such as surface tension. Then, is the phase-field model genuinely realistic? It was shown numerically by Kobayashi ([**220**], [**221**]) that the phase-field model with **anisotropy** can reproduce quite realistic patterns (cf. FIGURE 5.3).

When anisotropy is absent, although growth with tip-splitting is realized, as one can see from FIGURE 5.3 (a), the shape is far from that of dendrites. Assuming that the anisotropy coefficient $\epsilon$ depends on the normal velocity vector $v$ of the interface, it is usually the case that anisotropy is introduced as $\epsilon = \epsilon(v)$. However, in Kobayashi [**221**], giving consideration to computational time, the anisotropy is

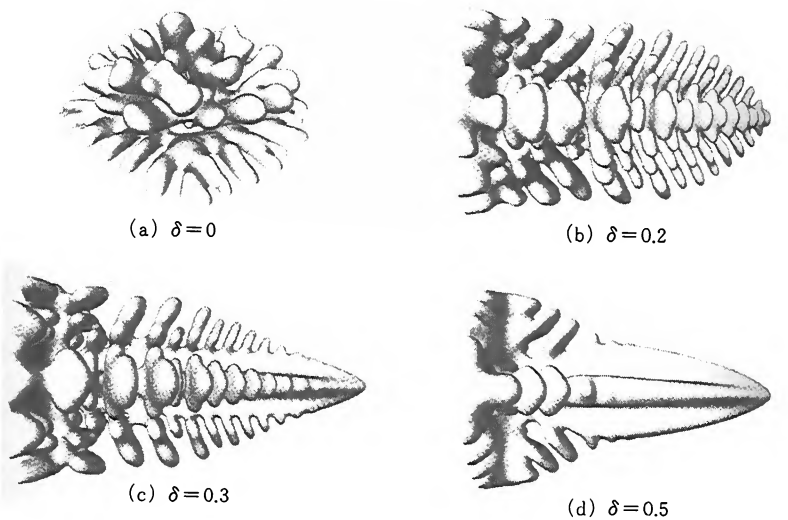


FIGURE 5.3. Various types of dendritic crystals according to the strength of anisotropy.

employed in the temperature-dependent term of the bistable nonlinearity, as in the following model:

$$\begin{cases} u_t = \Delta u + \phi_t, \\ \tau\phi_t = \epsilon^2\Delta\phi + \phi(1-\phi)\left(\phi - \frac{1}{2} + m(T, -\nabla\phi)\right). \end{cases} \tag{5.110}$$

In this model, $\nabla\phi$ is operative only on the interface (and almost 0 otherwise) and hence can be regarded as $v = -\nabla\phi$. The anisotropy term $m$ is given, in case of 4-mode anisotropy, by

$$\begin{cases} m(T, v) = -c\tan^{-1}(\gamma\sigma(v)T), \\ \sigma(\theta) = 1 - \frac{1}{4}\delta(1-\cos 4\theta), \end{cases} \tag{5.111}$$

where $c, \gamma, \delta$ are positive constants, and in particular, $\delta$ controls the strength of anisotropy. If we set the value of $\delta$ appropriately as in FIGURE 5.3 (c), the model can reproduce a pattern in which the tip is growing with constant speed and shape, showing very closely the same behavior as dendrites in experiments.

There are, however, almost no mathematical investigations of this model. As discussed in CHAPTER 3, even in terms of numerical simulations, no reasonable account has been given as to why side-branching develops from the tip. According to the strength of anisotropy, the tip sometimes grows oscillatorily as in FIGURE 5.3 (b). If the effect of anisotropy is too strong as in Figure 5.3 (d), a needle crystal is formed. Instability caused by discrete spectra (tip-splitting and Hopf bifurcation) and propagation instability (side-branching) caused by continuous spectra both appear in dendrite growth, and they interact to cause complex types of instability. Here lies the difficulty, as well as the excitement, in dealing with the problem of a dendritic crystal.

## 5.4. Singular Limit Eigenvalue Problem

We have shown that models described by partial differential equations are reduced, by passing to singular limits, to the geometric study of interface motion. In other words, information on the dynamics of a system is localized in restricted regions called interfaces. For example, in the mean curvature flow, the motion of an interface is solely determined by its curvature, a local geometric quantity.

It is, on the other hand, breathtaking to observe that actual dissipative systems can produce spectacularly varied patterns and dynamics. One reason why such varieties of patterns and dynamics emerge is that the speed of an interface not only depends on local geometric quantities such as curvature, but also interacts with the **spatially non-local field** generated by a control variable $v$. Models of Mullins-Sekerka type and those of Stefan type, obtained from the phase-field model, are examples of such a situation.

In this section, we discuss model systems of activator-inhibitor type in one-dimensional space, which allows us to understand the interaction in the simplest context. After describing briefly the singular limit system of the model, we discuss the stability and bifurcation of transition layer solutions of the original system of reaction-diffusion equations. In the study of spectral behaviors of the system in the singular limit, the **SLEP**-method (**S**ingular **L**imit **E**igenvalue **P**roblem) is very useful. This section is entirely based on [**281**], in which more detailed accounts can be found.

**5.4.1. One-dimensional Singular Limit of an Activator-Inhibitor System.** As described in §4.3.2, the condition $D_u < D_v$

is necessary for diffusion-driven instability to occur. As an extreme case of such situations, we consider the case in which $D_u = \epsilon^2 \ll 1$ and $D_v = O(1)$. In this case, we obtain a singularly perturbed system of an activator-inhibitor model:

$$\begin{cases} u_t = \epsilon^2 u_{xx} + f(u,v), & \\ & (x,t) \in I \times (0,\infty), \\ v_t = D_v v_{xx} + g(u,v), & \\ & \\ \dfrac{\partial u}{\partial x} = 0 = \dfrac{\partial v}{\partial x}, & (x,t) \in \partial I \times (0,\infty), \end{cases} \tag{5.112}$$

on a one-dimensional finite interval, say, $I = (0,1)$. Applying to this system the method of matched asymptotic expansion in §4.3.3, we obtain its singular limit system, which in the slow scale of time $s = \epsilon t$ is given by

$$\begin{cases} (\varphi_i)_s = (-1)^{i-1} c(V(\varphi_i(s))), \\ \\ DV_{xx} + G_{\Phi_n(s)}(V) = 0, \end{cases} \tag{5.113}$$

where each $\varphi_i(s)$ $(0 < \varphi_1(s) < \ldots < \varphi_n(s) < 1)$ denotes the position of the $i$-th transition layer at the instant $s$, and $\Phi_n(s) = (\varphi_1(s), \ldots, \varphi_n(s))$. The function $c(\cdot)$ is the wave speed function that appears in the velocity-curvature relation, and is determined by the value of $V$ (cf. PROPOSITION 4.31). The nonlinearity $G_{\Phi_n(s)}(V)$ assumes either $G_-(V)$ or $G_+(V)$ alternatively on successive subintervals $(\varphi_{i-1}(s), \varphi_i(s))$ $(i = 1, \ldots, n+1)$, and for definiteness, we agree that it is $G_-$ on the first subinterval $(0, \varphi_1(s))$.

We assume that $V$ is $C^1$-matched at each $x = \varphi_i(s)$ and satisfies the Neumann condition $V_x = 0$ on the boundary. Then note that $U$ is automatically determined by $V$ as $U = h_\pm(V)$. An intuitive picture of the dynamics is displayed in FIGURE 5.4. For the existence of time global solutions to (5.112) or its higher dimensional versions, we refer to [**178**], [**153**] and [**154**].

REMARK 5.15. Note that one cannot take the initial value $\Phi_n(0) = (\varphi_1(0), \ldots, \varphi_n(0))$ in an arbitrary manner. It has to be chosen so that the second equation of (5.113) has a $C^1$-matched solution $V(\cdot, s = 0)$ with the Neumann boundary conditions. Only on the set of such $\Phi_n(s)$ is the dynamics of (5.113) well-defined.

REMARK 5.16. It can often happen that two internal layers $\varphi_i$ and $\varphi_{i+1}$ collide and the phase in between disappears. Even at the

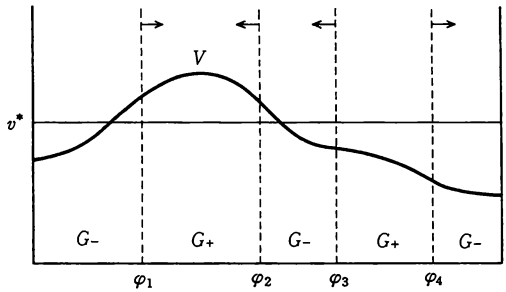


FIGURE 5.4. Interfaces driven by a non-local field $V$.

instant of disappearance, the function $V$ is $C^1$-matched, and hence continues to be well-defined. In this sense, the system (5.113) is such that the number of unknowns changes (decreases) in time. It is conjectured that solutions undergo such a **coarsening process** and eventually converge to equilibria.

PROPOSITION 5.17. *There exists a positive integer $N_0$ such that for any integer $n \geq N_0$, there is a unique equilibrium solution $\Phi_n^*$ of* (5.113) *with $n$-transition layers.*

REMARK 5.18. It is not necessarily true that $N_0 = 1$. Depending on the magnitude of $G_\pm(v)$ and the length $|I|$ of the interval, there exists no equilibrium solution with small $n$. If, for example, $|G_\pm(V)| \geq \delta > 0$ and $|I|$ is large, then $V$ cannot satisfy the boundary conditions because $V_{xx}$ changes faster than $\delta/D$. On the other hand, if both $G_-$ and $G_+$ are monotone decreasing and if there exist values $\overline{V}$ and $\underline{V}$ such that $G_-(\underline{V}) = 0 = G_+(\overline{V})$, then $N_0 = 1$ is realized.

The stability property of $\Phi_n^*$ plays an important role in the investigation of the asymptotic destiny of orbits (as $s \to \infty$).

PROPOSITION 5.19 (**Local Stability of $\Phi_n^*$**). *Each member of the family $\{\Phi_n^*\}_{n=N_0}^{\infty}$ is locally asymptotically stable.*

The last proposition says that the ultimate destiny of the system depends strongly on the initial conditions, and this in turn means that the system is capable of exhibiting many final states. How does the basin of attraction of the equilibrium solutions subdivide the space of initial values? This is a problem of global nature and should be investigated in the future.

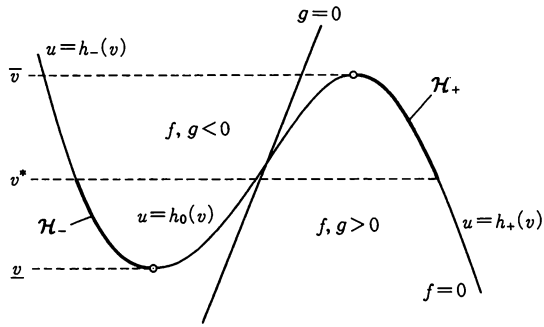


FIGURE 5.5. Shape of the nullcline of the nonlinearity $(f, g)$.

We will now show that the same result as above holds for the original reaction-diffusion system.

**5.4.2. Transition Layers in a Reaction-Diffusion System.** Let us deal with multiple-transition layer solutions of the activator-inhibitor system (5.112) on the finite interval $I = (0, 1)$.

As for the nonlinearity $(f, g)$, the FitzHugh-Nagumo type discussed in §4.3.3 is a typical example. In general, it suffices for our purpose to impose the following conditions on $(f, g)$.

(A.1) The nullcline of $f$, $\{(u, v) | f(u, v) = 0\}$, is of S-shape and consist of three smooth curves $u = h_-(v)$, $= h_0(v)$, $= h_+(v)$ defined respectively on $I_-, I_0, I_+$. Moreover, the inequalities $h_-(v) < h_0(v) < h_+(v)$ hold on $I^* = (\underline{v}, \overline{v})$, where $\underline{v} = \inf I_-$ and $\overline{v} = \sup I_+$ (cf. FIGURE 5.5).

(A.2) The nullcline of $g$ intersects that of $f$ transversally at either one point or three points. If an equilibrium point (the point of intersection of $f = 0$ and $g = 0$) lies on $u = h_-(v)$ (resp. on $u = h_+(v)$ or $u = h_0(v)$), then it is denoted by

$$P = (u_-, v_-) = (h_-(v_-), v_-)$$
$$(\text{resp. } Q = (u_+, v_+) = (h_+(v_+), v_+)$$
$$\text{or } R = (u_0, v_0) = (h_0(v_0), v_0)).$$

(A.3) Let $J(v)$ be defined by $J(v) = \int_{h_-(v)}^{h_+(v)} f(s, v) ds$. Then $J$ has an isolated zero at $v = v^*$ $(\underline{v} < v^* < \overline{v})$ such that $J'(v^*) < 0$.

(A.4) Let $\mathcal{H}_\pm$ be defined by

$$\mathcal{H}_- \equiv \{(u,v) \mid u = h_-(v),\ \ v_- < v < v^*\},$$
$$\mathcal{H}_+ \equiv \{(u,v) \mid u = h_+(v),\ \ v^* < v < v_+\},$$

with $v_-$ (resp. $v_+$) being replaced by $\underline{v}$ (resp. $\overline{v}$) if there is no equilibrium on $\mathcal{H}_-$ (resp. $\mathcal{H}_+$), cf. FIGURE 5.5. Then

$$f_u < 0 \qquad \text{on } \mathcal{H}_- \cup \mathcal{H}_+.$$

(A.5) $g|_{\mathcal{H}_-} < 0 < g|_{\mathcal{H}_+}$.

(A.6) The Jacobian satisfies

$$\det\left(\frac{\partial(f,g)}{\partial(u,v)}\right)\Big|_{\mathcal{H}_-\cup\mathcal{H}_+} > 0.$$

(A.7) $g_v|_{\mathcal{H}_-\cup\mathcal{H}_+} \le 0$.

When a spatially homogeneous equilibrium solution $\overline{U} = (\overline{u}, \overline{v})$ lies on $u = h_0(v)$, even if it is stable with respect to ODE, it can be destabilized with respect to PDE through the Turing-instability mechanism. Namely, if there is a certain difference between the diffusion rates of the activator $u$ and the inhibitor $v$ ($D_u < D_v$), a spatially inhomogeneous solution $\tilde{U}$ bifurcates and takes over $\overline{U}$. This is a good example of symmetry-breaking bifurcation.

Immediately after the bifurcation point, $\tilde{U}$ is very close to $\overline{U}$. As the bifurcation parameter deviates far from the bifurcation point, $\tilde{U}$ changes its shape substantially. If, for example, $D_u = \epsilon^2 \ll 1$, then that latter solution becomes a large-amplitude solution with internal transition layers appearing in the profile of the activator $u$.

The deformation process from the bifurcated solution to the singularly perturbed one as the parameter $D_u$ varies can be rigorously treated in the limit case where $D_v \to \infty$ (cf. [**280**]). The importance of internal layer solutions, however, is their existence under general conditions, regardless of whether the system is of Turing type or of excitable type. In fact, in the conditions on $(f,g)$ above, no reference is given as to how $\{f(u,v) = 0\}$ and $\{g(u,v) = 0\}$ should intersect. The important factors are the bistability contributed by $f$ and the existence of a variable $v$ that controls the motion of transition layers. The method for showing the existence of single-transition layer solutions is a typical example of obtaining solutions by matching two solutions of different spatial scales (cf. §1.2).

Let us now deal with the stationary problem by means of the method of matched asymptotic expansion. The problem is given by

$$\text{(5.114)} \qquad \begin{cases} \epsilon^2 u_{xx} + f(u,v) = 0, & \\ & x \in I, \\ \frac{1}{\sigma} v_{xx} + g(u,v) = 0, & \\ & \\ u_x = 0 = v_x, & x \in \partial I, \end{cases}$$

where $D_v$ is replaced by $D_v = 1/\sigma$ for the convenience of subsequent discussions. We also denote by $H^2_N(I)$ the subspace of $H^2(I)$ consisting of functions that satisfy the Neumann boundary conditions (which is the same as the $H^2(I)$-closure of the family of cosine functions).

**Outer Problem**

Setting formally $\epsilon = 0$ in (5.114), one obtains

$$\text{(5.115)} \qquad \begin{cases} f(u,v) = 0, & \\ & (u,v) \in L^2(I) \times H^2_N(I). \\ \frac{1}{\sigma} v_{xx} + g(u,v) = 0, & \end{cases}$$

The first equation is not a differential equation. There is freedom as to which branch one should choose. Here we use

$$\text{(5.116)} \qquad u = h^*(v) := \begin{cases} h_-(v), & v \le v^*, \\ h_+(v), & v \ge v^*, \end{cases}$$

in which $u = h_\pm(v)$ are two stable branches to which solutions of the ODE $\dot{u} = f(u,v)$ are attracted for fixed $v$. The reason why $v = v^*$ is chosen as the switching point is that it is the only value at which the lowest order inner problem (discussed later) will have a travelling wave solution with null-speed (note that we are dealing with equilibrium solutions). The function $u$ defined by (5.116) exhibits a discontinuity as $v$ passes $v^*$. Inserting (5.116) into the second equation of (5.115), one obtains

$$\text{(5.117)} \qquad \frac{1}{\sigma} v_{xx} + G^*(v) = 0, \cdot \qquad v \in H^2_N(I),$$

where $G^*(v) = g(h^*(v), v)$, which is a piecewise monotone decreasing function as depicted in FIGURE 5.6.

REMARK 5.20. Solutions of (5.117) are matched across $v = v^*$ in the $C^1$-sense, since $H^2_N(I) \subset C^1(I)$.

LEMMA 5.21. *There exists $\sigma_1^* > 0$ such that for $0 < \sigma < \sigma_1^*$ (5.117) has a unique monotone increasing solution $V^{*,\sigma}$.*

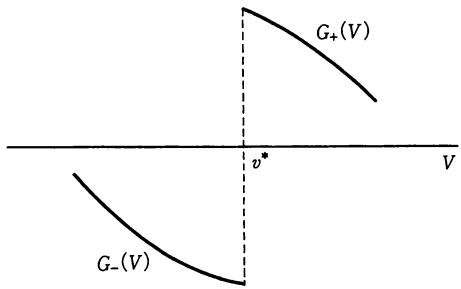


FIGURE 5.6. The graph of $G^*(V)$.

REMARK 5.22. There also exists a unique monotone decreasing solution. This solution, however, is obtained from the monotone increasing one by reflection. Therefore, we deal only with the monotone increasing one.

By means of (5.116), let us set $U^{*,\sigma}(x) = h^*(V^{*,\sigma}(x))$ to obtain an outer approximation

$$(U^{*,\sigma}(x), V^{*,\sigma}(x)). \tag{5.118}$$

The $C^1$-matching point $x_1^*(\sigma)$ for $V^{*,\sigma}$ (or the point of discontinuity for $U^{*,\sigma}$) is uniquely determined as a point $x^*$ at which $V^{*,\sigma}(x^*) = v^*$.

**Inner Problem**

Introducing a stretched variable $y = (x - x_1^*(\sigma))/\epsilon$ at $x = x_1^*$ and recasting the stationary problem (5.114) in terms of the stretched variable, one obtains in the limit as $\epsilon \to 0$ the following problem:

$$\begin{cases} \dfrac{d^2\tilde{u}}{dy^2} + f(\tilde{u}, v^*) = 0, \\ \\ \tilde{u}(\pm\infty) = h_\pm(v^*), \qquad \tilde{u}(0) = h_0(v^*). \end{cases} \tag{5.119}$$

We have already encountered this equation many times. Since $J(v^*) = 0$, this problem has a unique solution. Moreover, the limits of this solution at $\pm\infty$ agree with the left and right limits of the outer approximation at $x = x_1^*$. Combining these approximate solutions, a generalized implicit function theorem (cf. [**131**]) yields the following theorem ([**266**], [**190**]). The symbol $C_\epsilon^2(I)$ signifies the set of twice

continuously differentiable functions equipped with the norm

$$\|u\|_{C^2_\epsilon} = \sum_{k=0}^{2} \max_{x\in\overline{I}} \left| \left(\epsilon \frac{d}{dx}\right)^k u(x) \right|.$$

THEOREM 5.23 (Existence of a 1-transition layer solution). *For each $\sigma_0$ satisfying $0 < \sigma_0 < \sigma_1^*$, (5.114) has an $(\epsilon, \sigma)$-family of solutions*

$$D^1(\epsilon,\sigma) = \big(u^1(x;\epsilon,\sigma), v^1(x;\epsilon,\sigma)\big) \in C^2_\epsilon(\overline{I}) \times C^2(\overline{I})$$

*defined on $Q^1 = \{(\epsilon,\sigma) | 0 < \epsilon \le \epsilon_0,\ 0 \le \sigma \le \sigma_0\}$. $D^1(\epsilon,\sigma)$ is continuous and uniformly bounded on $Q^1$ with respect to the $C^2_\epsilon(\overline{I}) \times C^2(\overline{I})$-topology. Moreover, the following properties hold true:*

(i) $\lim_{\epsilon\to 0} u^1(x;\epsilon,\sigma) = U^{*,\sigma}(x)$ *uniformly on $\overline{I}\backslash I_\kappa$ for each $\kappa > 0$,*
(ii) $\lim_{\epsilon\to 0} v^1(x;\epsilon,\sigma) = V^{*,\sigma}(x)$ *uniformly on $\overline{I}$,*
(iii) $\lim_{\epsilon\to 0}(\tilde{u}^{\epsilon,\sigma}(y),\ \tilde{v}^{\epsilon,\sigma}(x)) = (\tilde{u}^*(y), v^*)$ *uniformly with respect to the $C(K)$-topology for any compact set $K \subset \mathbb{R}$.*

*In the above, $I_\kappa = (x_1^*(\sigma) - \kappa, x_1^*(\sigma) + \kappa)$ and*

$$\tilde{u}^{\epsilon,\sigma}(y) = u^1(x_1^*(\sigma) + \epsilon y;\epsilon,\sigma), \quad \tilde{v}^{\epsilon,\sigma}(y) = v^1(x_1^*(\sigma) + \epsilon y;\epsilon,\sigma).$$

$D^1(\epsilon,\sigma)$ is called a **normal 1-transition layer solution**. Using the following reflection principle, one can easily obtain $n$-transition layer solutions from $D^1(\epsilon,\sigma)$ in case of the Neumann boundary conditions.

PROPOSITION 5.24 (Reflection Principle). *Let $W(x;\underline{d})$ be a solution of (5.114) at $\underline{d} = (\tilde{\epsilon}^2, \tilde{\sigma}^{-1})$. Then, for each positive integer $n$, $R^n(W)(x)$, defined below, is a solution of (5.114) at $\frac{\underline{d}}{n^2} = (\epsilon^2, \sigma^{-1})$:*

$$R^n(W)(x) = \begin{cases} W(n(x - i/n);\underline{d}), & i \text{ even}, \\ W(n(1/n - (x-i)/n);\underline{d}), & i \text{ odd}, \end{cases}$$

(5.120)

$$\frac{i}{n} \le x \le \frac{i+1}{n} \quad (i = 0, 1, \dots, n-1).$$

Intuitively speaking, starting with a solution, the Neumann boundary conditions allow us to successively reflect it across the boundary to obtain a solution on a larger interval. In order to squeeze back to the original interval $I$, one simply needs to adjust the diffusion rate by multiplying by $1/n^2$. This is the content of the last proposition. Applying the reflection principle to $D^1(\epsilon,\sigma)$, we obtain the next corollary.

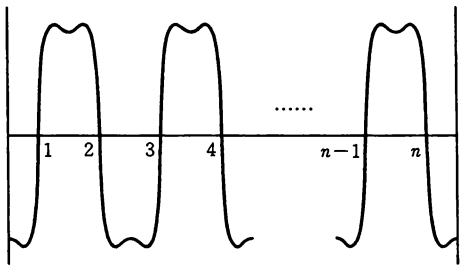


FIGURE 5.7. Normal $n$-layer solution.

COROLLARY 5.25 (Existence of normal $n$-transition layers). *The function* $D^n(\epsilon,\sigma) = (u^n(x;\epsilon,\sigma), v^n(x;\epsilon,\sigma))$ *defined by*

$$D^n(\epsilon,\sigma) = R^n(D^1(\tilde{\epsilon},\tilde{\sigma}))(x)$$

*is a solution of* (5.114) *with n internal transition layers, which exists for*

$$(\epsilon,\sigma) = (\tilde{\epsilon}/n, n^2\tilde{\sigma}) \in Q^n \equiv \{(\epsilon,\sigma) \mid 0 < \epsilon < \epsilon_0/n,\ \ 0 \le \sigma \le n^2\sigma_0\ \}.$$

$D^n(\epsilon,\sigma)$ *is called a* **normal $n$-transition layer solution** (FIGURE 5.7).

REMARK 5.26. We denote by $(U_n^{*,\sigma}(x), V_n^{*,\sigma}(x))$ the $L^2$-limit of $D^n(\epsilon,\sigma)$ as $\epsilon \to 0$, which is called the **reduced solution** of the normal $n$-transition layer solution. One can understand from the construction that $D^n(\epsilon,\sigma)$ consists of 1-transition layer solutions, each placed on subintervals $I_j$ $(j = 1,\dots,n)$ with width $1/n$.

**5.4.3. Singular Eigenvalues and Singular Eigenfunctions.** The linearized eigenvalue problem around the $n$-transition layer solution $D^n(\epsilon,\sigma)$ is given by

$$\mathcal{L}^\epsilon \begin{pmatrix} w \\ z \end{pmatrix} \equiv \begin{pmatrix} L^\epsilon & f_v^\epsilon \\ g_u^\epsilon & M^\epsilon \end{pmatrix} \begin{pmatrix} w \\ z \end{pmatrix} = \lambda \begin{pmatrix} w \\ z \end{pmatrix}, \tag{5.121}$$

$$(w,z) \in \left(H_N^2(I)\right)^2,$$

where

$$L^\epsilon \equiv \epsilon^2 \frac{d^2}{dx^2} + f_u^\epsilon, \tag{5.122}$$

$$M^\epsilon \equiv \frac{1}{\sigma}\frac{d^2}{dx^2} + g_v^\epsilon, \tag{5.123}$$

in which the partial derivatives are all evaluated at $D^n(\epsilon, \sigma)$, and $\lambda$ is the eigenvalue parameter.

Let us first outline our strategy to solve the eigenvalue problem (5.121). A difficulty common to singular eigenvalue problems associated with internal transition layers originates from the translational freedom of transition layers. The principal part of transition layer solutions is described by the front solution of the scalar bistable equation

$$\epsilon^2 u_{xx} - W'(u) = 0, \qquad x \in \mathbb{R}, \qquad u(\pm\infty) = \pm 1.$$

The linearization of the latter equation around the front solution has the 0-eigenvalue, with the associated eigenspace being spanned by its spatial derivative $u_x$. Since $u_x$ decays exponentially fast at $\pm\infty$, when it is rescaled and placed on a finite interval, it decays exponentially to 0 outside the transition layer region, and hence still serves as a 0-eigenfunction with exponentially small errors being neglected. The very slow motion discussed in §1.3 actually originates from such a situation.

When there are several transition layers, since these layers are considered as moving independently, it is expected that the number of eigenvalues close to 0 is the same as the number of transition layers. The eigenspace generated by the eigenfunctions corresponding to near-zero eigenvalues will control the motion of the pattern. Let us call eigenvalues that approach zero as $\epsilon \to 0$ **singular eigenvalues** (cf. REMARK 5.42 for those that cross the imaginary axis). From the reasoning above, one can expect that there are $n$ singular eigenvalues for $D^n(\epsilon, \sigma)$, which has $n$ transition layers. Transition layer solutions for scalar equations are all unstable (THEOREM 4.12). This is because the potential $W$ is the only driving force of motion of transition layers. When a control parameter $v$ is added to our system, the shape of the spatial distribution of $v$ controls the motion of transition layers and often stabilizes the pattern. Transition layers, appearing in the $u$-component, are moving around on the spatially controlled field generated by $v$, so to speak. Due to the interaction between two quantities with different scales, the dynamics is tuned in a subtle manner, making it difficult, as well as interesting, to deal with two-component systems.

We can divide the spectral analysis via the SLEP-method for $n$-transition layers into two steps:

(i) Contribution from the potential $W$.

(ii) Interaction with the control field generated by $v$.

Step (i) is essentially reduced to the analysis of the Sturm-Liouville problem for the equation associated with $u$. Exactly $n$ small (close to zero) eigenvalues are extracted in the analysis. In step (ii), the results obtained in (i) are substituted into the equation for $v$. It is here that difficulties due to the difference in spatial scales appear. According to the scale for $v$, the singular eigenfunctions obtained in (i) do not fit into the frame of ordinary functions as $\epsilon \to 0$. The essence of the SLEP-method lies in **characterizing the information possessed by singular eigenfunctions as distributions supported on the location of transition layers and incorporating them into the equation of the control field** $v$. Through such a process, the eigenvalue problem is reduced to a problem defined on the location of transition layers. In the one-space-dimensional case, the latter is an eigenvalue problem for a symmetric matrix. The basic of such an idea was first developed in [**282**] and [**281**], and was later applied to several problems ([**283**], [**284**], [**341**], etc).

Let us begin with the Sturm-Liouville problem:

$$\begin{cases} L^\epsilon \phi = \zeta \phi, & x \in I, \\ \\ \phi \in H_N^2(I), & \|\phi\|_{L^2(I)} = 1. \end{cases} \tag{5.124}$$

This is a self-adjoint problem, and hence the eigenvalues $\zeta$ are all real. We denote by $\{\zeta_i^\epsilon, \phi_i^\epsilon\}_{i=0}^\infty$ a complete orthonormal system of eigenpairs. How do the eigenvalues behave as $\epsilon$ changes? The following proposition says that we need to pay attention only to the first $n$ eigenvalues.

PROPOSITION 5.27. *The first $n$ eigenvalues $\{\zeta_i^\epsilon\}_{i=0}^{n-1}$ go to zero as $\epsilon$ tends to zero. The remaining eigenvalues are all negative and bounded uniformly away from zero.*

For the details of the proof, we refer to [**281**]. Let us consider the Dirichlet eigenvalue problem on a subinterval of length $1/n$ which contains only one transition layer. By applying comparison theorems, one can show that the largest eigenvalue of the Dirichlet problem separates $n$ singular eigenvalues from non-singular ones. The Dirichlet eigenfunction associated with the largest eigenvalue can be extended as an odd function onto the entire interval $I$. The extended function has $n - 1$ zeros in $I$. Therefore, the smallest singular eigenvalue

associated with the Neumann boundary conditions must have the same number of zeros.

One can show that on each subinterval of length $1/n$ the singular eigenfunctions $\{\phi_i^\epsilon\}_{i=0}^{n-1}$ are proportional to a scaled version of the derivative of the front solution for the scalar bistable equation. To be more precise, let us introduce some symbols:

$$\begin{aligned} &\phi_{ij}^\epsilon = \phi_i^\epsilon|_{I_j}; \text{ the restriction of the } i\text{-th eigenfunction} \\ &\qquad\qquad \text{to the } j\text{-th subinterval } I_j, \\ &\tilde{\phi}_{ij}^\epsilon = \tilde{\phi}_{ij}^\epsilon(y) \equiv \phi_{ij}^\epsilon(x_j^* + \epsilon y); \text{ representation of } \phi_{ij}^\epsilon \\ &\qquad\qquad \text{in terms of the stretched variable for } y \in \tilde{I}_j. \end{aligned} \tag{5.125}$$

They satisfy

$$\int_I |\phi_i^\epsilon|^2 dx = \sum_{j=1}^n \int_{I_j} |\phi_{ij}^\epsilon|^2 dx = \sum_{j=1}^n \int_{\tilde{I}_j} |\sqrt{\epsilon}\tilde{\phi}_{ij}^\epsilon|^2 dy.$$

In accordance with the last line above, we also define $\hat{\phi}_{ij}^\epsilon$ by

$$\hat{\phi}_{ij}^\epsilon \equiv \sqrt{\epsilon}\tilde{\phi}_{ij}^\epsilon \quad (y \in \tilde{I}_j).$$

Clearly,

$$\int_I |\phi_i^\epsilon|^2 dx = \sum_{j=1}^n \int_{\tilde{I}_j} |\hat{\phi}_{ij}^\epsilon|^2 dy.$$

We also denote by $\hat{\phi}_0^*$ and $\hat{\phi}_L^*$, respectively, the $L^2$-normalized and $L^1$-normalized versions of the principal eigenfunction of

$$\frac{d^2}{dy^2}\tilde{\phi} + f_u(\tilde{u}^*, v^*)\tilde{\phi} = \zeta\tilde{\phi},$$

namely

$$\|\hat{\phi}_0^*\|_{L^2(\mathbb{R})} = 1, \qquad \int_{\mathbb{R}} \hat{\phi}_L^* dy = 1.$$

These functions are related to the spatial derivative $\frac{d}{dy}\tilde{u}^*$ of the front solution as follows:

$$\hat{\phi}_0^* = \frac{\gamma^*}{c^*}\frac{d}{dy}\tilde{u}^*, \qquad \hat{\phi}_L^* = \gamma^*\frac{d}{dy}\tilde{u}^*, \tag{5.126}$$

where

$$c^* = \|\hat{\phi}_L^*\|_{L^2(\mathbb{R})}, \qquad \gamma^* = \frac{1}{h_+(v^*) - h_-(v^*)}. \tag{5.127}$$

Functions defined on stretched intervals $\tilde{I}_j$ are understood as being smoothly extended onto $\mathbb{R}$ by setting them equal to zero near $\pm\infty$.

LEMMA 5.28 (Precompactness of $\hat{\phi}_{ij}^{\epsilon}$). *There is a subsequence* $\hat{\phi}_{ij}^{\epsilon_m}$ *of* $\hat{\phi}_{ij}^{\epsilon}$, *with* $\lim_{m\to\infty}\epsilon_m = 0$, *such that*

$$\lim_{m\to\infty} \hat{\phi}_{ij}^{\epsilon_m} = \kappa_j^i \hat{\phi}_L^* \qquad \text{in } C^2(\mathbb{R}) \tag{5.128}$$

*uniformly for each pair* $(i,j)$ $(0 \le i \le n-1,\ 1 \le j \le n)$. *Moreover, the vectors* $\{c^*\mathbf{k}^i\}_{i=0}^{n-1}$, *in which* $\mathbf{k}^i$ *for each* $i$ *is defined by*

$$c^*\mathbf{k}^i = (\kappa_1^i, \dots, \kappa_n^i), \tag{5.129}$$

*constitute a orthonormal basis of* $\mathbb{R}^n$.

With these preparations at our disposal, we can now describe the behavior of $\zeta_i^{\epsilon}$ as $\epsilon \to 0$.

PROPOSITION 5.29 (Behavior of Singular Eigenvalues). *Denote by* $\{\zeta_i^{\epsilon}, \phi_i^{\epsilon}\}$ *the orthonormal eigenpairs of* (5.124) *under the Neumann boundary conditions. The first* $n$ *eigenvalues* $\zeta_0^{\epsilon} > \dots > \zeta_{n-1}^{\epsilon}$ *are positive and singular, satisfying the asymptotic relations*

$$\zeta_i^{\epsilon} = \hat{\zeta}_i(\epsilon,\sigma)\epsilon\sigma + e_i(\epsilon,\sigma). \tag{5.130}$$

*The functions* $\hat{\zeta}_i$ *and* $e_i$ $(i = 0, \dots, n-1)$ *are positive continuous functions defined on* $Q^n$ (*cf.* COROLLARY 5.25) *and satisfy the following:*

$$\begin{aligned} \hat{\zeta}^* &= \lim_{\epsilon\to 0} \hat{\zeta}_i(\epsilon,\sigma) \\ &= \frac{1}{n}\left(\frac{\gamma^*}{c^*}\right)^2 J'(v^*) \int_0^{x_1^*(\frac{\sigma}{n^2})} g(U^{*,\sigma/n^2}, V^{*,\sigma/n^2})dx > 0, \\ |e_i(\epsilon,\sigma)| &\le C\exp\left(-\frac{\gamma}{\epsilon}\right). \end{aligned} \tag{5.131}$$

*The remaining eigenvalues* $\zeta_i^{\epsilon}$ $(i \ge n)$ *are all negative and bounded away from zero uniformly in* $\epsilon > 0$. *Note also that the limit* $\hat{\zeta}^*$ *in* (5.131) *does not depend on* $i$.

**5.4.4. SLEP-Method.** The foremost difficulty in solving the eigenvalue problem (5.121) for $\mathcal{L}^{\epsilon}$ is that two different spatial scales coexist in $\mathcal{L}^{\epsilon}$. The coexistence is due to the fact that the normal $n$-transition layer solution has two spatial scales, coming from the outer and inner problems. In other words, the difficulty lies in how we can obtain the singular limit of $\mathcal{L}^{\epsilon}$ without losing two pieces of information coming from the two problems. Basically, we need to

prove the existence of $n$ singular eigenvalues (in the same manner as for $L^\epsilon$) and to study their asymptotic (as $\epsilon \to 0$) behavior.

The rescaled version of the singular eigenfunctions of $L^\epsilon$ that appeared in the previous subsection allows us to characterize the information contributed by the inner problem as distributions supported on the location of the transition layers. Thanks to such a characterization, one can finally reduce the problem (5.121) to an eigenvalue problem for a real $n \times n$ symmetric matrix. The solution of the latter problem determines the asymptotic behavior of singular eigenvalues of $\mathcal{L}^\epsilon$.

Let us start by separating the problem into singular and nonsingular parts.

Solving the first equation in (5.121) for $w$, we have

$$w = (L^\epsilon - \lambda)^{-1}(-f_v^\epsilon z). \tag{5.132}$$

This equation is meaningless if $\lambda$ coincides with one of the eigenvalues of $L^\epsilon$. However, since one can prove that eigenvalues of $\mathcal{L}^\epsilon$ belonging to the set $\Lambda_1 \equiv \{\lambda | \mathrm{Re}\lambda > -\mu\}$ (for some $\mu > 0$) do not coincide with those of $L^\epsilon$, (5.132) is meaningful. Applying the eigenfunction expansion to (5.132) and substituting the result into the second equation of (5.121), one obtains

$$\frac{1}{\sigma}\frac{d^2}{dx^2}z + \sum_{i=0}^{n-1} \frac{\langle -f_v^\epsilon z,\ \phi_i^\epsilon \rangle}{\zeta_i^\epsilon - \lambda} g_u^\epsilon \phi_i^\epsilon + g_u^\epsilon (L^\epsilon - \lambda)^\dagger (-f_v^\epsilon z) + g_v^\epsilon z = \lambda z, \tag{5.133}$$

where $(L^\epsilon - \lambda)^\dagger$ is a generalized resolvent operator defined by

$$(L^\epsilon - \lambda)^\dagger(\cdot) \equiv \sum_{i \geq n} \frac{\langle \cdot, \phi_i^\epsilon \rangle}{\zeta_i^\epsilon - \lambda} \phi_i^\epsilon, \tag{5.134}$$

$$(L^\epsilon - \lambda)^\dagger : L^2(I) \to L^2(I) \cap \{\phi_0^\epsilon, \ldots, \phi_{n-1}^\epsilon\}^\perp.$$

We have thus separated the part of singular eigenfunctions from the rest. (5.134) corresponds to the resolvent coming from the outer problem, omitting the contribution from the transition layer part. Its limit is characterized as follows.

PROPOSITION 5.30 (Asymptotic Limit of $(L^\epsilon - \lambda)^\dagger$). *The resolvent operator $(L^\epsilon - \lambda)^\dagger$ is bounded in $L^2$ uniformly in $\epsilon$ and converges*

*to a multiplication operator:*

(5.135)

$$\lim_{\epsilon\to 0}(L^\epsilon-\lambda)^\dagger(F^\epsilon h)=\frac{F^* h}{f_u^*-\lambda},\quad h\in L^2(I)\cap L^\infty(I),\quad \lambda\in\Lambda_1,$$

*where $F(u,v)$ is a smooth function and*

$$F^\epsilon\equiv F(D^n(\epsilon,\sigma)),\quad F^*\equiv F(U_n^{*,\sigma},V_n^{*,\sigma}).$$

*The convergence is in the strong $L^2$-sense, and if $h\in H^1(I)$, then the convergence is uniform on any bounded subset of $H^1(I)$.*

This proposition says that if the singular part is separated out, then the second derivative term $\epsilon^2\frac{d^2}{dx^2}$ in $L^\epsilon$ is negligible in the limit as $\epsilon\to 0$.

The eigenvalue problem for $\mathcal{L}^\epsilon$ is also expected to have the same number $n$ of singular eigenvalues as the number of transition layers, in a way similar to that for $L^\epsilon$. Since $L^\epsilon$ is self-adjoint, only real eigenvalues appear, and the comparison theorem enables us to rigorously prove the existence of exactly $n$ real singular eigenvalues and to explicitly characterize their asymptotic behaviors. Care must be exercised to treat $\mathcal{L}^\epsilon$, since complex eigenvalues may occur for some values of the time constant (cf. REMARK 5.42). One can show for (5.121) that the spectrum is bounded away from the imaginary axis, except for singular eigenvalues approaching the origin.

LEMMA 5.31. *There exists a constant $\delta>0$ such that eigenvalues $\lambda\in\mathbb{C}$ of $\mathcal{L}^\epsilon$ that satisfy $\lambda\notin B_\delta$ ($B_\delta$ is the closed disk of radius $\delta$ with center at the origin in the complex plane) must be such that*

$$\text{Re}\,\lambda<-\mu^*,\qquad 0<\epsilon<\epsilon_0,\tag{5.136}$$

*where $\mu^*$ is independent of $\delta$ and $\epsilon$.*

Thanks to the lemma, we can from now on concentrate only on singular eigenvalues $\lambda=\lambda(\epsilon)\in B_\delta$, $\lim_{\epsilon\to 0}\lambda(\epsilon)=0$. We can also assume that these eigenvalues are real (one can prove this fact). Under this situation, the denominators in the second term on the right hand side of (5.133) go to zero as $\epsilon\to 0$. The corresponding numerators can also be shown to go to zero. Therefore, in order to deal with these singular terms, we need to employ appropriate rescaling to obtain an asymptotic characterization. The terms in (5.133), other than these singular ones, constitute a nicely behaving operator in the following sense.

PROPOSITION 5.32 (Bounded operator $K^{\epsilon,\lambda}$). *Let $B^{\epsilon,\lambda}$ be a bilinear form on $H^1(I)$ defined by*

$$B^{\epsilon,\lambda}(z^1,z^2)=\frac{1}{\sigma}\langle z_x^1,z_x^2\rangle - \langle\{g_u^\epsilon(L^\epsilon-\lambda)^\dagger(-f_v^\epsilon)+g_v^\epsilon-\lambda\}z^1,z^2\rangle, \quad z^1,\ z^2\in H^1(I),\quad \lambda\in B_\delta. \tag{5.137}$$

*For sufficiently small $\epsilon\geq 0$ (including $\epsilon=0$), the equation*

$$B^{\epsilon,\lambda}(z,\psi)=\langle h,\psi\rangle \qquad \forall\psi\in H^1(I) \tag{5.138}$$

*has a unique solution $z=z(h)$ for each $h\in H^{-1}(I)$. If we denote the inverse operator by $K^{\epsilon,\lambda}$,*

$$K^{\epsilon,\lambda}h=z(h):H^{-1}(I)\to H^1(I), \tag{5.139}$$

*then it is continuous in $\epsilon$ and analytic in $\lambda$ in the sense of the operator norm.*

REMARK 5.33. If we define an operator $K^*$ by $K^*=\lim_{\epsilon\to 0}K^{\epsilon,\lambda}$, it is the inverse operator corresponding to a bilinear form $B^*$ defined by

$$B^*(z^1,z^2)=\frac{1}{\sigma}\langle z^1,z^2\rangle-\left\langle\frac{\det^*}{f_v^*}z^1,z^2\right\rangle, \tag{5.140}$$

where $\det^*=f_u^*g_v^*-f_v^*g_u^*$.

Letting $K^{\epsilon,\lambda}$ operate on both sides of (5.133), one obtains

$$z=\sum_{i=0}^{n-1}\frac{\langle -f_v^\epsilon z,\phi_i^\epsilon\rangle}{\zeta_i^\epsilon-\lambda}K^{\epsilon,\lambda}(g_u^\epsilon\phi_i^\epsilon), \tag{5.141}$$

which shows that $z$ can be expressed as a linear combination of the $K^{\epsilon,\lambda}(g_u^\epsilon\phi_i^\epsilon)$ $(i=0,\dots,n-1)$;

$$z=\sum_{i=0}^{n-1}\alpha_iK^{\epsilon,\lambda}(g_u^\epsilon\phi_i^\epsilon),$$

where $\mathbf{A}=(\alpha_0,\dots,\alpha_{n-1})$ is a real $n$-vector. Since the system $\{\phi_i^\epsilon\}_{i=0}^{n-1}$ is linearly independent, so is $\{K^{\epsilon,\lambda}\ (g_u^\epsilon\phi_i^\epsilon)\}_{i=0}^{n-1}$. When we

substitute the linear combination into (5.141), our problem now reduces to solving the following $n$-dimensional eigenvalue problem:

$$M^\epsilon \mathbf{A} = \begin{pmatrix} (\zeta_0^\epsilon - \lambda)\alpha_0 \\ \vdots \\ (\zeta_{n-1}^\epsilon - \lambda)\alpha_{n-1} \end{pmatrix}, \tag{5.142}$$

where $M^\epsilon = \{\langle -f_v^\epsilon \phi_i^\epsilon,\ K^{\epsilon,\lambda}(g_u^\epsilon \phi_j^\epsilon)\rangle\}_{i,j}$. Note that $M^\epsilon$ also depends on $\lambda$ through the operator $K^{\epsilon,\lambda}$. On the right hand side of (5.142), entries are multiplied by different coefficients which also go to zero as $\epsilon \to 0$. Therefore, (5.142), as it stands, is degenerate and may not be solved. This difficulty is resolved by the following characterization of rescaled singular eigenfunctions.

PROPOSITION 5.34 (Asymptotic limit of singular eigenfunction). *Let $\{\phi_i^{\epsilon_m}\}$ be an arbitrary subsequence as in* PROPOSITION 5.28. *The following identities are valid in the $H^{-1}(I)$-sense:*

$$\lim_{m\to\infty} -f_v^{\epsilon_m} \frac{\phi_i^{\epsilon_m}}{\sqrt{\epsilon_m}} = c_1^* \Delta_i \equiv c_1^* \sum_{j=1}^n \kappa_j^i \delta(x - x_j^*(\sigma)), \tag{5.143}$$

$$\lim_{m\to\infty} g_u^{\epsilon_m} \frac{\phi_i^{\epsilon_m}}{\sqrt{\epsilon_m}} = c_2^* \Delta_i \equiv c_2^* \sum_{j=1}^n \kappa_j^i \delta(x - x_j^*(\sigma)), \tag{5.144}$$

*where*

$$c_1^* = -\gamma^* J'(v^*), \qquad c_2^* = \gamma^* \Big( g(h_+(v^*), v^*) - g(h_-(v^*), v^*) \Big),$$

*and $\delta(x - x_j^*(\sigma))$ is the Dirac delta function with support at $x = x_j^*(\sigma)$.*

Let us apply the latter results to $M^\epsilon$. In the sequel, we denote the subsequence $\epsilon_m$ simply by $\epsilon$. We divide both sides of (5.142) by $\epsilon$. On the left hand side, we have

$$\frac{1}{\epsilon} M^\epsilon = \left\{ \left\langle -f_v^\epsilon \frac{\phi_i^\epsilon}{\sqrt{\epsilon}},\ K^{\epsilon,\lambda}\left( g_u^\epsilon \frac{\phi_j^\epsilon}{\sqrt{\epsilon}} \right) \right\rangle \right\}_{i,j},$$

and hence PROPOSITIONS 5.29, 5.34, and REMARK 5.33 give rise to the following limit equation (as $\epsilon \to 0$):

$$\hat{M}^* \mathbf{A} = (\sigma \hat{\zeta}^* - \tau^*)\mathbf{A}, \tag{5.145}$$

where

$$\hat{M}^* \equiv \lim_{\epsilon\to 0} \frac{M^\epsilon}{\epsilon} = c_1^* c_2^* \left\{ \left\langle \Delta_i, K^* \Delta_j \right\rangle \right\}_{i,j=0}^{n-1}, \qquad \tau^* \equiv \lim_{\epsilon\to 0} \frac{\lambda(\epsilon)}{\epsilon}.$$

To obtain the last limit, we used the fact that singular eigenvalues are of order $O(\epsilon)$, that is to say, the next result holds true.

LEMMA 5.35 (Order of singular eigenvalues). *The singular eigenvalues are expressed in the form*

$$\lambda = \epsilon\tau(\epsilon, \sigma), \tag{5.146}$$

*where $\tau$ is a bounded function, continuous up to $\epsilon = 0$.*

Note that although $M^\epsilon$ for $\epsilon > 0$ is not symmetric, the limit $\hat{M}^*$ is a symmetric matrix.

We have thus reduced our problem to the $n$-dimensional eigenvalue problem (5.145), called the SLEP-system. The matrix $\hat{M}^*$ depends on $\Delta_i$, and in turn $\Delta_i$, as it stands, may depend on the choice of the subsequence $\epsilon_m$, causing a difficulty.

We can resolve the difficulty by the following arguments, in which the matrix is deformed by coordinate change into a universal form independent of the choice of the subsequences. For this purpose, let us introduce the Green's function $G_N$ associated with $K^*$, described in REMARK 5.33, by

$$K^*\phi(x) = \langle G_N(x, \cdot), \phi\rangle \qquad \forall \phi \in H^{-1}(I). \tag{5.147}$$

The subscript $N$ signifies the Neumann boundary conditions. Let us then define a symmetric matrix $\mathbf{G}_N$ by

$$\mathbf{G}_N \equiv \{G_N(x_i^*(\sigma), x_j^*(\sigma))\}_{i,j=1}^n. \tag{5.148}$$

In terms of this matrix, we have

$$\langle \Delta_i, K^*\Delta_j\rangle = {}^t\mathbf{k}^i \mathbf{G}_N \mathbf{k}^j,$$

and hence $\hat{M}^*$ can be written as in the next lemma.

LEMMA 5.36 (Standard SLEP-Matrix). *Via an orthogonal transformation, the matrix $\hat{M}^*$ is similar to the symmetric matrix $\mathbf{G}_N$ determined by the Green's function of $K^*$:*

$$\hat{M}^* = {}^tP\hat{\mathbf{G}}_N P,$$

*where $P \equiv c^*(\mathbf{k}^0, \mathbf{k}^1, \ldots, \mathbf{k}^{n-1})$ (cf. LEMMA 5.28) and $\hat{\mathbf{G}}_N$ is given by*

$$\hat{\mathbf{G}}_N \equiv \frac{c_1^* c_2^*}{(c^*)^2}\mathbf{G}_N. \tag{5.149}$$

*The coefficients that appear above are defined in* (5.127), (5.143) *and* (5.144).

REMARK 5.37. The information contributed by the transition layers is concentrated on their position $\{x_i^*(\sigma)\}_{i=1}^n$ and on the coefficients $c^*$, $c_1^*$ and $c_2^*$.

Thus our problem has been reduced to

$$\hat{\mathbf{G}}_N \mathbf{A} = (\sigma\hat{\zeta}^* - \tau^*)\mathbf{A} \qquad \text{(standard SLEP-system)}. \tag{5.150}$$

A key to solving the standard SLEP-system is to investigate not $\hat{\mathbf{G}}_N$ itself but its inverse $\hat{\mathbf{G}}_N^{-1}$. We have the next result.

LEMMA 5.38 (Tri-diagonally of $\hat{\mathbf{G}}_N^{-1}$). *The matrix $\hat{\mathbf{G}}_N^{-1}$ is real, symmetric, and tri-diagonal. It has n distinct positive eigenvalues:*

$$0 < \gamma_0^{-1} < \gamma_1^{-1} < \ldots < \gamma_{n-1}^{-1}. \tag{5.151}$$

Since we are interested in the values of $\tau$, the latter lemma translates into the existence of $n$ distinct eigenvalues

$$\tau_i^* = \sigma\hat{\zeta}^* - \gamma_i \qquad (\tau_0^* < \tau_1^* < \ldots < \tau_{n-1}^*).$$

However, we still do not know the sign of $\tau_i^*$. In determining the sign, a key role is played by comparing our problem with an eigenvalue problem under the Dirichlet boundary conditions.

In fact, considering $\mathcal{L}^\epsilon$ under the Dirichlet boundary conditions, one can easily verify that the spatial derivative of the normal $n$-transition layer solution is an eigenfunction associated with the 0-eigenvalue. This is reflected in the singular limit as the existence of a solution $\tau^* = 0$ in the problem $\hat{\mathbf{G}}_D\mathbf{B} = (\sigma\hat{\zeta}^* - \tau^*)\mathbf{B}$. Comparing the eigenvalues of $\hat{\mathbf{G}}_N$ and those of $\hat{\mathbf{G}}_D$, one can conclude that $\tau_{n-1}^* < 0$.

THEOREM 5.39 (Eigenvalue of the standard SLEP-system). *The standard SLEP-system* (5.150) *has n real distinct solutions $\tau_i^*$ $(i = 0, \ldots, n-1)$:*

$$\tau_0^* < \tau_1^* < \ldots < \tau_{n-1}^* < 0. \tag{5.152}$$

Thanks to the implicit function theorem, we are now ready to state the following conclusion on the singular eigenvalues of $\mathcal{L}^\epsilon$.

THEOREM 5.40. *There exists $\hat{\epsilon} > 0$ such that for $0 < \epsilon < \hat{\epsilon}$ the operator $\mathcal{L}^\epsilon$ has n distinct real eigenvalues $\lambda_k^\epsilon(\epsilon)$ $(k = 0, \ldots, n-1)$. These eigenvalues are simple and continuous in $\epsilon$ and behave asymptotically (as $\epsilon \to 0$) as*

$$\lambda_k^\epsilon(\epsilon) \simeq \tau_k^*\epsilon \qquad k = 0, \ldots, n-1. \tag{5.153}$$

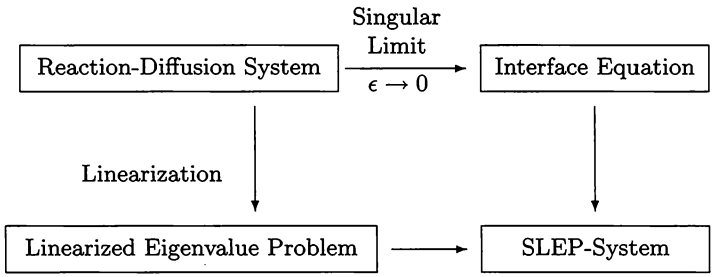


FIGURE 5.8. Relationship between the reaction-diffusion system and the SLEP-system.

*The corresponding singular eigenfunctions* $\Phi^k(\epsilon) = {}^t(w^k(\epsilon), z^k(\epsilon))$ *are asymptotically characterized as follows:*

(5.154)

$$\lim_{\epsilon\to 0} \Phi^k(\epsilon) = \Phi^k_* = \begin{pmatrix} w^k_* \\ \\ z^k_* \end{pmatrix} \equiv \begin{pmatrix} \displaystyle\sum_{j=1}^n q^k_j \delta_{x_j} - \frac{f^*_v}{f^*_u} c^*_2 \sum_{j=1}^n q^k_j K^* \delta_{x_j} \\ \\ \displaystyle c^*_2 \sum_{j=1}^n q^k_j K^* \delta_{x_j} \end{pmatrix},$$

*where* $\mathbf{q}^k = (q^k_1, \ldots, q^k_n)$ *with* $\|\mathbf{q}^k\| = 1$ *is an eigenvector of* $\hat{\mathbf{G}}_N$ *associated with* $\gamma_k$, *and* $\delta_{x_j}$ *is the Dirac delta function supported at* $x = x^*_j(\sigma)$.

Combining the theorems above with the consideration on the singular limit system given in §5.4.1, we obtain a commutative diagram (FIGURE 5.8).

REMARK 5.41. From PROPOSITION 5.31 and the estimate $\tau^*_{n-1} < 0$, it follows that the normal $n$-transition layer solution is (locally) **asymptotically stable**.

REMARK 5.42. In the reaction-diffusion system (5.112), if, in addition to the difference in diffusion rates, there is a substantial difference in the time constants of reaction, then the normal $n$-transition

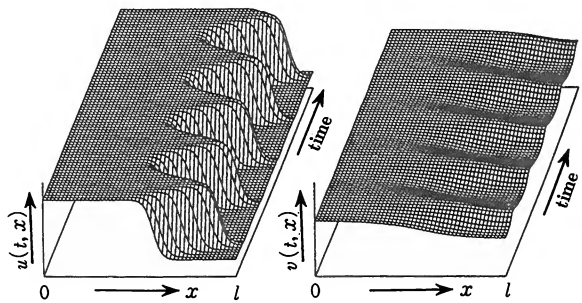


FIGURE 5.9. Breathing Solution: A numerical simulation on (5.155) with the nonlinear terms given by $f(u,v) = u(1-u^2) - v$, $g(u,v) = u + d - 8v$, at the parameter values $\epsilon = 0.05$, $d = -0.1$, $l = \pi/2$, $\sigma = 1$, $\tau = 0.04$.

layer solution can in general destabilize. In fact, let us consider the following system (with $\epsilon\tau$ multiplying $u_t$):

$$\text{(5.155)} \qquad \begin{cases} \epsilon\tau u_t = \epsilon^2 u_{xx} + f(u,v), \\ v_t = \frac{1}{\sigma} v_{xx} + g(u,v), \\ u_x = v_x = 0 \qquad \text{on } \partial I. \end{cases}$$

For this system, one can rigorously show by means of SLEP analysis that Hopf bifurcations occur as the parameter $\tau > 0$ gets small (cf. [**283**], [**186**]). In place of the destabilized equilibrium solution, time-periodic **breathing patterns** emerge after the Hopf bifurcation as in FIGURE 5.9. However, the analysis of Hopf bifurcation for the normal $n$-transition layer solution has not been thoroughly investigated yet.

REMARK 5.43. When the space dimension is equal to one, we can apply dynamical system theory to solve the problem of existence and stability of fronts and pulses on the infinite line. See, for instance, [**278**] and [**322**] in this direction.

## 5.5. Balanced Scaling in Singular Limit

As discussed in CHAPTER 4, the inequality $D_u < D_v$ is necessary for the Turing instability to occur. A special case of such a situation is realized by $D_u = \epsilon^2$ with $\epsilon$ small. As we have seen in the

previous section, singular perturbation techniques work very well in one-dimensional space in this case, allowing us to show the existence of normal $n$-transition layer solutions and to rigorously discuss their stability.

In high-dimensional spaces, the equilibrium problem is given by

$$\text{(5.156)} \qquad \begin{cases} \epsilon^2 \Delta u + f(u,v) = 0, & \\ & \text{in } \Omega, \\ \Delta v + g(u,v) = 0, & \\ \\ \frac{\partial u}{\partial n} = \frac{\partial u}{\partial n} = 0, & \text{on } \partial\Omega, \end{cases}$$

where $\Omega$ is a smooth domain in $\mathbb{R}^N$. As opposed to the one-dimensional case, however, the resolution of (5.156) is not so easy. The first difficulty lies in solving a reduced equation for (5.156), a counterpart of (5.117). Solutions of the reduced equation give a *seed* on which singular perturbation techniques are based. This difficulty does not arise for problems of boundary layer type, in which the interface is known a priori.

The reduced equation is given by a free-boundary problem (5.157) below, which is obtained formally from (5.156) by setting $\epsilon = 0$. The first equation of (5.156) (with $\epsilon = 0$) can be solved as $u = h_\pm(v)$ ($x \in \Omega^\pm$). The boundary between $\Omega^-$ and $\Omega^+$ defines the interface $\Gamma$. The determination of $\Gamma$ is a part of our problem. For simplicity, let us assume that $\Omega^+$ is strictly contained in $\Omega$ (or more precisely, $\Gamma = \partial\Omega^+$), and, denoting $G_\pm(v) \equiv g(h_\pm(v), v)$, the reduced problem asks us to find $V_\pm$ and $\Gamma$ that simultaneously satisfy

$$\text{(5.157)} \qquad \begin{cases} \Delta V_\pm + G_\pm(V_\pm) = 0, & x \in \Omega^\pm, \\ \\ \dfrac{\partial V_-}{\partial n} = 0, & x \in \partial\Omega, \\ \\ V_\pm = v^* & \text{on } \Gamma, \\ \\ V_- \text{ and } V_+ \text{ are } C^1\text{-matched on the interface } \Gamma. \end{cases}$$

Unfortunately, for the moment, there is no general result known for the solutions of (5.157), except for special cases, such as planar and radially symmetric solutions. On the other hand, even if we can find a solution $\Gamma$ of (5.157), it may not necessarily be meaningful to pursue the same line of arguments in higher-dimensional space as in the one-dimensional case.

The following result is known ([**287**]).

THEOREM 5.44. *Assume that the equilibrium problem* (5.156) *has a family of classical solutions* $\{(u^\epsilon, v^\epsilon)\}_{0\le\epsilon\le\epsilon_0}$ *with a family of interfaces* $\Gamma^\epsilon$ *that is smooth up to* $\epsilon = 0$. *Then the solution for small* $\epsilon$ *is unstable.*

REMARK 5.45. When $(u^\epsilon, v^\epsilon)$ is a solution of (5.156), its **interface** $\Gamma^\epsilon$ is defined by

$$\Gamma^\epsilon = \{\, x \mid u^\epsilon(x) = \alpha^* \}, \tag{5.158}$$

where $u = \alpha^*$ is an appropriate value between the two values $u = h_\pm(v^*)$ on stable branches, and $u^\epsilon$ takes this value within the transition layer.

REMARK 5.46. To be precise, in the conditions for THEOREM 5.44, it is required that $(u^\epsilon, v^\epsilon)$ have outer and inner asymptotic expansions up to the first order in $\epsilon$. That $\Gamma^\epsilon$ is smooth up to $\epsilon = 0$ means that there exists a smooth, compact, connected $(N-1)$-dimensional manifold $\Gamma^0$ such that $\Gamma^\epsilon$ converges to $\Gamma^0$ as $\epsilon \to 0$ with respect to the smooth topology.

The result in THEOREM 5.44 naturally gives rise to the following question. *How do the stable solutions behave as* $\epsilon \to 0$*?* The proof of the theorem above is carried out by showing, via a spectral analysis, that perturbations with appropriately **fine** wave lengths, given along the smooth interface $\Gamma^\epsilon$, do not decay but are in fact amplified.

For what wavelength does the solution destabilize? The analysis, described below for planar-wave solutions (cf. [**341**]), is enlightening. The planar-wave solutions here mean the one-dimensional transition layer solutions simply extended along the orthogonal directions.

THEOREM 5.47. *Let* $\Omega$ *be a two-dimensional rectangular domain. The planar-wave solution of* (5.156) *becomes unstable as* $\epsilon \to 0$. *The most unstable wavelength is of order* $O(\epsilon^{1/3})$.

REMARK 5.48. Assuming that the reduced equation (5.157) has a solution, the problem of constructing solutions of (5.156) is discussed in [**321**]. However, according to THEOREM 5.43, it is more adequate to consider the same problem for a rescaled version (5.159) below. The techniques in [**321**] also apply in the latter problem (cf. [**340**]).

THEOREM 5.47 is expected to be true not only for the planar-wave solution but also for the general internal layer solution $(u^\epsilon, v^\epsilon)$

of THEOREM 5.44. This strongly suggests that stable (internal layer) solutions of (5.156) possess a spatial scale of order $O(\epsilon^{1/3})$ for $0 < \epsilon \ll 1$.

On the other hand, the most unstable wavelength obtained from spectral analysis around constant trivial solutions cannot be used to predict the spatial scale of well-developed transition layers, because coarsening processes in between, such as coalescence of transition layers, cannot be captured by such an analysis.

If the conjecture above is true, and moreover, if the stable solution is spatially periodic, then its domain $\Omega_p$ of periodic unit will satisfy $|\Omega_p| = O(\epsilon^{1/3})$. Introducing a stretched variable by $y = x/\epsilon^{1/3}$, we obtain the following rescaled version of the equilibrium problem:

$$\begin{cases} \tilde{\epsilon}^2 \Delta_y u + f(u,v) = 0, \\ \qquad\qquad\qquad\qquad\quad y \in \tilde{\Omega}_p, \\ \Delta_y v + \tilde{\epsilon} g(u,v) = 0, \end{cases} \tag{5.159}$$

where $\tilde{\epsilon} = \epsilon^{2/3}$ and $\tilde{\Omega}_p$ is the stretched domain. We also assume that $(u,v)$ satisfies on the boundary $\partial\tilde{\Omega}_p$ appropriate boundary conditions, depending on the original periodic pattern. Strictly speaking, the shape of the periodic unit $\Omega_p$ needs to be determined. Note that $\tilde{\Omega}_p$ has a definite limit as $\tilde{\epsilon} \to 0$. Therefore, solutions of (5.159) determine the shape of stable solutions in the unit domain.

The meaning of $\epsilon^{1/3}$-scaling above becomes a little more transparent if it is interpreted in terms of the associated interface equation. Let us apply a scaling $y = x/\epsilon^{\alpha}$, where $0 < \alpha < 1$ is an unknown exponent, to the system of equations

$$\begin{cases} u_t = \epsilon^2 \Delta u + f(u,v), \\ \\ v_t = \Delta v + g(u,v), \end{cases} \tag{5.160}$$

to obtain the following:

$$\begin{cases} u_t = \epsilon^{2(1-\alpha)} \Delta_y u + f(u,v), \\ \\ v_t = \epsilon^{-2\alpha} \Delta_y v + g(u,v). \end{cases} \tag{5.161}$$

This can be rewritten as

$$\begin{cases} \epsilon^{-(1-\alpha)} u_t = \epsilon^{1-\alpha} \Delta u + \epsilon^{-(1-\alpha)} f(u,v), \\ \\ \epsilon^{2\alpha} v_t = \Delta v + \epsilon^{2\alpha} g(u,v). \end{cases} \tag{5.162}$$

Introducing a new time scale $\tau \equiv \epsilon^{1-\alpha}t$, the latter system is recast as

$$\begin{cases} u_\tau = \epsilon^{1-\alpha}\Delta u + \epsilon^{-(1-\alpha)} f(u,v), \\ \epsilon^{1+\alpha} v_\tau = \Delta v + \epsilon^{2\alpha} g(u,v). \end{cases} \tag{5.163}$$

Recalling (4.77) in CHAPTER 4, the interface equation for (5.163) as $\epsilon \to 0$ is given by

$$\begin{cases} \gamma(\tau) &= c(v|_\Gamma) - \epsilon^{1-\alpha}\kappa, \\ \epsilon^{1+\alpha} v_\tau^\pm &= \Delta_y v^\pm + \epsilon^{2\alpha} G_\pm(v^\pm), \end{cases} \tag{5.164}$$

in which $\gamma(\tau)$ stands for the normal speed of the interface and $v^\pm$ are defined in a manner similar to $V_\pm$ in (5.157). The third term in (4.77), which comes from the $v$-dependence of $f$, can be neglected. Since we are looking for patterns of order $O(1)$ even after $1/\epsilon^\alpha$-scaling, the contribution of the curvature term $\epsilon\kappa$ with respect to the original scale is of order $O(\epsilon^{1-\alpha})$, instead of $O(\epsilon)$. Therefore, the third term in (4.77) is of higher order than the second one. Since $1+\alpha > 2\alpha$, the second equation of (5.164) implies

$$v^\pm = v_0^\pm(y) + \epsilon^{2\alpha} v_1^\pm(y) + o(\epsilon^{2\alpha}). \tag{5.165}$$

For equilibrium solutions, we have $v_0^\pm(y) \equiv v^*$, where $v^*$ is such that $c(v^*) = 0$.

By means of the method of matched asymptotic expansion, one can show that $v_1^\pm$ takes a common value on the interface $\Gamma$. Therefore, substituting (5.165) into (5.164), we obtain

$$\begin{cases} \gamma(\tau) &= \epsilon^{2\alpha} c_v(v^*) v_1|_\Gamma - \epsilon^{1-\alpha}\kappa, \\ 0 &= \Delta_y v_1^\pm + G_\pm(v^*). \end{cases} \tag{5.166}$$

From the right hand side of (5.166), one can easily see that the first term, coming from translational wave speed, and the second term, representing curvature effects, balance only when $\alpha = 1/3$. In other words, **the spatial $\epsilon^{1/3}$-scaling is the only one in which contributions from the translational wave speed and curvature effect become comparable in the asymptotic expansion.**

This observation gives a very important viewpoint in dealing with pattern formation for high dimensional dissipative systems. Namely, stable spatio-temporal patterns in the singular limit tend to possess a scale in which contributions from possible principal parts in an

asymptotic expansion are equally balancing. We call such a scale the **balanced scaling in the singular limit** of the system.

It is our future task to examine to what extent a reasoning like the above is valid. We should be aware that such a balanced scaling in the singular limit has appeared already in CHAPTER 4, where the Fife scaling for spiral waves is discussed. Moreover, the interface equation for a model of di-block co-polymers (cf. §4.2.3) (which is a non-homogeneous version of the Mullins-Sekerka problem) has been derived along the same line of arguments as above ([**285**]).

## 5.6. Summary

**5.1** The mean curvature flow is defined, and a partial differential equation that the signed distance function to a hypersurface satisfies is derived.

**5.2** The level-set method is introduced as a means to describe the motion of hypersurfaces even after singularities are formed. Basic properties of viscosity solutions are explained. It is shown that a scalar bistable reaction-diffusion equation converges to the mean curvature flow in the singular limit.

**5.3** The phase-field model, which is very important in the discussion of interface dynamics, such as in crystal growth processes, is introduced. Moreover, it is shown that various types of interface equations are derived from the phase-field model by different scalings. Relationships between these interface equations are discussed.

**5.4** The spectral behavior of reaction-diffusion systems is analyzed in the singular limit. A detailed account is given of the SLEP-method, in which singular eigenfunctions are characterized as distributions supported on the locations of transition layers.

**5.5** In order to identify relevant scales to obtain meaningful singular limits, the idea of balanced scaling in the singular limit is described.

CHAPTER 6

# Transient Dynamics

So far, we have studied pattern formation problems by means of asymptotic methods. These methods enable us to grasp various types of dynamic modes that ultimately dominate the system. There are, however, many dynamic pattern formation phenomena which escape analysis by such asymptotic methods. One cannot deny that the latter types of phenomena, being transient, hard to grasp and impermanent, have been considered as the remotest objects to which mathematical analyses apply. How do we understand such transient phenomena from a viewpoint of dynamical system theory? Even though this is an important and interesting question, methods to answer it are still in their infancy compared with the development of asymptotic ones. One reason for this may be that the mathematical framework to describe such phenomena is aside the mainstream of research. However, it may be more appropriate to say that transient processes themselves have rarely been treated as an object of study.

In recent years, self-replicating patterns and self-similar spatio-temporal patterns ([**88, 303, 313, 316**], [**175**]) have attracted much research interest as typical examples of nonlinear phenomena observed in non-equilibrium systems. FIGURES 6.1 and 6.2 show two examples of such a dynamic behavior observed in the Gray-Scott model (6.1) below. Although these pictures exhibit a beautiful pattern, looking into them does not immediately give us clues to discern the dynamic driving mechanism that gives rise to such a pattern. One can observe in these pictures violent deformations of the solution, such as splitting of one pulse into two or disappearance of two pulses upon collision. These processes are intricately intermingled, making it difficult to understand the origin of such patterns. Recall, to appreciate the difficulty, that a rigorous proof has not yet been given to the pair annihilation of travelling pulses even in the classical FitzHugh-Nagumo equation.

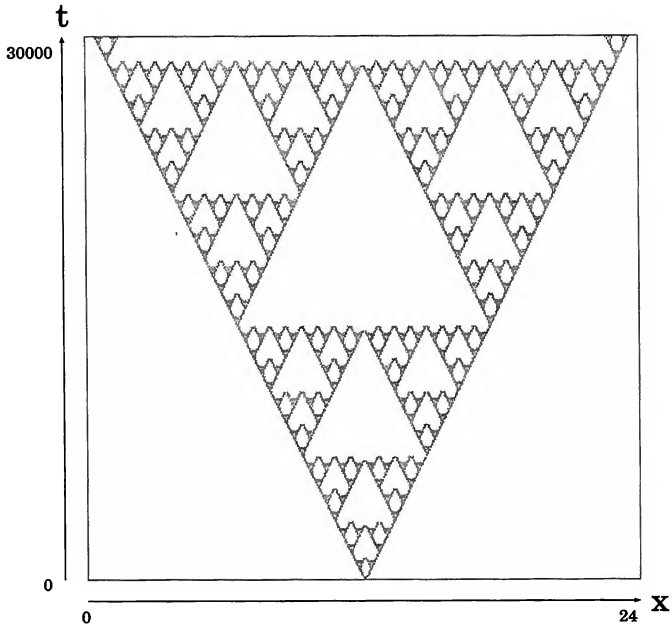


FIGURE 6.1. Self-similar spatio-temporal pattern for the Gray-Scott model. The parameters are $D_u = 1.15 \times 10^{-5}$, $D_v = 1.0 \times 10^{-5}$, $F = 0.02548$, $k = 0.05252$, and $L = 24$. The plot indicates the $v$-profile in gray-scale. A subtle combination of creation and annihilation of pulses forms a Sierpinski gasket-like pattern. This type of patterns was first found by Y. Hayase and T. Ohta [**175**] for the Bonhoeffer–van der Pol type of equations.

We are here dealing with a situation where seemingly transient dynamic behaviors are leading actors, while asymptotically stable states have disappeared from the main stage. As a more complicated dynamical behavior, FIGURE 6.21, below, will exhibit a spatio-temporal chaos observed in the Gray-Scott model. This is not a simple chaos that has an erratic spatio-temporal behavior. One can observe in it short-lived ordered states popping up in between irregular states. What should be the clue for us to start with in understanding such behaviors? We need to alter our way of thinking. **Let us think about**

**the geometric structures that guide solution orbits creating such a chaotic dynamism, rather than keeping track of the deformations of solutions in detail.** In other words, we should try to characterize geometric structures of the infinite dimensional phase space in which behaviors of solution orbits become easily detectable. In this respect, it turns out that unstable solutions are more important than stable ones, and that the overall geometric configuration of solutions plays a more important role than individual solutions. It is here that a global bifurcation analysis in an infinite dimensional space becomes indispensable. At the present moment, we have to rely on numerical methods, such as AUTO [**96**], which is a software package that allows us to detect bifurcation branches. Numerical methods, such as AUTO, are very useful because they give a great amount of information on an unstable solution, as well as on the behavior of its unstable manifold. This allows us to clarify the relationship between the traces of solution orbits and ordered solutions in infinite dimensional phase spaces. (We note here that AUTO was originally developed for ordinary differential equations and that it does not work, as it stands, for partial differential equations. Even if it works for the latter, the output is a complicated web-like pattern. In order to collect meaningful information out of it, one needs to perform detailed simulations for time evolution and to overcome some technical difficulties.) Although the output data of such numerical simulations are obtained for a particular model equation with a restricted range of parameters, the geometric characterization of such results is rather universal. In fact, it is possible to extract a mathematical framework from the data, and based on it, one can develop a rigorous theory of a universal nature (cf. [**110, 111, 112**]).

In this chapter, we focus our attention on the self-replication and spatio-temporal chaotic patterns in the Gray-Scott model to show the validity of our viewpoint. Putting it concisely, the keys to understanding the dynamics of self-replicating patterns are the **saddle-node bifurcation structure** of the relevant localized solution and the **critical distance** between objects. Morover, the dynamics of a spatio-temporal chaos is well-understood in terms of the global structure of **heteroclinic cycles** connecting ordered solutions.

## 6.1. Self-Replication Pattern as Transient Dynamics

Typical self-replication (or self-splitting) patterns in one space dimension are shown in FIGURE 6.2. The solution is obtained by solving

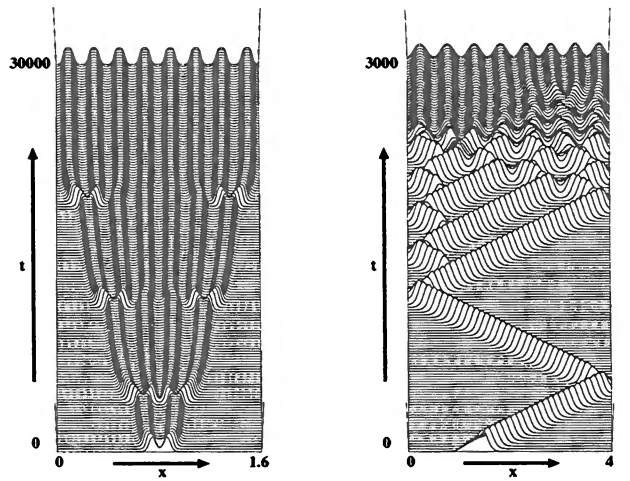


FIGURE 6.2. One-dimensional self-replication patterns. Two types of self-replication pattern obtained by solving the Gray-Scott model. Only the $v$-profile is exhibited in both pictures. (a) Self-replication pattern of static type: $D_u = 2 \times 10^{-5}$, $D_v = 10^{-5}$, $F = 0.04$, $k = 0.06075$, $L$ (length of the interval) $= 1.6$. (b) Self-replication pattern of propagation type: $D_u, D_v$ are the same as in (a). $F = 0.025$, $k = 0.0542$, $L = 4.0$.

the seemingly simple reaction-diffusion system, called the Gray-Scott model (cf. [**158**] and §6.3):

$$\begin{cases} \dfrac{\partial u}{\partial t} = D_u \Delta u - uv^2 + F(1-u), \\ \dfrac{\partial v}{\partial t} = D_v \Delta v + uv^2 - (F+k)v. \end{cases} \tag{6.1}$$

The system models the chemical reaction $U + 2V \to 3V$, $V \to P$ in a gel. The variables $u$ and $v$ stand for the concentration of the chemical substances $U$ and $V$, respectively. $D_u$ and $D_v$ are the corresponding diffusion rates. The parameter $F$ stands for the inflow of $U$, while $k$ represents the conversion rate of $V \to P$. In both (a) and (b)

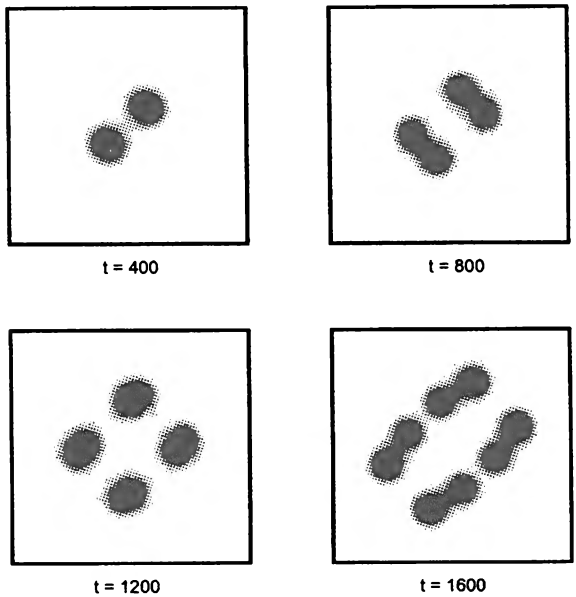


FIGURE 6.3. Two-dimensional self-replication patterns in the Gray-Scott model. The values of $D_u$, $D_v$ are the same as in FIGURE 6.2, and $F = 0.032$, $k = 0.063$, $L \times L = 1.0 \times 1.0$.

in FIGURE 6.2, the one-hump pattern undergoes successive splitting, eventually settling down to a spatially periodic structure, although the values of $F$ and $k$ are different. There is, however, a difference between these two cases in the intermediate stage. In (a), there is a period in which the solution stays still, as if it were a stationary solution, while in (b), there is a period in which the solution propagates as if it were a travelling wave. Case (a) is called a **self-replication pattern of static type**, and case (b) a **self-replication pattern of propagation type**. A splitting phenomenon in two-dimensional space is as in FIGURE 6.3, exhibiting itself as a cell-differentiation process (such a phenomenon was first discovered numerically in [**303**]).

REMARK 6.1. Generically, the two types of splitting behavior in FIGURE 6.2 are typically observed. A slightly more complicated splitting manner than FIGURE 6.2 was found in a transient area of parameter space from static type to traveling type. See REMARK 6.3 at the end of §6.3.

What is it that creates such a behavior of the dynamics? As one can see in FIGURE 6.2, the self-replication dynamics in a finite domain is an intermediate process, and one needs to choose an initial condition with localized compact support. In other words, the self-replication pattern is a typical example of transient dynamics that emerges from a special class of initial conditions. The collection of such orbits does not appear to give a meaningful set in the phase space. This causes a lot of trouble, because it means that one cannot understand such dynamics as above by relating it to a certain kind of invariant manifold, such as in pulse solutions corresponding to homoclinic orbits. We are therefore forced to take an approach different from the invariant manifold theory which has been a main theme of the theory of dynamical systems (however, we will see in §6.4, we can still apply a local invariant manifold theory to describe the onset of the splitting dynamics). We shall explain below how to grasp such *impermanent*, transient dynamic behaviors.

## 6.2. Elementary Transient Dynamics

**6.2.1. Transition via Saddle-to-Saddle Connection.** If we call a change from a *state* A to another one B a transition, we have already encountered an example of transition. A front solution connecting two equilibrium points is a typical example (cf. FIGURE 6.4 (a)), in which the state at fixed position $x$ exhibits a transition from A ($t = -\infty$) to B ($t = \infty$). This corresponds to a heteroclinic orbit connecting A and B, when observed from the travelling coordinate system. Note that if we consider a front solution in the travelling coordinate as a solution of the corresponding ordinary differential equation, then a stable equilibrium becomes an unstable saddle. In the example above, the transition occurs only once. If one wants to have transitions from one state to another occurring successively, one may consider the orbit $T$, as in FIGURE 6.4 (b), which stays near several connecting orbits between saddle points. (In the figure, we depict a two-dimensional situation which is necessarily structurally unstable. We therefore ask the reader to imagine a higher dimensional version of this situation. It may be more realistic to consider a chain recurrent

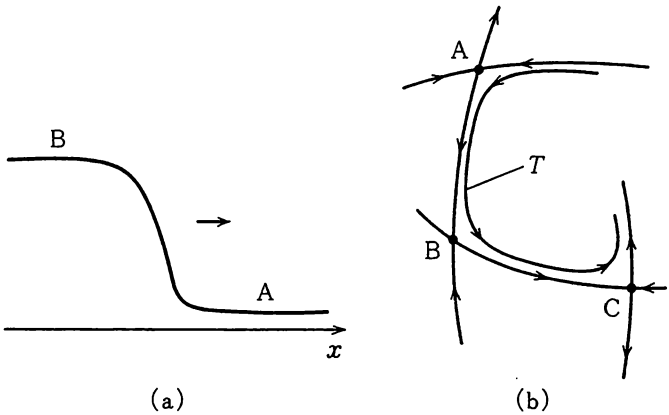


FIGURE 6.4. (a) A front solution. (b) Saddle-to-saddle connections.

situation, rather than the saddle connection, but we will not dwell on this point any more.) By choosing an appropriate initial condition, one can force the orbit $T$ to stay near the states A, B, and C for a long period of time and to make a transition from one to another. The latter situation may be generalized as follows. If several states (not necessarily equilibria) are connected by saddle-to-saddle orbits, there exists a nearby orbit that experiences successive transitions from one state to another. It is evident that the saddle-to-saddle connections in the phase space are a driving factor of the transient dynamics.

The scalar bistable reaction-diffusion equation (4.5) in CHAPTER 4 possesses spatially homogeneous solutions as a stable equilibrium under the Neumann boundary conditions (THEOREM 4.15). Therefore any solution of this equation with a transition layer must be unstable. In fact, one can prove in one space dimension, following the proof of THEOREM 4.11, that the transition layer solution has the same number of unstable eigenvalues as the number of transition layers for $0 < \epsilon \ll 1$. The behavior of the solution orbit corresponding to $T$ above in this case is such that the number of transition layers decreases as it goes through a transition from one equilibrium to another. The very slow motion discussed in CHAPTER 1 describes the dynamical process of the transition layer solution up to the time of a

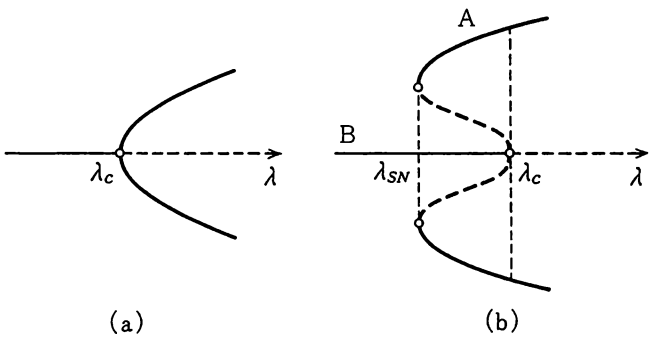


FIGURE 6.5. (a) Supercritical bifurcation. (b) Subcritical bifurcation.

pair-annihilation of transition layers. Therefore the coarsening process for the equations (4.5) and (4.12) is nothing but a transient dynamics which corresponds to an orbit going through successive transition from one unstable layered solution to another.

**6.2.2. Transition via Bifurcation.** In pattern formation problems, the system usually has a control parameter. It is often the case that when the parameter changes new solutions emerge successively, and varied patterns are observed. A typical example is a symmetry-breaking bifurcation. From the viewpoint of transient dynamics, a subcritical bifurcation as in FIGURE 6.5 (b) is more interesting than a supercritical bifurcation as in FIGURE 6.5 (a) in which a stable solution on a trivial branch destabilizes as the control parameter changes, continuously giving rise to stable solutions. The reason is that in the subcritical case, one can realize the situation where several stable solutions coexist and a jumping transition from one stable solution to another is likely to occur. To be a little more precise in the description, let us denote by $\lambda_c$ the bifurcation point and by $\lambda_{SN}$ the saddle-node bifurcation point. For $\lambda_{SN} < \lambda < \lambda_c$, there are three stable solutions. Two of the stable solutions disappear for $\lambda < \lambda_{SN}$ through the saddle-node bifurcation, leaving only one stable solution. In systems describing real phenomena, subcritical bifurcations appear not rarely, but frequently. For example, in the Turing pattern, hexagonal and roll patterns appear simultaneously ([**33, 192**]). If we consider a situation where the control parameter $\lambda$ changes slowly with time, then the system originally at the state A in FIGURE 6.5 (b)

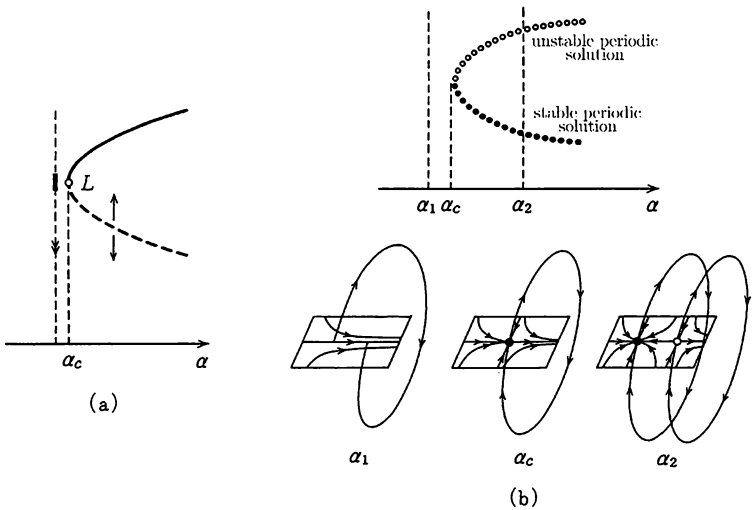


FIGURE 6.6. The aftereffect of limiting points. (a) Equilibrium solutions. (b) Periodic solutions. Pictures in the phase portrait exhibit the Poincaré map at the respective parameter values.

experiences a transition to the state B, as soon as the parameter $\lambda$ becomes smaller that $\lambda_{SN}$. It may look unrealistic to consider situations where the parameter depends on time. However, in realistic experiments we often adjust the in- and out-flow of materials. In describing the pigmentation patterns on seashells ([**257**],[**258**]), the domain size changes slowly with the growth of the animal. In these examples, it is rather natural to consider a system with a time-dependent parameter. Even if the parameter does not depend on time, if we appropriately fix it near ($<$) $\lambda_{SN}$, a transition phenomenon can occur for an adequate initial condition, as we will see in the next subsection. This is one reason why bifurcations of subcritical type will play very important roles later on.

**6.2.3. Aftereffect of a Limiting Point.** As observed in the previous subsection, if a bifurcation is of subcritical type, it necessarily creates a saddle-node bifurcation and naturally gives rise to a limiting point. From now on we use the terminology *limiting point* to designate a saddle-node bifurcation point in the parameter-solution

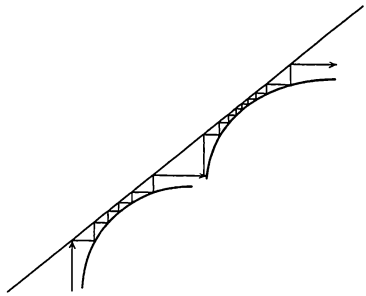

FIGURE 6.7. Intermittency

space. Let us consider the situation in FIGURE 6.6 (a), where there is a saddle-node bifurcation of equilibria with the limiting point $L$. If an initial condition is taken near the limiting point $L$ immediately after two equilibria disappear through the bifurcation, then the solution stays near the initial point for a long period of time, as if it is an equilibrium. This is so, because the vector field depends continuously on the parameter, even if the bifurcation itself takes place suddenly. When the branches consist of periodic solutions, then the solution with an initial condition near $L$ behaves almost like a periodic solution as in FIGURE 6.6 (b). Therefore, if an initial condition is chosen close to the profile of the limiting point of a saddle-node bifurcation, the solution for a certain time behaves in the same manner as the equilibrium (or periodic) solution which existed before the bifurcation. This is called an **aftereffect** of a limiting point, which naturally lasts only on a finite time interval. However, if the parameter is chosen sufficiently close to the bifurcation point and the initial condition close to the limiting point, the aftereffect survives for a very long period of time. In the dynamics of a one-dimensional map, such an aftereffect is known as an **intermittency** (see FIGURE 6.7). Let us show an example of aftereffect in a system of partial differential equations. It is well-known that travelling pulse solutions of the FitzHugh-Nagumo equation cease to exist when the diffusion rate $D$ of the inhibitor becomes large. The family of travelling pulse solutions has the structure of saddle-node bifurcation as in FIGURE 6.8 (a). When $D$ becomes larger than the bifurcation point, pulse solutions cease to exist. We emphasize that a branch of the unstable manifold of the slower pulse (which is unstable) is connected to

the trivial solution $(0,0)$. If we choose $D$ slightly above the value of the bifurcation point and choose a step-like function as an initial condition, then the solution at first structures itself as the shape of a travelling pulse as in FIGURE 6.8 (b), propagates for a while, and

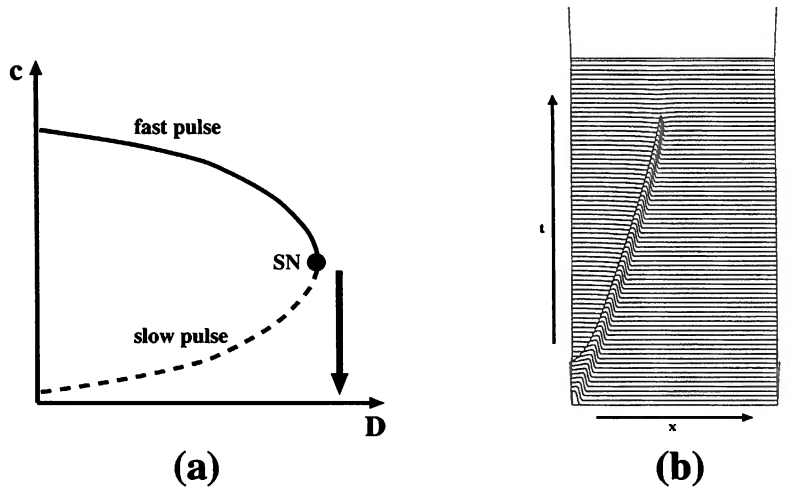


FIGURE 6.8. Aftereffect in the FitzHugh-Nagumo model.

then decays quickly to the trivial solution. This is a typical example in which the information of dynamics at the saddle-node bifurcation point reveals itself as an aftereffect. As one can see from this example, the behavior of the orbit after it escapes from the influence of the limiting point is determined by the destiny of (aftereffect of) the unstable manifold of the unstable solution.

It is possible to join several units of such behavior as above, creating a hierarchical structure as in the next subsection.

**6.2.4. Hierarchical Structure.** Let us consider an artificial model described by the following ordinary differential equation:

$$\frac{du}{dt} = -(u+1)(u^2-\alpha)(u^2-2u+1-\alpha), \qquad |\alpha| < \frac{1}{4}. \tag{6.2}$$

There are three branches of equilibrium solutions consisting of two parabolic curves and a straight line $u = -1$, as depicted in FIGURE 6.9, on the $(\alpha, u)$-plane. Here the branch of stable solutions is shown

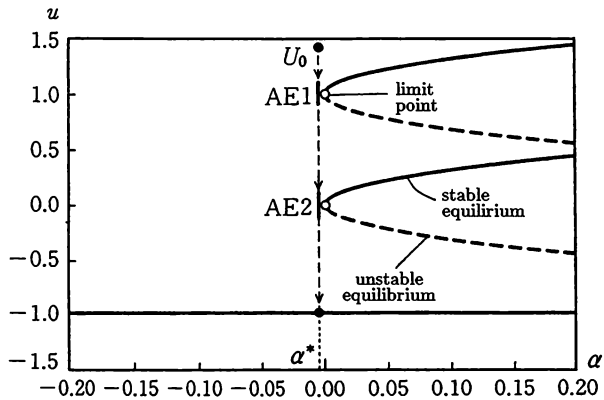


FIGURE 6.9. The hierarchical structure for ODE-model (6.2).

by solid lines and that of unstable ones by broken lines. The equilibrium $u = -1$ is always stable, regardless of the value $\alpha$. FIGURE 6.9 is called the **bifurcation diagram** of the model (6.2) with parameter $\alpha$. A remarkable point in the picture is that two saddle-node bifurcations occur at the same parameter value. Another feature, which is a trivial fact in scalar equations, is that the unstable manifolds of dotted solutions are connected to the stable solutions located immediately above and below. If we choose $\alpha = -0.001$ and the initial condition $U_0 = 0.5$, then how does the solution behave? The behavior is depicted in FIGURE 6.10 as the graph of $u(t)$ against $t$.

The heights of the horizontal steps in FIGURE 6.10 are almost equal to the values of equilibria corresponding to the limiting point of the saddle-node bifurcations. The closer the initial value to the limiting point, the longer the length of the corresponding horizontal step. If we observe such a solution in a short period of time, it looks like an equilibrium. If we observe it in a longer period, then it jumps to a neighborhood of another limiting point and stays there for a while. After these processes, the solution finally settles down to the stable equilibrium $u = -1$. Note that the solution go through only ordinary points before it reaches the equilibrium. Neither heteroclinic nor homoclinic orbits are involved in between. However, the jump from the vicinity of one limiting point to that of another in the orbit reflects how the aforementioned unstable manifold connects equilibria. In

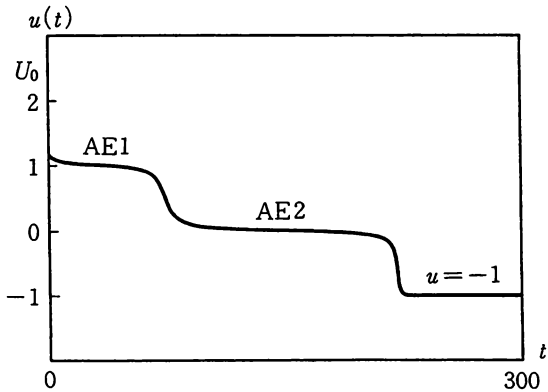


FIGURE 6.10. Aftereffect of a limiting point, shown in the $t$-$u$ plane.

this sense, we could say that the memory of the hierarchical structure of limiting points controls the behavior of the orbit. We emphasize again that the jump of orbit from one limiting point to another is possible only for the parameter values immediately after the equilibrium points disappear through saddle-node bifurcation. We call the global bifurcation structure described above the **hierarchical structure of limiting points**. In the following sections, we will examine, based upon the results of [**288, 289, 344**] and [**110, 111, 290**], how our viewpoint is useful in understanding the self-replication processes for a concrete example (6.1) of a reaction-diffusion system. We will, in particular, show how a theoretical framework is abstracted from global bifurcation diagrams obtained by numerical simulations.

## 6.3. Self-Replication Dynamics on a Finite Interval

The self-replication process consists of a splitting of localized pulse solutions which decay with exponential rates at infinity. It is therefore natural to consider the process on the infinite interval, as we will do in §6.4. However, the basic assumptions we will employ in §6.4 are actually suggested by global bifurcation diagrams for the system on a finite interval. Moreover, the analysis of the system on the finite interval is interesting in its own right. For example, one can prove, on finite intervals, the existence of the hierarchical structure of limiting points. Thererfore we now discuss the self-replication process

on finite intervals, and examine essential driving mechanisms of such a process.

**6.3.1. Hidden Structure Driving Self-Replication.** Let us explain the kinetics of the Gray-Scott model. We show that symmetry-breaking bifurcations occur at one of the equilibrium points. The examination of the global bifurcation structure popping up from such points will reveal the hierarchical structure of limiting points.

**Kinetics of Gray-Scott model**

The kinetics of the Gray-Scott model without diffusion is given by

$$\begin{cases} \dfrac{du}{dt} = -uv^2 + F(1-u), \\ \dfrac{dv}{dt} = uv^2 - (F+k)v. \end{cases} \tag{6.3}$$

The phase-portrait of (6.3) and its $(k, F)$-parameter dependence are as given in FIGURE 6.11. The system has a Bogdanov-Takens singularity (BT-point) and the equilibrium point $(1, 0)$, which is asymptotically stable regardless of the parameter values. Saddle-node bifurcation and Hopf bifurcation curves emanate from the BT-point. In one side of the saddle-node curve, two equilibrium points other than $(1, 0)$ emerge. One of the new equilibria is a spiral point from which (spatially homogeneous) periodic solutions bifurcate across the Hopf line. If diffusion effects are added, spatially inhomogeneous equilibria bifurcates from these equilibrium points, thanks to the Turing-instability mechanism discussed in CHAPTER 4. These bifurcated solutions are unstable[1] immediately after the bifurcation. As the parameter $k$ changes, these solutions recover their stability, which will be detailed in the subsequent sections. In bifurcation diagrams and simulation results for the Gray-Scott model (6.1) exhibited below, we fix the value of diffusion rates as $D_u = 2 \times 10^{-5}$ and $D_v = 10^{-5}$, unless otherwise stated.

[1]This is due to the fact that the equilibrium points as a solution of ODE are unstable even before the bifurcation. In this sense, it may not be appropriate to use the word *Turing bifurcation*, which means a bifurcation from *stable* equilibria. In this chapter, however, we generalize the notion and call destabilizations due to diffusion effects Turing instabilities.

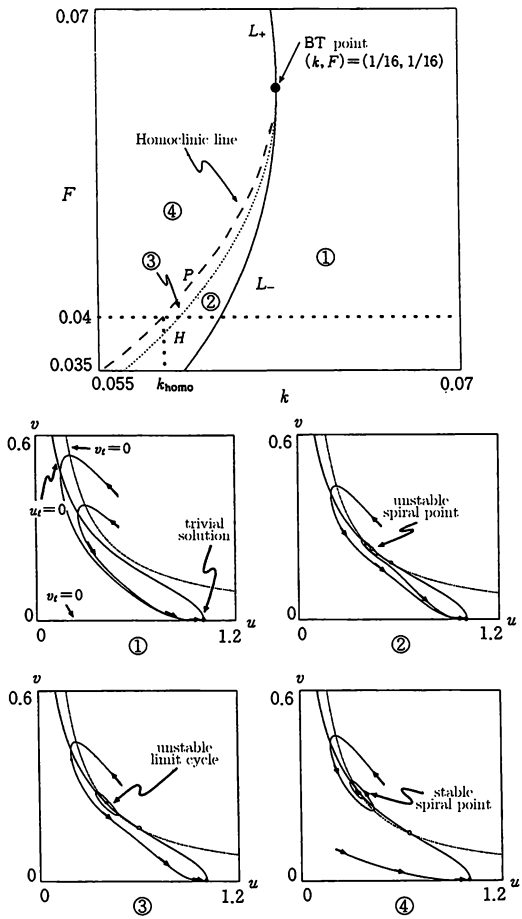


FIGURE 6.11. The unfolding of the BT-point of the GS-model with respect to the $(k, F)$-parameter and representative phase-portraits. The BT-point is a singularity of codimension 2, from which emanate the saddle-node bifurcation (solid line) and the Hopf bifurcation (dotted line) curves, as well as the homoclinic bifurcation curve (broken line). The homoclinic orbits are the limit of the family of periodic orbits created by the Hopf bifurcation as the amplitude grows.

### Limiting points of Turing bifurcation and basic self-replication structure

From the preliminary consideration in §6.2, it is suggested that the key to understanding a self-replication process is to clarify the bifurcation structures of localized equilibrium solutions. As a first such attempt, let us consider the simplest one-step splitting (cf. FIGURE 6.12 (a)) observed on finite intervals, in which a one-hump solution splits itself into a two-hump one and the process stops there. For a parameter value $k$ slightly larger than that for FIGURE 6.12 (a), a one-hump solution with the same initial condition does not split but remains as a stable solution (although the simulation is not exhibited here). The stable one-hump solution originates from an unstable equilibrium of (6.3) via Turing bifurcation. We emphasize, however, that the stable solution can never be captured by the local analysis around the Turing bifurcation point, and that a global bifurcation analysis based on numerical tracing of bifurcation branches is indispensable. We performed the following computations by using AUTO (cf. [**96**]) after we modified it for partial differential equations. We label branches of equilibria by the Fourier-mode number of the solution at the Turing bifurcation point. We also use the word *n-hump* in the sense that 1-hump = 2-modes is understood.

For the parameter value $F = 0.04$ with the system size $L = 0.3$, the global bifurcation diagram for the GS-model is as depicted in FIGURE 6.12. One can recognize Turing branches with 1 to 5 modes. The limiting points of 1 and 2 modes are realized at almost the same parameter value $k = 0.0608$. Although there is a larger parameter value of $k$ at which several limiting points line up, it has nothing to do with replication; in fact the equilibria on the branches nearby are unstable and everything goes to the trivial state $(1, 0)$ even starting from an initial data of 1-hump shape (around $k = 0.068$). This suggests that just a line-up of limiting points is not enough to have interesting dynamics, and the interrelation through unstable manifolds among different saddle-node branches plays a crucial role, as we will see below. Taking the parameter values $k$ slightly below the limiting point of the 2-mode Turing branch and choosing an appropriate 2-mode Turing solution as an initial condition, one obtains the time evolution of the solution profiles as in FIGURE 6.12 (a), (b). In both of these simulations, the solution behaves as a 2-mode equilibrium solution for a period of time, splits into two parts, and then

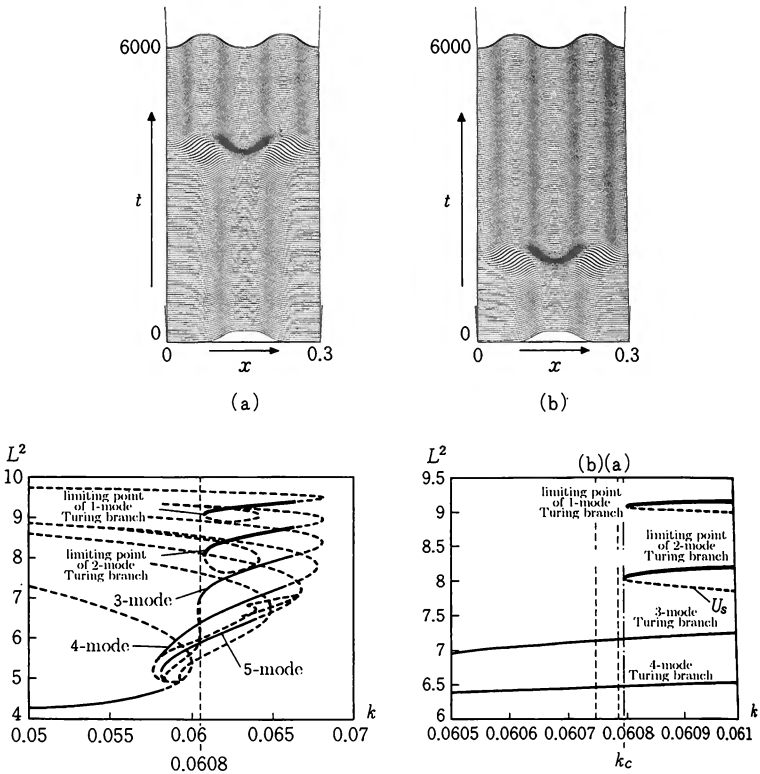


FIGURE 6.12. The aftereffect of a limiting point for 2-mode solutions and the splitting into a 4-mode solution in the GS-model. The limiting point of a 1-mode solution is at $k = 0.06080211$, while that of a 2-mode one is at $k = 0.06079793$. They are very close to each other. The vertical axis in the bifurcation diagram stands for the $L^2$-norm of solutions. The simulations of time evolution are performed at the following parameter values. For (a): $k = 0.06079$, $L = 0.3$. For (b): $k = 0.06075$, $L = 0.3$. $F = 0.04$ is used for both cases.

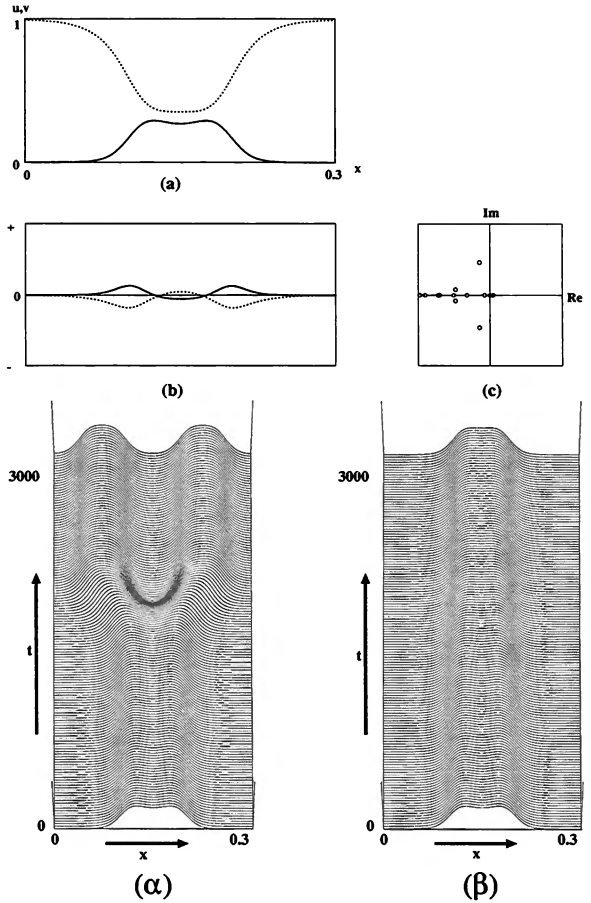


FIGURE 6.13. The destiny of the one-dimensional unstable manifold of the unstable solution $U_s$. (a) The profile of $U_s$ ($u$: solid line, $v$: broken line) for $k = 0.06009$. (b) The unstable eigenfunction: The $u$ (resp. $v$)-component has a positive (resp. negative) bump in the middle, which indicates the initiation of splitting. (c) The distribution of eigenvalues of linearization at $U_s$. There exists a unique real unstable eigenvalue. ($\alpha$) and ($\beta$) show the time evolution starting from small perturbations of $U_s$, obtained by adding to $U_s$ small positive (for ($\alpha$)) and negative (for ($\beta$)) multiples of the eigenfunction in (b).

settles down to a 4-mode solution. In (a), the aftereffect of the limiting point lasts for a very long period of time, since the parameter $k$ is very close to the critical value $k_c$. In this case, one can clearly observe the aftereffect of the limiting point, as discussed in §6.1. For parameter values less than the critical one $k_c$ at which limiting points line up, there are no 1- or 2-mode stable solutions, and only 3- and 4-mode stable solutions exist (see the magnified diagram in FIGURE 6.12). From the two-dimensional diagram in FIGURE 6.12, it may as well happen that the orbit starting near the 2-mode solution converges to the 3-mode solution. However, this is not the case, the reason being that FIGURE 6.12 is only a projection of the infinite dimensional phase space onto a two-dimensional subspace, and in the function space the orbit corresponding 2-to-4 splitting and 3-mode solution are far apart. To show that it is not by luck that the 2-mode (one-hump) solution self-replicates into a 4-mode (two-hump) one, let us examine the behavior of the unstable manifold of the unstable solution. FIGURE 6.13 (a) shows the profile of the 2-mode unstable solution $U_s$. FIGURE 6.13 (c) exhibits the distribution of eigenvalues for the linearization around $U_s$, indicating the existence of a unique (real) unstable eigenvalue. The corresponding eigenfunction has the shape of profile depicted in FIGURE 6.13 (b). It has a dent in the middle, indicating the onset of splitting. In fact, if we multiply the eigenfunction by small positive and negative constants and add them to $U_s$ as a small perturbation, the solutions starting with these functions behave as in ($\alpha$) and ($\beta$) of FIGURE 6.13. The pictures strongly suggest that the destinies of the one-dimensional unstable manifold of $U_s$ are the 4-mode and 2-mode solutions. Therefore, we are justified in saying that the self-replication dynamics in FIGURE 6.12 is not caused by chance but necessarily appears as the reflection of the basic self-replication structure consisting of the aftereffect of the limiting point for 2-mode solutions and the heteroclinic connection from the 2-mode unstable solution to a 4-mode stable solution.

**6.3.2. Hierarchical Structure of Equilibrium Solutions.** The basic structure of a splitting process discussed in the previous subsection was a one-step process. When the system size $L$ becomes large, successive self-replication processes emerge as in FIGURE 6.2, which deserves to be called a transient dynamics. For $L = 0.5$, $k = 0.06075$, the solution undergoes two steps of splitting and settles down to a 4-hump equilibrium as depicted in FIGURE 6.14. The corresponding bifurcation diagram is shown in FIGURE 6.15. The limiting

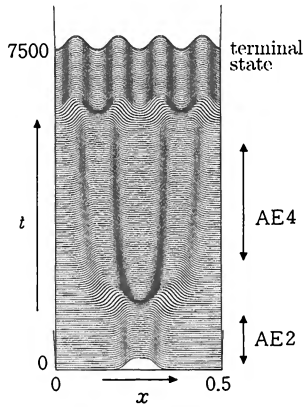


FIGURE 6.14. Self-replication patterns in the Gray-Scott model with $k = 0.06075$, $L = 0.5$.

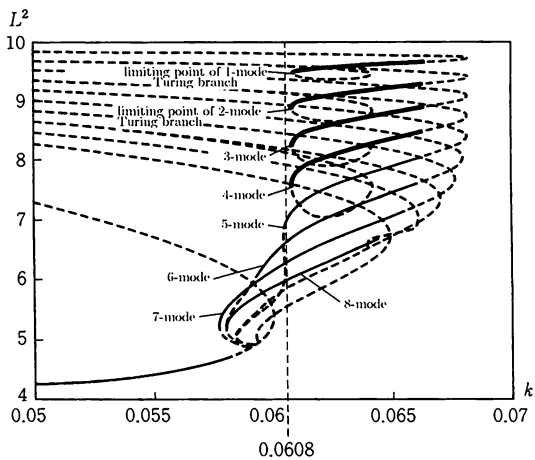


FIGURE 6.15. The bifurcation diagram of equilibrium solutions for the Gray-Scott model ($L = 0.5$). Bold lines stand for stable branches and gray lines represent unstable ones. One can observe a hierarchical structure of limiting points of Turing branches near $k = 0.0608$.

points of 1- through 4-mode solution branches arrange themselves almost on the vertical line passing through a point near $k_c \approx 0.0608$. In order to explain the dynamics in FIGURE 6.14, it is convenient to use a caricature, FIGURE 6.16 (a). As our initial condition we employ the 2-mode Turing solution (FIGURE 6.16) at the parameter value $k = 0.0609$. The solution behaves like the 2-mode equilibrium (AE2-part) for a while, splits quickly, behaves like the 4-mode equilibrium (AE4-part), splits again, and finally converges to the 8-mode (4-hump) Turing solution. In the graph of the $L^2$-norm of the orbit (FIGURE 6.16 (b)), the value is almost equal to 8.8 at AE2 and almost equal to 7.6 at AE4, which are almost identical, respectively, to the $L^2$-norms of 2- and 4-mode limiting points, exhibiting the aftereffect of limiting points. One can in fact confirm numerically that the aftereffect of the 4-mode equilibrium last longer by choosing the parameter $k$ closer to the 4-mode limiting point. In this way, we can verify that the hierarchical structure of limiting points described in the previous subsection is actually embedded in the infinite dimensional phase space of the reaction-diffusion system. It is discussed in [**289**] that such structures as above are not rare exceptions but emerge naturally in a class of systems (see REMARK 6.2). We do not pursue the issue any more here.

The preceding discussions reveal that one can answer the following questions by analyzing the global bifurcation diagram of equilibrium solutions.

- For what parameter values and for what kind of initial conditions does a splitting occur?
- How many times do splittings occur, and to which equilibrium does the solution settle down?

It is important to notice that a saddle-node bifurcation structure controls the onset of splitting. It is also worth noticing that as the system size becomes large and the number of splittings increases, the information obtained from the bifurcation diagram alone is not sufficient to give a satisfactory description to the transient process. In FIGURE 6.2 (a), for example, after the solution splits into 2-hump or 4-hump profile, the distance between the humps gradually increases. During the latter process, however, the solution profile is not close to that of 2-hump or 4-hump equilibrium solutions (where the humps are equally distributed on the interval). This suggests that the information obtained from the branches of equilibria is not sufficient, and that one needs to know more about the interaction among humps.

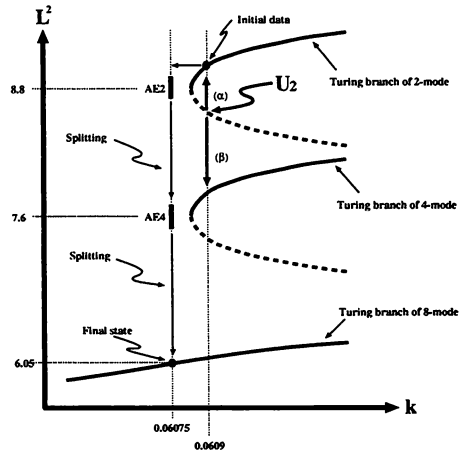


(a)

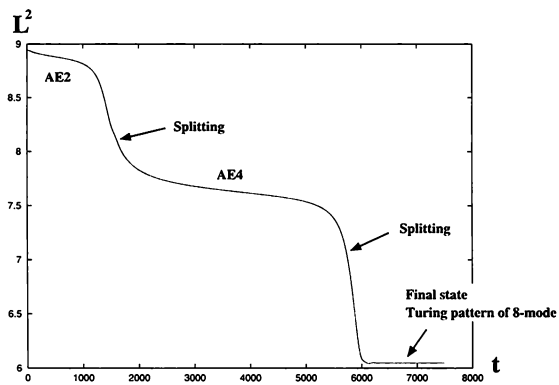


(b)

FIGURE 6.16. (a) A schematic bifurcation diagram with $L = 0.5$. The 2-mode stable Turing solution at $k = 0.0609$ in the figure is adopted as the initial value for FIGURE 6.13. The shape of unstable solution $U_2$, the associated distribution of the spectrum, and the behavior of the unstable manifold are the same as in FIGURE 6.13. AE2 and AE4 represent aftereffects of limiting points. (b) The $L^2$-norm of the orbit in (a) plotted against time. The $L^2$-norms of the flat parts AE2 and AE4 are almost equal to those in (a).

It is numerically observed that splittings appear to begin as soon as the distance between two adjacent humps exceed a certain length. To understand such a dynamic behavior, it is no doubt necessary to consider how pulses (humps) interact with each other. From such a consideration, one can in particular define a **critical distance**, which is a minimum distance between pulses for splitting to occur, as we will see in the next section.

REMARK 6.2. Hierarchical structures of branches of localized equilibrium solutions are not special to the Gray-Scott model. Similar structures are found in a large class of model equations. For example, the Gierer-Meinhardt model from morphogenesis,

$$\begin{cases} a_t &= \epsilon^2 \Delta a - a + \dfrac{a^2}{h}, \\ \epsilon^2 h_t &= \Delta h - \mu \epsilon^2 h + a^2, \end{cases}$$

also displays splitting, as was shown by Doelman and van der Ploeg ([**104**]). Hence it is expected to have a structure similar to the Gray-Scott model. In fact it has a hierarchical structure of saddle-node bifurcations as in FIGURE 6.17, which drives self-replication dynamics.

REMARK 6.3. As is shown in FIGURE 6.2, the Gray Scott model has at least two splitting manners, static and propagating types. By a careful parameter search, another type of splitting was found as in FIGURE 6.18, called the splitting of travelling breather type, in the transition area from static type to propagating type. It turns out that this dynamics can be captured by unfolding the codimension 2 singularity of saddle-node and translational bifurcations ([**112**]).

## 6.4. Pulse Interaction and Self-Replication Dynamics on the Infinite Interval

When one wants to talk about self-replication, it is first of all necessary for the pattern in question to have specific shape and size differentiable from others, so that it has an entity to be called a *self*. Candidates in the Gray-Scott model are stationary pulses and travelling pulses. We shall consider below a stationary pulse, namely, the homoclinic orbit to the stable equilibrium $(1, 0)$ in the stationary problem of (6.1), as a unit of *self*. The existence and stability of such a stationary pulse have been established by Doelman et al.

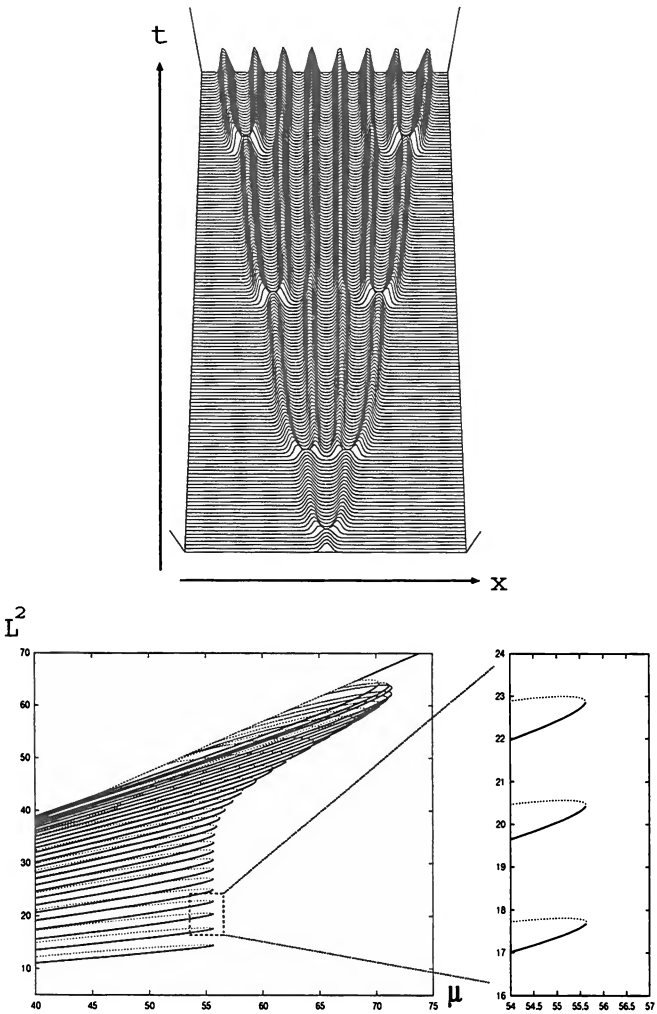


FIGURE 6.17. A self-replicating dynamics in the Gierer-Meinhardt model. The top figure shows a self-replicating pattern for the Gierer-Meinhardt system for $\epsilon^2 = 0.05$ and $\mu = 56.5$ (see the text for the equations). The associated global bifurcation diagram by AUTO clearly indicates the existence of the hierarchy structure of saddle-node bifurcations.

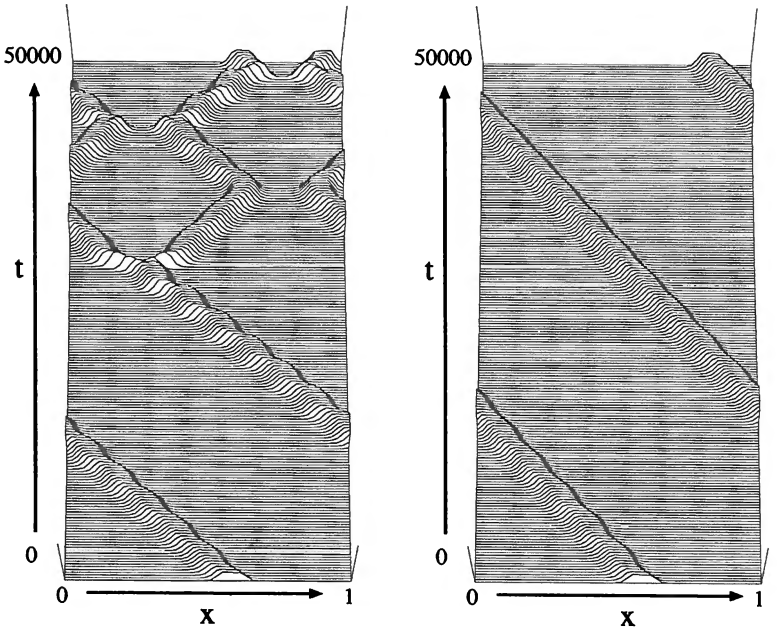


FIGURE 6.18. Self-replication of travelling breather type for the Gray-Scott model. Diffusion coefficients are the same as in FIGURE 6.2, and $F$ is fixed to be 0.0291. The boundary condition is of periodic type. At $k$=0.05799 (left), the amplitude of oscillation of travelling pulse gradually increases, and when it exceeds a critical level, the pulse splits into two travelling ones. On the other hand, if $k$ is increased slightly up to $k$=0.058 (right), then the oscillation decays and it settles down to the stable travelling pulse. In fact, there exists a branch of travelling breathers bifurcating from a travelling pulse via Hopf bifurcation, but it is subcritical and hence unstable. See [**112**] for details.

([**100**], [**99**]) in certain scaling limits. For parameter values in a special region, exact solutions are known ([**168, 169**]). Based upon the considerations in previous sections, we will propose a mathematical

framework that allows us to sensibly understand self-replication patterns in the infinite interval. The framework is effective for a wide class of systems, including the Gray-Scott model, and gives us a lot of information as to when splitting initiates and how it subsequently unfolds.

As for two-dimensional spots, there are very few rigorous existence results at present (see [**353**], for instance). The methodology shown below, nevertheless, could be extended to higher dimensional spaces, once the existence of spot-solutions is postulated.

**6.4.1. Weak Interaction and the Flow Describing the Onset of Splitting.** When stable pulses interact, staying far apart from each other, the pulse dynamics strongly resembles that of point-masses under the influence of a potential field. The driving force of such dynamics is caused by *weak* interactions through the tails of pulses, and hence it is possible to derive governing equations of motion (for instance, see [**109**], in which a PDE-approach is employed). However, what we would like to consider in this section is not stable pulses but dynamic interactions between unstable pulses, such as pulses which undergo splitting. In particular, our main interest is to clarify how weak repulsive interactions and the instability of splitting are related each other.

Roughly speaking, the dynamics consists of two steps. In the first step, a chosen parameter gives rise to a critical distance, and the weak repulsive interactions dominate the dynamics before the critical distance is reached. In the second step, after the critical distance is reached, splitting-dynamics is enacted in a short time scale. The discussions below in this section apply not only to the Gray-Scott model but also to any system which conforms to the following general framework. The results in this section are due to [**111**] and [**110**], to which we refer for the details of proof.

REMARK 6.4. The reduction method to ODEs presented in the sequel has the same spirit as in §1.3 for very slow motion. A key feature in both cases is that translation of fronts or pulses forms a good approximation of the local invariant manifold.

REMARK 6.5. It is well-known in bifurcation theory ([**163**], [**233**]) that unfoldings of singularities of codimension $k$ ($\geq 2$) lead to a variety of exotic dynamics. The stationary pulse with saddle-node singularity presented below is the simplest, but a nontrivial application of this idea. A natural extension is to investigate how the dynamics of pulses

associated with other singularities looks like. In fact, the splitting of traveling breather type shown in FIGURE 6.18 is born near a codimension 2 singularity of saddle-node and translational bifurcations for the Gray-Scott model (see [**112**]). This approach, i.e., to find a kind of *organizing center* of high codimension singularity and describe complex dynamics as its unfolding, seems quite powerful; however, it is in general quite difficult to show the existence of such singularities rigorously, partly due to the large amplitude of the patterns involved.

Let us consider an equation of the form

$$\mathbf{u}_t = \mathcal{L}(\mathbf{u}; k), \quad t > 0,\ x \in \mathbb{R}^1, \tag{6.4}$$

where $\mathbf{u} \in \mathbb{R}^n$, $\mathcal{L}(\mathbf{u}; k) = D\mathbf{u}_{xx} + F(\mathbf{u}; k)$ and $k$ is a bifurcation parameter such as $k$ in (6.1). All of the assumptions listed below can be checked at least numerically for several models. Therefore they seem to give a natural and reasonable framework (see [**289**] and [**109**]).

Suppose that the bifurcation structure of (6.4) with respect to $k$ enjoys the following properties:

**S1)** $\mathbf{0} = (0, \cdots, 0) \in \mathbb{R}^n$ is always a stable equilibrium of (6.4). That is, $\mathcal{L}(\mathbf{0}; k) \equiv \mathbf{0}$ and the eigenvalues of the linearized matrix $F'(\mathbf{0}; k)$ are all to the left of the imaginary axis for any $k$. For (6.1), the equilibrium (1,0) should be shifted to (0,0) by translation.

**S2)** There exists $k = k_c$ such that a saddle-node bifurcation occurs at $k = k_c$, and for $k > k_c$, there exist two branches of stationary pulse solutions $\{P^s(x; k)\}$ and $\{P^u(x; k)\}$ of (6.4) decaying exponentially at infinity. These solutions have $\mathbb{Z}_2$-symmetry, and $P^s(x; k)$ is stable, while $P^u(x; k)$ is unstable (see FIGURE 6.19).

**S3)** Let $X = \{L^2(\mathbb{R}^1)\}^n$ with the norm $\|\cdot\|$. We denote by $L^s(k) = \mathcal{L}'(P^s(x; k))$ and $L^u(k) = \mathcal{L}'(P^u(x; k))$ the linearized operators of (6.4) in $X$ around the stationary solutions $P^s(x; k)$ and $P^u(x; k)$, respectively. For $k > k_c$ close to $k_c$, $L^s(k)$ has two critical real simple eigenvalues, 0 and $\lambda^s(k) < 0$. The spectra of $L^s(k)$ other than these two, say $\Sigma_1(L^s(k))$, have negative real parts and stay uniformly away from the imaginary axis:

$$\Sigma_1(L^s(k)) \subset \{z \in \mathbb{C} \mid \mathrm{Re}\,(z) < -\rho_0\} \quad \text{for a } \rho_0 > 0.$$

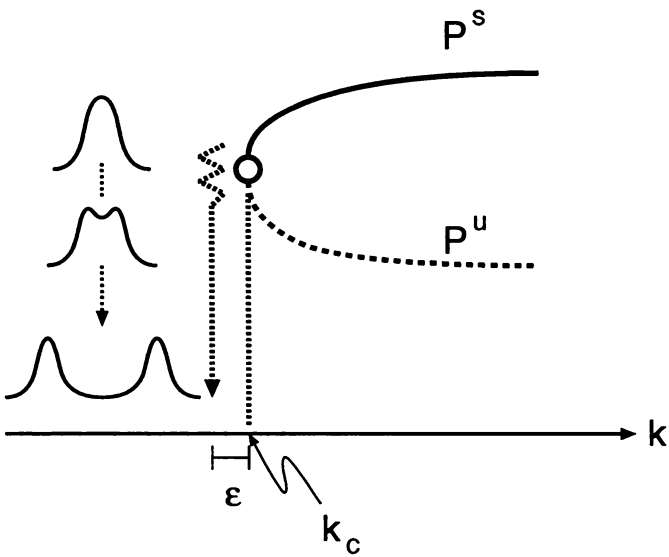


FIGURE 6.19. $P^s$ and $P^u$ merge at the saddle-node point at $k = kc$. Splitting occurs for $k$ slightly to the left of $k = k_c$, $k = k_c + \epsilon$ (with small negative $\epsilon$).

The eigenfunction corresponding to 0 is $P^s_x$, which comes from translation invariance. Let $\xi^s(x;k)$ be an eigenfunction corresponding to $\lambda^s(k)$ (see FIGURE 6.13(b)).

Similar conditions hold for the operator $L^u(k)$. That is, the spectrum of $L^u(k)$ consists of 0, $\lambda^u(k) > 0$ and $\Sigma_1(L^u(k))$, where

$$\Sigma_1(L^u(k)) \subset \{z \in \mathbb{C} \mid \mathrm{Re}\,(z) < -\rho_0\}.$$

The eigenfunctions corresponding to 0 and $\lambda^u(k)$ are respectively denoted by $P^u_x$ and $\xi^u(k)$.

**S4)** At $k = k_c$, the two branches of solutions merge and satisfy

$$P^s(x,k_c) = P^u(x;k_c) =: P(x),$$
$$\lambda^s(k_c) = \lambda^u(k_c) = 0,$$
$$\xi^s(x;k_c) = \xi^u(x;k_c) =: \xi(x).$$

We consider (6.4) in a neighborhood of $k = k_c$. Suppose $k = k_c + \epsilon$ and rewrite (6.4) as

$$\mathbf{u}_t = \mathcal{L}(\mathbf{u}) + \epsilon g(\mathbf{u}), \tag{6.5}$$

where

$$\begin{aligned}
&\mathcal{L}(\mathbf{u}) = \mathcal{L}(\mathbf{u}; k_c) = D\mathbf{u}_{xx} + F(\mathbf{u}),\\
&F(\mathbf{u}) = F(\mathbf{u}; k_c),\\
&\epsilon g(\mathbf{u}) = \mathcal{L}(\mathbf{u}; k_c + \epsilon) - \mathcal{L}(\mathbf{u}).
\end{aligned}$$

For (6.1), $\mathbf{u} = (u, v)$ and $\mathcal{L}(\mathbf{u})$ stands for the equation on the right hand side of (6.1) with $k = k_c$. $g(\mathbf{u})$ is given by $g(\mathbf{u}) = (0, -v)$.

Thanks to **S4)** we have $L^s(k_c) = L^u(k_c)$, so we denote it simply by $L$. The eigenvalue 0 of $L$ is semisimple, and its kernel is spanned by $P_x$ and $\xi$. Let $L^*$ denote the adjoint operator of $L$. $L^*$ has the same properties as $L$. In particular, 0 is also a semisimple eigenvalue of $L^*$ with the associated eigenfunctions denoted by $\phi^*$ and $\xi^*$. Note that $P_x$ is an odd function, since $P$ is an even function. As for the other eigenfunctions, we assume that they fulfil the following properties.

**S5)** $\xi$ and $\xi^*$ are even and $\phi^*$ is odd, and they are normalized so that

$$\langle P_x, \phi^* \rangle_{L^2} = \langle \xi, \xi^* \rangle_{L^2} = 1.$$

The relations $\langle P_x, \xi^* \rangle_{L^2} = \langle \xi, \phi^* \rangle_{L^2} = 0$ hold automatically, because the integrands are odd.

**S6)** $P(x)$, $\phi^*(x)$ and $\xi(x)$, $\xi^*(x)$ are exponentially monotone decaying. That is, there exist $\mathbf{a}$, $\mathbf{a}^*$, $\mathbf{b}$, $\mathbf{b}^* \in \mathbb{R}^n$ and $\alpha > 0$ such that

$$\begin{aligned}
&P(x) \to e^{-\alpha|x|}\mathbf{a}, \quad \xi(x) \to e^{-\alpha|x|}\mathbf{b},\\
&\phi^*(x) \to \pm e^{-\alpha|x|}\mathbf{a}^*, \quad \xi^*(x) \to e^{-\alpha|x|}\mathbf{b}^*
\end{aligned}$$

as $x \to \pm\infty$.

REMARK 6.6. The bifurcation structure **S1)** $\sim$ **S4)** and the symmetry of eigenfunctions **S5)** can be numerically verified (cf. [**289**]) for (6.1). The symmetry properties in **S5)** are natural consequences of the fact that the saddle-node bifurcation is symmetry-preserving, i.e., the associated critical eigenfunction has $\mathbb{Z}_2$-symmetry. Note that the profile of $\xi$, shown in FIGURE 6.13 (b), has a small dent in the middle, which triggers the splitting.

One can observe, from the numerical simulation (FIGURE 6.2 (a)) performed on a large domain, that weak repulsive forces seem to act between localized pulses. Splittings start occurring, which are initiated as an aftereffect of the saddle-node bifurcation followed by large deformation of profile, as the distances between pulses reach a certain length. Let us now examine how the splitting and the weak repulsive interactions through the tails influence each other to give rise to a whole self-replication dynamics. The weak interaction between pulses is described well by approximating the solution profile as a superposition of several shifted copies of a single pulse on the infinite interval. The collection of such superpositions constitutes an approximate local invariant manifold in the phase space. The flow on the manifold then gives a very good description of the weak interaction. The dynamic description we present below, moreover, takes into consideration the unstable process of pulse splitting. Namely, the neutral modes associated with the tangent space of the approximate local invariant manifold include not only ones coming from translational invariance of pulses but also a critical mode that triggers splitting. In this sense, our situation is a typical example of dynamics near a multiple singularity caused by the Euclidean invariance and a critical mode associated with a certain kind of destabilization.

Let us consider the interaction of $N+1$ pulses near the saddle-node point. The location of each pulse is denoted by $x_j$ and the depth of dimple at the onset of splitting is expressed by $r_j\xi(x-x_j)$ for each $j$. Then the first approximation by superposition is given by the following:

$$\begin{aligned} P(x;\mathbf{h}) &= \sum_{j=0}^{N} P(x-x_j), \quad \xi(x;\mathbf{h},\mathbf{r}) = \sum_{j=0}^{N} r_j\xi(x-x_j), \\ S(x;\mathbf{h},\mathbf{r}) &= \sum_{j=0}^{N}\{P(x-x_j)+r_j\xi(x-x_j)\} = P(x;\mathbf{h})+\xi(x,\mathbf{h},\mathbf{r}), \end{aligned}$$

where $x_0 = 0$ and

$$x_j = x_j(\mathbf{h}) = \sum_{i=1}^{j} h_i \ (j \geq 1) \quad \text{for } \mathbf{h} = (h_1, h_2, \cdots, h_N) \in \mathbb{R}^N$$
$$\text{and } \mathbf{r} = (r_0, r_1, \cdots, r_N) \in \mathbb{R}^{N+1},$$

(see FIGURE 6.20).

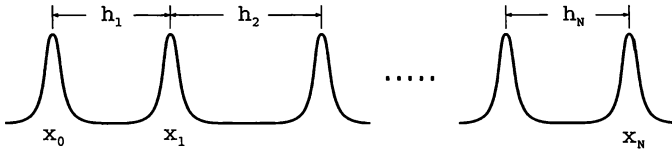


FIGURE 6.20. Weak interaction among pulses

We define the translation operator $\Xi$ by

$$\Xi(l)\mathbf{u} = \mathbf{u}(x - l).$$

By using the operator, we define a set

$$\mathcal{M}(h^*, r^*) = \{\Xi(l)S(\,\cdot\,;\mathbf{h},\mathbf{r}) \mid l \in \mathbb{R}^1,\ \min\mathbf{h} > h^*,\ |r_j| < r^*\},$$

a quantity

$$\delta(\mathbf{h}) = \sup_{x\in\mathbb{R}^1} |\mathcal{L}(P(x;\mathbf{h}))|,$$

and functions

$$\begin{aligned} H_j(\mathbf{h}) &= \langle \mathcal{L}(P(x+x_j;\mathbf{h})), \phi^*\rangle_{L^2}, \\ \widetilde{H}_j(\mathbf{h}) &= \langle \mathcal{L}(P(x+x_j;\mathbf{h})), \xi^*\rangle_{L^2} \end{aligned}$$

for $j = 0, 1, \dots, N$, where $\min\mathbf{h} = \min\{h_1, \dots, h_N\}$. Thanks to **S6)**, $\delta(\mathbf{h}) = O(e^{-\alpha \min \mathbf{h}})$.

Let $\Delta_1 = \Delta_1(\mathbf{h}, \mathbf{r}, \epsilon) = \delta(\mathbf{h}) + |\mathbf{r}|^2 + |\epsilon|$. Then, we have

THEOREM 6.7. *There exist positive constants $h^*$, $r^*$, $\epsilon^*$, $C_0$ and a neighborhood $U$ of $\mathcal{M}(h^*, r^*)$ such that if the initial data $\mathbf{u}(0) \in U$, then there exist functions $l(t) \in \mathbb{R}^1$, $\mathbf{h}(t) \in \mathbb{R}^N$ and $\mathbf{r}(t) \in \mathbb{R}^{N+1}$ such that*

$$\|\mathbf{u}(t) - \Xi(l(t))S(\mathbf{h}(t), \mathbf{r}(t))\|_\infty \le C_0\Delta_1(\mathbf{h}(t), \mathbf{r}(t), \epsilon) \tag{6.6}$$

*as long as $\min\mathbf{h}(t) > h^*$, $|r_j(t)| < r^*$ and $|\epsilon| < \epsilon^*$, where $\mathbf{u}(t)$ is a solution of (6.5). Moreover, the derivatives of $l$, $\mathbf{h}$ and $\mathbf{r}$ are estimated as*

$$\dot{l},\ \dot{\mathbf{h}},\ \dot{\mathbf{r}} = O(\Delta_1). \tag{6.7}$$

We will now give the explicit forms of the equations for $\mathbf{h}$ and $\mathbf{r}$. For this purpose, let us introduce the following constants:

$$\begin{aligned} &M_0 = 2\alpha\langle D\mathbf{a}, \mathbf{a}^*\rangle, \quad \widetilde{M_0} = -2\alpha\langle D\mathbf{a}, \mathbf{b}^*\rangle, \\ &M_1 = \frac{1}{2}\langle F''(P)\xi\cdot\xi, \xi^*\rangle_{L^2}, \quad M_2 = -\langle g(P), \xi^*\rangle_{L^2}. \end{aligned}$$

We assume that these constants satisfy the following condition.

**S7)** The constants $M_0$, $\widetilde{M}_0$, $M_1$ and $M_2$ are all positive.

REMARK 6.8. The sign of the constant $M_0$ determines whether the interaction between pulses is attractive or repulsive. For the Gray-Scott model, **S7)** can be confirmed numerically (see also [**109**]), which implies repulsion.

The nonlinear ODEs for the distance $\mathbf{h}$ among pulses and the depth $\mathbf{r}$ of dimple are given by the following equations. For a fixed $\beta$, $\frac{2}{3}\alpha < \beta < \alpha$, let us define

$$\begin{aligned}
\delta_j &= \delta_j(\mathbf{h}) = e^{-\alpha h_j} + e^{-\alpha h_{j+1}} \ (j = 1, 2, \dots, N-1), \\
\delta_0 &= e^{-\alpha h_1}, \quad \delta_N = e^{-\alpha h_N}, \\
\widehat{\delta}_j &= e^{-\beta h_j} + e^{-\beta h_{j+1}} \ (j = 1, 2, \dots, N-1), \\
\widehat{\delta}_0 &= e^{-\beta h_1}, \quad \widehat{\delta}_N = e^{-\beta h_N}, \\
\Lambda_j &= \Delta_1^{\frac{1}{2}}(\delta_j + |\epsilon|) + (\widehat{\delta}_j + |\epsilon|)|r_j| + \Delta_1^{\frac{1}{2}}|r_j|^2 + |r_j|^3.
\end{aligned}$$

We are ready to state

THEOREM 6.9. *The following equations are valid as long as* $\min \mathbf{h}(t) > h^*$ *and* $|r_j(t)| < r^*$*:*

$$\dot{l} = -H_0(\mathbf{h}) + O(\Lambda_0), \tag{6.8}$$

$$\dot{h}_j = H_{j-1}(\mathbf{h}) - H_j(\mathbf{h}) + O(\Lambda_{j-1} + \Lambda_j), \tag{6.9}$$

$$\dot{r}_j = M_1 r_j^2 - \epsilon M_2 - \widetilde{H}_j(\mathbf{h}) + O(\Lambda_j), \tag{6.10}$$

*where* $H_j$ *and* $\tilde{H}_j$ *are given for* $j = 1, \dots, N-1$ *by*

$$\begin{aligned}
H_j(\mathbf{h}) &= M_0(e^{-\alpha h_{j+1}} - e^{-\alpha h_j})\left(1 + O(e^{-\gamma \min \mathbf{h}})\right), \\
\widetilde{H}_j(\mathbf{h}) &= \widetilde{M}_0(e^{-\alpha h_{j+1}} + e^{-\alpha h_j})\left(1 + O(e^{-\gamma \min \mathbf{h}})\right),
\end{aligned}$$

*and for* $j = 0, N$ *by*

$$\begin{aligned}
H_0(\mathbf{h}) &= M_0 e^{-\alpha h_1}\left(1 + O(e^{-\gamma \min \mathbf{h}})\right), \\
H_N(\mathbf{h}) &= -M_0 e^{-\alpha h_N}\left(1 + O(e^{-\gamma \min \mathbf{h}})\right), \\
\widetilde{H}_0(\mathbf{h}) &= \widetilde{M}_0 e^{-\alpha h_1}\left(1 + O(e^{-\gamma \min \mathbf{h}})\right), \\
\widetilde{H}_N(\mathbf{h}) &= \widetilde{M}_0 e^{-\alpha h_N}\left(1 + O(e^{-\gamma \min \mathbf{h}})\right),
\end{aligned}$$

*with* $\gamma$ *being a suitable positive constant.*

THEOREM 6.10. *There exist* $C_1 > 0$, $C_2 > 0$ *such that* $r_j(t)$ *is monotone increasing with*

$$\dot{r}_j \geq C_2(r_j^2 + |\epsilon| + \widehat{\delta}_j(\mathbf{h})),$$

*as long as* $|r_j| \geq C_1\sqrt{\widehat{\delta}_j + |\epsilon|}$, *while it satisfies*

$$\begin{aligned}(6.11)\qquad \dot{r_j} =&(M_1 + O(\Delta_1^{\frac{1}{2}}))r_j^2 - \epsilon M_2 - \widetilde{H}_j(\mathbf{h}) \\ &+ (\delta_j + |\epsilon|)O(e^{-\gamma \min \mathbf{h}} + \sqrt{|\epsilon|} + |\mathbf{r}|),\end{aligned}$$

*as long as* $|r_j| \leq C_1\sqrt{\widehat{\delta}_j + |\epsilon|}$.

REMARK 6.11. Interesting results of [**97**] and [**98**] show how the two pulses behave, even when the two pulses are not well-separated. These are an analysis in the mildly-strong regime, in between the weak and strong regimes.

**6.4.2. Manner of Splitting: $2^n$-splitting or Edge-splitting.** What is the manner of splitting starting from a single pulse? Naively, one may think that all of the pulses split almost simultaneously and hence the number of pulses increases as $2^n$ after splitting $n$ times. On the other hand, FIGURE 6.2 (a) suggests that only the pulses located at edges are able to split, namely, **edge-splitting**. The goal of this section is to answer the question raised above when the system size is infinite.

By constructing an invariant manifold near the saddle-node point, the flow on it was given as (6.8)∼(6.10), which describes the weak interaction regime and the initial stage of the strong interaction regime (i.e., so long as the depth of the wedge in the middle of the pulse is shallow). It turns out that the weak and strong interactions are not independent. In fact, the onset of splitting is determined through the process of weak interaction. Namely, there exists a distance, called the **critical distance**, such that each pulse does not start splitting until the distance to the neighboring pulses exceeds it, driven by the weak repulsive interaction. Through the analysis of the principal part of (6.8)∼(6.10), we shall prove that pulses at the two ends primarily reach the critical distance before others do, establishing the edge-splitting. Analysis including error estimates (see [**110**]) is not given here, but it gives the same result as what we present below.

### Asymptotic behavior of pulse distances

If the pulses are separated far away from each other and free from instabilities (i.e., $k > k_c$), they are expected to interact only through the tails and move slowly. We discuss this type of **weak interaction** among pulses, and characterize the asymptotic behavior of the distances in between as $t$ tends to $\infty$.

In fact, if the remainder terms are neglected, the system of equations for $h_j(t)$ of (6.9) decouples from $r_j(t)$ as follows:

(6.12)
$$\begin{cases} \dot{h}_1 = -M_0(e^{-\alpha h_2} - 2e^{-\alpha h_1}), \\ \dot{h}_j = -M_0(e^{-\alpha h_{j-1}} - 2e^{-\alpha h_j} + e^{-\alpha h_{j+1}}) \quad (j = 2, \dots, N-1), \\ \dot{h}_N = -M_0(e^{-\alpha h_{N-1}} - 2e^{-\alpha h_N}), \end{cases}$$

where $\dot{h}$ stands for $\frac{dh}{dt}$. Note that (6.12) is exactly the same ODEs derived under the assumption that the pulse is stable. For later use, it is more convenient to introduce new variables : $G_j = M_0 e^{-\alpha h_j}$ and a new time scale $t \to \alpha t$. In terms of $G_j$, (6.12) becomes

(6.13)
$$\begin{cases} \dot{G}_1 = (G_2 - 2G_1)G_1, \\ \dot{G}_j = (G_{j-1} - 2G_j + G_{j+1})G_j \quad (j = 2, \dots, N-1), \\ \dot{G}_N = (G_{N-1} - 2G_N)G_N, \end{cases}$$

where we used the same notation $t$ for the new time. By the definition of $G_j$, we only need to consider (6.13) in the non-negative region. Since $M_0 > 0$, thanks to **S7)** and REMARK 6.5, the interaction is of repulsive type; that is, adjacent pulses repel each other. Intuitively, it seems clear that the distance between pulses eventually diverges as time goes to $\infty$. Here the main issue is to clarify the order of divergence with respect to $t$ and the ordering among the pulses. In particular, we shall prove the following.

PROPOSITION 6.12. *Suppose that $h_j(0) < l$ $(j = 1, \dots, N)$ holds for a given $l > 0$. Then $h_1$ and/or $h_N$ first attains $l$ for some finite $t^*$, i.e., $h_j(t^*) = l$ $(j = 1$ and/or $N)$.*

The proof follows from several lemmas, stated below.

LEMMA 6.13. *It follows from* (6.12) *that if $\max_{j=2,\dots,N-1} h_j$ is larger than $h_1$ and $h_N$, then $\max_{j=2,\dots,N-1} h_j$ is a strictly monotone decreasing function of $t$.*

The proof of this lemma is left to the reader, since it is a direct consequence of the form of (6.13). In terms of $G_j$, PROPOSITION 6.12 is equivalent to the following:

> *For a given constant $L > 0$, suppose that the conditions $G_j(0) > L$ are satisfied for all $j$. Then $G_1$ and/or $G_N$ first attain(s) $L$ at $t = t^*$.*

In order to prove this, we first show that the lengths of internal intervals never reach $L$ primarily for finite time.

LEMMA 6.14. *If $G_j(0) > L$ for all $j$, then each $G_j$ for $j = 2, \dots, N-1$ never attains the value $L$ primarily in finite time.*

PROOF. Whenever the inequalities $G_j > L$ hold, we have

$$\begin{aligned}\dot{G}_j &= (G_{j-1} - 2G_j + G_{j+1})G_j \\ &\geq (2L - 2G_j)G_j \qquad (j = 2, \dots, N-1).\end{aligned}$$

Hence

$$\frac{\dot{G}_j}{(2L - 2G_j)G_j} \leq 1,$$

$$\frac{1}{L}\left(\frac{\dot{G}_j}{2L - 2G_j} + \frac{\dot{G}_j}{2G_j}\right) \leq 1,$$

$$\frac{d}{dt}\left(\frac{\log G_j}{2} - \frac{\log |L - G_j|}{2}\right) \leq 1. \tag{6.14}$$

Suppose $G_j = L$ holds primarily at $t = t_c$. Then after integrating (6.14), we have

$$\int_0^{t_c} \frac{d}{dt}\left(\frac{\log G_j}{2} - \frac{\log |L - G_j|}{2}\right) dt \leq \int_0^{t_c} 1 dt,$$

$$\left[\frac{\log G_j}{2} - \frac{\log |L - G_j|}{2}\right]_0^{t_c} \leq t_c.$$

This implies that $G_j \to L$ is equivalent to $t_c \to +\infty$. □

The following comparison lemma is crucial in characterizing the asymptotic behavior of (6.13).

LEMMA 6.15. *Suppose that $U_j$ and $V_j$ $(j = 1, \dots, N)$ are bounded solutions of (6.13) and satisfies $U_j(0) > V_j(0)$. Then $U_j(t) > V_j(t)$ holds for $t \in [0, +\infty)$.*

PROOF. Let $W_j = U_j - V_j$; then

$$\begin{aligned}\frac{dW_j}{dt} &= (\Delta U)_j U_j - (\Delta V)_j V_j \\ &= U_j(\Delta(U-V)_j) + (U_j - V_j)(\Delta V)_j \\ &= U_j(\Delta W)_j + (\Delta V)_j W_j,\end{aligned}$$

where $(\Delta U)_j = U_{j-1} - 2U_j + U_{j+1} (j = 1, \dots, N)$ and $U_0 = U_{N+1} = 0$. Moreover let $\psi_j = e^{ct} W_j$ with $c \in \mathbb{R}$; then it satisfies

$$\begin{aligned}\frac{d\psi_j}{dt} &= ce^{ct} W_j + e^{ct} \frac{dW_j}{dt} \\ &= ce^{ct} W_j + e^{ct}(U_j(\Delta W)_j + (\Delta V)_j W_j) \\ &= U_j(\Delta\psi)_j + (c + (\Delta V)_j)\psi_j.\end{aligned} \tag{6.15}$$

Here $(\Delta V)_j$ remains bounded; $c + (\Delta V)_j$ is negative for sufficiently small $c$ for all time. Suppose that $\psi_{j_0}$ ($j_0 \in \{1, \dots, N\}$) first becomes negative at $t = t_0$. We have

$$\frac{d\psi_{j_0}}{dt}(t_0) < 0, \tag{6.16}$$

replacing $t_0$ by a suitable one, if necessary. On the other hand, since $c + (\Delta V)_{j_0} < 0$, the right-hand side of (6.15) with $j = h_0$ is positive:

$$U_{j_0}(\Delta\psi)_{j_0} + (c + (\Delta V)_{j_0})\psi_{j_0} > 0, \tag{6.17}$$

which is a contradiction. □

In order to characterize the asymptotic behavior of $G_j(t)$, we introduce new unknowns $K_j$ and a new time $T$ as

$$G_j(t) = K_j(\log t)/t \quad \text{and} \quad T = \log t.$$

Then $K_j(T)$ satisfies

$$\begin{cases} K_1' = (K_2 - 2K_1)K_1 + K_1, \\ K_j' = (K_{j-1} - 2K_j + K_{j+1})K_j + K_j, \\ K_N' = (K_{N-1} - 2K_N)K_N + K_N, \end{cases} \tag{6.18}$$

where $K'$ denotes $\frac{dK}{dT}$.

LEMMA 6.16. *There exist two equilibrium points,* $(0, \dots, 0)$ *and* $(\overline{K}_1, \cdots, \overline{K}_N)$, *for* (6.18) *in non-negative space, where*

$$\overline{K}_j = \frac{j}{2}(N - j + 1).$$

*$K_j(T)$ remains $O(1)$ (i.e., $G_j = O(1/t)$) and $K_j$ $(j = 1, \dots, N)$ converges to $\overline{K}_j$ as $T$ tends to $\infty$.*

PROOF. The proof for the first half can be checked in a straightforward way; hence we focus on the second part.

First of all, it is easy to check that

$$(G_1, \dots, G_N) = \left(\overline{K}_1/(t+t_1), \dots, \overline{K}_N/(t+t_1)\right)$$

is a solution of (6.13). Take appropriate $t_1$ and $t_2$ so that $(G_1(0), \dots, G_N(0))$ and $(\overline{K}_1, \dots, \overline{K}_N)$ satisfy the following inequalities:

$$\left(\frac{\overline{K}_1}{t_1}, \dots, \frac{\overline{K}_N}{t_1}\right) < (G_1(0), \dots, G_N(0)) < \left(\frac{\overline{K}_1}{t_2}, \dots, \frac{\overline{K}_N}{t_2}\right). \tag{6.19}$$

In view of LEMMA 6.15, for $t \in [0, +\infty)$

$$\left(\frac{\overline{K}_1}{t+t_1}, \dots, \frac{\overline{K}_N}{t+t_1}\right) < (G_1(t), \dots, G_N(t)) < \left(\frac{\overline{K}_1}{t+t_2}, \dots, \frac{\overline{K}_N}{t+t_2}\right), \tag{6.20}$$

which clearly shows that $G_j = O(1/t)$. Moreover, for each $j$, we have

$$\frac{t\overline{K}_j}{t+t_1} < tG_j(t) < \frac{t\overline{K}_j}{t+t_2}, \tag{6.21}$$

$$\lim_{t\to\infty} \frac{t\overline{K}_j}{t+t_1} < \lim_{t\to\infty} tG_j(t) < \lim_{t\to\infty} \frac{t\overline{K}_j}{t+t_2}. \tag{6.22}$$

We conclude that

$$\lim_{T\to\infty} K_j(T) = \lim_{t\to\infty} tG_j(t) = \overline{K}_j. \tag{6.23}$$

□

Now we are ready to prove PROPOSITION 6.12.

PROOF. LEMMA 6.14 implies that $G_j$ $(j = 2, \cdots, N-1)$ do not attain $L$ in finite time as long as $G_1 > L$ and $G_N > L$ are satisfied, where $L = e^{-\alpha l}$. On the other hand, it follows from LEMMA 6.16 that $G_j$ $(j = 1, 2, \cdots, N)$ decreases with the order $O(1/t)$, which leads to the conclusion. □

### Critical distance and edge splitting

In the previous section we discussed the weak repulsive interaction among pulses, and we showed that edge distances eventually primarily reach $l$ for a given $l$. In this subsection we take into account

the deformation of pulses, i.e., $r_j$ measuring the depth of dimple for each pulse (see (6.10)). The dynamics of $r_j$ is completely determined, once $\{h_j\}_{j=1}^N$ are known and the remainder terms in (6.10) are neglected. In fact, the resulting ODE has a quadratic nonlinearity and has two equilibrium points, unless $h_j$ and $h_{j+1}$ exceed the length defined by

$$-\epsilon M_2 - \widetilde{M}_0(e^{-\alpha h_{j+1}} + e^{-\alpha h_j}) = 0.$$

Note that the sign of $\epsilon$ corresponds to which side of the saddle-node point the parameter $k$ is chosen on (see FIGURE 6.19). Once the left-hand side of the last equation becomes positive (i.e., $\epsilon < 0$), the equation (6.10) ceases to have equilibria and its solution $r_j$ now can cross zero and grow large, i.e., initiation of splitting. The minimum of the above length is given by edge pulses, namely,

$$-\epsilon M_2 - \widetilde{M}_0 e^{-\alpha h_j} = 0 \qquad (j = 1 \text{ or } N).$$

For negative $\epsilon$, **the critical distance** $\ell_c$ is defined by

$$e^{-\alpha \ell_c} = -M_2 \varepsilon / \widetilde{M}_0. \tag{6.24}$$

When $r_j = 0$ is satisfied for some $j$, we say that the **onset of splitting** occurs for the $j$-th pulse. The goal of this subsection is to show that the onset of splitting primarily occurs only at edge pulses under natural assumptions for initial conditions. We prove this for the principal part of ODEs (6.8)$\sim$(6.10) in the following discussions. Based upon such discussions, one can rigorously describe successive edge splitting starting from a single pulse. However, we skip this and refer for the details to [**111**] and [**110**].

It is obvious that if all the pulses are separated sufficiently far, they immediately start splitting simultaneously. Therefore the interesting question is what would happen when each distance is initially less than the critical one. Let us therefore assume the following for the initial data $h_j(0)$ and $r_j(0)$.

**H1** The initial values $h_j(0), r_j(0)$ belong to the weak-interaction regime, i.e., $\min \mathbf{h}(t) > h^*$ and $|r_j(t)| < r^*$, and satisfy the following inequalities:

$$\begin{aligned} &e^{-\alpha h_1(0)} > e^{-\alpha \ell_c}, \quad e^{-\alpha h_N(0)} > e^{-\alpha \ell_c}, \\ &e^{-\alpha h_j(0)} > \frac{e^{-\alpha \ell_c}}{2} \qquad (j = 2 \ldots, N-1), \end{aligned} \tag{6.25}$$

where $\ell_c$ is the critical distance defined by (6.24). The initial data for $r_j$ satisfies

$$r_j(0) < 0 \qquad (j = 0 \dots, N), \tag{6.26}$$

Moreover, $r_j(0)$ is smaller than the unstable equilibrium point.

REMARK 6.17. When we take account of remainder terms, we need the following assumption, in addition to the above one, for $r_j(0)$:

$$|r_j(0)| \le C_1 \sqrt{\widehat{\delta}_j(0) + |\epsilon|}, \tag{6.27}$$

where the positive constant $C_1$ appears in THEOREM 6.7.

The principal part for $l, h_j, r_j$ is given by

$$\dot{l} = -M_0 e^{-\alpha h_1}, \tag{6.28}$$

$$\dot{h}_1 = -M_0(e^{-\alpha h_2} - 2e^{-\alpha h_1}), \tag{6.29}$$

$$\dot{h}_j = -M_0(e^{-\alpha h_{j-1}} - 2e^{-\alpha h_j} + e^{-\alpha h_{j+1}}), \tag{6.30}$$

$$\dot{h}_N = -M_0(e^{-\alpha h_{N-1}} - 2e^{-\alpha h_N}), \tag{6.31}$$

$$\dot{r}_0 = M_1 r_0^2 - \epsilon M_2 - \widetilde{M}_0 e^{-\alpha h_1}, \tag{6.32}$$

$$\dot{r}_j = M_1 r_j^2 - \epsilon M_2 - \widetilde{M}_0(e^{-\alpha h_{j+1}} + e^{-\alpha h_j}), \tag{6.33}$$

$$\dot{r}_N = M_1 r_N^2 - \epsilon M_2 - \widetilde{M}_0 e^{-\alpha h_N}. \tag{6.34}$$

PROPOSITION 6.18. *Under the assumption* **H1**, *for sufficiently small* $|\epsilon|$, *the onset of splitting occurs primarily for* $h_1$ *and/or* $h_N$. *Namely, edge-distance is the first to attain the critical value, and* $r_0$ (*and/or* $r_N$) *crosses* 0 *primarily and becomes strictly positive while* $r_j$ ($j = 2, \dots, N-1$) *remain negative.*

PROOF. We prove that $h_1$ (and/or $h_N$) is (are) the first to reach the critical distance $\ell_c$. In order for the $j$-th pulse ($j = 2, \dots, N-1$) to split, the inequality $e^{-\alpha h_{j+1}} + e^{-\alpha h_j} < e^{-\alpha \ell_c}$ must hold, which implies that either $e^{-\alpha h_j}$ or $e^{-\alpha h_{j+1}}$ has to be strictly smaller than $e^{-\alpha \ell_c}/2$. On the other hand, it follows from **H1** and PROPOSITION 6.12 that either $e^{-\alpha h_1}(t) = e^{-\alpha \ell_c}/2$ or $e^{-\alpha h_N}(t) = e^{-\alpha \ell_c}/2$ is attained before the internal ones $e^{-\alpha h_j}(t)$ ($j = 2, \dots, N-1$) become smaller than $e^{-\alpha \ell_c}/2$. Namely, edge pulses already start splitting before internal ones do. Now we will show that the wedge depth for edge pulses $r_0$ (and/or $r_N$) becomes strictly positive, while internal ones remain negative. Let us take an appropriate constant $c$ ($1 < c < 2$) so that $e^{-\alpha \ell_c}/2 \le e^{-\alpha h_1}, e^{-\alpha h_N} \le e^{-\alpha \ell_c}/c$. It follows from LEMMA 6.16 that

it takes at least time $O(1/|\varepsilon|)$ for $e^{-\alpha h_1}$ (and/or $e^{-\alpha h_N}$) to change from $e^{-\alpha \ell_c}/c$ to $e^{-\alpha \ell_c}/2$. On the other hand, we have

$$\dot{r}_0 = M_1 r_0^2 - \epsilon M_2 - \widetilde{M}_0 e^{-\alpha h_1} \tag{6.35}$$

$$\geq M_1 r_0^2 - \epsilon M_2 - \frac{\widetilde{M}_0 e^{-\alpha \ell_c}}{c} \tag{6.36}$$

$$= M_1 r_0^2 - \left(1 - \frac{1}{c}\right) M_2 \epsilon. \tag{6.37}$$

Let $t_0$ be the time when $e^{-\alpha h_1}$ (and/or $e^{-\alpha h_N}$) reach(es) $e^{-\alpha \ell_c}$. If $r_0$ (and/or $r_N$) is (are) already positive, the proof is done. If not, let $t_1$ be the time when, say $r_0 = \bar{r} > 0$, and $p = (1 - 1/c)M_2 > 0$. Then, from (6.37),

$$t_1 - t_0 \leq \frac{1}{M_1 \sqrt{-p\epsilon}} \arctan\left(\frac{r_0}{\sqrt{-p\epsilon}}\right)\Bigg|_{r_0 = r_0(t_0)}^{\bar{r}} \sim O\left(\frac{1}{\sqrt{|\epsilon|}}\right). \tag{6.38}$$

This implies that it takes only $O(1/\sqrt{|\epsilon|})$ for $r_0$ (and/or $r_N$) to cross 0 and become positive. Recall that the differential inequality (6.37) holds for the much longer time $O(1/|\epsilon|)$. Combining the above discussions, we conclude that $r_0$ (and/or $r_N$) become(s) positive before $e^{-\alpha h_N}$ becomes $e^{-\alpha \ell_c}/2$ for sufficiently small $|\epsilon|$. □

Finally we briefly touch on the successive splitting from a single symmetric 1-pulse. It is clear from (6.8)∼(6.10) that the reflectional symmetry at the center of the initial pulse survives for all time. After initiation of splitting, the wedge depth becomes deeper, and then two new pulses are born, but they are not yet well-separated. Since the description of this process is beyond our analysis for the moment, some assumptions are necessary to study the successive splitting, namely, the existence of an orbit connecting the initial stage of splitting to the next stage of the weak-interaction regime. Under those assumptions, we can prove the edge-splitting for all time for the principal part of ODEs (6.8)∼(6.10), see [**110, 111**].

REMARK 6.19. The methods described in this section are equally effective on sufficiently large intervals. For problems on finite intervals, such as in the Gray-Scott model in which pulse interaction is repulsive and the boundary conditions are of homogeneous Neumann

type, the solution profile converges to a stable spatially-periodic equilibrium solution after experiencing several splitting stages. The spatial period of the latter equilibrium is determined by the length of the interval and the critical distance.

## 6.5. Spatio-Temporal Chaos and Heteroclinic Cycle

As we have already witnessed, what is vivid and hence of more interest to us is the intermediate dynamical process rather than the ultimate dynamics. As we will see below, the spatio-temporal chaos passing through several ordered states is a typical example of transient dynamics in the sense above, as well as a recurrent dynamics. In order to understand such transient dynamics, the geometric viewpoint based on global bifurcation pictures employed above again plays an important role. In the following discussions, we will describe the outline of the procedure of dealing with such dynamics, referring to [**290**] for details.

The pictures in FIGURE 6.21 are results of a numerical simulation performed for the Gray-Scott model. As one can seen in the left side picture, the solution stays near one state for a period of time and after a while make a transition to another state, and seems to repeat this kind of behavior indefinitely.

The behavior is certainly different from a pure random one, because in a short time scale one can observe that the solution stays near an ordered state. We claim that this is a special case of spatio-temporal chaos. To understand such a behavior, our strategy is not to display evidences of chaos by employing various statistical quantities, even though such quantities give important pieces of information. What we would like to discuss is whether there is a geometric viewpoint that allows us to understand what kind of spatial patterns a solution orbit goes through and why it behaves in such a manner. Let us deal with the questions along the following steps:

1. Identify the dynamism of self-reproduction.
2. Identify the self-destruction mechanism.
3. Construct a dynamic self-reproduction and self-destruction cycle by combining the previous two in an appropriate way.

This is an attempt to construct a heteroclinic cycle in an infinite dimensional phase space. A precursor of such an idea has already been employed in [**256**]. Since the first stage of self-reproduction dynamics has already been described, we now consider the self-destruction process in the second step above.

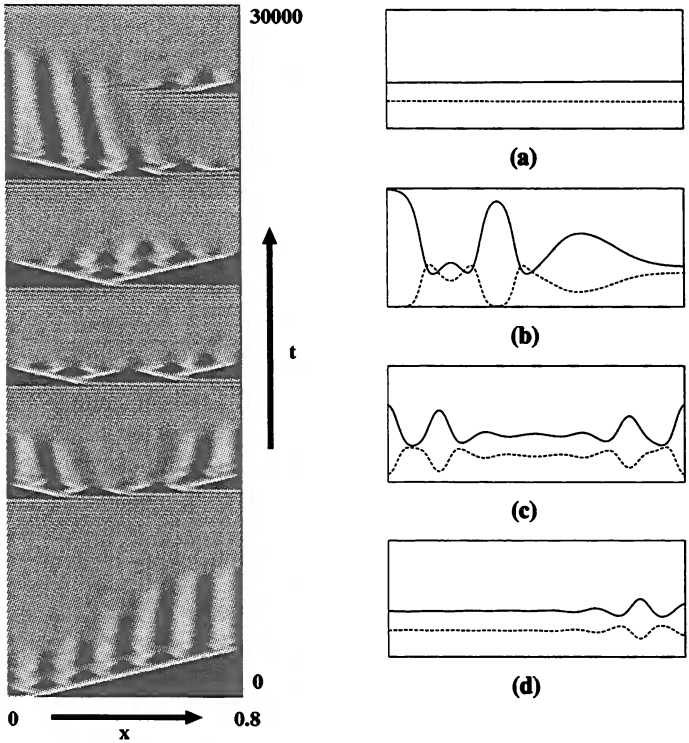


FIGURE 6.21. Spatio-temporal chaotic patterns in the Gray-Scott model ($D_u = 2 \times 10^{-5}$, $D_v = 10^{-5}$, $F = 0.035$, $k = 0.05632$ and $L = 0.8$). The profiles on the right exhibit a cycle of characteristic behaviors, starting from a nearly constant state $P$, settling down to $(1, 0)$ on several spatial subintervals to ignite self-replication waves, pretending to be a stationary pattern for a while before breaking down through a self-collapsing process, and returning near the original state $P$.

**6.5.1. Self-destruction.** In conventional pattern formation theory, as its name indicates, the main theme is to describe the spontaneous formation of a spatially non-uniform state from a uniform one through fluctuation. The reverse direction, i.e., a destruction

process, however, is equally important in transient dynamics. In fact, if destruction processes of what has been constructed are missing, then systems in general may not be able to change from one state to another successively. What, then, do we mean when we say that dissipative structures undergo a self-destruction process? One can think of two ways in which a pattern collapses. In one, the pattern collapses by itself, without interacting with others. The other way is that it collapses because of a strong interaction with others (usually copies of itself). A well known example of the latter is the pair annihilation of travelling pulses in the FitzHugh-Nagumo equation (with the diffusion coefficient $D$ of the inhibitor being zero or small), upon head-on collision. As was shown in FIGURE 6.8, however, the same pulse undergoes a self-destruction process for specific parameter values.

To our surprise, it turns out that the principle of self-destruction is the same as that of self-replication. The only difference is that the destiny of the unstable manifold is a stable *constant* equilibrium in the case of self-destruction, and hence the solution profile plunges into the trivial state, instead of increasing the number of humps, which is already exemplified in FIGURE 6.22.

Let us observe the self-destruction process in a numerical simulation of the Gray-Scott model. We consider the self-destruction of a 6-hump (=12-mode) equilibrium solution. The number 6 is chosen for convenience in later discussions. We obtain the bifurcation diagram in FIGURE 6.22, tracing the branches of equilibria by using AUTO. One can see that a saddle-node bifurcation point exists in the diagram, and it originates from the 6-hump (12-mode) equilibrium created by a subcritical bifurcation from the branch of constant equilibria (denoted by $P$). Immediately after the bifurcation, the branch of the 6-hump solutions and the $P$-branch are connected by the unstable manifold, and this situation continues up to the saddle-node bifurcation point $k = k_{\min}$. Note that the constant equilibria on the $P$-branch recover their stability at the Hopf bifurcation point $k = k_{\text{Hopf}}$. Since the 6-hump equilibrium solutions branch off from the $P$-branch at an unstable equilibrium, they are unstable immediately after the bifurcation. However, they recover stability at the turning point $k = k_{\min}$, thus being able to accommodate the destinies of orbits that have undergone self-replication processes. If we choose the parameter $k$ slightly less than $k_{\min}$ and start from an initial value with a 6-hump cosine-like function, the solution profile evolves

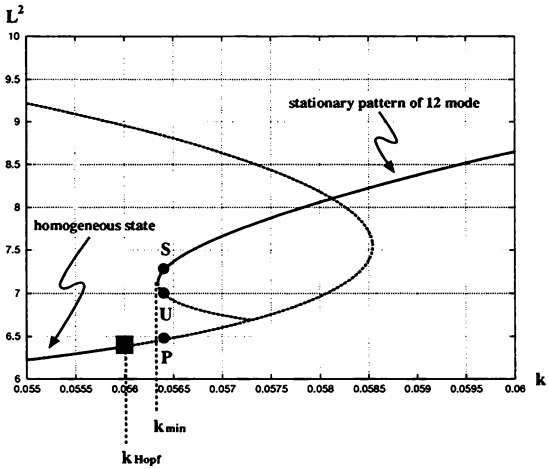


FIGURE 6.22. The saddle-node bifurcation created by the branch of 12-mode equilibria bifurcated from a $P$-branch of constant equilibria. The self-destruction of the 12-mode solution into $P$ occurs when the parameter $k$ is chosen slightly less that $k_{\min} \approx 0.0573408$. Compare FIGURE 6.23.

as in FIGURE 6.23. The solution shapes itself quickly into a 6-hump equilibrium from the 6-hump cosine-like profile, keeps the state for a while, and eventually collapses into a uniform state. In this case, the dimension of the unstable manifold of the unstable equilibrium $U$ is 1, and the manifold is connected to $P$. Even if the initial profile is a rather large perturbation from a cosine-like function, the solution shapes itself into a 12-mode (6-hump) profile, and thereafter follows the same course of events as above. This means that the basin of the self-destruction process is rather large.

## 6.6. Construction of a Heteroclinic Loop

We now embark on constructing a cycle of construction-destruction dynamics by appropriately combining the self-replication process (in which patterns of the same profile as the original are successively produced) and the self-destruction process (in which the created patterns collapse). In FIGURE 6.14, the solution does not change once it settles down to 4-hump equilibrium after two steps of self-replication.

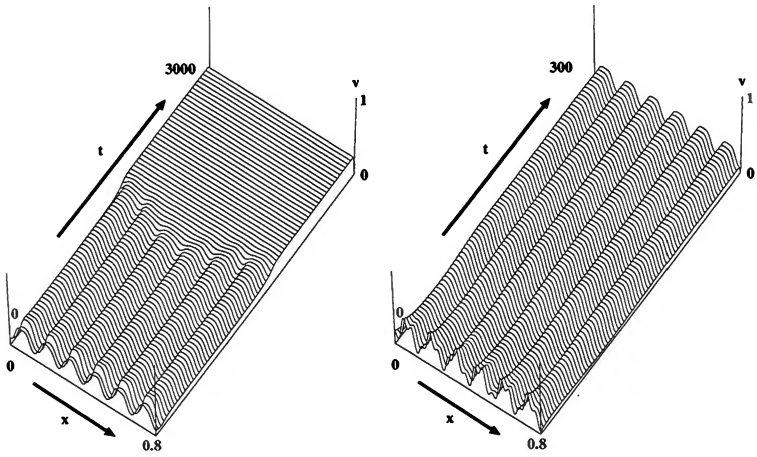


FIGURE 6.23. (a) The aftereffect of the unstable manifold connecting the saddle-node bifurcation point to $P$ in FIGURE 6.17, when the initial condition is a 12-mode cosine function. The solution profile approaches that of a 6-hump solution once, and then collapses to $P$. (b) Even if the initial condition is perturbed rather strongly from the cosine one, the solution shapes itself into a 6-hump solution, and collapses to the constant equilibrium, following the same course of events as (a). Parameter values are $F = 0.040$, $k = 0.05772$, $L = 0.8$ for both (a) and (b).

If the equilibrium at the final step is on a branch of a saddle-node bifurcation, such as that discussed in the previous subsection, one can adjust parameters so that it collapses to the constant state $P$. If the state $P$ is stable, however, the dynamic process stops there, and cannot pass through other states indefinitely. Therefore, in order to have a chaotic cycle, $P$ must be unstable, so that the orbit approaches $P$ along its stable manifold during the self-destruction process, and then escapes from it along its unstable manifold in the direction to produce a spatial pattern again. We need to see whether the answers to the following are affirmative:

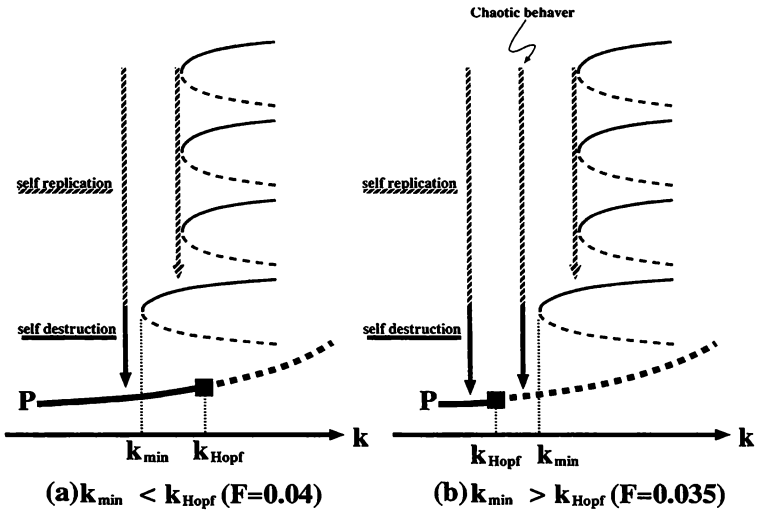


FIGURE 6.24. (a) $F = 0.04$. Since $k_{\text{min}} < k_{\text{Hopf}}$, both self-replication and self-destruction occur. However, once the orbit settles down to $P$, which is stable, it remains there forever. (b) $F = 0.035$. Since $k_{\text{Hopf}} < k_{\text{min}}$, it is possible to choose a parameter $k$ for which self-destruction to $P$ occurs and $P$ is unstable. In this case spatio-temporal chaos is possible.

1. Are there parameter values for which self-replication and self-destruction occur simultaneously and repeatedly?
2. Do the stable and unstable manifolds of $P$ have the saddle structure described above?

The global configuration and stability properties of bifurcation solutions again play decisive roles in answering these questions. The bifurcation diagrams of equilibria and the constant solution $P$ in the Gray-Scott model for parameter values $F = 0.04$ and $K = 0.035$, respectively, are schematically depicted for the sake of explanation in FIGURE 6.24 (see [**290**] for more detailed diagrams). These two diagrams may look the same at first glance, but there is a big difference in the relative position between $k_{\text{min}}$ and $k_{\text{Hopf}}$. As one can read off from the pictures, $k_{\text{min}}$ is the minimum value among the saddle-node bifurcation points and hence is the threshold to determine whether

self-destruction occurs or not. The constant equilibrium $P$ undergoes a Hopf bifurcation at $k_{\text{Hopf}}$, where it recovers stability. In both cases of FIGURE 6.24, one can observe self-replication and self-destruction patterns, respectively, on the broken and solid parts of the arrows. However, in case (a), if the parameter is chosen with $k < k_{\min}$ so that self-destruction is possible, the orbit settles down to $P$ after self-destruction, since $P$ is stable. On the other hand, in case (b), where $k_{\text{Hopf}} < k_{\min}$, if the parameter $k$ is chosen with $k_{\text{Hopf}} < k < k_{\min}$, the orbit after self-destruction to the unstable state $P$ escape from it and possibly passes through various states indefinitely. In fact, for $k = 0.05632$ the solution behaves as in FIGURE 6.21. We may thus conclude that $k_{\min} = k_{\text{Hopf}}$ is the threshold value to predict whether spatio-temporal chaos emerges or not.

As is seen in FIGURE 6.21, it is clearly visible that ordered states emerge and disappear. What is the origin of such an iteration of spatially ordered states? One can confirm *formally* at $k = k_{\min}$ that there is a heteroclinic cycle as in FIGURE 6.24 on the infinite line $\mathbb{R}$. This provide us with an answer to the question raised earlier: *What kind of spatial patterns does a chaotic orbit experience?* If we shift the parameter slightly, spatio-temporal chaos emerges from this heteroclinic cycle, reminding us of the Shilnikov-bifurcation or the homoclinic tangle in finite dimensional chaos theory.

We thus realize that we can characterize the spatio-temporal chaos described above only through arguments based on global solution structures, not by reducing the analysis near the onset to that of lower dimensional ordinary differential equations.

## 6.7. Concluding Remark

We have considered, through several examples, what are the mathematical mechanisms that drive complicated transient pattern dynamics in dissipative systems. Since the dynamics takes place in an infinite dimensional phase space, it is very much a challenge to try to describe in detail how an orbit behaves in relation to other solutions. Recent developments in our computational ability have enabled us to pursue such an attempt to a certain degree. Thanks to such studies, we have been able to clarify, to some extent, the skeleton structure and guiding principle needed to understand the complex dynamics in partial differential equations of dissipative type. Probably, the most important thing is that the information gained from this will give us hints on constructing a framework of mathematical

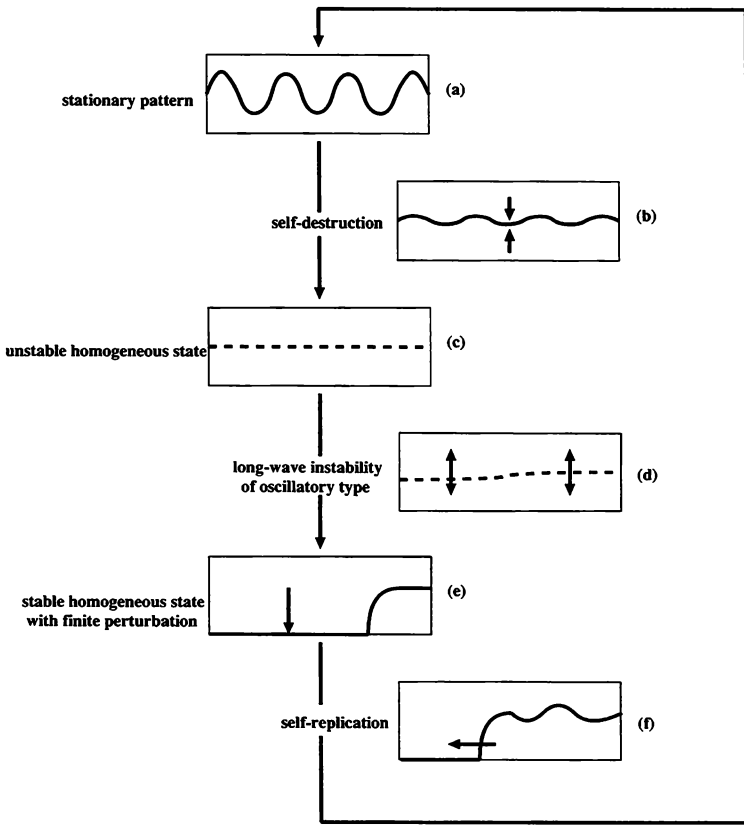


FIGURE 6.25. Heteroclinic cycle on the infinite line passing through an unstable homogeneous state $P$, $(1,0)$, and a spatially periodic pattern. Strictly speaking, such a cycle does not exist on a finite interval, since $(1,0)$ is stable in the PDE sense. However, after replacing $(1,0)$ by $(1,0)$ *with trigger* (the resulting cycle is called a *generalized* heteroclinic cycle), we can observe an aftereffect of the generalized cycle numerically as shown in FIGURE 21. Here, $(1,0)$ *with trigger* means that there is some portion of the interval where $(u,v)$ is not equal to $(1,0)$ and from which a replication wave can start propagating. Such a generalized cycle can be defined at $k = k_{\min}$ in FIGURE 6.24 (b).

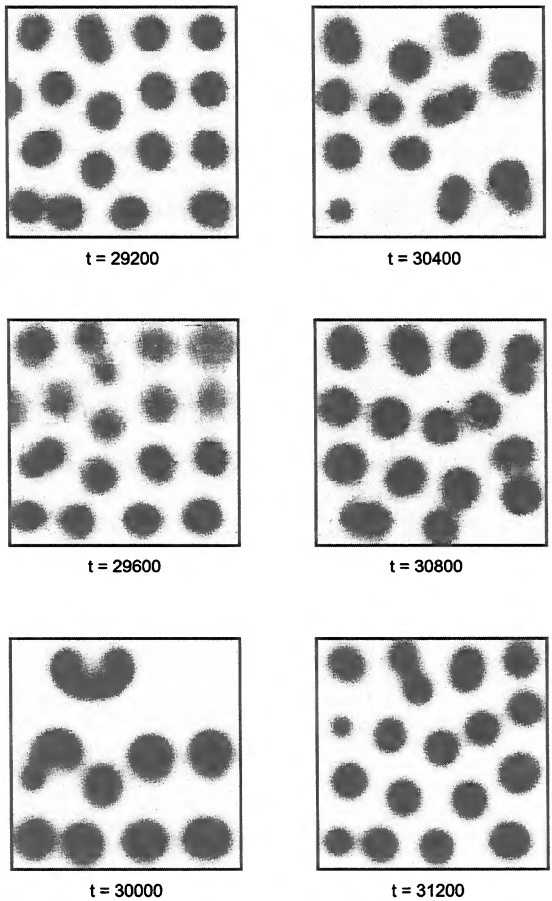


FIGURE 6.26. Two-dimensional spatio-temporal chaos in the Gray-Scott model. $D_u$ and $D_v$ are the same as in FIGURE 6.2, and $F = 0.018$, $k = 0.054$, $L \times L = 1.0 \times 1.0$. Self-replication and self-destruction coexist, which makes the following cycle locally in space. Several spots disappear almost simultaneously due to crowdedness ($t = 30000$); then the remaining spots have enough resources to split and fill the space ($t = 30800$), which causes crowdedness again.

theory. Although we omitted the details, we can give a rigorous proof to parts of what we have described above, which in turn tells us about essential ingredients. We are thus able to give universality to a phenomenon observed in a particular model. To set up a framework of standing hypotheses, imagination based on numerical simulation is very helpful.

REMARK 6.20. A similar type of spatio-temporal chaos consisting of creation and destruction of spots can be observed also in two-dimensional space as in FIGURE 6.26. Several spots disappear almost simultaneously; then the surrounding spots start to replicate and invade the empty zone. After the domain is filled up with almost identical spots, then, after some time, several spots die out unpredictably. This process continues indefinitely.

# Future Perspectives

Mathematics for pattern formation is diverse and has deep relationships with other sciences. The description of spiral waves in CHAPTER 4, for example, involves chemistry experiments, modeling, numerical simulations, and qualitative theories of nonlinear dynamics as a framework, each giving a feedback to others. It is easy to talk about the integral relationship among these aspects, but it is very difficult in reality to fully undertake any one of them. Even though one single individual may not cover all of these aspects, it is impossible in reality to capture the whole picture of the phenomenon if one neglects the multi-faceted character of the matter. In the sequel, I will display my personal viewpoints related to these aspects from a rather broad standpoint. Constructive criticisms are very much welcome.

## The First Principle and Phenomenology

Most of the model equations treated in this book are phenomenological ones. In this sense, their role is different from that played by the Navier-Stokes equation in fluid dynamics. For example, as a model system of equations describing the transmission of nerve-impulses, the Hodgkin-Huxley equation (whose simplified version is the FitzHugh-Nagumo equation) is well known. Its derivation is based on many experiments and physical considerations, as well as on intuitions gained from experience and qualitative reasoning. This situation substantially differs from the case of the Navier-Stokes equation in which the governing equations with several parameters are uniquely derived from fundamental hypotheses (the first principles) on fluids. In order to make the Hodgkin-Huxley equation more accurate, for example, it is necessary to do more realistic parameter fittings based on a lot of detailed experimental data. It is easily seen, however, that such a direction of study unnecessarily complicates the model and is

expensive. This reminds us of a centipede strolling along graciously, who suddenly gets confused when asked how it could control so many legs all at once in such a harmonious way.

One loses sight of the essence if too much emphasis is placed on details. It is therefore more and more urgent to propose, from the standpoint of mathematics, qualitative models which capture the essence of a huge complicated system with a lot of substrata. Our time is already such an age. Mathematics is indispensable in dealing with the dynamics of the financial market and large communication network systems. How is it possible to build highly reliable qualitative models? Naturally, there is no simple almighty answer to such a question. One approach may be the method of exploiting differences in scales, discussed in this book, to describe dynamics from coarse-grained viewpoints. Also interesting are the ideas of systematically integrating dynamical behaviors gained in each scale and considering interactions between them. As the self-replication models and chaos theories in CHAPTER 6 suggest, a simple model or principle can produce highly complicated dynamics. We can give, to a certain extent, theoretical predictions of such complicated dynamics. For example, it has recently been reported ([**175**]) that the Sierpinsky gasket structure is realized as a spatio-temporal pattern in a reaction-diffusion system. The comparison between the Navier-Stokes equation and the Hodgkin-Huxley equation is due to an article (AMS Notices **45**(9) 1998) by John Guckenheimer, which is worthwhile reading.

### From Matter to Dynamism

One may think that the standpoint of gene analysis is antipodal position to what we have presented in this book, but this may not be necessarily so. The work by Kondo et al. in [**229**] has received much attention because it claims that the phenomenological model (the Turing model described in CHAPTER 4) can predict to high accuracy the development of fish coat patterns. A cautious researcher may say about the result that it imitates the phenomenon in detail but fails to explain its essence. The viewpoint of Kondo et al., on the contrary, seems to advantageously claim that the *essence* is nothing more than what is revealed by the model. Moreover, they have made a step forward, recently, to try to relate a specific gene to the role of

a parameter in the model, namely, to try to identify a genetic control with parameter adjustment.

What does this mean? It is highly probable that a simple qualitative model, which is the remotest from reality, can give, precisely because it is so, an explanation of macroscopic dynamics. One of the missions of modern science has been to identify an ultimate matter, such as genes. While the mission has been successful, it simultaneously has gotten rid of dynamical viewpoints. Matter certainly initiates dynamics, but is definitely different from dynamics. Even though phenomenological models are often abstract, they help us to understand dynamics.

### Local versus Global

A universal question that appears in nonlinear problems is the relationship between *local* and *global*. The idea of the renormalization group method was related precisely to how one can extract global information from local information. Also, the reason why various types of pattern appear more in systems of equations than in scalar equations is that local and global effects coexist and interact in the former. In CHAPTER 4, we discussed Turing instability and the existence of stationary waves. In order for such a wave to exist, it was necessary for the inhibitor to diffuse much faster than the activator. The reason why a stable stationary wave can exist is that the inhibitor quickly spreads throughout the region to create a global inhibitory field in space and to prevent the activator from moving.

The structure of solutions of an equation, and its parameter-dependent global bifurcation diagram, in particular, is a typical example in which local and global are connected via certain kinds of singularity. Fujii, Mimura and Nishiura in [**146**] numerically show that the global bifurcation diagram of equilibrium solutions to a reaction-diffusion system is obtained by amplifying the local structure near a multiple bifurcation point. Namely, they identified the organizing center of global structure as the multiple bifurcation point. Such an attempt to connect local to global via singularities has also been employed in CHAPTER 6, where it is shown that the multiple bifurcation point combining the Bogdanov-Takens and Turing singularities plays a decisive role in creating a hierarchical structure of limiting points that drives self-replication dynamics.

### Role of Simulation

Needless to say, the role played by computers in mathematics has penetrated every scientific endeavor. Just as one cannot replace radio-telescope and electron-microscope by magnifying glasses any more, nobody can refuse the use of computers. The reason for this is simply because the machine stimulates human imagination. If it instantaneously gives an answer to a problem that a human being could not compute in a hundred years, then one may feel as if God is one's partner.

However, there is a pitfall. Some years ago, I had an opportunity to chat with a researcher from the Netherlands who had developed a bifurcation-branch-tracing software. He said, "Now thousands of research papers with the first author being a machine will appear." Although a lot of papers with low quality have been published, as he predicted, the important things are what we should have the machine compute and how we interpret the output. It is in the latter that mathematics plays a very crucial role. There is a periodical journal called *Experimental Mathematics*. It publishes varieties of articles, including topics such as algebraic geometry, combinatorics and wavelets, among which one can find articles that elucidate subtle relationships between mathematics and computation. It is also the case that saving the vast data produced by a large scale computation is costly. Computations without any clear policy and vision will eventually be eradicated.

For phenomena that are not reproducible or very difficult to actually put into experiments, such as evolution processes, fluctuations in financial markets, brain functions, and the origin of life, it is becoming a common practice to construct models and perform experiments in computer simulations. The computer simulations have a lot to do with our recognition of chaos. It is not, however, yet certain how deeply and widely the relationship between simulation and mathematics will unfold. This is a research frontier that may give rise to unexpected relationships between the two.

### Geometrization

A big difference between classical and modern theories of singular perturbation is that geometrization has been pursued in the latter.

Matching conditions in a singular perturbation problem is interpreted in geometric singular perturbation theory as an easily understandable notion of transversality ([**199**]). The idea of the renormalization group method, having a close relation to self-similar solutions and fractals, also possesses the advantage of providing us with an easy grasp of geometric pictures. For background related to these points, I recommend [**19**] (see also [**9**] and [**299**]).

Dynamical system approaches often give rise to geometric viewpoints. Kirchgässner and Mielke (cf. [**263**]) proposed, and showed the effectiveness of treating non-evolutionary types of partial differential equations as a dynamical system by regarding one of the spatial variables as time. The advantage of such a viewpoint is that one can construct center manifolds to understand various types of solutions as geometric objects. The method of singular limit analysis, described in CHAPTER 5, is also an example of geometrization, in the sense that the original dynamics is reduced to the motion of hypersurfaces called interfaces. This viewpoint has been steadily uncovering the nature of complicated interface motions, such as in a series of works [**265, 267, 296**] by Mimura and Ohta et al. These results at the same time present unsolved mathematical problems, especially questions related to the effectiveness and limitation of singular limit systems.

# Bibliography


[1] Alexander, J., Gardner, R. and Jones, C., *A topological invariant arising in the stability analysis of travelling waves*, J. Reine Angew. Math. **410**(1990) 167-212.

[2] Alikakos, N.D., Bates, P.W. and Chen, X., *Convergence of the Cahn-Hilliard equation to the Hele-Shaw model*, Arch. Rational Mech. Anal. **128**(1994) 165-205.

[3] Alikakos, N.D., Bates, P.W. and Fusco, G., *Slow motion for the Cahn-Hilliard equation in one space dimension*, J. Diff. Eqs. **90**(1991) 81-135.

[4] Alikakos, N.D., Bronsard, L. and Fusco, G., *Slow motion in the gradient theory of phase transition via energy and spectrum*, Cal. Var. Partial Differential Equations **6**(1998) 39-66.

[5] Alikakos, N.D. and Fusco, G., *Slow dynamics for the Cahn-Hilliard equation in higher space dimensions: the motion of bubbles*, Arch. Rational Mech. Anal. **141**(1998) 1-61.

[6] Amick, C.J. and McLeod, J.B., *A singular perturbation problem in needle crystals*, Arch. Rat. Mech. Anal. **109**(1990) 139-171.

[7] Angenent, S.B., *The Morse-Smale property for semilinear parabolic equation*, J. Diff. Eqs. **62**(1986) 427-442.

[8] Argentina, M., Coullet, P. and Mahadevan, L., *Colliding waves in a model excitable medium: preservation, annihilation, and bifurcation*, Phys. Rev. Lett. **79**(1997) 2803-2806.

[9] Aronson, D.G. and Vazquez, J.L., *Anomalous exponents in nonlinear diffusion*, J. Nonlinear Sci. **5**(1995) 29-56.

[10] Aronson, D.G. and Weinberger, H.F., *Nonlinear diffusion in population genetics, combustion, and nerve pulse propagation*, J.A.Goldstein, ed., Partial Differential Equations and Related Topics, Lecture Notes in Math. **466**(1975) 5-49.

[11] Aronson, D.G. and Weinberger, H.F., *Multidimensional nonlinear diffusion arising in population genetics.*, Adv. Math. **30**(1978) 33-76.

[12] Athanasopoulos, L., Caffarelli, L. and Salsa, S., *Regularity of the free boundary in parabolic phase-transition problems*, Acta Math. **176**(1996) 245-282.

[13] Athanasopoulos, L., Caffarelli, L. and Salsa, S., *Phase transition problems of parabolic type: flat free boundaries are smooth*, Comm. Pure Appl. Math. **51**(1988) 77-112.

[14] Bahiana, M. and Oono, Y., *Cell dynamical system approach to block copolymers*, Phys. Rev. A **41**(1990) 6763-6771.

[15] Bär, M. and Eiswirth, M., *Turbulence due to spiral breakup in a continuous excitable medium*, Phys. Rev. E **48**(1993) 1635-1637.

[16] Bär, M. and Or-Guil,M., *Alternative scenarios of spiral breakup in a reaction-diffusion model with excitable and oscillatory dynamics*, Phys. Rev. Lett. **8**(1999) 1160-1163.

[17] Barbieri, A., Hong, D.C. and Langer, J.S., *Velocity selection in the symmetric model of dendritic crystal growth*, Phys. Rev. **A35**(1986) 1802-1808.

[18] Bardi, M., Crandall, M.G., Evans, L.C., Soner, H.M., and Souganidis, P.E., *Viscosity Solutions and Applications*, Lec. Note in Math. **1660**, Springer (1997).

[19] Barenblatt, G.I., *Scaling, self-similarity and intermediate asymptotics*, Cambridge Univ. Press (1996).

[20] Barkley, D., *Euclidean symmetry and the dynamics of rotating spiral waves*, Phys. Rev. Lett. **72**(1994) 164-167.

[21] Barles, G. Soner, H.M., and Souganidis, P.E., *Front propagation and phase field theory*, SIAM J. Cont. Opt. **31**(1993), 439-469.

[22] Bar-Ziv, R. and Moses, E., *Instability and pearling states produced in tubular membranes by competition between curvature and tension*, Phys. Rev. Lett. **73**(1994) 1392-1395.

[23] Bates, P.W. and Fife, P.C., *Spectral comparison principles for the Cahn-Hilliard and phase-field equations, and time scales for coarsening*, Physica D **43**(1990) 335-348.

[24] Bazalii, B.V., *The Stefan problem for the Laplace equation taking into account the curvature of the free boundary.*, Ukrainian Math. J. **49**(1997) 1465-1484.

[25] Ben Amar, M. and Brener, E., *Parity-broken dendrites*, Phys. Rev. Lett. **75**(1995) 561-564.

[26] Ben-Amar, M. and Moussalam, B, *Numerical results on two-dimensional dendritic solid*, Physica D **25**(1986) 155-164.

[27] Ben-Amar, M. and Pomeau, Y., *Theory of dendritic growth in a weakly undercooled melt*, Euro. Phys. Lett. **2**(1986) 307-314.

[28] Ben-Jacob, E., Brand, H., Dee, G., Kramer, L. and Langer, J.S., *Pattern propagation in nonlinear dissipative systems.*, Physica D **14**(1985) 348-364.

[29] Ben-Jacob, E., Goldenfeld, N.D., Langer, J.S. and Schon, G., *Boundary-layer model of pattern formation in solidification*, Phys. Rev. **A29**(1984) 330-340.

[30] Bernoff, A.J., *Spiral wave solutions for reaction-diffusion equations in a fast reaction/slow diffusion limit*, Physica D**53**(1991) 125-150.

[31] Bers, A.N., *Space-time evolution of plasma instabilities -Absolute and convective*, in *Handbook of Plasma Physics*, M. N. Rosenbluth and R. Z. Sagdeev, eds., North-Holland (1983) 451-517.

[32] Bethuel, T., Brezis, H. and Helein, F., *Ginzburg-Landau Vortices*, Boston, Birkhäuser (1994).

[33] Boissonade, J., Dulos, E., and De Kepper, P., *Turing Patterns: From Myth to Reality*, in R. Kapral and K. Showalter (eds.), *Chemical Waves and Patterns*, Chap. 7, pp. 221-268.

[34] Bramson, M., *Convergence of solutions of the Kolmogorov equation to travelling waves.*, Memoirs of the AMS **44**(285)(1983).

[35] Brener, E., *Needle-crystal solution in three-dimensional dendritic growth*, Phys. Rev. Lett. **71**(1993) 3653-3656.

[36] Bricmont, J., Kupiainen, A. and Lin, G., *Renormalization group and asymptotics of solutions of nonlinear parabolic equations*, Comm. Pure Appl. Math. **47**(1994) 893-922.

[37] Bricmont, J. and Kupiainen, A., *Stability of moving fronts in the Ginzburg-Landau equation*, Commun. Math. Phys. **159**(1994) 287-318.

[38] Bricmont, J. and Kupiainen, A., *Renormalization group and the Ginzburg-Landau equation*, Commun. Math.Phys. **150**(1992) 193-208.

[39] Bronsard, L. and Kohn, R.V., *On the slowness of the phase boundary motion in one space dimension*, Comm. Pure Appl. Math. **43**(1990) 983-997.

[40] Bronsard, L. and Kohn, R.V., *Motion by mean curvature as the singular limit of Ginzburg-Landau dyanmics*, J. Diff. Eqs. **90**(1991) 211-237.

[41] Brower, R., Kessler, D., Koplik, D., and Levine, H., *Geometrical approach to moving-interface dynamics*, Phys. Rev. Lett. **51**(1983) 1111-1114.

[42] Brower, R., Kessler, D., Koplik, D., and Levine, H., *Geometrical models of interface evolution*, Phys. Rev. A **29**(1984) 1335-1342.

[43] Brunet, E. and Derrida, B., *Shift in the velocity of a front due to a cutoff*, Phys. Rev. E **56**(1997) 2597-2604.

[44] Brunovsky, P. and Fiedler, B., *Connecting orbits in scalar reaction diffusion equations*, Dyanmics Reported **1**(1988) 57-90.

[45] Caffarelli, L.A., *The regularity of free boundaries in higher dimensions*, Acta Math. **139**(1977) 155-184.

[46] Caffarelli, L.A., *Some aspects of the one-phase Stefan problem*, Indiana Univ. Math. J. **27**(1978) 73-77.

[47] Caffarelli, L.A. and Friedman, A., *Continuity of the temperature in the Stefan problem*, Indiana Univ. Math. J. **28**(1979) 53-70.

[48] Caginalp, G., *An analysis of a phase field model of a free boundary*, Arch. Rat. Mech. Anal. **92**(1986) 205-245.

[49] Carginalp, G., *Stefan and Hele-Shaw type models as asymptotic limits of the phase field equations*, Phys. Rev. A **39**(1989) 5887-5896.

[50] Carginalp, G. and Chen, X., *Phase field equations in the singular limit of sharp interface problems*, On the Evolution of Phase Boundaries (Gurtin, M. and McFadden, G.B., eds.), IMA Vol. of Mathematics and its Applications **43**, Springer-Verlag (1992) 1-28.

[51] Caginalp, G. and Fife, P.C., *Phase field methods for interfacial boundaries*, Phys. Rev. B **33**(1986) 7792-7794.

[52] Caginalp, G. and Fife, P.C., *Dyanmics of layered interfaces arising from phase boundaries*, SIAM J. Appl. Math. **48**(1988) 506-518.

[53] Caginalp, G. and Nishiura, Y., *The existence of traveling waves for phase equations and convergence to sharp interface models in the singular limit*, Quarterly of Appl. Math. **49**(1991) 147-162.

[54] Cahn, J.W. and Hilliard, J.E., *Free energy of a nonuniform system I. Interfacial free energy*, J. Chem. Phys. **28**(1958) 258-267.

[55] Carpenter, G, *A geometric approach to singular perturbation problems with applications to nerve impulse equations*, J. Diff. Equations **23**(1977) 335-367.

[56] Carr, J., *Applications of centre manifold theory*, Springer-Verlag (1981).

[57] Carr, J., Gurtin, M.E. and Slemrod, M., *Structured phase transitions on a finite interval*, Arch. Rational Mech. Anal. **86**(1984)·317-351.

[58] Carr, J. and Pego, R.L., *Metastable patterns in solutions of* $u_t = \epsilon^2 u_{xx} - f(u)$, Comm. Pure Appl. Math. **42**(1989) 523-576.

[59] Casten, R.C. and Holland, C.J., *Instability results for reaction diffusion equations with Neumann boundary conditions*, J. Diff. Eqs. **27**(1978) 266-273.

[60] Castets, V., Dulos, E., Boissonade, J. and De Kepper, P., *Experimental evidence of a sustained standing Turing-type nonequilibrium chemical pattern*, Phys. Rev. Lett. **64**(1990) 2953-2956.

[61] Chafee, N., *Asymptotic behavior for solutions of a one dimensional parabolic equation with Neumann boundary conditions*, J. Diff. Eqs. **18**(1975) 111-135.

[62] Chafee, N. and Infante, E.F., *A bifurcation problem for a nonlinear partial differential equation of parabolic type*, Applicable Anal. **4**(1974) 17-37.

[63] Chalmers, B., *Principles of solidification.*, Krieger, Huntington, N.Y. (1977)

[64] Chen, L.Y., Goldenfeld, N. and Oono, Y., *Renormalization group and singular perturbations: Multiple scales, boundary layers, and reductive perturbation theory.*, Phys. Rev. E **54**(1996) 376-394.

[65] Chen, L.Y, Goldenfeld, N., Oono, Y. and Paquette, G., *Selection, stability and renormalization*, Physica A **204**(1994) 113-133.

[66] Chen, X., *The Hele-Shaw problem and area-preserving curve-shortening motions*, Arch. Rational Mech. Anal. **123**(1993) 117-151.

[67] Chen, X-F., Hong, J. and Yi, F., *Existence, uniqueness and regularity of classical solutions of the Mullins-Sekerka problem*, Comm. Partial Differential Equations **21**(1996), 1705-1727.

[68] Chen, X. and Reitich, F., *Local existence and uniqueness of solutions of the Stefan problem with surface tension and kinetic undercooling*, J. Math. Anal. Appl. **164**(1992) 350-362.

[69] Chen, X-Y., *Dynamics of interfaces in reaction diffusion systems*, Hiroshima Math. J. **21**(1991)47-83.

[70] Chen, X-F., *Generation and propagation of the interface for reaction-diffusion equation*, J. Diff. Eqs. **96**(1992) 116-141.

[71] Chen, X-Y., Jimbo, S. and Morita, Y., *Stabilization of vortices in the Ginzburg-Landau equation with a variable diffusion coefficient*, SIAM J. Math. Anal. **29**(1998) 903-912.

[72] Chen, Y.G., Giga, Y. and Goto, S., *Uniqueness and existence of viscosity solutions of generalized mean curvature flow equations*, J. Diff. Geom. **33**(1991) 744-786.

[73] Choksi, R., *Scaling Laws in Microphase Separation of Diblock Copolymers*, J. Nonlinear Sci. **11** (2001) 223 - 236.

[74] Chow, S.-N. and Hale, J., *Methods of Bifurcation Theory*, Springer-Verlag (1982).

[75] Collet, P. and Eckmann, J-P., *The existence of dendritic fronts.*, Commun. Math. Phys. **107**(1986) 39-92.

[76] Collet, P. and Eckmann, J-P., *The stability of modulated fronts.*, Helvetica Phys. Acta **60**(1987) 969-991.

[77] Collet, P. and Eckmann, J-P., *Instabilities and fronts in extended systems*, Princeton Series in Physics (1990).

[78] Collet, P. and Eckmann, J-P., *The time dependent amplitude equation for the Swift-Hohenberg problem*, Commun. Math. Phys. **132**(1990) 139-153.

[79] Collet, P. and Eckmann, J-P., *Space-time behavior in problems of hydrodynamic type: a case study*, Nonlinearity **5**(1992) 1265-1302.

[80] Collet, P. and Eckmann, J-P., *Solutions without phase-slip for the Ginzburg-Landau equation*, Commun. Math. Phys. **145**(1992) 345-356.

[81] Collet, P., Eckmann, J-P. and Epstein, H., *Diffusive repair for the Ginzburg-Landau equation*, Helv. Phys. Acta **65**(1992) 56-92.

[82] Conway, E., Hoff, D. and Smoller, J., *Large time behavior of solutions of systems of reaction diffusion equations*, SIAM J. Appl. Math. **35**(1978) 1-16.

[83] Crandall, M.G., Ishii, H. and Lions, P.L., *User's guide to viscosity solutions of second order partial differential equations*, Bull. Amer. Math. Soc. **27**(1992) 1-67.

[84] Cross, M.C. and Hohenberg, P.C., *Pattern formation outside of equilibrium*, Rev. Modern Physics, **65**(1993) 851-1112.

[85] Davydov, V.A., Zykov, V.S. and Mikhaĭlov, A.S., *Kinematics of autowave structures in excitable media*, Soviet Phys. Uspekhi **34**(1991) 665-684.

[86] De Giorgi, E., *Convergence problems for functionals and operators*, Proceedings of the International Meeting on Recent Methods in Nonlinear Analysis (E. De Giorgi et al., eds), Pitagora, Bologna (1978) 131-188.

[87] De Kepper, P., Boissonade, J. and Epstein, I., *Chlorite-Iodide reaction: A versatile system for the study of nonlinear dynamical behavior*, J. Phys. Chem. **94**(1990) 6525-6536.

[88] De Kepper, P., Perraud, J.J., Rudovics, B. and Dulos, E., *Experimental study of stationary Turing patterns and their interaction with traveling waves in a chemical system*, International Journal of Bifurcation and Chaos **4**(1994) 1215-1231.

[89] Dee, G., *Dynamical properties of propagating front solutions of the amplitude equation*, Physica D **15**(1985) 295-304.

[90] Dee, G., *Propagation into an unstable state*, J. Sta. Phys. **39**(1985) 705-717.

[91] Dee, G. and Langer, J.S., *Propagating Pattern Selection*, Phys. Rev. Lett. **50**(1983) 385-386.

[92] DeMottoni, P. and Schatzman, M., *Development of interfaces in* $\mathbf{R}^N$, Proc. Royal Soc. Edinb. **116A**(1990) 207-220.

[93] DiBenedetto, E. and Vespri, V., *On the singular equation* $\beta(u)_t = \Delta u$, Arch. Rational Mech. Anal. **132**(1995) 247-309.

[94] Diekmann, O. (Temme,N.M., ed.), *Nonlinear Diffusion Problems*, MC Syllabus **28**, Mathematisch Centrum, Amsterdam, (1982).

[95] Dockery, J.D., Keener, J.P. and Tyson, J.J., *Dispersion of traveling waves in the Belousov-Zhabotinsky reaction*, Physica D**30**(1988) 117-191.

[96] Doedel, E.J., Champneys, A.R., Fairgrieve, T.F., Kuznetsov,Y.A., Sandstede, B. and Wang, X., *AUTO97: Continuation and bifurcation software for ordinary differential equations (with HomCont)*, ftp://ftp.cs.concordia.ca/pub/doedel/auto (1997).

[97] Doelman, A., Eckhaus, W. and Kaper, T.J., *Slowly-modulated two pulse solutions in the 1-D Gray-Scott model I: Asymptotic construction and stability*, SIAM J. Appl. Math. **61**(2001) 1080-1102.

[98] Doelman, A., Eckhaus, W. and Kaper, T.J., *Slowly-modulated two pulse solutions in the 1-D Gray-Scott model II: Geometric theory, bifurcations and splitting dynamics*, SIAM J.Appl.Math. **61**(2001) 2036-2062.

[99] Doelman, A., Gardner, R.A. and Kaper, T.J., *Stability analysis of singular patterns in the 1-D Gray-Scott model: A matched asymptotic approach*, Physica D **122**(1998) 1-36.

[100] Doelman, A., Kaper, T.J. and Zegeling, P.A., *Pattern formation in the one-dimensional Gray-Scott model*, Nonlinearity **10**(1997) 523-563.

[101] Ebert, U. and van Saarloos, W., *Front propagation into unstable states: Universal algebraic convergence towards uniformly translating pulled fronts*, Physica D **146**(2000) 1-99.

[102] Ebert, U., van Saarloos, W. and Peletier, L.A., *Universal algebraic convergence in time of pulled fronts: The common mechanism for difference-differential and partial differential equations*, to appear in Eur. J. Appl. Math.

[103] Eckhaus, W., *The Ginzburg-Landau manifold is an attractor*, J. Nonlinear Sci. **3**(1993) 329-348.

[104] Doelman, A. and van der Ploeg, H., *Homoclinic stripe patterns* (2001), preprint.

[105] Eckmann, J-P. and Gallay, Th., *Front Solution for the Ginzburg-Landau Equation*, Commun. Math. Phys. **152**(1993) 221-248.

[106] Eckmann, J-P., Gallay, Th. and Wayne, C.E., *Phase slip and the Eckhaus instability*, Nonlinerity **8**(1995) 943-961.

[107] Eckmann, J-P. and Wayne, C.E., *Propagating fronts and the center manifold theorem*, Commun. Math. Phys. **136**(1991) 285-307.

[108] Eckmann, J-P., Wayne, C-E. and Wittwer, P., *Geometric stability analysis for periodic solutions of the Swift-Hohenberg equation*, Commun. Math. Phys. **190**(1997) 173-211.

[109] Ei, S.-I., *The motion of weakly interacting pulses in reaction diffusion systems*, J. Dynam. Diff. Eqs. **14**(2002) 85-137.

[110] Ei, S.-I., Nishiura, Y. and Sandstede, B., *Pulse interaction approach to self-replicating dynamics in reaction-diffusion systems*, preprint 2000.

[111] Ei, S.-I., Nishiura, Y. and Ueda, K., *$2^n$-splitting or edge-splitting? A manner of splitting in dissipative systems*, Japan J. Indus. and Appl. Math. **18**(2001) 181-205.

[112] Ei, S.-I., Nishiura, Y. and Ueda, K., *Wave-splitting of traveling breather type*, in preparation.

[113] Ei, S. and Ohta, T., *Equation of motion for interacting pulses*, Phys. Rev. E **50**(1994) 4671-4678.

[114] Elliott, C.M. and Zheng, S., *On the Cahn-Hilliard equation*, Arch. Rational Mech. Anal. **96**(1986) 339-357.

[115] Escher, J. and Nishiura, Y., *Smooth unique solutions for a modified Mullin-Sekerka model arising in diblock copolymer melts*, to appear in Hokkaido Math.J.

[116] Escher, J., Prüss, J. and Simonett, G., *Analytic solutions for a Stefan problem with Gibbs-Thomson correction.*, preprint.

[117] Escher, J., Prüss, J. and Simonett, G., *Smooth solutions for the Stefan problem with surface tenssion*, in preparation.

[118] Escher, J. and Simonett, G., *On Hele-Shaw models with surface tension*, Math. Res. Lett. **3**(1996) 467-474.

[119] Escher, J. and Simonett, G., *Classical solutions for the quasi-stationary Stefan problem with surface tension*, Differential equations, asymptotic analysis, and mathematical physics (Potsdam,1996), Math. Res. **100**, Akademie-Verlag, Berlin, 1997, 98-104.

[120] Escher, J. and Simonett, G., *Classical solutions for Hele-Shaw models with surface tension*, Adv. Diff. Eqs. **2**(1997) 619-642.

[121] Escher, J. and Simonett, G., *A center manifold analysis for the Mullins-Sekerka model*, J. Diff. Eqs. **143**(1998) 267-292.

[122] Evans, J., *Nerve axon equations, I: Linear approximations*, Indiana Univ. Math. J. **21**(1972) 877-955.

[123] Evans, J., *Nerve axon equations, II: Stability at rest*, Indiana Univ. Math. J. **22**(1972) 75-90.

[124] Evans, J., *Nerve axon equations, III: Stability of the nerve impulse*, Indiana Univ. Math. J. **22**(1972) 577-594.

[125] Evans, J., *Nerve axon equations, IV: The stable and unstable impulses*, Indiana Univ. Math. J. **24**(1975) 1169-1190.

[126] Evans, L.C., *Partial Differential Equations*, Grad. Stud. in Math. **19**, Amer. Math. Soc. (1998).

[127] Evans, L.C. and Spruck, J., *Motion of level sets by mean curvature I*, J. Diff. Geom. **33**(1991) 635-681.

[128] Evans, L.C. and Spruck, J., *Motion of level sets by mean curvature II*, Trans. Amer. Math. Soc. **330**(1992) 321-332.

[129] Evans, L.C., Soner, H.M. and Souganidis, P.E., *Phase transitions and generalized motion by mean curvature*, Comm. Pure. Appl. Math **45**(1992) 1097-1123.

[130] Fiedler, B. and Mallet-Paret, J., *Connections between Morse sets for delay-differential equations*, J. Reine Angew. Math. **397**(1989) 23-41.

[131] Fife, P.C., *Boundary and interior transition layer phenomena for pairs of second order equations*, J. Math. Anal. Appl. **54**(1976) 497-521.

[132] Fife, P.C., *Propagator-controller systems and chemical patterns*, in *Non-Equilibrium Dynamics in Chemical Systems*, eds. Vidal, C. and Pacault, A., Springer, Berlin (1984) 76-88.

[133] Fife, P.C., *Understanding the patterns in the BZ reagent*, J. Stat. Phys. **39**(1985) 687-701.

[134] Fife, P.C., *Dynamics of internal layers and diffusive interfaces*, CBMS-NSF Regional Conference Series in Applied Mathematics **53**, SIAM, Philadelphia (1988).

[135] Fife, P.C., *Dynamical aspects of the Cahn-Hilliard equation*, Barrett Lectures, University of Tennessee, Spring(1991).

[136] Fife, P.C., *Models for phase separation and their mathematics*, Electron. J. Diff. Eqs. **48**(2000)(electronic).

[137] Fife, P.C. and Greenlee, W.M., *Interior transition layers for elliptic boundary value problems with a small parameter*, Usp. Matem. Nauk **29**(4)(1974) 103-130; Russ. Math. Surveys **29**(4)(1974) 103-131.

[138] Fife, P.C. and Hilhorst, D., *The Nishiura-Ohnishi free boundary problem in the 1D case*, SIAM J. Math. Anal. **33**(2001) 589-606.

[139] Fife, P.C. and McLeod, J.B., *The approach of solutions of nonlinear diffusion equations to travelling wave solutions*, Bull. Amer. Math. Soc. **81**(1975) 1076-1078.

[140] Fife, P.C. and McLeod, J.B., *The approach of solutions of nonlinear diffusion equations to travelling front solutions*, Arch. Rat. Mech. Anal. **65**(1977) 335-361.

[141] Fisher, R.A., *The advance of advantageous genes*, Ann. Eugenics **7**(1937) 355-369.

[142] Friedman, A., *The Stefan problem in several space variables*, Trans. Amer. Math. Soc. **133**(1968) 51-87.

[143] Friedman, A., *Variational Principles and Free-Boundary Problems*, Wiley-Interscience, New York (1982).

[144] Friedman, A. and Kinderlehrer, D., *A one phase Stefan problem*, Indiana Univ. Math. J. **24**(1975) 1005-1035.

[145] Friedman, A. and Reitich, F., *The Stefan problem with small surface tension*, Trans. Amer. Math. Soc. **328**(1991) 465-515.

[146] Fujii, H., Mimura, M. and Nishiura, Y., *A picture of the global bifurcation diagram in ecological interacting and diffusing systems*, Physica D **5**(1982) 1-42.

[147] Fusco, G., *A geometric approach to the dynamics of* $u_t = \epsilon^2 u_{xx} + f(u)$ *for all* $\epsilon$, Lecture Notes in Physics **359**(1990) 53-73.

[148] Fusco, G. and Hale, J.K., *Slow motion manifolds. Dormant instability and singular perturbations*, J. Dynamics Diff. Eqs. **1**(1989) 75-94.

[149] Gage, M. and Hamilton, R.S., *The heat equation shrinking convex plane curves*, J. Diff. Geom. **23**(1986),69-96.

[150] Gallay, Th., *A center-stable manifold theorem for differential equations in Banach spaces*, Commun. Math. Phys. **152**(1993) 249-268.

[151] Gallay, Th., *Local stability of critical fronts in nonlinear parabolic partial differential equations*, Nonlinearity **7**(1994) 741-764.

[152] Gardner, R. and Jones, C.K.R.T., *A stability index for steady state solutions of boundary value problems for parabolic systems*, J. Diff. Eqs. **91**(1991) 181-203.

[153] Giga, Y., Goto, S., and Ishii, H., *Global existence of weak solutions for interface equations coupled with diffusion equations*, SIAM J. Math. Anal. **23**(1992) 821-835.

[154] Giga, Y. and Sato, M., *Neumann problem for singular degenerate parabolic equations*, Diff. and Integral Eqns. **6**(1993) 1217-1230.

[155] Gilbarg, D. and Trüdinger, N.S., *Elliptic partial differential equations of second order*, Springr-Verlag, New York (1983).

[156] Giusti, E., *Minimal Surfaces and Functions of Bounded Variation*, Birkhäuser (1984).

[157] Goldenfeld, N., *Lectures on Phase Transition and the Renormalization Group*, Addison-Wesley (1992).

[158] Gray, P. and Scott, S.K., *Autocatalytic reactions in the isothermal, continuous stirred tank reactor: oscillations and instabilities in the system $A + 2B \rightarrow 3B$, $B \rightarrow C$*, Chem. Eng. Sci. **39**(1984) 1087-1097.

[159] Grayson, M., *The heat equation shrinks embedded plane curves to round points*, J. Diff. Geom. **26**(1987) 285-314.

[160] Grinrod, P., *Theory and Application of Reaction-Diffusion Equations; Patterns and Waves*, Second Ed., Clarendon Press, Oxford (1996).

[161] Gurtin, M.E., *On the two phase problem with interfacial energy and entropy*, Arch. Rational Mech. Anal. **96**(1986) 199-241.

[162] Gurtin, M.E., *Multiphase thermomechanics with interfacial structure*, Arch. Rational Mech. Anal. **104**(1988) 195-221.

[163] Golubitsky, M. and Schaeffer, D.G., *Singularities and Groups in Bifurcation Theory*, I and II, Springer (1985 and 1988).

[164] Gurtin, M and Matano, H, *On the structure of equilibrium phase transitions within the gradient theory of fluids*, Quarterlly Appl. Math. **46**(1988) 302-317.

[165] Hagberg, A. and Meron, E., *From labyrinthine patterns to spiral turbulence*, Phys. Rev. Lett. **72**(1994) 2494-2497.

[166] Hale, J.K., *Asymptotic Behavior of Dissipative Systems*, Amer. Math. Soc., Providence (1998).

[167] Hale, J.K. and Massatt, P., *Asymptoptic behavior of grandient-like systems*, Dynamical Systems II (A. R. Bednarek and L. Cesari, eds.), Academic Press (1982) 85-101.

[168] Hale, J.K., Peletier, L.A. and Troy, W.C., *Stability and instability in the Gray-Scott model: The case of equal diffusivities*, Appl. Math. Lett. **12**(1999) 59-65.

[169] Hale, J.K., Peletier, L.A. and Troy, W.C., *Exact homoclinic and heteroclinic solutions of the Gray-Scott model for autocatalysis*, SIAM J. Appl. Math. **61**(2000) 102-130.

[170] Hale, J.K. and Sakamoto, K., *Existence and stability of transition layers*, Japan J. Appl. Math. 5(1988) 367-405.

[171] Hammersley, J.M. and Mazzarino, G., *A differential equation connected with the dendritic growth of crystals*, IMA J. Appl. Math. **42**(1989) 43-75.

[172] Hanzawa, E.I., *Classical solutions of the Stefan problem*, Tohoku Math. Jour. **33**(1981) 297-335.

[173] Hartman, P., *Crystal growth: An introduction*, North-Holland, Amsterdam (1973).

[174] Hastings, S., *On traveling wave solutions of the Hodgkin-Huxley equations*, Arch. Rat. Mech. Anal. **60**(1976) 229-257.

[175] Hayase, Y. and Ohta, T., *Sierpinski gasket in a reaction-diffusion system*, Phys. Rev. Letters **81**(1998) 1726-1729.

[176] Henry, D., *Geometric Theory of Semilinear Parabolic Equations*, Springer Lecture Notes in Math. **840**(1981).

[177] Henry, D., *Some infinite dimensional Morse-Smale systems defined by parabolic differential equations*, J. Diff. Eqs. **59**(1985) 165-205.

[178] Hilhorst, D., Nishiura, Y. and Mimura, M., *A free boundary problem arising in some reacting-diffusing systems*, Proc. Roy. Soc. Edinburgh **118A**(1991) 355-378.

[179] Hohenberg, P.C. and Halperin, B.I., *Theory of dynamic critical phenomena*, Rev. Mod. Phys. **49**(1977) 435-479.

[180] Honjo, H. and Sawada, Y., *Quantitative measurements on the morphology of a $NH_4Br$ dendritic crystal growth in a capillary*, J. Crystal Growth **58**(1982) 297-303.

[181] Horway, G. and Cahn, L.W., *Dendritic and spheroidal growth*, Acta. Metall. **9**(1961) 695-705.

[182] Howard, L.N. and Kopell, N., *Slowly varying waves and shock structures in reaction-diffusion equations*, Stud. Appl. Math. **56**(1977) 95-145.

[183] Huang, S.C. and Glicksman, M.E., *Fundamentals of dendritic solidification. I: Steady state tip growth; II: Development of sidebranch structure*, Acta Metall. **29**(1980) 701-734.

[184] Huisken, G., *Flow by mean curvature of convex surfaces into spheres*, J. Diff. Geom. **20**(1984) 237-266.

[185] Ikeda, H., *Singular perturbation approach to stability properties of travelling wave solutions of reaction-diffusion systems*, Hiroshima Math. J. **19**(1989) 587-630.

[186] Ikeda, T. and Nishiura, Y., *Pattern selection for two breathers*, SIAM J. Appl. Math. **54**(1994) 195-230.

[187] Ikeda, H., Nishiura, Y. and Suzuki, H., *Stability of travelling waves and a relation between the Evans function and SLEP equation*, J. Reine Angew. Math **475**(1996) 1-37.

[188] Ilmanen, T., *Convergence of the Allen-Cahn equation to Brakke's motion by mean curvature*, J. Diff. Geom. **38**(1993) 417-461.

[189] Iooss, G., Mielke, A. and Demay, Y., *Theory of steady Ginzburg-Landau equation in hydrodynamic stability problems*, European J. Mech. B/Fluids **3**(1989) 229-268.

[190] Ito, M., *A remark on singular perturbation methods*, Hiroshima Math. J. **14**(1984) 619-629.

[191] Ivantsov, G.P., *Temperature field around a spherical, cylindrical or pointed crystal growing in a supercooled melt* (for the English translation, see [**305**]), Doklady Akad. Nauk SSSR **58**(1947) 567-569.

[192] Jensen, O., Pannbacker, V.O., Mosekilde, E., Dewel, G. and Borckmans, P., *Localized structures and front propagation in the Lengyel-Epstein model*, Phys. Rev. E **50**(1994) 736-749.

[193] Jimbo, S. and Morita, Y., *Stability of non-constant steadystate solutions to a Ginzburg-Landau equation in higher space dimensions*, Nonlinear Anal. **22**(1994) 753-770.

[194] Jimbo, S. and Morita, Y., *Ginzburg-Landau equation and stable solutions in a rotational domain*, SIAM J. Math. Anal. **27**(1996) 1360-1385.

[195] Jimbo, S. and Morita, Y., *Stable solutions with zeros to the Ginzburg-Landau equation with Neumann boundary condition*, J. Diff. Eqs. **128**(1996) 596-613.

[196] Jimbo, S., Morita, Y. and Zhai, J., *Ginzburg-Landau equation and stable steady state solutions in a non-trivial domain*, Comm. Partial Diff. Eqs. **20**(1995) 2093-2112.

[197] Jimbo, S. and Zhai, J., *Ginzburg-Landau equation with magnetic effect: non-simply-connected domains*, J. Math. Soc. Japan **50**(1998) 663-684.

[198] Jones, C.K.R.T., *Stability of the travelling wave solution of the FitzHugh-Nagumo system*, Trans. Amer. Math. Soc. **286**(1984) 431-469.

[199] Jones, C.K.R.T., *Geometric Singular Perturbation Theory*, Springer Lecture Notes in Math. **1609**(1994) 44-118.

[200] Jones, C.K.R.T., Kopell, N. and Langer, R., *Construction of the FitzHugh-Nagumo pulse using differential forms*, in *Patterns and Dynamics in Reactive Media*, Swinney, H., Aris, G., and Aronson, D., Eds., IMA Vol. Math. Appl. **37**, Springer-Verlag (1991) 101-115.

[201] Kapral, R. and Showalter, K., *Chemical Waves and Patterns*, Kluwer Academic Publishers (1995).

[202] Kamenomostskaja,S.L., *On Stefan's problem*, Mat. Sbornik **53**(1961) 485-514 (Russian).

[203] Karma, A., *Universal limit of spiral wave propagation in excitable media*, Phys. Rev. Lett. **66**(1991) 2274-2277.

[204] Karma, A., *Scaling regime of spiral wave propagation in single-diffusive media*, Phys. Rev. Lett. **68**(1992) 397-400.

[205] Kawasaki, K. and Ohta, T., *Kink dynamics in one-dimensional nonlinear systems*, Physica **116A**(1982) 573-593.

[206] Keener, J.P., *A geometrical theory for spiral waves in excitable media*, SIAM J. Appl. Math. **46**(1986) 1039-1059.

[207] Keener, J.P., *The core of the spiral*, SIAM J. Appl. Math. **52**(1992) 1370-1390.

[208] Keener, J.P., *Symmetric spirals in media with relaxation kinetics and two diffusing species*, Physica D **70**(1994) 61-73.

[209] Keener, J.P. and Tyson, J.J., *Spiral waves in the Belousov-Zhabotinsky reaction*, Physica D **21**(1986) 307-324.

[210] Kessler, D., Koplic, J., and Levin, H., *Geometrical models of interface evolution. III: Theory of dendrite growth*, Phys. Rev. A **31**(1985) 1712-1717.

[211] Kessler, D., Koplic, J. and Levin, H., *Steady-state dendritic crystal growth*, Phys. Rev. A **33**(1986) 3352-3357.

[212] Kessler, D.A. and Kupferman, R., *Spirals in excitable media: The free-boundary limit with diffusion*, Physica D **97**(1996) 509-516.

[213] Kessler, D.A. and Levine, H., *Diffusive boundary layers in the free-surface excitable medium spiral*, Phys. Rev. E **55**(1997) 3847-3850.

[214] Kessler, D.A., Levine, H. and Reynolds, W.N., *Theory of the spiral core in excitable media*, Physica D **70**(1994) 115-139.

[215] Kinderlehrer, D. and Nirenberg, L., *Regularity in free boundary problems*, Ann. Scuola Norm. Sup. Pisa Cl. Sci. (4) **4**(1977) 373-391.

[216] Kinderlehrer, D. and Nirenberg, L., *The smoothness of the free boundary in the one phase Stefan problem*, Comm. Pure Appl. Math. **31**(1978) 257-282.

[217] Kirchgassner, K., *On the nonlinear dynamics of travelling fronts*, J. Diff. Eqs. **96**(1992) 256-278.

[218] Kirrmann, P., Schneider, G. and Mielke, A., *The validity of modulation equations for extended systems with cubic nonlinearities*, Proc. Roy. Soc. Edin. **122A**(1992) 85-91.

[219] Kishimoto, K. and Weinberger, H.F., *The spatial homogeneity of stable equilibria of some reaction diffusion systems on convex domains*, J. Diff. Eqs. **58**(1985) 15-21.

[220] Kobayashi, R., *Modeling and numerical simulations of dendritic crystal growth*, Physica D **63**(1993) 410-423.

[221] Kobayashi, R., *A numerical approach to three-dimensional dendritic solidification*, Experimental Math. **3**(1994) 59-81.

[222] Koch, H., *Classical solutions to phase transition problems are smooth*, Comm. Partial Diff. Eqs. **23**(1998) 389-437.

[223] Kohn, R.V. and Müller, S., *Surface energy and microstructure in coherent phase transitions*, Comm. Pure Appl. Math. **47**(1994) 405-435.

[224] Kohn, R.V. and Sternberg, P., *Local minimisers and singular parturbations*, Proc. Roy. Soc. Edinburgh **111A**(1989) 69-84.

[225] Kokubu, H., *Homoclinic and heteroclinic bifurcation of vector fields*, Japan J. Appl. Math. **5**(1987) 455-501.

[226] Kokubu, H., Mischaikow, K., Nishiura, Y., Oka, H. and Takaishi, T., *Connecting Orbit Structure of Monotone Solutions in the Shadow System*, J. Diff. Eqs. **140**(1997) 309-364.

[227] Kokubu, H., Nishiura, Y., Oka, H., *Heteroclinic and homoclinic bifurcations in bistable reaction diffusion systems*, J. Diff. Eqns. **86**(1990) 260-341.

[228] Kolmogoroff, A., Petrovsky, I. and Piscounoff, N., *Étude de l'équation de la diffusion avec croissance de la quantité de matière et son application à un problème biologique*, Bull. Univ. Moscou Sér. Internat. Sect. A **1**(1937), #6, 1-25.

[229] Kondo, S., Asai, R., *A reaction-diffusion wave on the skin of the marine angel fish Pomacanthus*, Nature **376**(1995) 765-768.

[230] Kruskal, M.D. and Segur, H., *Asymptotics beyond all orders in a model of crystal growth*, Stud. Appl. Math. **85**(1991) 129-181.

[231] Kryloff, N. and Bogoliuboff, N., *Les méthodes de la mécanique non linéaire appliquées à la théorie des oscillations stationnaires*, Monogr. Acad. Sci. Ukraine No. 8, Kiev, 1934 (99 Russian pages; 10-page French summary).

[232] Kunihiro, T., *A geometrical formulation of the renormalization group method for global analysis*, Prog. Theor. Phys. **94**(1995) 503-514.

[233] Kuznetsov, Y-A., *Elements of Applied Bifurcation Theory*, Springer-Verlag (1997).

[234] Ladyzenskaja, O.A., Solonnikov, V.A, and Ural'ceva, N.N., *Linear and quasilinear equations of parabolic type*, Translations of Mathematical Monographs. Vol.56, American Mathematical Society, Providence, R.I. (1968).

[235] Landau, L.D. and Lifshitz, E.M., *Course of Theoretical Physics*, Vol. 10, Pergamon, New York, 1981.

[236] Langer, J.S., *Studies in the theory of interfacial stability II: Moving symmetric model*, Acta Metall. **25**(1977) 1121-1137.

[237] Langer, J.S., *Instabilities and pattern formation in crystal growth*, Reviews of Modern Physics **52**(1980) 1-28.

[238] Langer, J.S., *Instabilities and pattern formation*, Academic Press (1982).

[239] Langer, J.S., *Dendrites, viscous fingers, and the theory of pattern formation*, Science **243**(1989) 1150-1156.

[240] Langer, J.S. and Müller-Krumbhaar, H., *Theory of dendritic growth II: Instabilities in the limit of vanishing surface tension*, Acta. Metall. **26**(1978) 1689-1695.

[241] Langer, R., *Existence and uniqueness of pulse solution to the FitzHugh-Nagumo equations*, Ph.D. Thesis, Northeastern University,1980.

[242] Lee, K.J., McCormick, W.D., Pearson, J.E. and Swinney, H.L., *Experimental observation of self-replicating spots in a reaction-diffusion system*, Nature **369**(1994) 215-218.

[243] Lee, K.J. and Swinney, H.L., *Lamellar structures and self-replicating spots in a reaction-diffusion system*, Phys. Rev. E **51**(1995) 1899-1915.

[244] Lengyel, I. and Epstein, I.R., *A chemical approach to designing Turing patterns in reaction-diffusion systems*, Proc. Natl. Acad. Sci. USA **89**(1992) 3977-3979.

[245] Lin, F.H., *Some dynamical properties of Ginzburg-Landau vortices*, Commun. Pure Appl. Math. **49**(1996) 323-359, and *A remark on the previous paper "Some dynamical properties of Ginzburg-Landau vortices"*, Commun. Pure Apple. Math. **49**(1996) 361-364.

[246] Lin, F.H., *Complex Ginzburg-Landau equations and dynamics of vortices, filaments, and codimension 2 submanifolds*, Commun. Pure Appl. Math. **51**(1998) 385-441.

[247] Lin, X.B., *Shadowing lemma and singularly perturbed boundary value problems*, SIAM J. Appl. Math. **49**(1989) 26-54.

[248] Luckhaus, S., *Solution of the two phase Stefan problem with the Gibbs-Thompson law for the melting temperature*, European J.Appl.Math. **1**(1990) 101-111.

[249] Maginu, K., *Stability of periodic travelling wave solutions of a nerve conduction equation*, J. Math. Biology **6**(1978) 49-57.

[250] Maginu, K., *Geometrical characteristics associated with stability and bifurcations of periodic traveling waves in reaction-diffusion systems*, SIAM J. Appl. Math. **45**(1985) 750-774.

[251] Mallet-Paret, J., *Negatively invariant sets of compact maps and an extension of a theorem of Cartwright*, J. Diff. Eqs. **22**(1976) 331-348.

[252] Matano, H., *Convergence of solutions of one-dimensional semilinear parabolic equations*, J. Math. Kyoto Univ. **18**(1978) 224-243.

[253] Matano, H., *Asymptotic behavior and stability of solutions of semilinear diffusion equations*, Publ. Res. Inst. Math. Sci. **15**(1979) 401-458.

[254] Matano, H., *Nonincrease of the lap number of a solution for a one-dimensional semilinear parabolic equation*, J. Fac. Sci. Univ. Tokyo Sect. 1A Math. **29**(1982) 401-441.

[255] Mazin, W., Rasmussen, K.E., Mosekilde, E., Borckmans, P. and Dewel, G., *Pattern formation in the bistable Gray-Scott model*, Mathematics and Computers in Simulation **40**(1996), 371-396.

[256] Merkin, J.H., Petrov, V., Scott, S.K. and Showalter, K., *Wave-induced chemical chaos*, Phys. Rev. Lett. **73**(1996) 546-549.

[257] Meinhardt, J.H., *The algorithmic beauty of sea shells*, Springer (1995).

[258] Meinhardt, J.H. and Klinger, M., *A model for pattern formation on the shells of molluscs*, J. Theoret. Biol. **126**(1987) 63-89.

[259] Meiron, D., *Selection of steady states in the two-dimensional symmetric model of dendritic growth*, Phys. Rev. A **33**(1986) 2704-2715.

[260] Meirmanov, A.M., *On the classical solution of the multidimensional Stefan problem for quasilinear parabolic equations*, Math. USSR Sb. **40**(1981) 157-178.

[261] Meirmanov, A.M., *The Stefan Problem.*, De Gruyter, Berlin (1992).

[262] Meron,E., *Pattern formation in excitable media*, Physics Reports **218**(1992) 1-66.

[263] Mielke, A., *Reducation of quasilinear elliptic equations in cylindrical domains with applications*, Math. Meth. Appl. Sci. **10**(1988) 51-66.

[264] Mikhailov, A.S., *Kinematical theory of spiral waves in excitable media: Comparison with numerical simulations*, Physica D **52**(1991) 379-397.

[265] Mimura, M. and Nagayama, M., *Non-anihilation of traveling pulses in reaction-diffusion systems*, to appear in SIAM J.Appl.Math.

[266] Mimura, M., Tabata, M. and Hosono, Y., *Multiple solutions of two-point boundary value problems of Neumann type with a small parameter*, SIAM J. Math. Anal. **11**(1980) 613-631.

[267] Mimura, M. and Tsujikawa, T., *Aggregating pattern dynamics in a chemotaxis model including growth*, Physica A **230**(1996) 499-543.

[268] Modica, L., *The gradient theory of phase transitions and the minimal interface criterion*, Arch. Rational Mech. Anal. **98**(1987) 123-142.

[269] Modica, L., *Gradient theory of phase transitons with boundary contact energy*, Ann. Inst. H. Poincaré: Analyse Non Linéaire **5**(1987) 453-486.

[270] Mori, H. and Kuramoto, Y., *Dissipative Structures and Chaos*, Springer-Verlag, Berlin (1998).

[271] Müller, S., *Singular perturbation as a selection criterion for periodic minimizing sequences*, Calculus of Variations and PDE **1**(1993) 169-204.

[272] Morita, Y. and Mimoto, Y., *Collision and collapse of layers in a 1D scalar reaction-diffusion equation*, Physica D **140**(2000) 151-170.

[273] Müller-Krumbhaar, H and Langer, J.S, *Theory of dendritic growth III: Effects of surface tension*, Acta Metall. **26**(1978) 1697-1708.

[274] Mullins, W.W. and Sekerka, R.F., *Stability of a planar interface during solidification of a dilute binary alloy*, J. Appl. Phys. **3**(1964) 444-451.

[275] Murray, J.M., *Mathematical Biology*, Springer-Verlag (1989).

[276] Neu, J., *Vortices in complex scalar fields*, Physica D **43**(1990) 385-406.

[277] Newell, A.C., Passot, T. and Lega, J., *Order parameter equations for patterns*, Annual Rev. Fluid Mech. **25**(1993) 399-453.

[278] Nii, S., *A topological proof of stability of N-front solutions of the FitzHugh-Nagumo equations*, J. Dynam. Diff. Eqs. **11**(1999) 515-555.

[279] Nicolis, G. and Prigogine, I., *Self-organization in Nonequilibrium Systems; from Dissipative Structures to Order through Fluctuations*, Wiley, New York (1977).

[280] Nishiura, Y., *Global structure of bifurcating solutions of some reaction-diffusion systems*, SIAM J. Math. Anal. **13**(1982) 555-593.

[281] Nishiura, Y., *Coexistence of infinitely many stable solutions to reaction diffusion systems in the singular limit*, Dynamics Reported **3**(1994) 25-103.

[282] Nishiura, Y. and Fujii, H., *Stability of singularly perturbed solutions to systems of reaction diffusion equations*, SIAM J. Math. Anal. **18**(1987) 1726-1770.

[283] Nishiura, Y. and Mimura, M., *Layer oscillations in reaction-diffusion systems*, SIAM J. Appl. Math. **49**(1989) 481-514.

[284] Nishiura, Y., Mimura, M., Ikeda, H. and Fujii, H., *Singular limit analysis of stability of travelling wave solutions in bistable reaction-diffusion systems*, SIAM J. Math. Anal. **21**(1990) 85-122.

[285] Nishiura, Y and Ohnishi, I, *Some mathematical aspects of the micro-phase separation in diblock copolymers*, Physica D **84**(1995) 31-39.

[286] Nishiura, Y and Ohnishi, I, *Rugged landscape with fine structure*, preprint.

[287] Nishiura, Y. and Suzuki, H., *Nonexistence of higher dimensional stable Turing patterns in the singular limit*, SIAM J. Math. Anal. **29**(1998) 1087-1105.

[288] Nishiura, Y. and Ueyama, D., *A hidden bifurcational structure for self-replicating dynamics*, ACH-Models in Chemistry **135**(1998) 343-360.

[289] Nishiura, Y. and Ueyama, D., *A Skeleton Structure of Self-replicating Dynamics*, Physica D **130**(1999) 73-104.

[290] Nishiura, Y., Ueyama, D., *Spatial-temporal chaos for the Gray-Scott model*, Physica D **150**(2001) 137-162.

[291] Nochetto, R.H., *A class of nondegenerate two-phase Stefan problems in several space variables*, Comm. Partial Diff. Eqs. **12**(1987) 21-45.

[292] Novick-Cohen, A. and Segel, L.A., *Nonlinear aspects of the Cahn-Hilliard equation*, Physica D **10**(1984) 277-298.

[293] Ohnishi, I., Nishiura, Y., Imai, M. and Matsushita, Y., *Analytical solutions describing the phase separation driven by a free energy functional containing a long-range interaction term*, Chaos **9** (1999) 329-341.

[294] Ohta, T., Jasnow, D. and Kawasaki, K., *Universal scaling in the motion of random interfaces*, Phys. Rev. Lett. **49**(1982) 1223-1226.

[295] Ohta, T. and Kawasaki, K., *Equilibrium morphology of block copolymer melts*, Macromolecules **19**(1986) 2621-2632.

[296] Ohta, T. and Kiyose, J., *Collision of Domain Boundaries in a Reaction-Diffusion System*, J. Phys. Soc. Japan **65**(1996) 1967-1970.

[297] Ohta, T. and Mimura, M., *Pattern dynamics in excitable reaction-diffusion media*, in *Formation, Dynamics and Statistics of Patterns* **1**, Kawasaki, K., Suzuki, M. and Onuki, A., Eds., World Scientific (1990) 55-112.

[298] Ohta, T., Mimura, M. and Kobayashi, R., *Higher-dimensional localized pattern in excitable media*, Physica D **34**(1989) 115-144.

[299] Oono, Y., *Renormalization and Asymptotics*, Int. J. Modern Phys. **B 14**(2000) 1327-1361.

[300] Osher, S. and Sethian, A., *Fronts propagating with curvature dependent speed: Algorithms based on Hamilton-Jacobi formulations*, J. Comp. Phys. **79**(1988) 12-49.

[301] Otto, E., *Chaos in dynamical systems*, Cambridge Univ. Press (1993).

[302] Ouyang, Q. and Flesselles, J.M., *Transition from spirals to defect turbulence driven by a convective instability*, Nature **379**(1996) 143-146.

[303] Pearson, J.E., *Complex patterns in a simple system*, Science **216**(1993) 189-192.

[304] Pego, R.L., *Front migration in the nonlinear Cahn-Hilliard equation*, Proc. Roy. Soc. London **A 422**(1989) 261-278.

[305] Pelce, P., *Dynamics of Curved Fronts*, Accademic Press (1988).

[306] Pelce, P. and Sun, J., *Wavefronts interaction in steadily rotating spirals*, Physica D **48**(1991) 353-366.

[307] Penrose, O. and Fife, P.C., *Thermodynamically Consistent Models of Phase-field Type for the Kinetics of Phase Transitions*, Physica D **43**(1990) 44-62.

[308] Petrov, V., Scott, S.K. and Showalter, K., *Excitability, wave reflection, and wave splitting in a cubic autocatalysisreaction-diffusion system*, Phil. Trans. Roy. Soc. Lond. A **347**(1994) 631-642.

[309] Pillet, C.A., *Stabilization of needle-crystals by the Gibbs-Thomson effect*, Commun. Math. Phys. **140**(1991) 241-274.

[310] Powell, J.A., Newell, A.C. and Jones, C.K.R.T., *Competition between generic and nongeneric fronts in envelope equations*, Phys. Rev. A **44**(1991) 3636-3652.

[311] Powers, T.R. and Goldstein, R.E., *Pearling and pinching: Propagation of Rayleigh instabilities*, Phys. Rev. Lett. **78**(1997) 2555-2558.

[312] Rachevsky, N., *Mathematical Biophysics*, Univ. of Chicago Press (1938).

[313] Rasmussen, K.E., Mazin, W., Mosekilde, E., Dewel, G. and Borckmans, P., *Wave-splitting in the bistable Gray-Scott model*, International Journal of Bifurcation and Chaos, **6**(1996) 1077-1092.

[314] Ren, X. and Wei, J., *On energy minimizers of the di-block copolymer problem*, preprint (2001).

[315] Reynolds, W.N., Pearson, J.E. and Ponce-Dawson, S., *Dynamics of self-replicating patterns in reaction diffusion systems*, Phys. Rev. Lett. **72**(1994) 1120-1123.

[316] Reynolds, W.N., Ponce-Dawson, S. and Pearson, J.E., *Self-replicating spots in reaction-diffusion systems*, Phys. Rev. E **56**(1997) 185-198.

[317] Rinzel, J. and Terman, D., *Propagation in a bistable reaction-diffusion system*, SIAM J. Appl. Math. **42**(1982) 1111-1137.

[318] Rubinstein, J., Schatzman, M. and Sternberg, P., *Collapse of vortex links in the Ginzburg-Landau flow*, C. R. Acad. Sci. Paris Sér. I Math. **322**(1996) 31-35.

[319] Rubinstein, L.I., *The Stefan Problem*, Translations of Mathematical Monographs **27**, American Mathematical Society, Providence, R.I. (1971).

[320] Sakamaoto, K., *Construction and stability analysis of transition layer solutions in reaction-diffusion systems*, Tohoku Math. J. **42**(1990) 17-44.

[321] Sakamoto, K., *Internal layers in high-dimensional domains*, Proc. Roy. Soc. Edinburgh **128A**(1998) 359-401.

[322] Sandstede, B., *Stability of multiple-pulse solutions*, Trans. American Math. Soc. **350**(1998) 420-472.

[323] Sandstede, B. and Scheel, A., *Absolute versus convective instability of spiral waves*, Phys. Rev. E **62**(2000) 7708-7715.

[324] Sandstede, B. and Scheel, A., *Absolute and convective instabilities of waves on unbounded and large bounded domains*, Physica D **145**(2000) 233-277.

[325] Sandstede, B. and Scheel, A., *Super-spiral structures of meandering and drifting spiral waves*, Phys. Rev. Lett. **86**(2001) 171-174.

[326] Sandstede, B., Scheel, A. and Wulff, C., *Bifurcations and dynamics of spiral waves*, J. Nonlinear Sci. **9**(1999) 439-478.

[327] Sattinger, D.H., *On the stability of waves of nonlinear parabolic systems*, Adv. Math. **22**(1976) 312-355.

[328] Sattinger, D.H., *Weighted norms for the stability of traveling waves*, J. Diff. Eqs. **25**(1977) 130-144.

[329] Schneider, G., *Error estimates for the Ginzburg-Landau approximation*, ZAMP (Z. Angew. Math. Phys.) **45**(1994) 433-457.

[330] Schneider,G., *A new estimate for the Ginzburg-Landau approximation on the real axis*, J. Nonlinear Sci. **4**(1994) 23-34.

[331] Schneider, G., *Analyticity of Ginzburg-Landau modes*, J. Diff. Equ. **121**(1995) 233-257.

[332] Schneider, G., *Diffusive stability of spatial periodic solutions of the Swift-Hohenberg equation*, Commun. Math. Phys. **178**(1996) 679-702.

[333] Sijbrand, J., *Properties of center manifolds*, Trans. Amer. Math. Soc. **289**(1985) 431-469.

[334] Simon, L., *Asymptotics for a class of non-linear evolution equations with applications to geometric problems*, Ann. of Math. **118**(1983) 525-571.

[335] Skinner, G.S. and Swinney, H.L., *Periodic to quasiperiodic transition of chemical spiral rotation*, Physica D **48**(1991) 1-16.

[336] Soner, M.H., *Convergence of the phase-field equations to the Mullins-Sekerka problem with kinetic undercooling*, Arch. Rational Mech. Anal. **131**(1995) 139-197.

[337] Sternberg, P., *The effect of a singular perturbation on noncovex variational problems*, Arch. Rational Mech. Anal. **101**(1988) 209-260.

[338] Stokes, A.N., *On two types of moving front in quasilinear diffusion*, Math. Biosci. **3**(1976) 307-315.

[339] Stoth, B.E.E., *Convergence of the Cahn-Hilliard equation to the Mullins-Sekerka problem in spherical symmetry*, J. Diff. Eqns. **125**(1996) 154-183.

[340] Suzuki, H., *Asymptotic characterization of stationary interfacial patterns for reaction diffusion systems*, Hokkaido Math. J. **26**(1997) 631-667.

[341] Taniguchi, M. and Nishiura, Y., *Instability of planar interfaces in reaction-diffusion systems*, SIAM J. Math. Anal. **25**(1994) 99-134.

[342] Turing, A.M., *The chemical basis of morphogenesis*, Phil. Trans. Roy. Soc. Lond. **B327**(1952) 37-72.

[343] Tyson, J.J. and Kenner, J.P., *Singular perturbation theory of travelling waves in excitable media (a review)*, Physica D **30**(1988) 327-361.

[344] Ueyama, D., *Dynamics of self-replicating patterns in the one-dimensional Gray-Scott model*, Hokkaido Math. J. **28**(1999) 175-210.

[345] van Harten, A., *On the validity of the Ginzburg-Landau equation*, J. Nonlinear Sci. **1**(1991) 397-422.

[346] van Saarloos, W., *Front propagation into unstable states: Marginal stability as a dynamical mechanism for velocity selection*, Phys. Rev. A **37**(1988) 211-229.

[347] van Saarloos, W., *Front propagation into unstable states II: Linear versus nonlinear marginal stability and rate of convergence*, Phys. Rev. A **39**(1989) 6367-6390.

[348] van Saarloos, W. and Hohenberg, P.C., *Fronts, pulses, sources and sinks in generalized complex Ginzburg-Landau equations*, Physica D **56**(1992) 303-367.

[349] van Saarloos, W. and Weeks, J.D., *Boundary-layer formulation of dendritic growth: Existence of a family of steady-state needle solutions*, Phys. Rev. Lett. **55**(1985) 1685-1688.

[350] Visintin, A., *Models of Phase Transitions*, Progress in Nonlinear Differential Eequations and Their Applications, Volume 28, Birkhauser, Boston (1996).

[351] Ward, M.J., *Metastable bubble solutions for the Allen-Cahn equation with mass conservation*, SIAM J. Appl. Math. **56**(1996) 1247-1279.

[352] Wayne, C.E., *Invariant manifolds for parabolic partial differential equations on unbounded domains*, Arch. Rational Mech. Anal. **138**(1997) 279-306.

[353] Wei, J., *Pattern formations in two-dimensional Gray-Scott model: Existence of single-spot solutions and their stability*, Physica D **148**(2001) 20-48.

[354] Weinstein, M.I. and Xin, J., *Dynamic stability of vortex solutions of Ginzburg-Landau and nonlinear Schrödinger equations*, Commun. Math. Phys. **180**(1996) 389-428.

[355] Williams, L.M., Muschol, L., Qian, X., Losert, W., and Cummins, H.Z., *Dendritic side-branching with periodic localized perturbations: Directional solidification of pivalic acid-coumarin 152 mixtures*, Phys. Rev. E **48** (1993) 489-499.

[356] Winfree, A.T., *Varieties of spiral wave behavior: An experimentalist's approach to the theory of excitable media*, Chaos **1**(1991) 303-334.

[357] Yamaguchi, T., *Turing structure and pattern formation in reaction-diffusion systems*, J. National Institute of Material and Chemical Reserach, **5**(4)(1997) 151-164.

[358] Yanagida, E., *Stability of stationary distributions in a space-dependent population growth process*, J. Math. Biol. **15**(1982) 37-50.

[359] Yanagida, E., *Stability of fast travelling pulse solutions of FitzHugh-Nagumo equations*, J. Math. Biol. **22**(1985), 81-104.

[360] Zelenyak, T.I., *Stabilization of solutions of boundary value problems for a second order parabolic equation with one space variable*, Diff. Eqs. **4**(1968) 17-22.

# Index

# Selected Titles in This Series

(*Continued from the front of this publication*)

181 **Ya. G. Berkovich and E. M. Zhmud′,** Characters of finite groups. Part 2, 1999

180 **A. A. Milyutin and N. P. Osmolovskii,** Calculus of variations and optimal control, 1998

179 **V. E. Voskresenskiĭ,** Algebraic groups and their birational invariants, 1998

178 **Mitsuo Morimoto,** Analytic functionals on the sphere, 1998

177 **Satoru Igari,** Real analysis—with an introduction to wavelet theory, 1998

176 **L. M. Lerman and Ya. L. Umanskiy,** Four-dimensional integrable Hamiltonian systems with simple singular points (topological aspects), 1998

175 **S. K. Godunov,** Modern aspects of linear algebra, 1998

174 **Ya-Zhe Chen and Lan-Cheng Wu,** Second order elliptic equations and elliptic systems, 1998

173 **Yu. A. Davydov, M. A. Lifshits, and N. V. Smorodina,** Local properties of distributions of stochastic functionals, 1998

172 **Ya. G. Berkovich and E. M. Zhmud′,** Characters of finite groups. Part 1, 1998

171 **E. M. Landis,** Second order equations of elliptic and parabolic type, 1998

170 **Viktor Prasolov and Yuri Solovyev,** Elliptic functions and elliptic integrals, 1997

169 **S. K. Godunov,** Ordinary differential equations with constant coefficient, 1997

168 **Junjiro Noguchi,** Introduction to complex analysis, 1998

167 **Masaya Yamaguti, Masayoshi Hata, and Jun Kigami,** Mathematics of fractals, 1997

166 **Kenji Ueno,** An introduction to algebraic geometry, 1997

165 **V. V. Ishkhanov, B. B. Lur′e, and D. K. Faddeev,** The embedding problem in Galois theory, 1997

164 **E. I. Gordon,** Nonstandard methods in commutative harmonic analysis, 1997

163 **A. Ya. Dorogovtsev, D. S. Silvestrov, A. V. Skorokhod, and M. I. Yadrenko,** Probability theory: Collection of problems, 1997

162 **M. V. Boldin, G. I. Simonova, and Yu. N. Tyurin,** Sign-based methods in linear statistical models, 1997

161 **Michael Blank,** Discreteness and continuity in problems of chaotic dynamics, 1997

160 **V. G. Osmolovskiĭ,** Linear and nonlinear perturbations of the operator div, 1997

**Far-from-Equilibrium Dynamics**

Yasumasa Nishiura

This book is devoted to the study of evolution of nonequilibrium systems. Such a system usually consists of regions with different dominant scales, which coexist in the space-time where the system lives. In the case of high nonuniformity in special directions, one can see patterns separated by clearly distinguishable boundaries or interfaces.

The author considers several examples of nonequilibrium systems. One of the examples describes the invasion of the solid phase into the liquid phase during the crystallization process. Another example is the transition from oxidized to reduced states in certain chemical reactions. An easily understandable example of the transition in the temporal direction is a sound beat, and the author describes typical patterns associated with this phenomenon.

The main goal of the book is to present a mathematical approach to the study of highly nonuniform systems and to illustrate it with examples from physics and chemistry. The two main theories discussed are the theory of singular perturbations and the theory of dissipative systems. A set of carefully selected examples of physical and chemical systems nicely illustrates the general methods described in the book.

ISBN 0-8218-2625-5

9 780821 826256

MMONO/209